

The Tor Exhumation Approach – A New Technique to Derive Continuous In-Situ Soil Erosion and Surface Denudation Models

Dissertation

zur

Erlangung der naturwissenschaftlichen Doktorwürde
(Dr. sc. nat.)

vorgelegt der

Mathematisch-naturwissenschaftlichen Fakultät

der

Universität Zürich

von

Gerald Raab

aus

Österreich

Promotionskommission

Prof. Dr. Markus Egli (Leitung & Vorsitz)

Prof. Dr. Fabio Scarciglia

Prof. Dr. Max Maisch

Prof. Dr. Christine Alewell

Zürich, 2019

ABSTRACT

Landscapes and soils are subjected to changing environmental conditions, resulting in a non-linear evolution over time. Capturing the variations of surface denudation and soil erosion over geological time-scales remains challenging due to the lack of suitable archives. Common denudation studies using cosmogenic nuclides and catchment-wide approaches provide only average denudation or erosion rates. However, the natural denudation variations over time are mostly neglected. In addition, soil formation can also change in dependency of soil production and erosion rates or aeolian additions — a fact that has not had much data collected over millennia due to the limitations of present-day investigation techniques. The fragmented and incomplete knowledge of these temporal fluctuations hinders an understanding of how landscapes and soils respond to environmental changes. This study tackled this knowledge gap using modern surface dating techniques (surface exposure dating — ^{10}Be) within the well-defined conditions of the granite upland plateau of the Sila Massif (Calabria, Italy).

In pursuit of unravelling soil erosion history, specific rock formations, so called “tors”, were investigated as potential soil erosion and landscape denudation archives. Tors are large residual rocks having a height of some meters that are still attached to the underlying bedrock. It was hypothesised that the by surface exposure dating quantified exhumation speed of tors reflects the surrounding surface lowering and associated soil erosion. The exhumation theory was not only tested on tors but also on detached bedrock (boulders) and exposed rock-outcrops along steep slopes (scarps). In addition, alternative soil age estimation techniques were explored and allochthonous soil material (volcanic glass) was geochemically traced to its original location and time of input for additional correlations with local soil formation ages.

The multi-method approach for soil-age estimations revealed that local radiocarbon ages provide information about minimum soil ages of about 14,000 years. Semi-quantitative dating with chemical weathering indices resulted in a soil age span from 16 – 67 ka, averaging at 45 ka. Geochemical fingerprinting of volcanic glass allowed a stratigraphic correlation of volcanic eruption sequences of distant volcanos. Using chemical mass balances and laser ablation on thin sections showed that large proportions of the volcanic deposits derived from Lipari (Aeolian Islands) and a minor part from Etna (Sicily). This correlation framed certain soil horizons to be older than 30,000 years but younger than 92,000 – 81,000 years.

The postulated exhumation approach deciphered for the first time the temporal evolution of surface denudation and soil erosion over Holocene to Pleistocene time. Among the three investigated landforms tors provided the most consistent denudation results and covered the longest exposure time-span (100,000 years). Hence, the exhumation history of granite tors in the upland plateau vastly enabled the determination of continuous soil erosion rates over geological time-scales. Linking of the deciphered soil erosion and surface denudation variation

with paleoenvironmental data resulted in a local surface evolution model and an event chronology. The role of excepted soil-forming factors (e.g. topography, vegetation, climate) was thereby captured for the first time over a continuous geological time-scale up to the Pleistocene. Slope angles and vegetation density appear to regulate soil erosion intensity, while climate transitions can initiate relatively abrupt increases.

In detail, extremely low rates of mostly below $100 \text{ t km}^{-2} \text{ year}^{-1}$ (about $0.12 \text{ mm year}^{-1}$) were detected prior to 21,000 years. During these conditions soil formation seemed to have occurred, being also stimulated by the volcanic ash input. During the transition from the Pleistocene to the Holocene (cool-dry to warm-humid), soil erosion rates increased up to a maximum of about $0.31 \text{ mm year}^{-1}$ at slopes and $0.16 \text{ mm year}^{-1}$ at planar surfaces. Since this peak phase at about 17,000 – 5,000 years, soil erosion appears to have decreased back to $\sim 0.12 \text{ mm year}^{-1}$. However, modern soil redistribution rates obtained from fallout radionuclide investigations ($^{239+240}\text{Pu}$) suggest soil erosion rates of the last five decades to be $\geq 1,000 \text{ t km}^{-2} \text{ year}^{-1}$ (about $1.22 \text{ mm year}^{-1}$). These rates are far above the tor-derived surface denudation rates and the natural rates of soil production. The continuation of the local anthropogenic influence of the area will definitely lead to a distinct decrease in soil depth and with time to a rockier surface.

In conclusion, the exhumation approach tested on tors detected soil erosion and surface denudation variation over an unprecedented time-scale and enabled a linkage to influential environmental factors. Tors proved to be a very suitable archive that retain information about surface evolution and its fluctuation over a geological time-scale. Further explorations of tors as archive can help to decrease the knowledge gap of surface denudation and soil erosion variations of the past from regional to potentially global scales.

ZUSAMMENFASSUNG

Landschaften und Böden sind wechselnden Umweltbedingungen ausgesetzt, die im Laufe der Zeit zu einer nichtlinearen Entwicklung führen. Die Erfassung der Variationen von Denudation und Bodenerosion über geologische Zeiträume hinweg bleibt eine Herausforderung, da geeignete Archive fehlen. Gängige Denudationsstudien mit kosmogenen Nukliden und einzugsgebietsweiten Ansätzen liefern nur durchschnittliche Denudations- oder Erosionsraten. Die natürlichen zeitlichen Schwankungen der Denudation und Erosion werden meist vernachlässigt. Darüber hinaus kann sich auch die Bodenbildung in Abhängigkeit von der Bodenproduktion, der Erosionsrate oder von äolischen Einträgen ändern – eine Tatsache, die mit den heutigen Untersuchungstechniken kaum über Jahrtausende hinweg erfasst wird. Die fragmentierte und unvollständige Kenntnis dieser zeitlichen Schwankungen erschwert das Verständnis, wie Landschaften und Böden auf Umweltveränderungen reagieren. Diese Wissenslücke wurde in dieser Studie mit modernen Oberflächendatierungstechniken (^{10}Be) unter genau definierten Bedingungen auf dem Granitplateau des Sila-Massivs (Kalabrien, Italien) in Angriff genommen.

Um die Geschichte der Bodenerosion zu enträtseln, wurden bestimmte Gesteinsformationen, sogenannte „Tors“, als potenzielle Archive für Bodenerosion und Landschaftsentblößung untersucht. Tors sind große, meterhohe Restgesteine, die noch am darunter liegenden Grundgestein haften. Es wurde die Hypothese aufgestellt, dass die durch Oberflächenexposition quantifizierte Exhumierungsgeschwindigkeit von Toren, die Absenkung der umgebenden Oberfläche und die damit verbundene Bodenerosion widerspiegelt. Die Exhumierungstheorie wurde nicht nur an Toren, sondern auch an abgelösten Felsbrocken (Boulder) und exponierten Untergrundgestein entlang steiler Hänge (Scarps) getestet. Darüber hinaus wurden alternative Techniken zur Abschätzung des Bodenalters zur Untersuchung beigezogen. Allochthones Bodenmaterial (vulkanisches Glas) wurde geochemisch an seinem ursprünglichen Ort und Zeitpunkt des Eintrags zurückverfolgt, um weitere Korrelationen mit dem lokalem Bodenbildungsalter zu ermöglichen.

Der Multi-Methoden-Ansatz zur Abschätzung des Bodenalters ergab, dass lokale Kohlenstoffalter Informationen über das Mindestalter des Bodens von etwa 14'000 Jahren liefern. Semiquantitative Datierungen mit chemischen Verwitterungsindizes ergaben eine Altersspanne des Bodens von 15'600 bis 66'700 Jahren und einen Durchschnitt von 45'300 Jahren. Geochemische Fingerabdrücke von Vulkanglas ermöglichten eine stratigraphische Korrelation von Vulkanausbruchsequenzen entfernter Vulkane. Die Verwendung chemischer Massenbilanzen und Laserablation an Dünnschliffen zeigte, dass der Großteil der vulkanischen Ablagerung von Lipari (Äolischen Inseln) und ein kleinerer Anteil vom Ätna

(Sizilien) stammen. Durch diese Korrelation wurden bestimmte Bodenhorizonte älter als 30'000 Jahre, aber jünger als 92'000 – 81'000 Jahre eingestuft.

Der postulierte Exhumierungsansatz entschlüsselte zum ersten Mal die zeitliche Entwicklung von Denudation und Bodenerosion über die Zeit des Holozäns bis zum Pleistozän. Unter den drei untersuchten Landformen lieferten die Tore die konsistentesten Denudationsergebnisse und deckten den längsten Expositionszeitraum (100'000 Jahre) ab. Die Exhumierungsgeschichte von Granittoren im Hochland ermöglichte daher die Bestimmung kontinuierlicher Bodenerosionsraten über erhebliche geologische Zeitskalen. Die Verknüpfung der entschlüsselten Variationen von Bodenerosion und Denudation mit Paläoumweltdaten führte zu einem lokalen Oberflächenentwicklungsmodell und einer Ereignischronologie. Die Rolle von anerkannten Bodenbildungsfaktoren (z. B. Topographie, Vegetation, Klima) wurde dabei zum ersten Mal über einen kontinuierlichen geologischen Zeitraum bis zum Pleistozän erfasst. Hangwinkel und Vegetationsdichte scheinen die Intensität der Bodenerosion zu regulieren, während Klimaübergänge relativ abrupte Zunahmen auslösen können.

Im Detail wurden vor mehr als 21'000 Jahren extrem niedrige Raten von meist unter $100 \text{ t km}^{-2} \text{ Jahr}^{-1}$ (ca. $0,12 \text{ mm Jahr}^{-1}$) festgestellt. Unter diesen Bedingungen schien es zu Bodenbildung gekommen zu sein, die auch durch den Vulkanascheeintrag angeregt wurde. Während des Übergangs vom Pleistozän zum Holozän (kühl-trocken zu warm-feucht) stiegen die Bodenerosionsraten an Hängen bis zu einem Maximum von ca. $0,31 \text{ mm Jahr}^{-1}$ und ebenen Oberflächen bis zu $0,16 \text{ mm Jahr}^{-1}$ an. Seit dieser Spitzenphase um ca. 17'000 – 5'000 Jahren scheint die Bodenerosion auf $\sim 0,12 \text{ mm Jahr}^{-1}$ zurückgegangen zu sein. Die modernen Umverteilungsraten des Bodens, die im Rahmen von Radionukliduntersuchungen ($^{239+240}\text{Pu}$) ermittelt wurden, zeigen Bodenerosionsraten der letzten fünf Jahrzehnte von $\geq 1'000 \text{ t km}^{-2} \text{ Jahr}^{-1}$ (ca. $1,22 \text{ mm Jahr}^{-1}$). Diese Raten liegen weit über den von Toren abgeleiteten Denudationsraten und den natürlichen Raten der Bodenproduktion. Die Fortsetzung des lokalen anthropogenen Einflusses in dem Gebiet wird definitiv zu einer deutlichen Abnahme der Bodentiefe und mit der Zeit zu einer felsigeren Oberfläche führen.

Zusammenfassend lässt sich festhalten, dass der an Toren getestete Exhumierungsansatz Bodenerosion und Denudation über einen beispiellosen Zeitraum erfasste und eine Verknüpfung mit einflussreichen Umweltfaktoren ermöglichte. Tors haben sich als sehr geeignete Archive erwiesen, die Informationen über die Oberflächenentwicklung und deren Fluktuation über einen geologischen Zeitraum hinweg bewahren. Weitere Untersuchungen von Toren als Archiv können dazu beitragen die Wissenslücke über Denudations- und Bodenerosionsschwankungen der Vergangenheit auf regionalen und potentiell globalen Maßstab zu verringern.

ABBREVIATIONS

a	Latin: annum = year; ka = kilo years = 1000 years;
AMS	Accelerator mass spectrometry
B.P.	Before present. Present is defined as the year 1950.
CRONUS	Cosmic-ray produced nuclide systematics (project)
DRIFT	Diffuse reflection infrared Fourier transform
ESEM-EDS	Environmental scanning electron microscope energy dispersive system
FRNs	Fallout radionuclides
GPS	Global positioning system
HF	Hydrofluoric acid
ICP-OES	Inductively coupled plasma optical emission spectrometry
ICP-MS	Inductively coupled plasma mass spectrometry
LA-ICP-MS	Laser ablation inductively coupled plasma mass spectrometry
LGM	Last glacial maximum
REEs	Rare earth elements
SEM	Scanning electron microscope
TCNs	Terrestrial cosmogenic nuclides
TEA	Tor exhumation approach
XRD	X-ray powder diffraction
XRF	X-ray fluorescence
ZORA	Zurich open repository and archive

CONTENTS

1. INTRODUCTION	1
1.1. CHALLENGES OF CONVENTIONAL SOIL EROSION ARCHIVES	4
1.2. HYPOTHESES AND AIMS	6
2. STUDY AREA	8
3. METHODS	10
3.1. THEORY OF TERRESTRIAL COSMOGENIC NUCLIDES	10
3.2. TERRESTRIAL IN-SITU COSMOGENIC RADIONUCLIDE DATING	11
3.3. RADIOCARBON DATING	11
3.4. FALLOUT RADIONUCLIDES	13
3.5. CHEMICAL WEATHERING INDICES	13
3.6. GEOCHEMICAL FINGERPRINTING OF IGNEOUS MINERALS	15
4. RESULTS	15
4.1. MANUSCRIPT I	16
4.2. MANUSCRIPT II	16
4.3. MANUSCRIPT III	16
4.4. ORIGINAL PUBLICATIONS	17
5. DISCUSSION OF MAIN RESULTS	19
5.1. ALTERNATIVE SOIL AGE ESTIMATIONS	19
5.2. TOR EXHUMATION APPROACH (TEA)	20
5.3. ANTHROPOGENIC SOIL EROSION?	24
5.4. NATURAL DRIVER AND PREVENTOR OF SOIL EROSION	24
6. CONCLUSIONS	25
7. OUTLOOK AND PERSPECTIVES	25
7.1. PROPOSED NEXT STEPS	25
7.2. BROADER APPLICABILITY AND VALUE	26
REFERENCES	28
ACKNOWLEDGEMENTS	34
APPENDICES	34
CURRICULUM VITAE	38

1. INTRODUCTION

Soil is the fragile skin of Earth that anchors life as a permeable near-surface layer at the intersection of interfaces such as the atmosphere, biosphere, and lithosphere (NRC 2001; Brantley, 2006; Wilding, 2006; Anderson, 2007). The mixture of minerals, air, water and organic material, functions as an active feed-through reactor where continuous exchanges and transformations of mass and energy occur (Banwart et al., 2017). The capabilities of soil (Fig. 1) include, among others, water filtration (e.g.

groundwater protection), discharge control (e.g. flood prevention), storage of carbon and other nutrients, biomass production, biological habitat and chemical recycling. Moreover, soil serves as platform for man-made structures (e.g. roads, houses), agriculture (e.g. crops, livestock), as well as raw material (e.g. bricks, porcelain). This makes it one of the most precious resources on our planet. Although, soil is considered a self-renewable resource, its formation is complex, nonlinear and can take several thousands of years (Fig. 2). Soil formation starts with parent material (e.g. rock or additional material influxes) that is

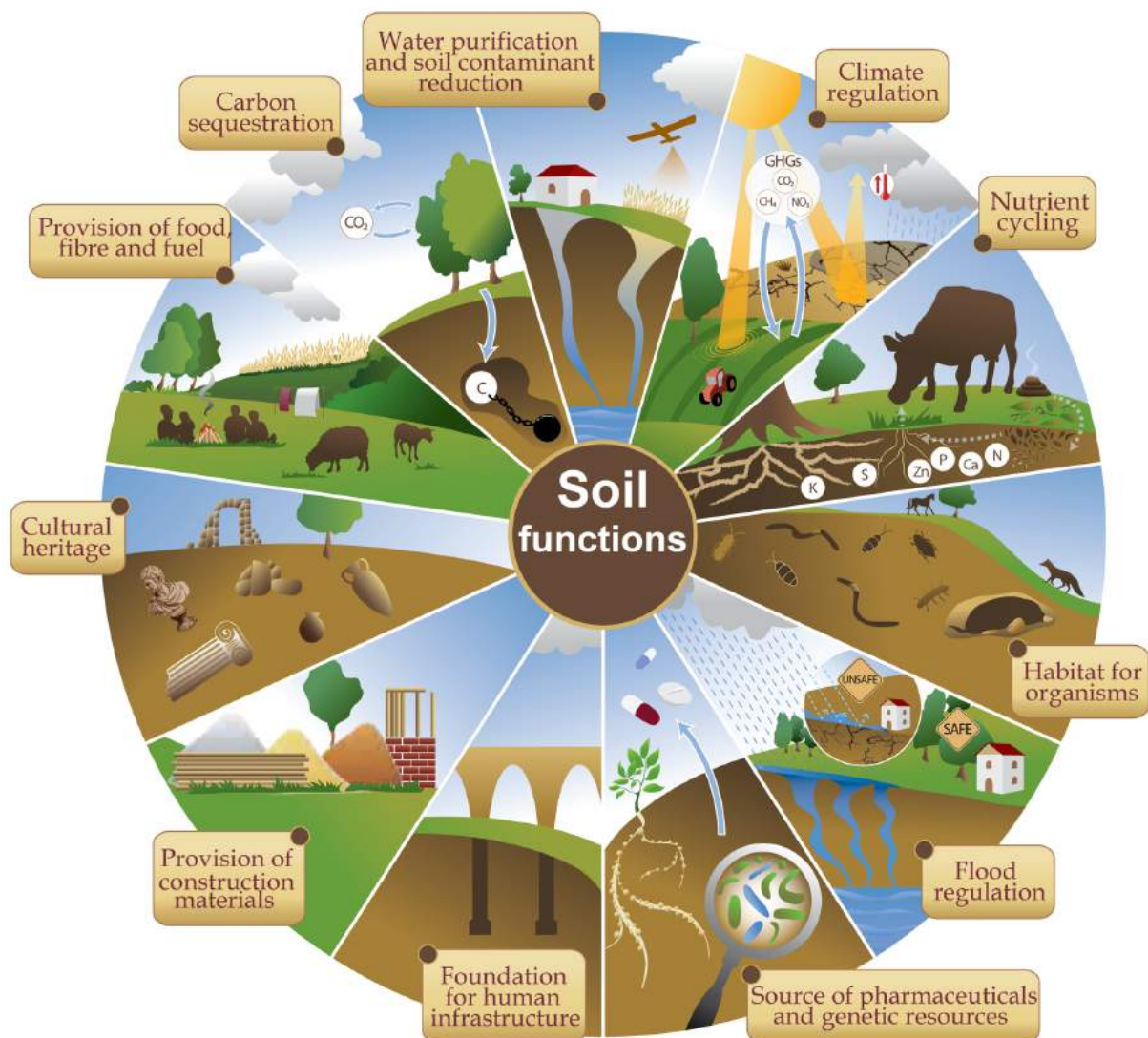


Figure 1: This overview of the broad spectrum of soil functions displays the numerous ecosystem services that soil provides to enable life on Earth (FAO, 2015). GHGs =Green House Gases.

converted through weathering (e.g. physical, chemical and hydrological processes) to a hospitable substrate for organisms (Graham et al., 2010). The bioactivity of organisms, in and on the substrate, assist with translocation of material, the chemical transformation of minerals and nutrients, retaining moisture

for these reactions, enrich it with organic matter and protect it from material loss by denudation (e.g. wind and water erosion; leaching through weathering). Soils evolve over time depending on local environmental conditions such as climate (e.g. temperature and precipitation), relief (e.g. surface gradient) or material additions

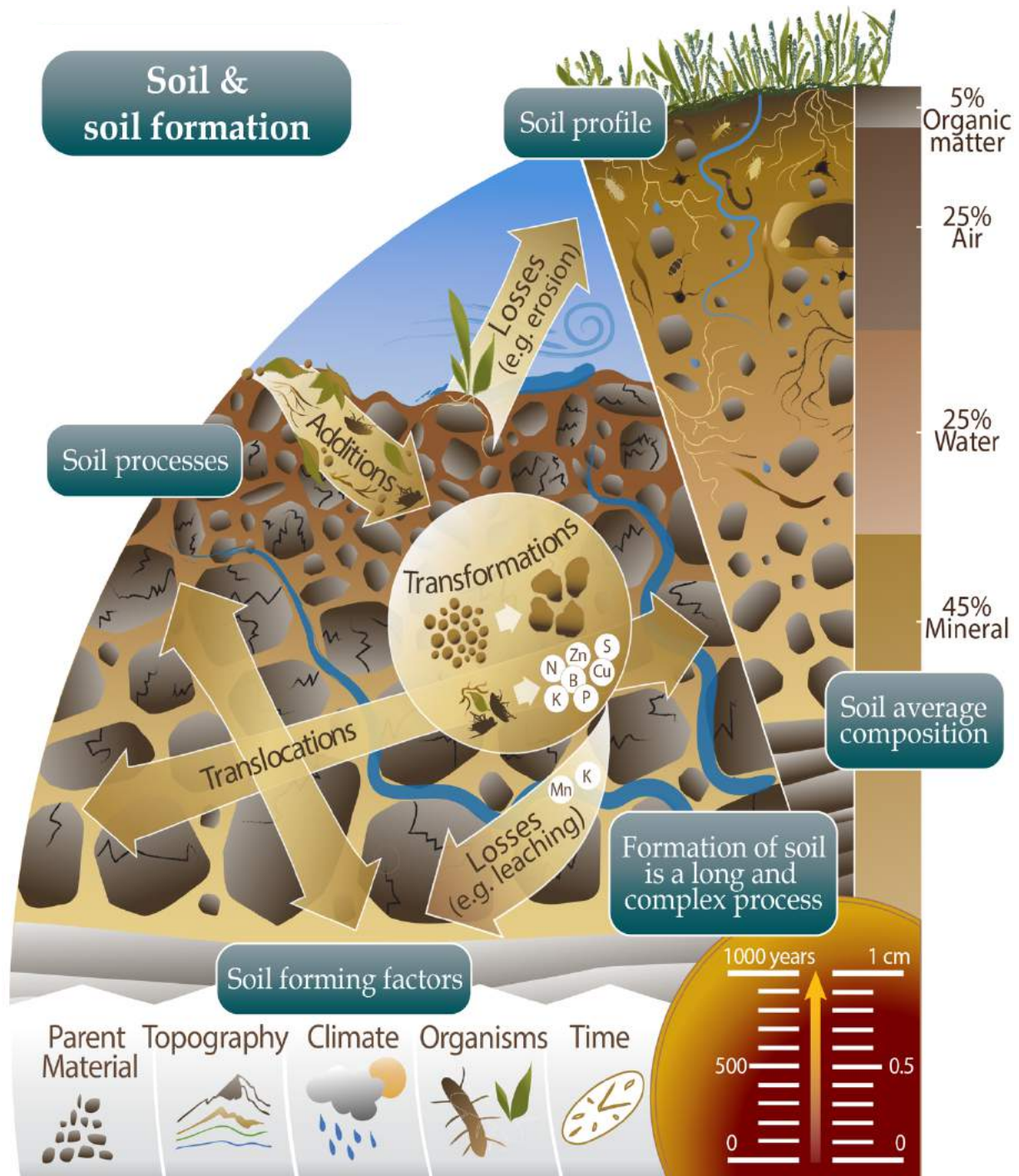


Figure 2: A brief overview of how soil is formed, including its soil forming factors, the diverse soil processes, a conceptual soil profile and the average composition and formation time of soil (modified after FAO, 2015).

(e.g. aeolian or organic material). The responsible environmental conditions can change across space and time, which can also hinder the related soil formation or even reduce the soil thickness. Changes might be even very abrupt, either by catastrophic and natural events (e.g. landslides) or by the influence of anthropogenic activities (e.g. deforestation, intensification of agriculture, overgrazing).

Therefore, in a temporal model, soil evolution is regarded as being irregular and conceptualised by 'progressive' or 'regressive' phases (Fig. 3; Johnson & Watson-Stegner, 1987; Sommer et al., 2008). Progressive phases (e.g. soil deepening) then occur when soil production exceeds denudation and regressive phases (e.g. soil erosion through wind and water) occur when denudation surpasses soil production.

Consequently, soil erosion dominant phases reduce the capabilities of its functions. In a broader aspect, soil erosion can lead, among other things, to water

shortage clogged river beds, eutrophication of water with direct harmful impact on biotas and man-made structures (e.g. hydropower plants), dust storms (e.g. health issues) and reduced crop yields (causing starvation — which can initiate migration or local/regional conflicts).

Hence, the loss of soil can be considered to be, after pollution and global warming, one of the most impactful environmental (and economic) threats the world faces (Butzer, 1974; Blaikie 2016).

According to the United Nations, a third of the planet's land surface, particularly the valuable soil, has already been lost or heavily degraded (UN news, 2017). Additionally, the demand and stress put on soil steadily increase due to the world population continuously rising (Pimentel et al., 1995, 2006; Richter & Markewitz, 2001). The recent increase in extreme weather events (e.g. droughts, floods) further accelerate surface degradation and increases the vulnerability of erodible landscapes and its soils.

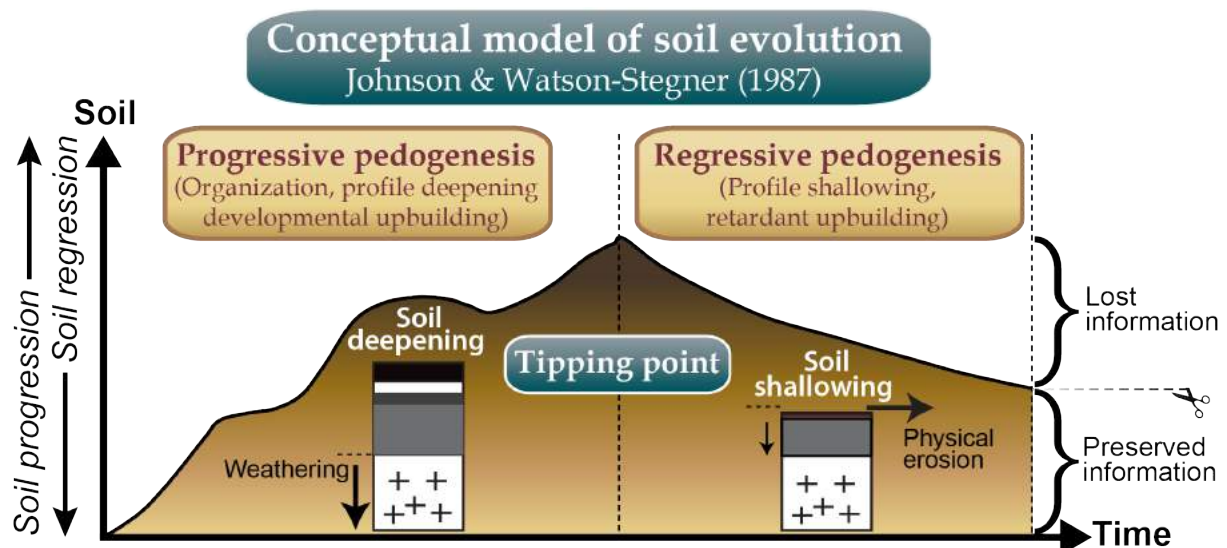


Figure 3: The concept of non-linear soil formation after Johnson & Watson-Steger (1987). Phases of progressive and regressive pedogenesis alternate depending on the changing environmental conditions. Information about past soil depth and volume is lost by soil regressive phases.

However, compared to other global issues like climate change, the issue of soil erosion has often been neglected in the past. Consequently, there are many data sets about climate records reaching back millions of years, but there are only a few soil erosion records covering c. the last millennium (Boardman & Poesen, 2007; Poesen, 2018).

This lack of records has resulted in poor information about past spatial and temporal dynamics and keeps the knowledge in this field fragmented and incomplete (Pimentel, 2006). In particular, the effects of changing environmental conditions on soil erosion and surface denudation are poorly identified and understood over geological time-scales.

The absence of data complicates accurate predictions about future surface development, risk assessments of landscapes, tailoring of suitable counter-measures and leads to poor policy-making.

In order to provide a holistic understanding of soil surface destructive processes, (paleo-)environmental records have to be compared with long-term soil erosion archives.

1.1. CHALLENGES OF CONVENTIONAL SOIL EROSION ARCHIVES

Paleoenvironmental investigations can offer insight into the evolution of soils and landscape surfaces (Fig. 4). However, soils are often problematic and not suitable for the reconstruction of time-varying surface-destructive processes. They merely reflect the overall situation at a given time (Johnson & Watson-Stegner, 1987) and provide only fragmented information on temporal discontinuities of denudation and soil erosion fluctuations (Bouchard & Jolicoeur, 2000; Migoń & Lidmar-Bergström, 2002; Migoń & Thomas, 2002; Tylor & Shirliff, 2003; Ehlen, 2005; Hall et al., 2012).

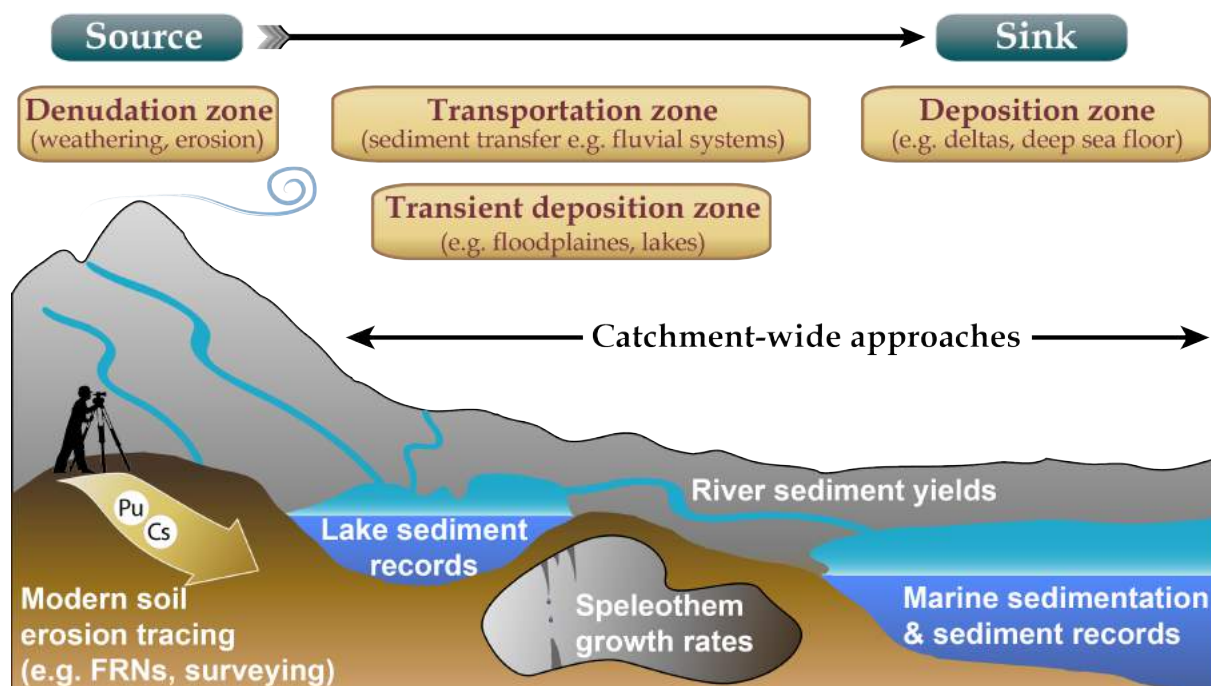


Figure 4: Sketch of diverse conventional archives to quantify soil erosion and surface denudation rates. Usually catchment-wide approaches are used to determine erosion and denudation rates for source areas.

However, pioneering work for measuring erosion and also chemical weathering rates in soils (point data, small areas) was done by, among others, Schaller et al. (2010a,b), Norton et al. (2010) and Heimsath et al. (2001a,b; 2012). Qualitative or quantitative estimates of erosion rates over different time-scales have been derived from river sediment yields (Kirchner et al., 2001), lake and marine sedimentation (Mourier et al., 2010) and speleothem growth rates (Clift et al., 2014). Under specific conditions, the quantification of soil erosion over a few millennia has been possible by using the recorded data of weakly-disturbed lake sediment (Enters et al., 2008; Bajard et al., 2017). Modern techniques use surveying techniques (e.g. erosion bolt) or even isotopes (e.g. $^{239+240}\text{Pu}$, ^{137}Cs) to trace soil erosion and accumulation in more detail but are limited to a time-scale of a few decades (Alewell et al., 2014).

In comparison, the accumulative or catchment-wide approaches can cover time-spans from several millennia to a few million years. This is often achieved with the use of cosmogenic nuclide (e.g. ^{10}Be) derived basin-average denudation (and erosion) rates (e.g. Kirchner et al., 2001; Norton et al., 2011; Portenga & Bierman, 2011). However, they encounter other difficulties by using sedimentary records of depositional zones (e.g. basins) to determine the rate of material loss in distant denudational zones (e.g. mountain crests, uplands). First, catchment-wide approaches basically lack the ability to distinguish between soil-erosion from erosion as a

general landscape process. Secondly, material flows that caused sediment deposition can have been diverted and also can have substantially changed over time. This can cause sediment chronologies to be incomplete and challenges the quantification of the actual lost material at specific erosional sites. Moreover, catchments are also susceptible to erosion, which can therefore also weaken the continuity of these archives. Lastly, it is usually only possible to estimate average erosion rates. The fact that soil erosion is a discontinuous process having varying temporal changes is therefore mostly not taken into account. Hence, current methods cannot provide needed answers to questions such as (i) How did soil denudation and, thus, soil erosion rates vary over late Pleistocene-to-Holocene time? (ii) How did soils develop over time? (iii) Can progressive and regressive phases be detected? and (iv) How do current soil erosion rates compare to past rates? Thus, new approaches are needed to comprehensively quantify the elements involved in surface evolution history (Fig. 5).

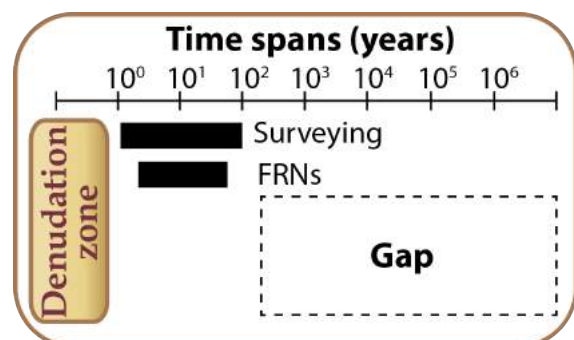


Figure 5: Currently, knowledge about past soil erosion rates in the denudation zone is limited because of the lack of appropriate methods.

1.2. HYPOTHESES AND AIMS

In order to resolve these issues, one has to diverge from conventional methods and archives (e.g. catchment wide approaches) and start new investigations on landscape features that optimally preserve the temporal information while evolving over a continuous time-frame. In addition, the ideal archive should allow for the deciphering of surface denudation rates and subsequent soil erosion rates in many regions around the world.

Landscapes affected by deep weathering processes and subsequent intense erosion and denudation may be characterised by boulder fields, “tors” and “bornhardt” landforms, i.e. tower-like or dome-shaped, often castellated, residual hills of rock (Migoñ, 2006). Specifically, the residual rock formations named tors often appear to have continuously “grown” from the landscape due to their higher physical resistance compared to the surrounding more easily erodible material. Tors occur at numerous locations world-wide and their presence seems to be unrelated to one

specific environmental condition. For example, they can be found in the Arctic, Antarctica, Mediterranean, deserts, tropical landscapes as well as in former glaciated areas (Migoñ, 2006). Thus, we saw great potential in tors as a new soil erosion and surface denudation archive.

We hypothesised that determination of the speed of the tor exhumation can be used to deduce the local (in-situ) soil erosion rates over different time periods (Holocene and potentially up to the Pleistocene) (Fig 6). By using modern geochronological techniques (e.g. terrestrial cosmogenic nuclides (TCNs), the rock surfaces of tors can be dated along vertical profiles. This should allow the determination of their exhumation rate and subsequently the re-modelling of soil erosion and surface denudation rates over multiple time-intervals (continuously and over millennia). The aim of this thesis was to perform, with the use of TCNs, the first investigation on the suitability, capabilities and limitations of the properties of tors to be used in order to provide an in-situ soil erosion and surface denudation archive.

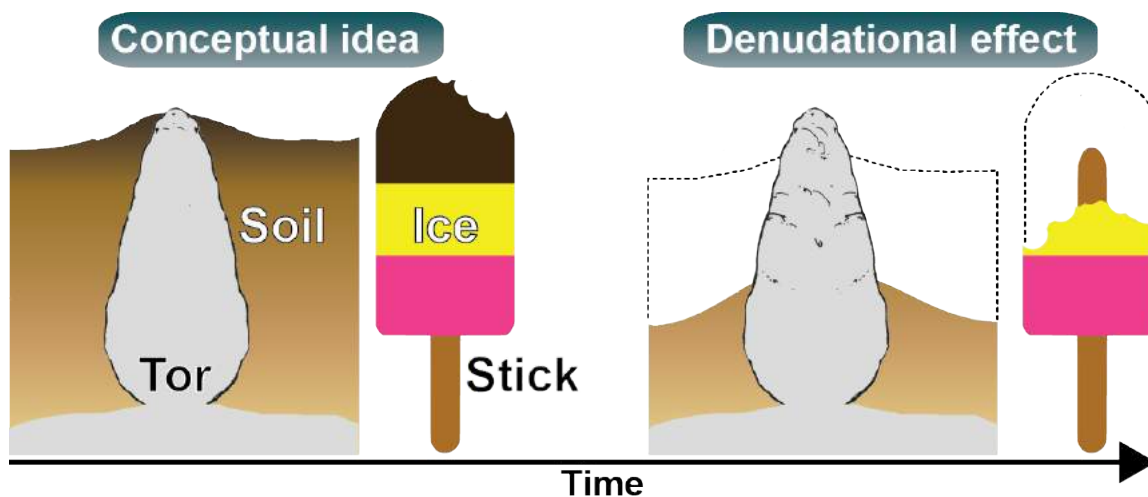


Figure 6.: The conceptual idea is comparatively illustrated with an ice on a stick. The stick represents the tor, and the ice the soil. Denudation (or ice melting) reduces the surrounding soil (ice) depth and volume. This can be quantified using modern dating techniques.

Testing a new approach to quantify soil erosion history over millennia requires local soils to be geochronological characterised beforehand. Rock surfaces will already have been dated by the use of TCNs near and below the soil surface. This opens up the opportunity to test new ways (e.g. relative dating techniques) to determine soil ages. The provenance of soil material in complex landscapes such as in southern Italy is often unknown. To better understand soil evolution trajectories, the age and origin of the material needs to be known. Geo-forensic techniques are a useful tool in order to trace the origin and weathering trajectories. From the use of these general considerations, the following hypotheses have arisen:

Hypotheses of Manuscript I

(i) Using a multi-method geo-forensic approach, the origin of volcanic deposits and the subsequent weathering trajectories of soils can be detected. (ii) By comparing the chemical ratios of the soils and primary particles with the assumed origin of the volcanic material and dated eruptions, soil ages can be derived. (iii) In this context chemical mass balance calculations of the allochthonous material and soils are a useful additional tool to determine the eruption source. (iv) In addition, by relating weathering indices (WI) of relatively identical soils with known ages to WI of local soils, age ranges can be determined.

Hypotheses of Manuscript II

(i) Exhumation rates of tors can be quantified. (ii) The concentration of TCNs increase with increasing heights above ground along rock tor surfaces. (iii) Exhumation rates provide time sequences and reflect surface denudation and soil erosion rates. (iv) Estimated rates are in the range of catchment-derived rates. (v) Progressive and regressive phases can be detected. (vi) Modern rates (past c. 60 years) derived from FRNs, reflect tor derived trends.

Hypotheses of Manuscript III

(i) Tors at similar topographic position have similar surface denudation developments. Higher erosion rates are expected at steeper surfaces. (ii) Soil erosion rates are equivalent among time periods having equal environmental conditions (climate, vegetation). Higher erosion rates are expected in transition phases (warm — cool or cool-warm). (iii) Tors uniquely provide insight into the soil erosion history. The exhumation approach is not transferable to other stable (or unstable) landscape features. Bedrock outcrops of slopes represent only the latest stage of surface denudation.

2. STUDY AREA

There are numerous tor provinces around the world where this study could have been conducted. Since this was the first attempt to evaluate a tor exhumation approach as soil erosion archive, it was beneficial to do so under the best controlled environmental conditions. By limiting the number of denudation-influencing variables, the chances for an undistorted chronology were the highest. In addition, a low number of environmental factors facilitate the identification of driving forces. Of course, some surface denudation variables, such as climate and vegetation, can hardly be kept constant over a time interest of several decamillennia. Yet, changing surface properties (e.g. density, mineralogical composition) and great mass-fluxes (e.g. landslides, glacial incisions) that would complicate the final evaluation can be greatly diminished, or even eliminated, by carefully choosing the study area.

The Sila Massif upland plateau in southern Italy (Fig. 7–9) provided the best geomorphological and geological setting to test our hypothesis under well-defined conditions. The massif is tectonically stable (Olivetti et al., 2012) and consists of an uplifted batholith with a homogenous granite-bearing landscape (Molin et al., 2004). Therefore, the main mineralogical composition and physical properties can be considered constant over the course of the investigated time-frame. The gentle topography enabled a predominant tracing of soil erosion and not mass wasting (e.g. landslides). The isolation of the box-shaped upland ruled out material influxes from other erosional areas and the gentle plateau surface has never been glaciated. Additionally, literature about climate (Allen et al., 1999), vegetation (Allen et al., 1999; Pelle et al., 2013) and anthropological influences (Peréz-Obiol & Sadori 2007) is available. Further descriptions of the Sila Massif are found in the manuscripts.

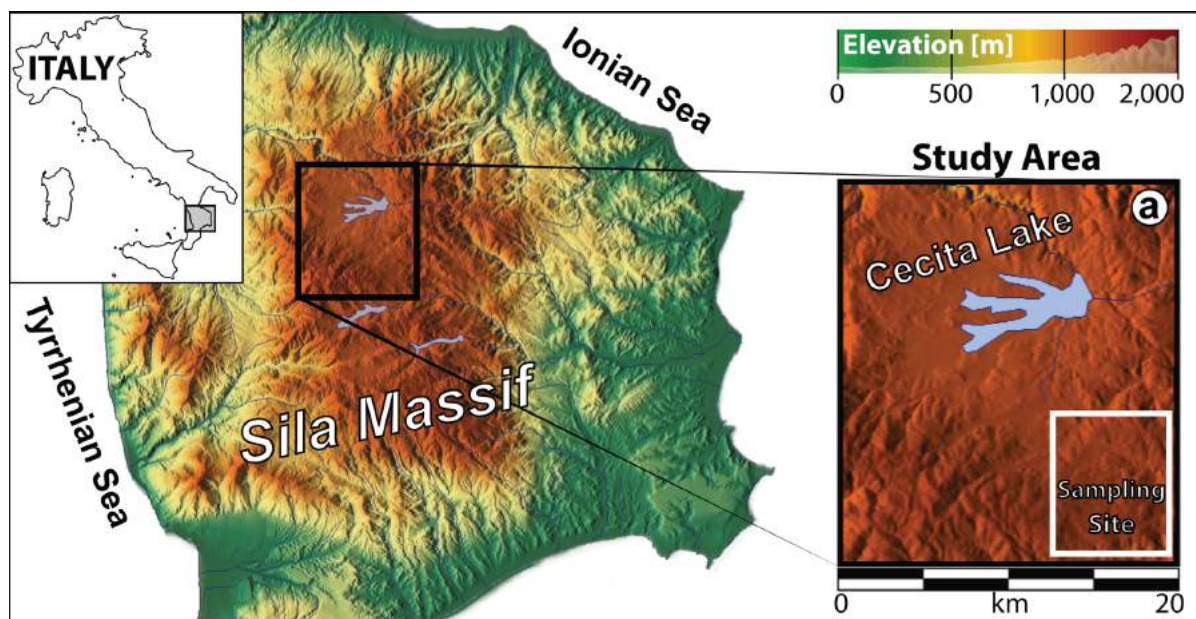


Figure 7: Topographic map of the Sila Massif in Calabria, southern Italy. The actual sampling site where the hypothesis has been tested is indicated in (a).



Figure 8: Impression of the Sila Upland plateau taken in spring 2016.



Figure 9: Example of a granite tor in our study area.

3. METHODS

3.1. THEORY OF TERRESTRIAL COSMOGENIC NUCLIDES

Earth is bombarded from all directions by galactic cosmic rays that originate mostly from supernova explosions outside of the solar system (Lal, 1988; Dunai & Lifton, 2014). When these particles enter the Earth's atmosphere, cascades of secondary particles (mostly protons, neutrons and a small fraction of muons, pions, positrons and electrons) are generated by their interactions with its composing elements (e.g. nitrogen, oxygen, argon).

In turn, (meteoric) cosmogenic nuclides (e.g. ^{10}Be , ^{14}C) are produced in the atmosphere (Fig. 10). When these secondary particles reach the lithosphere, they also cause (in-situ) nuclear reactions within the mineral lattices of rocks (Ivy-Ochs & Schaller, 2009). By measuring the terrestrial cosmogenic nuclide concentration of a defined mass, one can obtain the length of exposure time if the local production rate is known.

In general, in-situ nuclide production rates in the lithosphere are lower compared to the meteoric rates in the atmosphere (Dunai, 2010). This is because the reactions in the atmosphere cause the intensity to attenuate with increasing atmospheric depth (Dunai, 2010). Additionally, depending on the latitude, Earth's magnetic fields reduce the intensity of cosmic rays (Masarik & Beer, 1999). At low latitudes, the geomagnetic field lines are parallel to the lithosphere and will repel more incoming

cosmic rays — compared to high latitudes, close to the poles, where they are perpendicularly aligned to the surface.

Over the past ten million years, the incoming flux of galactic cosmic rays is assumed to have been more or less constant (Wielers et al., 2013). However, the geomagnetic field and the atmospheric pressure have varied during that time. Production rates were therefore potentially influenced by these changes.

In addition to these global effects, local factors have also to be considered for the estimation of in-situ production rates. The main influence is the surrounding topography, which can reduce the local production rate at a surface by (partly) shielding it from the incoming particles (e.g. more particles can interact with the surface at a free mountain peak than in a deep and narrow canyon or cave).

Also, the direction and angle of the surface determines interaction intensity (Dunne et al., 1999). Because the in-situ production rate is attenuated with lithospheric depth, the sampling depth (e.g. sample thickness and density) also governs the in-situ production rate (Gosse & Philips, 2001).

In summary, the rate of terrestrial cosmogenic isotope production at the sampling spot is a function of latitude, altitude, time, topographic shielding, surface geometry, sampling depth and density.

3.2. TERRESTRIAL IN-SITU COSMOGENIC RADIONUCLIDE DATING

This dating technique is a geochronological method to determine the exposure time of (rock) surfaces on Earth (Ivy-Ochs & Schaller, 2009). Rock surface exposure ages are determined using the following steps. First, the material of a surface is collected. The sampling depth, surface geometry, topographic shielding, altitude and geographic position is noted. In the second step, a specific mineral present in the entire composition of the surface material is physically and/or chemically extracted. Quartz, with its wide natural abundance, weathering resistance and uniform production rates makes it the mineral of choice (especially in granite landscapes). In the third step the extracted quartz is cleaned (HF leaching) and the trapped cosmogenic nuclides within the lattices of the quartz are chemically isolated and collected (Kohl & Nishiizumi, 1992) using target chemistry (von Blanckenburg et al., 1996). In the final step, the nuclide concentration is quantified by counting the number of atoms using AMS (see Christl et al., 2013). Ages are estimated with the use of normalised production rates (see Balco et al., 2008) prior scaled to the local production conditions of the sampled surface. Among the cosmogenic nuclides produced in quartz (^3He , ^{10}Be , ^{14}C , ^{21}Ne , ^{26}Al), Beryllium is commonly preferred, because its superior half-life of 1.387 Ma (Chmeleff et al., 2010), allows the dating of 4 – 5 Ma exposed surfaces under ideal conditions.

3.3. RADIOCARBON DATING

Radiocarbon dating is an established method and the single most powerful technique to date organic material younger than 50 ka. It is based on comparing three different carbon isotopes ^{12}C , ^{13}C and ^{14}C . While ^{12}C and ^{13}C are naturally occurring stable isotopes, ^{14}C is a cosmogenic nuclide produced in the atmosphere (Fig. 10). The atmospheric ^{14}C oxidises to $^{14}\text{CO}_2$ and is absorbed by plants by photosynthesis. Carbon is passed through the food chain in the same ratios of ^{12}C , ^{13}C and ^{14}C as in the atmosphere. After death, organic material loses ^{14}C due to beta decay, according to its radioactive half-life (5730 yr). ^{12}C and ^{13}C remain at the same quantity. Radiocarbon age is determined by comparing the amount of ^{14}C to the remaining stable carbon. However, the carbon ratio in the atmosphere has varied over time (e.g. due to changes of the Earth's magnetic field and the industrial revolution) and therefore also in plants and animals. Due to this variation over time, results are corrected using a calibration curve which employs other dating techniques (e.g. dendrochronology) to verify the carbon ages. Uncalibrated ages are given in BP and calibrated ages in calBP.

In order to perform radiocarbon dating today, only a few grams of organic material are needed to be chemically cleaned and treated before being burned in sealed ampoules. The captured $^{14,13,12}\text{CO}_2$ is converted to graphite and their differing carbon ratios are measured using AMS.

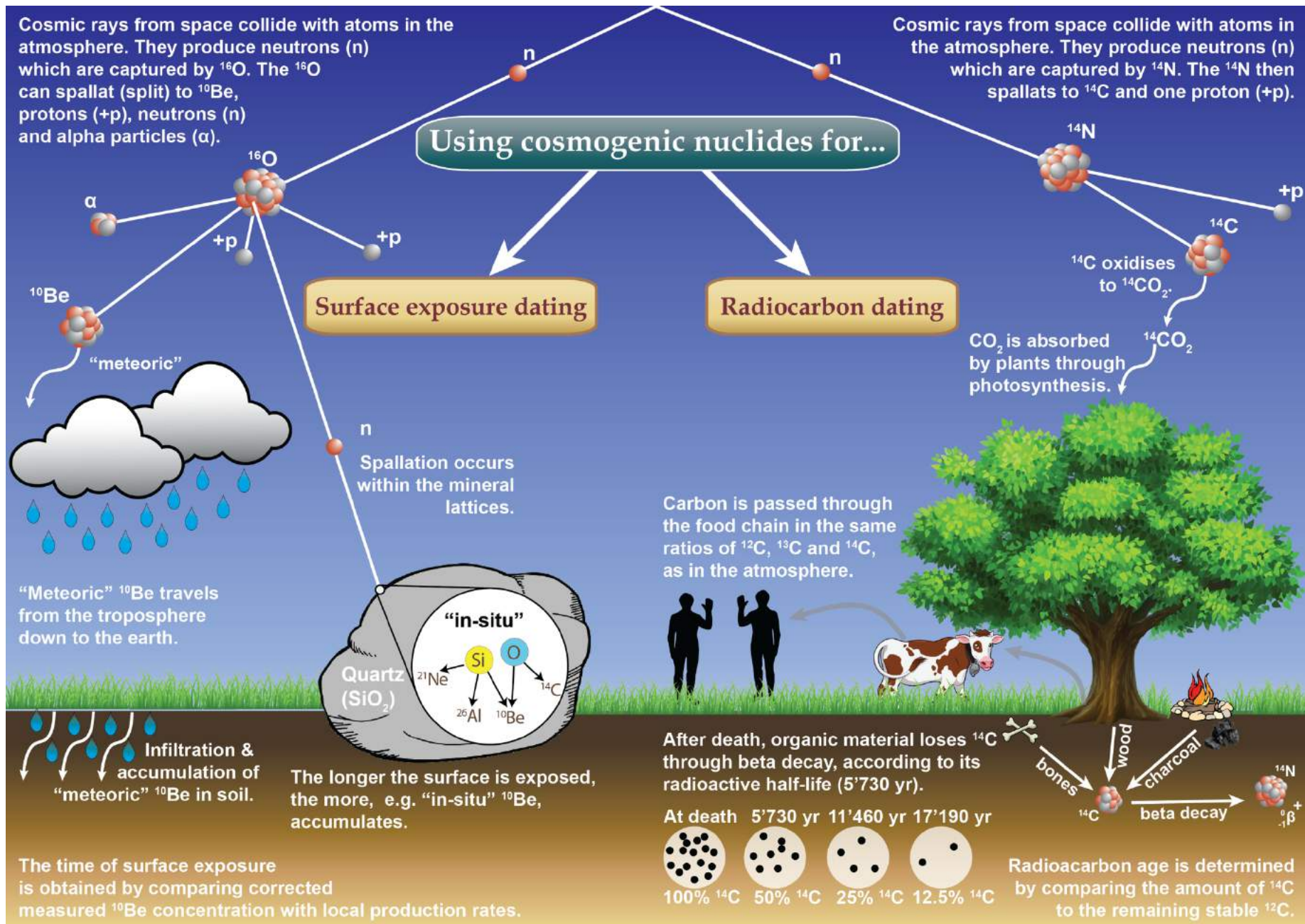


Figure 10: Production of atmospheric (^{10}Be , ^{14}C) and in-situ (^{10}Be , ^{26}Al , ^{14}C , ^{21}Ne) cosmogenic nuclides by secondary particles and how they are used for geochronological dating techniques.

3.4. FALLOUT RADIONUCLIDES

Thermonuclear weapon tests in the 1950s – 1960s and nuclear power plant accidents (e.g. Chernobyl, Fukushima) resulted in a global distribution of artificial radionuclides such as $^{239+240}\text{Pu}$ or ^{137}Cs (Fig. 11). These fallout radionuclides (FRNs) are quickly and tightly absorbed by fine soil particles, in nature chemically hardly mobile and thus primarily only transported by physical processes such as soil erosion. Therefore, FRNs are an effective modern resource to trace soil erosion and/or deposition over the last ~ 50 – 60 yr (Wallbrink & Murray, 1993). In recent years $^{239+240}\text{Pu}$ have gained popularity as soil redistribution tracers due to (i) their longer half-life, (ii) their greater homogeneity at reference sites and (iii) better measurement precision and time compared to other FRNs (e.g. ^{137}Cs) (Alewell et al., 2017). Currently Pu isotopes are measured using ICP-MS after being isolated out of a given soil sample volume by the use of target chemistry (Ketterer et al., 2004). Soil redistribution rates are quantified by conversion models on the basis of the differences in measured $^{239+240}\text{Pu}$ inventories (total radionuclide activity per unit area) between an undisturbed local reference site (flat, well-vegetated and unploughed surface) and potential erosion (inclined surface) or depositional (e.g. foot of slope) sites. As expected, erosional sites have a lower activity, and depositional sites a higher one compared to the reference site (Mabit et al., 2008).

3.5. CHEMICAL WEATHERING INDICES

During their formation, rocks are mostly subjected to conditions of several hundred degrees Celsius and thousands of tons of pressure. Minerals formed under these conditions that reach Earth's surface have to adapt to a new environmental situation – for example by chemical weathering. Chemical weathering changes the composition of rocks and minerals over time and through spontaneous thermo-dynamic processes leads to a more stable state at current surface conditions. In turn soils are generated and the concentration and distribution of chemical elements within soils is controlled. Elements having high field strength (e.g. Ti, Zr), due to high cationic charge and small radii, remain mostly preserved and relatively immobile in soils and parent material. This contrasts to the mobile elements (e.g. Na, Mg, Mn, K), which are being leached out (Fig. 11). Therefore, in time parent material and soils become depleted in mobile elements and enriched in immobile elements. Chemical weathering indices (CWIs) use these temporal changes to quantify the alteration of minerals and the weathering degree of soils by using appropriate chemical element ratios. CWIs are commonly used to evaluate soil fertility and development (e.g. Delvaux et al., 1989) and ideally allow the comparison of different locations of various weathered materials of different ages (Harnois, 1988). The necessary inorganic chemical data are usually determined by an XRF.

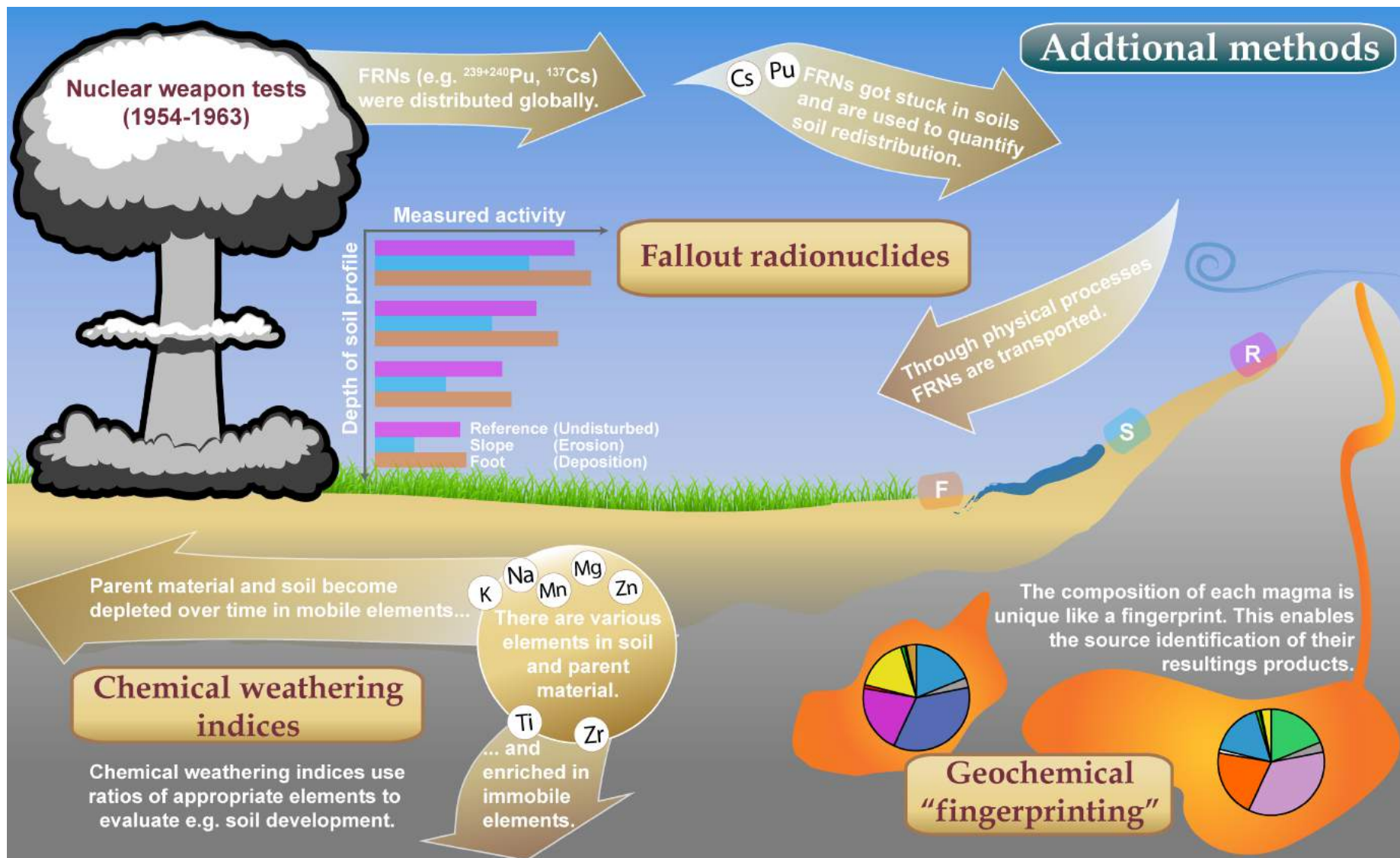


Figure 11: The fallout radionuclides $^{239+240}\text{Pu}$ were used during this study. Soil redistribution was evaluated by evaluating the activity differences between erosional and reference sites. Slopes (erosional sites) are expected to have a lower activity compared to the reference site. Chemical weathering indices were used for semi-quantitative dating. Older soils are expected to be enriched with immobile elements. In addition, geochemical fingerprinting was applied to identify the source of allochthonous soil material (volcanic glass). The assigned pie charts illustrate the different chemical composition of the magmas.

3.6. GEOCHEMICAL FINGERPRINTING OF IGNEOUS MINERALS

Minerals of igneous rocks are formed by bonding of elements within a structured lattice during the cooling of a magmatic source. In addition to necessary major (e.g. Si, Al, O, Mg, Ca, Fe) and minor elements (e.g. Na, K, Cr, Mn), trace elements (e.g. Co, Lu, Hf, Ce, Th) are also accumulated in the mineral structure.

In general, distribution trends of trace elements (in particular rare earth elements — REEs) are used as indicators to identify the past geotectonic position of a magmatic source (e.g. subduction zone, oceanic island). However, each magma batch still has a slightly different chemistry to any

other (Fig. 11). The individual chemical pattern is therefore a unique geochemical fingerprint. By using the individual geochemical signature of a source, unaltered sample material can be identified and its origin identified. If the timing of the magmatic cooling of the source is known, its age can be estimated.

4. RESULTS

Several researchers have contributed to this project. Those who have made substantial contributions to data acquisition, sample processing and manuscript preparations appear as authors on the presented manuscripts. A summary of the individual contributions is stated in Table 1.

Table 1: Contributions of individual researchers to the presented manuscripts I–III.

Task	Manuscript I	Manuscript II	Manuscript III
Fieldwork	<i>Raab G. Halpern D. Scarciglia F. Egli M.</i>	<i>Raab G. Ruppli A. Scarciglia F. Egli M.</i>	<i>Raab G., Scarciglia F. Egli M.</i>
Participating in fieldwork	<i>Raimondi S.</i>	<i>Norton K. Dahms D.</i>	<i>Norton K. Dahms D.</i>
Sample preparation for soil analyses	<i>Raab G. Halpern D.</i>	<i>Raab G. Ketterer M.E.</i>	
Sample preparation for surface exposure dating		<i>Raab G. Ruppli A. Brandová D.</i>	<i>Raab G. Brandová D.</i>
Performed analytical measurements of sampled material	<i>Raab G.^{6,7,8} Halpern D.² Pettke T.^{3,5} Hermann J.^{3,5} Aguilar Sanchez A.M⁶</i>	<i>Christl M.¹ Ketterer M.E.⁴</i>	<i>Christl M¹</i>
Calculations and modelling	<i>Raab G. Norton K.</i>	<i>Raab G. Egli M.</i>	<i>Raab G.</i>
Data evaluation and interpretation	<i>Raab G. De Castro Portes R. Norton K. Scarciglia F. Egli M.</i>	<i>Raab G. De Castro Portes R Scarciglia F. Egli M.</i>	<i>Raab G. Egli M.</i>
Drafting the manuscript, tables and/or figures	<i>Raab G. Egli M. Scarciglia F.</i>	<i>Raab G., Egli M. Scarciglia F.</i>	<i>Raab G., Egli M. Scarciglia F.</i>

¹AMS, ²DRIFT, ³ESEM-EDS, ⁴ICP-MS, ⁵LA-ICP-MS, ⁶SEM, ⁷XRD, ⁸XRF

4.1. MANUSCRIPT I

The first manuscript was dedicated to the investigation of the soil formation history and origin of volcanic material in the study area of the Sila Massif. Therefore, the geochemical signature and chronological information of the local soil was obtained using a multi-method approach. The chemical characteristics of volcanic clasts and glass particles in the soil were used to determine the eruption sources and times. The volcanic events served as proxies for potential soil formation phases during the Pleistocene and Holocene. Radiocarbon ages provided minimum soil ages (about 8 – 10 ka, max. 14 ka). Estimates on the basis of chemical indices resulted in a soil age range of 15.6 – 66.7 ka (45.3±11.1 ka average; Fig. 13). Overall the investigation improved the general understanding of the local landscape evolution, providing an essential base for testing the tor exhumation approach (Manuscript II).

Reference: Raab G., Halpern D., Scarciglia F., Raimondi S., Norton K.P., Pettke T., Hermann J., de Castro Portes R., Aguilar Sanchez A.M., & Egli M. (2017). Linking tephrochronology and soil characteristics in the Sila and Nebrodi Mountains, Italy. Catena 158: 266-285. DOI: 10.1016/j.catena.2017.07.008

4.2. MANUSCRIPT II

The second publication was dedicated to exploring the potential of isolated rock masses (tors) as long-term soil erosion and surface denudation archives. It presents the

first results of ^{10}Be exposure ages along vertical tor profiles in the Sila Massif. The ^{10}Be concentrations of all sampled tors increased with heights. Therefore, surface denudation rates and changes of rates for the last 100 ka could be successfully deciphered (Fig. 12). Temporal continuous (in-situ) surface denudation models were created on the basis of three tors at potential erosional sites (ridge and slopes). A surface evolution model for the Sila Massif upland was created. The model incorporated the findings of Manuscript I and explains progressive and regressive surface phases (Fig. 13). Through modern fallout radionuclide techniques ($^{239+240}\text{Pu}$), the time-series could be extrapolated to the present. The modern soil redistribution rates indicated a significant increase in soil erosion rates above past natural rates.

Reference: Raab G., Scarciglia F., Norton K., Dahms D., Brandová D., Portes R., Christl M., Ketterer M.E., Ruppli A. & Egli M. (2018). Denudation Variability of the Sila Massif Upland (Italy) from decades to millennia using ^{10}Be and $^{239+240}\text{Pu}$. Land Degradation and Development (Special issue) 29: 3736-3752. DOI: 10.1002/ldr.3120

4.3. MANUSCRIPT III

In Manuscript III the vertical exposure age profiling of tors used in Manuscript II was further tested on other landscape features – boulders and scarps. Each investigated landform group revealed a distinct different pattern. Three scarps showed a rapid surface exposure age and

could only provide surface denudation information of the past 8-15 ka. Three boulders provided similar exposure ages to tors, but their ^{10}Be concentrations varied considerably at the same heights above ground. The two additional investigated tors in potential depositional zones (planes, small basins) had consistent concentration-heights relationship as the three of Manuscript II. The plane/basin based tors had a lower denudation intensity compared to the slope based tors (Fig. 13). Overall, tors provided the oldest exposure ages and exhibited similar denudation trends at similar topographic position. Denudation apparently increased during the transition to warmer and humid conditions, while it decreased with increasing vegetation density. Finally, an event chronology for the study area was presented.

Reference: Raab G., Egli M., Norton K., Dahms D., Brandová D., Christl M., & Scarciglia F. (2018). Climate and relief-induced controls on the temporal variability of denudation rates in a granitic upland. *Earth Surface Processes and Landscapes*. DOI: 10.1002/esp.4681

4.4. ORIGINAL PUBLICATIONS

The final part of the result section includes the original published manuscripts, which are available at the corresponding journals as well as on personal websites (e.g. www.geraldraab.com) and repositories (e.g. ZORA).

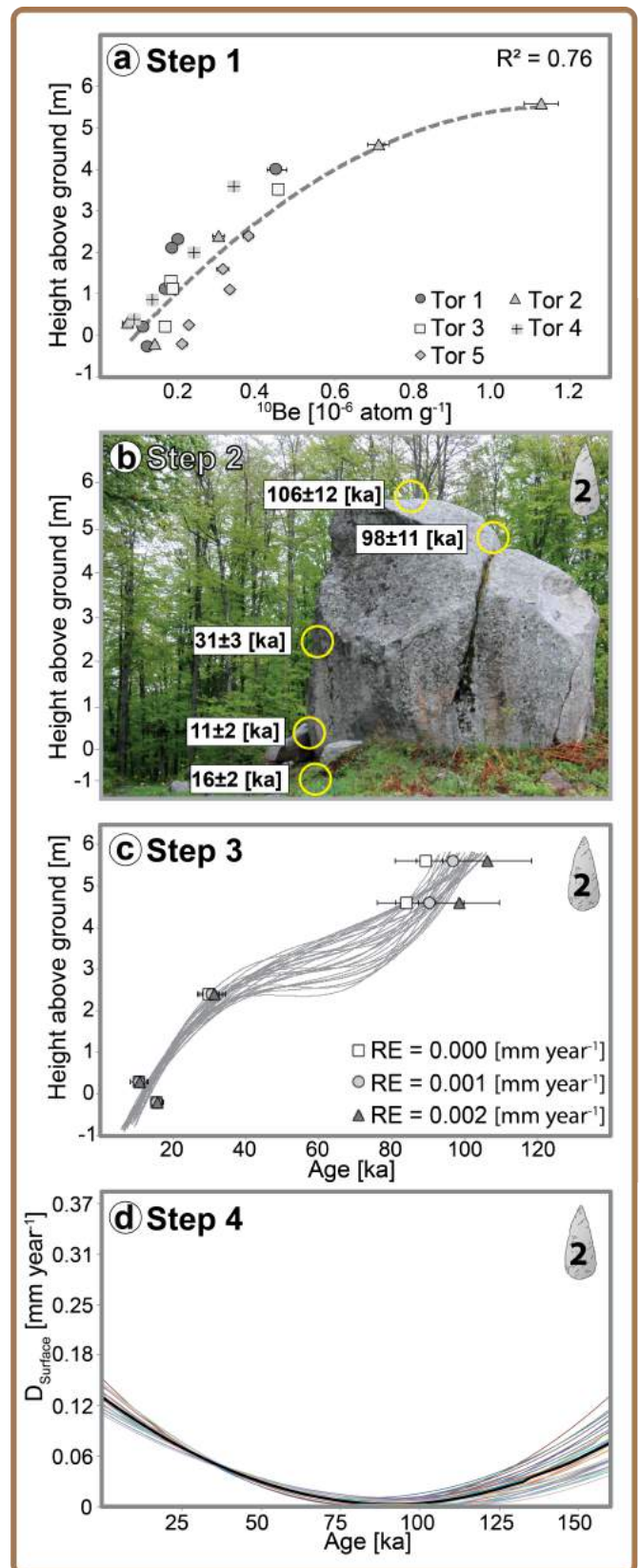


Figure 12: TEA scheme: To obtain denudation models, (a) corrected ^{10}Be concentrations are converted to (b) surface ages (e.g. Tor 2). Within the age variations, (c) various exhumation trends are modelled using Monte Carlo simulations. Mathematical derivations of these functions are used to model (d) surface denudation (D_{Surface}). RE= rock surface erosion rate.



Linking tephrochronology and soil characteristics in the Sila and Nebrodi mountains, Italy



Gerald Raab^a, Dieter Halpern^a, Fabio Scarciglia^b, Salvatore Raimondi^c, Kevin Norton^d, Thomas Pettke^e, Jörg Hermann^e, Raquel de Castro Portes^a, Asel Maria Aguilar Sanchez^f, Markus Egli^{a,*}

^a Department of Geography, University of Zurich, Winterthurerstrasse 190, 8057 Zurich, Switzerland

^b Department of Biology, Ecology and Earth Sciences (DiBEST), University of Calabria, Via P. Bucci – Cubo 15B, 87036 Arcavacata di Rende, CS, Italy

^c Dipartimento dei Sistemi Agro-Ambientali, Università degli Studi di Palermo, Viale delle Scienze, 90128 Palermo, Italy

^d School of Earth and Environment, Victoria University of Wellington, PO Box 600, 6140 Wellington, New Zealand

^e Institute of Geological Sciences, University of Bern, Baltzerstrasse 1 + 3, 3012 Bern, Switzerland

^f Institute for Building Materials, ETH Zurich, 8093 Zurich, Switzerland

ARTICLE INFO

Keywords:

Volcanic sediments
Geo-forensics
Soil evolution
Dating
Quaternary

ABSTRACT

Recent studies have demonstrated that soils formed on pyroclastic ash deposits are much more common in the Mediterranean area than previously assumed. These soils are an important key to understanding past volcanic events and landscape evolution. Chronological information in soils of Quaternary volcanic events, however, remains still poorly understood in southern Italy. Using a multi-method forensic approach, we explore the origin and age of volcanic deposits (soils) in Sicily and Calabria. The geochemical signature of the soil was compared to the chemical fingerprint of the magmas of potential source areas of southern Italian volcanoes. The results indicate that the investigated soils on the Nebrodi (Sicily) and Sila (Calabria) mountains were both impacted by materials having a high-K calc-alkaline series volcanism. The Aeolian Islands (in particular Lipari and Vulcano) are the most likely source of origin, but contributions also from the Etna (particularly the Biancavilla ignimbrites and Plinian eruptions) occurred. Weathering and leaching processes, along with a potential contribution from the underlying non-volcanic bedrock, has altered the main chemical composition of soils, often precluding direct relation to potential source areas. Immobile elements and their ratios (e.g. the Nb/Y vs Zr/Ti plot) or trace elements (Co, Th) and rare earth elements (laser ablation ICP-MS analyses of glass particles, volcanic clasts and pumice-like materials) gave precious hints of the origin of the volcanic deposits. Radiocarbon dating of the H₂O₂ resistant soil organic fraction indicates a minimum age of 8–10 ka of the soils. The weathering index WIP (weathering index according to Parker) and the chemical composition of volcanic glasses and clasts were tested as proxies for the age of the volcanic deposits and time for soil formation. The soils and landscape are characterised by multiple volcanic depositional phases for the last about 50 ka in the Sila mountains and about 70 ka or more in the Nebrodi mountains. Chemical-mineralogical analyses enabled the detection of deposition phases during the Pleistocene and also Holocene. The multi-method approach enabled the identification of potential source areas, provided a tentative age estimate of the start (and in part duration) of ash deposits and therefore improved our understanding of volcanic landscape evolution.

1. Introduction

Volcanic eruptions are spectacular natural events (Giaccio et al., 2008) that have captured man's curiosity since prehistoric times. On the one hand, they can be of great benefit to man (e.g. increased soil fertility), but on the other hand they can also cause great harm (Fisher and Schmincke, 1984; Sulpizio et al., 2014; Sandri et al., 2016). In a large

part of the world, today's landscape has been predominately formed since the late Quaternary period. In those last two and half million years, the Mediterranean region was marked by numerous spectacular natural and highly explosive volcanic events (Paterne et al., 2008; Scarciglia et al., 2008; Bourne et al., 2015). These events have clearly left their marks on the landscapes. Fine volcanic material generally affects large areas around volcanic centers (Giaccio et al., 2008).

* Corresponding author.

E-mail address: markus.egli@geo.uzh.ch (M. Egli).

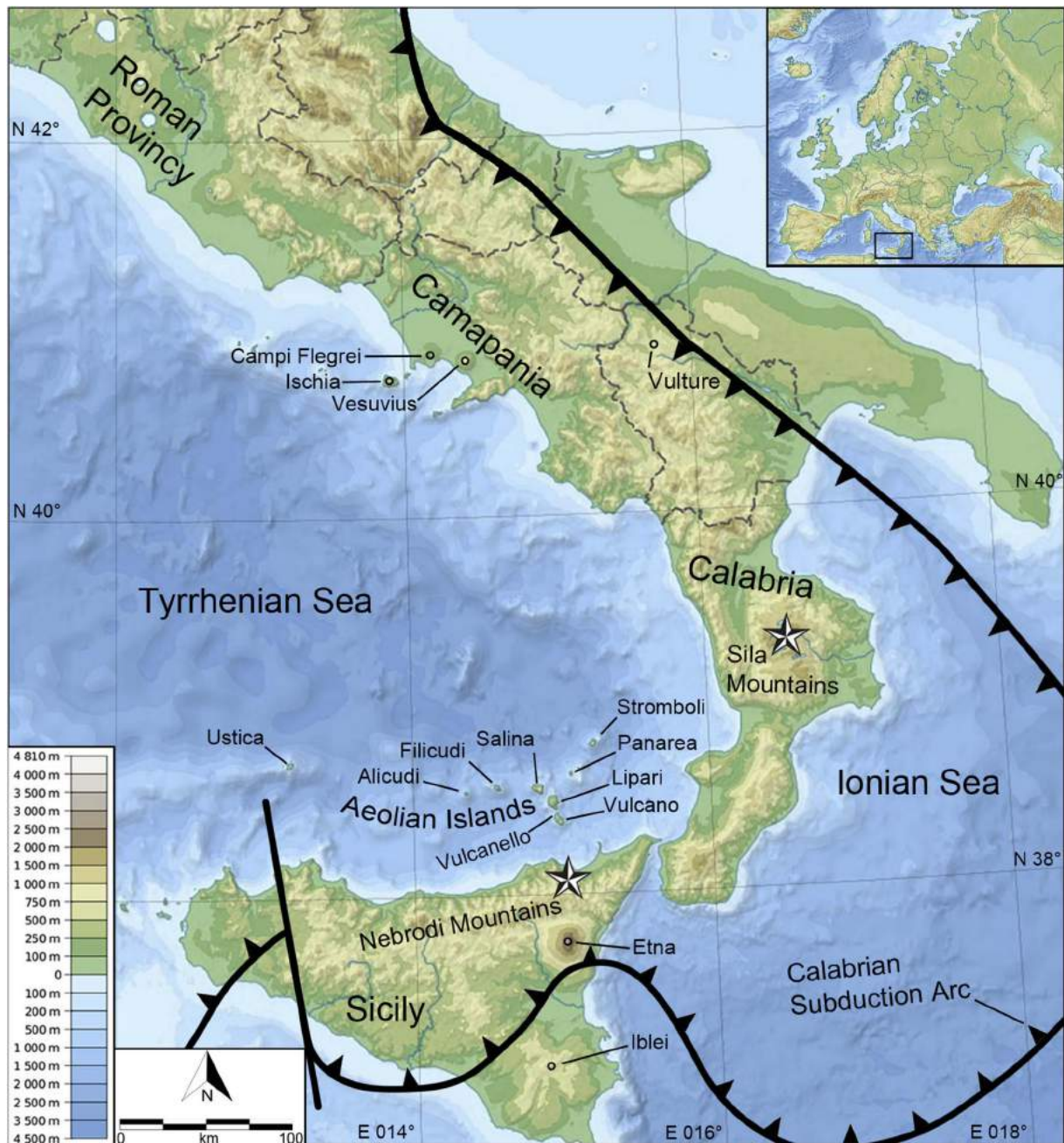


Fig. 1. Location of the study areas. The two stars mark the investigation sites in the Nebrodi and Sila mountains.

Chemical evaluation of this fine grained material is a powerful tool for Quaternary studies, providing not only a target for dating, but also a means to correlate specific deposits to a specific source, sometimes located at a great distance (Giaccio et al., 2008). According to Zimmerer et al. (2016), information about timescales of magmatism and ages of eruptions is crucial to understanding the history as well as the hazards of active and dormant volcanic areas. These authors also claim that knowledge of eruption ages can be further used to calculate hazard parameters such as recurrence intervals and repose periods, as well as to identify vent migration patterns that are crucial to eruption forecasting. In spite of their social and geological importance, chronologies for Quaternary volcanic events remain poorly understood (Zimmerer et al., 2016). To date, several numerical methods have been used for dating volcanic sediments, such as radiocarbon (^{14}C), potassium-argon decay ($^{40}\text{K}/^{39}\text{Ar}$), fission-track geochronology, uranium-lead decay ($^{235}\text{U}/^{207}\text{Pb}$) or cosmogenic nuclides (^{10}Be).

However, the necessary conditions for successful application of these numerical methods are often not fulfilled and hence relative dating techniques remain an essential tool (Favilli et al., 2009a, 2009b). A multi-method approach, i.e. a combination of numerical analyses and relative dating methods, can possibly yield more accurate results (Giaccio et al., 2008). The Italian Mediterranean Basin is a complex and volcanically active zone in Europe (Pichler, 1984) with abundant ash fall. Despite their wide spread occurrence (about 7% of the soil area has volcanic deposits as parent material; Costantini and Dazzi, 2013), the source of volcanic sediments is still unknown in many areas. Throughout Sicily and mid- to southern-Italy, the large physical presence of volcanic materials is a constant reminder of the intense volcanic activity of the area. The origin of much of this volcanic material is unknown due to the abundance and activity of different volcanoes in close proximity (Giaccio et al., 2008). Here we attempted to trace the origin of volcanic sediments in southern Italy (Sicily/Calabria) and to

Table 1
General characteristics of the study sites Nebrodi (Sicily) and Sila (Calabria) in southern Italy.

Site	Coordinates WGS 84 (N/E)	Elevation m a.s.l.	Geologic substrates along the profile	Vegetation	Slope	Exposure °N	Soil type WRB (IUSS Working Group, 2015)	Land use
Nebrodi mountains – Sicily								
Nebrodi I	37°59'15.5"/14°58'41"	1269	Volcanic deposits, Quartz-arenite	Fen, grass, maquis	0°	0	Vitric Cambisol	Regional park (pasture)
Nebrodi II	37°59'01.6"/14°57'52"	1279	Volcanic deposits (ash, lapilli), marl, Quartz-arenite	Fen, grass, maquis	11°	345	Vitric Cambisol	Regional park (pasture)
Nebrodi III	37°59'05.9"/14°59'17"	1243	Quartz-arenite	Fen, grass, maquis	8°	90	Vitric Andosol	Regional park (pasture)
Nebrodi IV	37°59'02.1"/14°57'51"	1264	Volcanic deposits (ash, lapilli), marl, Quartz-arenite	Fen, grass, maquis	4°	0	Vitric Cambisol	Regional park (pasture)
Sila mountains – Calabria								
Sila I	39°16'50"/16°32'19"	1572	Volcanic deposits, granite	Shrubs, grass	2°	195	Vitric Cambisol	National park (pasture)
Sila II	39°16'50"/16°32'19"	1572	Volcanic deposits, granite	Shrubs, grass	2°	195	Vitric Cambisol	National park (pasture)

derive an approximate age of the timing of their deposition. To this end, we tested the following hypotheses: 1) the chemical signatures of the volcanoes where these sediments originate from can still be found in the soil, 2) radiocarbon dating and weathering indices of the soils can help to constrain the numerical or at least relative age of the deposits of interest.

2. Materials and methods

2.1. Study area

Two investigation sites in southern Italy were chosen for this study (Fig. 1). One site is on the east end of the Nebrodi mountains, Sicily. The second study region is in the centre of the Sila mountain plateau, Calabria. The two sites differ in some aspects. Sila has a granite parent material of the Calabride complex (Cirriuncione et al., 2015). In contrast, the bedrock of the Nebrodi mountains derives from the allochthonous flysch basin sequences of the Numidian flysch formation, which also contains quartzarenite sandstones (Thomas, 2011) besides limestone and clays. The Sila (with a max. altitude of slightly above 1900 m a.s.l.) and Nebrodi mountains (highest peaks slightly above 1800 m a.s.l.) have a comparable elevation and climate (Table 1). Both locations are characterised by a Mediterranean warm climate at the lower altitudes and temperate to cool climate at the highest altitudes. Hill tops (at about 1300 m a.s.l.) and hill slopes of the Sila mountains have an annual average temperature of 9–12 °C with an annual precipitation of 1000–1800 mm (Le Pera and Sorriso-Valvo, 2000), and temperatures at high and medium mountain altitudes in Nebrodi ranging between 9 and 13 °C in average, with precipitation rising to over 1000 mm/year (Tuttolomondo et al., 2014; Floresta meteorological station 1250 m a.s.l.: MAAT 9.3°). Looking at plant diversity, Nebrodi is mostly covered by grass, maquis and fen in contrast to Sila where shrubs and grass make up the cover, along with patches of pine- or beech-forest (Table 1).

2.2. Sampling strategy

In total, four profiles (all at a similar altitude of about 1300 m a.s.l.) on the Nebrodi mountains and two profiles on the Sila mountains (at approx. 1500 m a.s.l.; Table 1) were investigated in detail. The soil profiles on the Nebrodi mountains were selected by using ferns as bio-indicators as they are primarily found on acidic substrates which are a common feature of volcanic soils (Siddig et al., 2015). In the Sila mountains, the sites were selected based on already-existing investigations (Scarciglia et al., 2008; Pelle et al., 2013; Vingiani et al., 2014). All soil profiles (Fig. 2) can be considered as representative of

the main soil types. About 1–2 kg per soil horizon (continuous sampling over the horizon) were taken using open pits. In addition, soil cylinders were used to determine bulk density of the soil material. The ash layers in the areas of Nebrodi II and IV and in the area Nebrodi III (Fig. 3a) were mapped and their thickness registered using a Pürckhauer soil corer. The mapped areas were 77,000 m² and 26,000 m² respectively, and the variability of the ash layer (or Andosol-like epipedon) thickness on the Nebrodi mountains was assessed.

2.3. Physical and chemical analyses

All bulk samples were sieved to < 2 mm (fine earth) after oven drying (70 °C) for 48 h. The soil skeleton represents the weight ratio of the fraction ≥ 2 mm of the total bulk sample. After a pre-treatment of the fine earth with H₂O₂ (3%), particle-size distribution of the fine-earth was measured using a combined method consisting of wet-sieving the coarser particles (2000–32 μm) and determining the finer particles (< 32 μm) by means of an X-ray sedimentometer (SediGraph 5100). The SediGraph was used without autosampler to prevent, as far as possible, a disturbance of the stirring process caused by ferromagnetic material that may be potentially present. Coarse, rounded volcanic material (lapilli), retrieved from the Nebrodi soils, was removed and separately milled for further analyses. Soil pH (in 0.01 M CaCl₂) was determined on air-dried fine-earth samples using a soil:solution ratio of 1:2.5. Fe, Al and Mn concentrations were determined (in duplicate) after treatment with NH₄-oxalate (buffered at pH 3; McKeague et al., 1971). The extracts were centrifuged for 8 min at 4000 rpm and filtered (mesh size 0.45 μm, S & S, filter type 030/20). Element concentrations were measured using atomic absorption spectroscopy (AAAnalyst 700, Perkin Elmer). Element concentrations were furthermore controlled using standard addition (recovery ≥ 95%). The oxalate (Al_o, Mg_o, Fe_o) treatment extracts both the weakly- and poorly crystalline phases and some of the organic phases, but normally does not dissolve the strong humus-metal complexes (Mizota and van Reeuwijk, 1989). Loss on ignition (LOI) was performed by igniting 2 g of oven-dried fine earth at 1000 °C for 2 h. Measurement of the total element content of fine earth and lapilli and arenite (after crushing) was done by means of X-ray fluorescence (XRF) (Beckhoff et al., 2006). Approximately 5 g of soil material was milled to < 50 μm and analysed as loose powder in sample cups using an energy dispersive X-ray fluorescence spectrometer (SPECTRO X-LAB 2000, SPECTRO Analytical Instruments, Germany). For comparison additional data of analysed glass particles of the Sila soil were provided by Scarciglia et al. (2008). Scanning electron microscopy analyses, coupled with energy dispersive spectroscopy (SEM-EDS), were performed on Au-coated thin sections to assess and characterise volcanic components (Scarciglia et al., 2008). Total

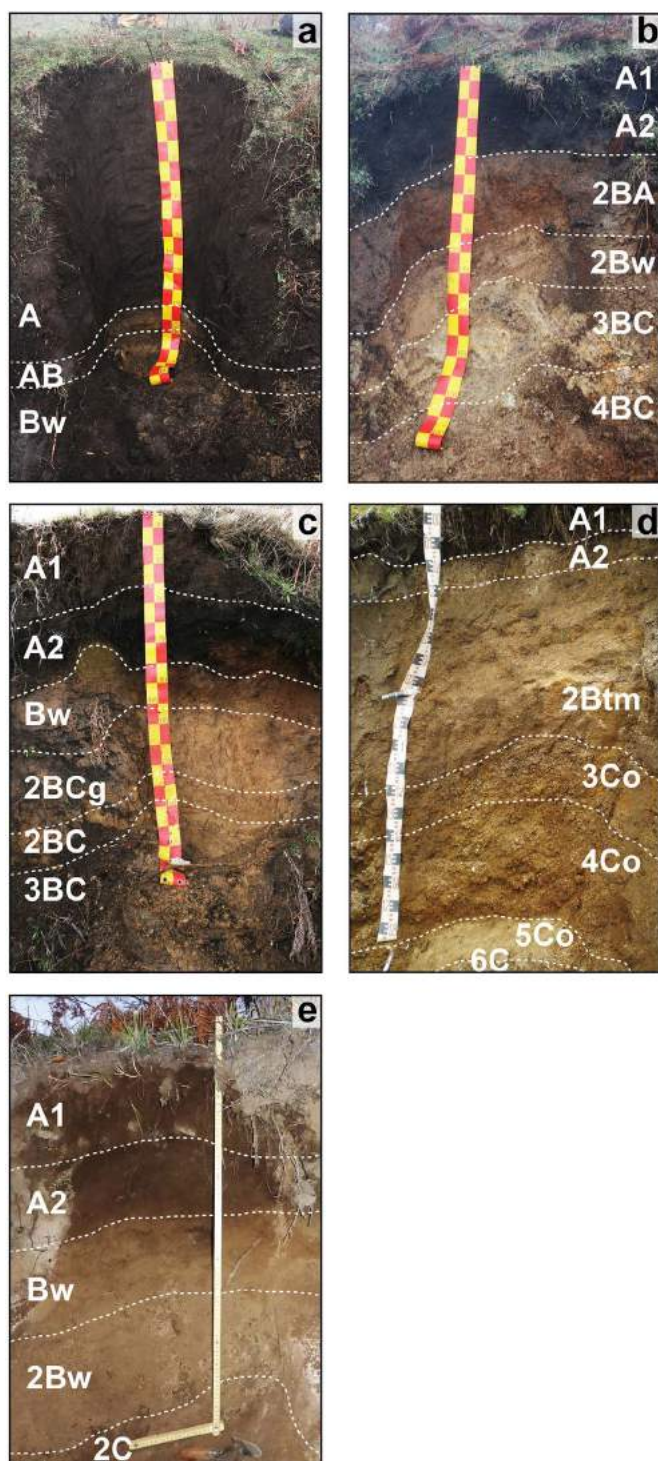


Fig. 2. Soil profiles (with soil horizon designation) at the investigated sites, a = Nebrodi I, b = Nebrodi II, c = Nebrodi III, d = Nebrodi IV and e = Sila II.

organic carbon (C) and nitrogen (N) values were obtained using a Leco® C-H-N elemental analyser (CHNS-932, USA). For this task, oven-dried finely milled soil material was used.

2.4. Soil mineralogy

For a general qualitative overview of soil minerals present, XRD (Bruker AXS D8 Advance, $\text{CuK}\alpha$) and DRIFT (Diffuse Reflection Infrared Fourier Transform; Bruker, Tensor 27) measurements of the fine silt and clay fraction ($< 32 \mu\text{m}$) were performed. The DRIFT analyses were run

from 250 to 4000 cm^{-1} . About 30 mg of finely-ground soil material and 270 mg of KBr were homogenised in a mill using a fine ball-mill (Zr) for 30 s and at 10 rpm. Prior to measurement, the samples were dried in an oven at 70°C for 2 h. The individual spectra were interpreted using OPUS 6 software. For X-ray analyses, randomly oriented samples were scanned from 2 to $80^\circ 2\theta$ with steps of $0.02^\circ 2\theta$ at 10 s intervals using a Bruker AXS D8 Advance ($\text{CuK}\alpha$). The measured spectra were evaluated using DIFFRACplus EVA.

2.5. ESEM-EDS and LA-ICP-MS measurements

Selected samples were polished (up to $1 \mu\text{m}$) with a diamond spray and then carbon coated. The SEM analyses were performed using a SEM FEI QUANTA 200 3D under high vacuum and SSD (solid state detector) operating at an accelerating voltage of 20 kV. The energy dispersive X-ray spectroscopy (EDX) was equipped with an Si(Li)EDX Detector that enabled point measurements on volcanic glass particles.

The chemical composition (major and trace elements) of glass particles, pumice and volcanic clasts of selected samples was determined by using a laser ablation ICP-MS (LA-ICP-MS). The system at the University of Bern consists of a Geolas Pro 193 nm ArF Excimer laser (Lambda Physik, Germany) coupled with an ELAN DRCE quadrupole mass spectrometer (QMS; Perkin Elmer, USA). Details on the setup and optimisation strategies can be found in Pettke et al. (2012). Daily optimisation of the analytical conditions were done to satisfy a ThO production rate of below 0.2% (i.e., Th/ThO intensity ratio < 0.002) and to achieve robust plasma conditions monitored by a Th/U sensitivity ratio of 1 as determined on the SRM612 glass standard. Analyses were done using 10 Hz laser repetition rate and 32–90 μm beam sizes, the maximum possible chosen to minimise limits of detection. External standardisation was done employing GSD-1G from USGS, SRM612 from NIST was measured for quality control (employing reference concentrations reported for both in Peters and Pettke, 2017) and bracketing standardisation provided a linear drift correction. Internal standardisation employed the sum of total major element oxides = 97 wt%. Data reduction was done off-line with the SILLS program (Guillong et al., 2008), with rigorous limits of detection calculated for each element in every analysis following the formulation detailed in Pettke et al. (2012).

2.6. Radiocarbon dating

Partial oxidative degradation of organic materials (OM) leaves behind intrinsically resistant as well as mineral-protected OM. This fraction can be extracted using a H_2O_2 leaching protocol (Favilli et al., 2008). This method is based on the oxidation of OM by 10% H_2O_2 (Plante et al., 2004, modified; Eusterhues et al., 2005). 2 g of air-dried, untreated soil ($< 2 \text{ mm}$) were wetted for 10 min with distilled water in a 300-ml beaker. Afterwards, 180 ml of 10% H_2O_2 were added. The procedure was run at a temperature of 50°C in a closed system for 168 h (7 days). Furthermore, additional charcoal samples were taken from two already studied soil profiles (CL4 and 5; cf. Moser et al., 2017). The charcoal samples were treated using the ABOx procedure (Brock et al., 2010; Wood et al., 2012). The ABOx procedure includes a treatment at room temperature in 6 M HCl for 1 h, followed by 2 M NaOH for 30 min, during which time the solution is replaced until it remains colourless. The charcoal is subsequently oxidised in $\text{H}_2\text{SO}_4/\text{K}_2\text{Cr}_2\text{O}_7$ (2 M/0.1 M) at 60°C in a sealed tube for 20 h. The charcoal was washed three times with ultrapure water between each treatment.

The samples (cleaned charcoal and soil sample fractions) were heated under vacuum in quartz tubes with CuO (oxygen source) to remove any absorbed CO_2 in the CuO. The tubes were then evacuated again, sealed and heated in the oven at 900°C to obtain CO_2 . The CO_2 of the combusted sample was mixed with H_2 (1:2.5) and catalytically reduced over iron powder at 535°C to elemental carbon (graphite). After reduction, the mixture was pressed into a target and carbon ratios were

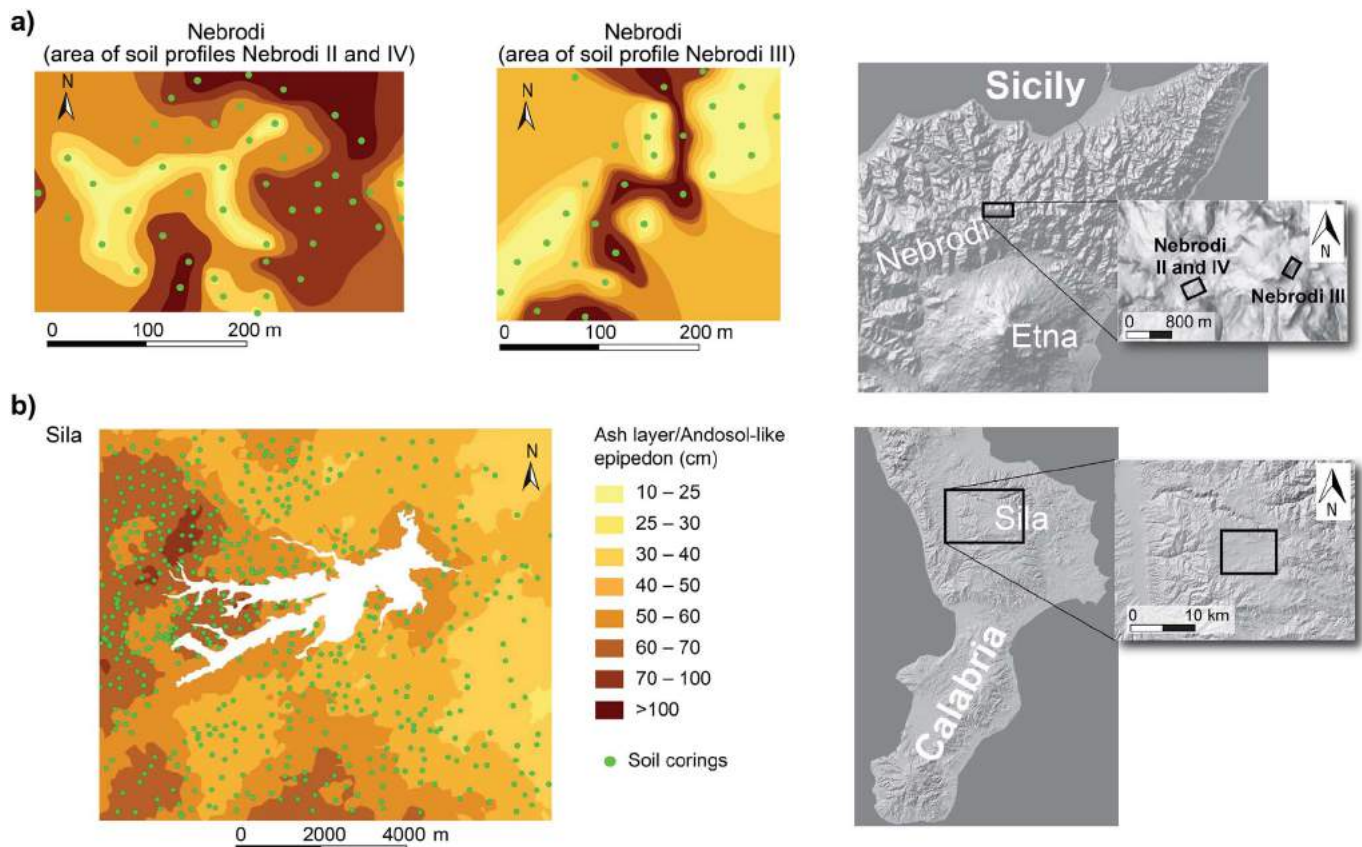


Fig. 3. Maps of ash layer thickness/Andosol-like epipedon based on soil coring investigations a) at the sites Nebrodi II, III and IV and b) around the Cecita Lake (Sila) after Scarciglia et al. (2008). The maps are created based on the DEM 20 SINAnet (Calabria; project SIGIEC, Sistemi Territoriali S.r.l., 2012) and SITR (Sistema Informativo Territoriale Regionale, Regione siciliana).

measured by Accelerator Mass Spectrometry (AMS) using 0.2 MV radiocarbon dating facility (MICADAS) of the Ion Beam Physics at the Swiss Federal Institute of Technology Zurich (ETHZ). The calendar ages were obtained using the OxCal 4.2 calibration program (Bronk Ramsey, 2001, 2009) based on the IntCal 13 calibration curve (Reimer et al., 2013). Calibrated ages are given in the 1σ and 2σ range (minimum and maximum value for each).

2.7. Chemical weathering indices and semi-quantitative and relative dating

To characterise mineral alteration and the weathering degree of soil material several indices have been utilized. According to Parker (1970), weathering and leaching generate a loss of mobile elements over time, and therefore an enrichment of non-mobile elements. Consequently, similar soils within the same geographic position should have a similar index value in the same time span. The older a soil surface the more easily weatherable elements are leached and relatively immobile elements enriched. As such, the bulk chemistry of a given soil should be a function of its age. A large number of such proxies have been proposed and over the years, often with variable relevance for the investigated system. In this study the utility of a number of these geochemical proxies were tested for deriving an age estimation of volcanic-influenced soils. The index B of Kronberg and Nesbitt (1981) and the chemical index of alteration (CIA) of Nesbitt and Young (1982) are based on the same considerations and provide a quantitative measure of feldspar weathering (Buggle et al., 2011). Index B is defined by the molar ratio of:

$$B = \frac{\text{CaO} + \text{K}_2\text{O} + \text{Na}_2\text{O}}{\text{Al}_2\text{O}_3 + \text{CaO} + \text{K}_2\text{O} + \text{Na}_2\text{O}} \quad (1)$$

The CIA is defined as:

$$\text{CIA} = 100 \left[\frac{\text{Al}_2\text{O}_3}{\text{Al}_2\text{O}_3 + \text{CaO} + \text{Na}_2\text{O} + \text{K}_2\text{O}} \right] \quad (2)$$

The index B and CIA refer to silicate weathering. The investigated soils have all a pH around 5 (Table 2). Consequently, the total CaO content refers to silicate CaO because no carbonates are present. As stated by Dahms et al. (2012) and Egli et al. (2008), the molar ratio of $(\text{K} + \text{Ca})/\text{Ti}$ can be used to determine the time of surface exposure and can also be deployed as a weathering index, based on the fact that K and Ca are mobile elements, while Ti is considered to be an immobile element because of its higher ionic potential (Egli and Fitze, 2000; Stiles et al., 2003; Buggle et al., 2011). Harnois (1988) presented a CIA without considering potassium because K may either be enriched or depleted in soil. He therefore suggested a chemical index of weathering (CIW):

$$\text{CIW} = 100 \left[\frac{\text{Al}_2\text{O}_3}{\text{Al}_2\text{O}_3 + \text{CaO} + \text{Na}_2\text{O}} \right] \quad (3)$$

In addition the plagioclase index of alteration (PIA) of Fedo et al. (1995), which is an Al-content corrected version of the CIW, was tested together with the WIP (Parker, 1970).

The PIA is given by:

$$\text{PIA} = 100 \left[\frac{\text{Al}_2\text{O}_3 - \text{K}_2\text{O}}{\text{Al}_2\text{O}_3 + \text{CaO} + \text{Na}_2\text{O} - \text{K}_2\text{O}} \right] \quad (4)$$

the WIP, calculated by using the weight percent, by (Price and Velbel, 2003):

$$\text{WIP} = 100 \left[\frac{2\text{Na}_2\text{O}}{0.35} + \frac{\text{MgO}}{0.9} + \frac{2\text{K}_2\text{O}}{0.25} + \frac{\text{CaO}}{0.7} \right] \quad (5)$$

Finally the chemical proxy of alteration (CPA) of Buggle et al.

Table 2
Typical chemical characteristics of the soils.

Site	Horizon	pH (CaCl ₂)	C (g/kg)	N (g/kg)	C/N	Al _o ^a (g/kg)	Mn _o ^a (mg/kg)	Fe _o ^a (g/kg)	Al _o + 1/2Fe _o (g/kg)
Nebrodi I	A1	4.92	110.0	9.62	11.4	7.86	497	5.95	10.84
	A2	4.69	94.3	8.23	11.5	10.68	524	6.03	13.70
	A3	4.72	72.4	6.40	11.3	11.74	581	6.82	15.15
	A4	4.85	72.5	6.26	11.6	9.66	459	6.05	12.69
	AB	4.82	9.5	0.51	18.5	1.03	202	2.15	2.11
	Bw	4.68	3.9	0.16	24.4	0.36	169	0.73	0.73
Nebrodi II	A1	5.76	48.1	3.83	12.6	4.94	750	6.95	8.42
	A2	5.62	66.0	4.51	14.6	14.57	856	7.410	18.28
	2BA	4.95	32.4	1.94	16.7	38.41	604	23.26	50.04
	2Bw	4.92	44.0	3.16	13.9	63.32	716	23.21	74.93
	3BC	4.42	3.1	–	–	1.22	1005	3.71	3.08
	4BC	4.02	3.0	0.04	–	0.86	3	2.83	2.28
Nebrodi III	A1	4.99	19.1	1.32	14.4	1.45	180	1.91	2.41
	A2	4.75	40.2	2.40	16.8	11.28	356	7.50	15.03
	Bw	4.73	9.5	0.34	28.3	10.86	214	6.67	14.20
	2BCg	4.28	2.4	–	–	0.93	233	2.19	2.03
	2BC	4.07	2.7	0.11	24.3	0.86	197	1.68	1.70
	3BC	3.92	2.6	0.00	–	1.22	254	2.04	2.24
Nebrodi IV	A1	5.00	32.1	2.84	11.3	10.49	453	5.31	13.15
	A2	5.00	11.9	1.21	9.9	22.96	425	7.15	26.54
	2Btm	4.75	10.8	1.00	10.7	1.35	361	13.01	7.86
	3Co	5.10	5.7	0.69	8.2	10.64	537	11.09	16.19
	4Co	5.30	4.3	0.57	7.6	6.81	1446	16.45	15.04
	5Co	5.75	1.5	0.57	2.7	0.30	1013	2.76	1.68
Sila I	6C	4.50	3.4	0.53	6.4	–	23	2.13	–
	A1	4.80	58.6	4.45	13.2	5.73	326	4.21	7.84
	A2	5.00	39.1	2.98	13.1	6.77	306	4.00	8.77
	Bw	5.00	13.2	1.18	11.2	8.83	59	1.23	9.45
	2Bw	5.10	7.9	0.75	10.5	9.95	13	0.42	10.16
	2C	4.90	4.2	0.47	8.9	9.21	32	0.23	9.33
Sila II	A1	5.13	52.6	3.64	14.4	4.18	340	3.96	6.16
	A2	5.01	35.3	2.39	14.8	4.20	385	11.72	10.06
	Bw	5.08	19.4	1.21	16.1	6.65	50	2.14	7.72
	2Bw	5.23	5.2	0.05	–	1.23	25	0.42	1.44
2C	5.24	5.4	–	–	5.48	11	0.08	5.52	

^a Oxalate-extractable fraction.

(2011) was also tested.

$$CPA = 100 \left[\frac{Al_2O_3}{Al_2O_3 + Na_2O} \right] \quad (6)$$

Semi-quantitative dating was achieved by using weathering data (total elemental contents and calculation of weathering indices) given in Mirabella et al. (2005) and relating this dataset to numeric surface ages (also provided in Mirabella et al., 2005). Using regression curves (weathering indices vs surface age) an age estimation could be performed for sites (or soil horizons) having a given geochemical composition of the same source but unknown ages.

3. Results

3.1. General soil characteristics

The investigated soils had an upper mineral A horizon and showed typical features of volcanic soils having vitric properties (Table 1). The displayed colours in the A horizons – according to the Munsell soil colour charts – ranged from black to dark brown in wet conditions, when dry, the soils displayed lighter colours (Table 3). Nebrodi I has in the topsoil a relatively high silt content (loam) and in the subsoil the material is sandier (sandy loam). The profile is mainly made of volcanic ash and has one massive umbric (10YR1.7/1) A horizon that extends from the top to 130 cm depth, followed by two more, but comparatively shallower, horizons. Furthermore, the soil is slightly acidic. Soil profile Nebrodi II is characterised by loam, sandy clay loam or sandy loam textural classes (Soil Survey Division Staff, 2010). The site Nebrodi II has a sandy loam or loam texture all over the profile. Also Nebrodi II

has two umbric (7.5YR3/1 and 7.5YR7/1) A-horizons, which predominantly consist of ash material and extend from the surface to a depth of 50 cm. Similarly to Nebrodi I and II, Nebrodi III has two dark (umbric) (10YR3/2 and 10YR1.7/1) A-horizons consisting of ash material and having the characteristics of a sandy loam texture. The soil profile of Nebrodi IV generally has a lighter colour, clay loam texture in the upper part and clay in the lowermost part of the profile. The soil profile Nebrodi IV had one distinctive argic horizon (Bt) with a high content of clays and a reddish-colour. The entire profile consists of five different parent materials, overshadowing any trend in chemical or physical constituents. In contrast to the Nebrodi profiles, the Sila profiles displayed a variety of brown colours and were shallower. In general, the soil thickness (A + B horizon) was between 90 and 160 cm at the Nebrodi sites and around 80 cm on the Sila mountains. In the topsoil, volcanic material was recognisable. The ash deposits at Nebrodi are sometimes > 100 cm thick (Fig. 3). The bulk density values in the upper part of the profiles were low, which is typical for soils having vitric properties (Table 3). According to the WRB (IUSS Working Group WRB, 2015), the diagnostic criteria for an andic horizon are: Al_o + 1/2Fe_o > 2%, a bulk density < 0.9 g cm⁻³ and a phosphate retention ≥ 85%. The phosphate retention was not measured. The A and sometimes the B horizons often had a density below or close to 0.9 g cm⁻³. Most of the samples did, however, not completely fulfil the criteria of Al_o + 1/2Fe_o > 2%. Only the Nebrodi II profile and the Nebrodi IV profile (A2 horizon) met these requirements. Although the profiles contain a considerable amount of ashes and lapilli, several of them cannot be classified as Andosols. Except Nebrodi I, all other profiles in the Nebrodi mountains are composed of several substrates. Consequently, Fe_o and Al_o often strongly vary along the profiles.

Table 3
Physical characteristics of the investigated soils.

Site	Horizon	Depth (cm)	Munsell colour (moist)	Soil skeleton (wt%)	Bulk density (g/cm ³)	Sand (%)	Silt (%)	Clay (%)
Nebrodi I	A1	0–20	10YR1.7/1	0.9	0.84	34.8	44.7	20.5
	A2	20–50	10YR1.7/1	1.0	0.92	–	–	–
	A3	50–90	10YR1.7/1	0.7	0.93	–	–	–
	A4	90–130	10YR1.7/1	0.6	1.01	–	–	–
	AB	130–140	7.5YR3/1	0.6	1.49	68.3	16.6	15.1
	Bw	140–160	2.5Y5/6	0.6	1.58	57.0	18.9	24.1
Nebrodi II	A1	0–15	7.5YR3/1	1.3	1.00	41.7	27.7	30.6
	A2	15–50	7.5YR1.7/1	0.8	0.86	46.2	33.5	20.3
	2BA	50–65	7.5YR 4/4	19.2	0.89	55.0	30.4	14.6
	2Bw	65–90	7.5YR 4/4	49.3	0.74	59.0	29.6	11.4
	3BC	90–130	10YR 5/4	43.9	1.54	41.4	18.1	40.5
	4BC	130–170	10YR5/4	35.8	1.39	–	–	–
Nebrodi III	A1	0–50	10YR3/2	0.9	1.32	63.6	18.3	18.1
	A2	50–75	10YR1.7/1	4.3	0.98	–	–	–
	Bw	75–110	7.5YR4/3	17.6	1.27	69.5	20.6	9.9
	2BCg	110–135	10YR4/4	1.2	1.57	–	–	–
	2BC	135–155	10YR5/4	0.1	1.55	–	–	–
	3BC	155–170	10YR6/4	20.1	1.46	67.7	16.6	15.7
Nebrodi IV	A1	0–20	10YR2/1	5.0	0.80	36.6	33.5	29.9
	A2	20–35	10YR2/1	10.0	0.80	–	–	–
	2Btm	35–115	10YR3/6	10.0	0.90	54.0	31.0	15.0
	3Co	115–135	10YR3/4	40.0	1.10	–	–	–
	4Co	135–180	7.5YR4/4	35.0	1.10	–	–	–
	5Co	180–200	2.5Y4/4	10.0	1.25	–	–	–
Sila I	6C	> 200	2.5Y4/0	25.0	1.30	13.5	20.0	66.4
	A1	0–20	10YR3/4	2.0	0.87	37.1	38.0	24.9
	A2	20–40	10YR3/4	2.0	0.97	–	–	–
	Bw	40–60	10YR4/6	5.0	1.13	60.7	33.4	5.9
	2Bw	60–80	10YR6/4	5.0	1.37	–	–	–
	2C	80–100	10YR/6/3	10.0	1.37	70.9	22.4	6.7
Sila II	A1	0–20	10YR3/4	10.9	0.90	–	–	–
	A2	20–40	10YR3/4	15.1	0.83	–	–	–
	Bw	40–60	10YR4/6	15.8	1.11	–	–	–
	2Bw	60–80	10YR6/4	20.4	1.43	–	–	–
	2C	80–100	10YR/6/3	21.0	1.19	–	–	–

However, a maximum was measured in most cases in the B-horizon (Table 2). The majority of the soils at the Nebrodi sites had a pH-value (Table 2) of around 5 in the topsoil but showed a decrease of up to around 4 in the deeper B-horizons. This trend is most likely due to the ash input (unweathered fresh material) in the upper horizons giving rise to a higher pH. In the Sila mountains all the soils had a pH-value close to 5 with a tendency to increase with depth. In all the soils, organic carbon was found in most cases to a considerable depth. The organic C content, and therefore also the LOI, were particularly high in the soil Nebrodi I (Table 4). The thickness of the ash-bearing layer showed a considerable spatial variation at both mapped areas in the Nebrodi mountains, with 17 to > 100 cm close to Nebrodi II and 7 to > 100 cm close to Nebrodi III (Fig. 3).

3.2. Soil mineralogy

The DRIFT analysis (Table 5) of six soil profiles enabled the detection of a wide range of minerals that were confirmed by XRD analyses (Fig. 4). Kaolinite or halloysite (peaks at 3620 cm⁻¹ and 3694 cm⁻¹ in the IR spectra), gibbsite (at 3525 cm⁻¹), mica (given in the XRD spectra at 1.0 nm) and quartz (confirmed by XRD and the quartz doublet at 780 and 800 cm⁻¹ in the IR spectra) were present in all profiles. In most profiles, a minor amount of smectitic phases (at 3624 cm⁻¹) seemed to be present. Typical for sediments and soils having a volcanic origin or input, a small amount of imogolite-type material (ITM: sum of imogolite and proto-imogolite allophane) was detected in many samples. Nebrodi IV, Sila I and Sila II showed also the presence of some amphibole in several horizons. Using XRD also iron oxides and traces of fayalite (olivine) were detected (Fig. 4).

3.3. Scanning electron microscopy data and related chemical analyses

The SEM-EDS analyses of thin sections enabled the detection of glass particles and volcanic clasts in all topsoil samples (Fig. 5). The glass particles often had small dimensions in the range of about 20–200 µm. They appear weathered at different extents (Fig. 5), showing coalescing etch pits and/or clay neogenesis (see Scarciglia et al., 2008). The main chemical composition of the site Sila (analysed on spots from better-preserved, fresh surfaces) appears quite homogeneous and has an essentially rhyolitic composition with a high silica (SiO₂ between about 75 and 78%) and alkali contents (Na₂O + K₂O between about 7 and 9%) and a TiO₂ content mostly in the range of 0.1–0.8% (Scarciglia et al., 2008; Vingiani et al., 2014). Using SEM-EDS, the samples of the Nebrodi site showed an average SiO₂ in the range of 62–72% and TiO₂ content of about 1.2% (0–2.7%).

LA-ICP-MS analyses were done on individual volcanic particles of the Nebrodi samples (Horizons A2 and A4 of Nebrodi I; A horizon of Nebrodi IV). Major and trace element contents are given in Table 6. Glasses, pumice-like material and volcanic clasts (sometimes considerably altered) were detected and measured (Fig. 5). Some samples analysed with SEM-EDS were re-measured. The more or less unweathered glass particles with minimal alteration have a quite uniform composition with a SiO₂ content of about 71–71 wt-% and a low TiO₂ content near 0.1 wt-%. The weathered volcanic clasts have, as an average, a lower SiO₂ (about 54–70 wt-%) and a higher TiO₂ content (0.2–1.1 wt-%). Some prominently vesicular (pumice-like) particles were also measured having a SiO₂ content of about 53 wt-% and TiO₂ of about 0.8 wt-%. The trace elements showed distinct variations among the distinguished material groups of the Nebrodi samples. Within the groups, the variability was limited suggesting a co-genetic link.

Table 4

Total elemental content (given as oxides) of all soil samples. LOI = loss on ignition; OM = organic matter, whereby the total organic C was determined via CHN-analyser and multiplied by the factor 1.72; IVC = inorganic volatile compounds, estimated by LOI minus OM.

Site	Horizon	Depth (cm)	Na ₂ O (g/kg)	MgO (g/kg)	Al ₂ O ₃ (g/kg)	SiO ₂ (g/kg)	P ₂ O ₅ (g/kg)	K ₂ O (g/kg)	CaO (g/kg)	TiO ₂ (g/kg)	MnO (g/kg)	Fe ₂ O ₃ (g/kg)	LOI (g/kg)	OM (g/kg)	IVC (g/kg)
Nebrodi I	A1	0–20	19.2	13.7	169	490	6.5	19.1	16.7	10.1	1.7	58	196	189.1	7
	A2	20–50	18.8	13.7	184	522	6.3	20.1	14.4	10.7	1.8	60	148	162.1	0
	A3	50–90	18.0	13.6	184	526	6.3	19.8	14.5	10.6	1.8	59	146	124.6	22
	A4	90–130	20.5	14.5	191	524	6.6	19.9	15.8	10.9	1.8	60	135	124.7	10
	AB	130–140	17.8	19.2	195	649	2.0	27.1	12.2	6.6	0.8	37	33	16.3	17
	Bw	140–160	16.1	20.3	175	658	0.6	28.2	12.4	6.2	0.5	37	46	6.8	39
Nebrodi II	A1	0–15	14.7	15.9	168	566	3.6	20.2	19.4	9.0	1.8	57	124	82.7	42
	A2	15–50	14.9	13.1	191	491	5.7	17.4	17.8	10.7	2.0	66	170	113.4	57
	2BA	50–65	18.4	13.6	248	425	8.1	10.4	13.5	16.1	1.5	85	160	55.7	105
	2Bw	65–90	18.8	11.8	266	381	9.7	7.8	15.1	15.9	2.2	81	192	75.7	116
	3BC	90–130	8.6	10.3	100	764	0.5	13.8	4.5	4.6	1.5	42	51	5.4	45
	4BC	130–170	5.4	12.0	96	744	0.1	10.1	4.6	5.1	0.0	47	75	5.2	70
Nebrodi III	A1	0–50	19.8	16.4	164	673	1.4	27.7	8.9	5.4	0.7	31	52	32.9	19
	A2	50–75	18.5	15.0	211	542	4.8	21.8	9.2	10.0	1.2	56	110	69.1	41
	Bw	75–110	18.3	16.1	233	572	4.5	22.2	10.6	9.7	0.9	50	62	16.3	46
	2BCg	110–135	19.6	15.5	165	692	0.5	29.7	6.6	4.9	0.6	32	34	4.1	30
	2BC	135–155	16.6	17.5	166	692	0.5	30.3	7.2	4.6	0.5	30	35	4.7	30
	3BC	155–170	13.5	19.4	168	656	0.4	27.6	7.2	6.2	0.6	41	60	4.4	56
Nebrodi IV	A1	0–20	18.5	11.4	139	623	2.0	23.0	11.5	6.9	1.1	45	120	55.2	64
	A2	20–35	13.1	12.0	167	600	1.1	17.9	9.1	9.3	1.2	59	110	20.5	90
	2Btm	35–115	16.7	13.4	221	458	4.2	10.7	18.6	14.9	1.3	80	161	18.5	143
	3Co	115–135	26.1	14.8	238	447	6.8	9.0	34.1	15.5	2.0	83	124	9.7	115
	4Co	135–180	18.0	8.8	251	422	5.1	5.4	21.2	17.1	3.1	84	165	7.4	158
	5Co	180–200	13.7	10.6	123	710	0.1	19.8	7.5	6.2	1.8	44	63	2.6	61
	6C	> 200	4.3	9.4	86	732	0.1	11.7	3.9	4.8	0.1	66	82	5.8	76
Sila I	A1	0–20	18.3	11.3	191	508	2.4	23.8	19.8	7.1	0.8	49	168	100.8	67
	A2	20–40	17.6	11.4	199	528	2.2	25.3	21.1	7.1	0.8	50	137	67.3	69
	Bw	40–60	22.6	9.0	230	535	2.1	27.3	28.1	6.0	0.4	45	94	22.7	72
	2Bw	60–80	23.4	8.9	233	545	2.5	27.7	30.8	6.5	0.3	49	73	13.6	60
	2C	80–100	25.3	8.4	218	577	1.9	29.8	33.6	5.5	0.3	43	58	7.1	50
Sila II	A1	0–20	18.5	13.4	227	519	2.1	23.7	19.7	8.3	1.0	57	111	90.4	20
	A2	20–40	20.2	9.5	247	487	3.1	24.6	27.5	7.5	0.4	56	117	60.8	56
	Bw	40–60	26.7	8.9	239	530	2.7	25.1	35.2	6.1	0.3	46	80	33.4	47
	2Bw	60–80	33.7	9.7	254	543	2.9	24.7	36.9	5.9	0.3	45	44	8.9	35
	2C	80–100	26.9	8.8	247	542	3.0	25.5	37.6	6.1	0.3	44	58	9.2	49
Lapilli ^a	2BA	50–65	43.7	18.0	224	538	9.4	14.1	40.0	21.8	1.6	90	–	–	–
	2Bw	65–90	48.6	18.5	201	558	8.1	15.2	48.0	19.8	1.7	81	–	–	–
	2Bw	65–90	43.0	14.9	269	485	11.9	7.9	37.5	26.1	1.5	104	–	–	–
Arenite ^b		12.6	21.6	123	511	2.3	21.5	268.9	5.0	0.5	34	–	–	–	

^a Lapilli of the Nebrodi II site.

^b Average composition of the arenite at the Monti Nebrodi sites.

3.4. Determination of the volcanic origin

Total alkali versus silica (TAS) diagrams are often used to determine the origin of igneous rocks and their extent of fractional crystallisation (Johannsen, 1937). However, the classical TAS diagram is not deemed suitable for determining the origin of unweathered rocks from bulk geochemical data of weathered soils, as enrichment and depletion of potassium or sodium in the soils, coupled with desilication, may have occurred. Weathering processes overshadow such a straightforward relation and may lead to potential errors. Instead, immobile or trace elements (Figs. 5 and 6) and their ratios including the Th-Co plot of Hastie et al. (2007) and the Nb/Y-Zr/Ti plot of Pearce (1996) were thus employed (Fig. 8a and b).

The source of the Sila volcanic material is not conclusive. The Hastie plots revealed the origin of a potassium rich calc-alkaline to shoshonitic origin for Sila I, Sila II and the extracted lapilli. Most samples of the Nebrodi sites can be characterised as trachy-andesite, whereas the Sila samples are related to the rhyolite/dacite domain. According to the Ti/Nb – Ti/Zr ratios (Fig. 6a), the Sila data showed a good agreement with the Roman Province, however this was not the case for any other chemical system (Figs. 6 and 7). Some overlap occurred with Campania (Figs. 6b, 7c) and Vultur (Fig. 6d). The most consistent trend was found for the Rb-Co (Fig. 6d), Zr/Rb – Th/Rb (Fig. 7b) and the K₂O/Na₂O – K₂O + Na₂O plots (Fig. 7a; Paterne et al., 1988) which suggest that the

Sila site is predominantly related to the Aeolian Islands.

The Nebrodi samples showed a clearer trend and this suggests sources from the Campania and Aeolian Islands domain as seen in the Ti/Nb-Ti/Zr (Fig. 6a), Sr-Rb (Fig. 7b) and Pb/Hf-Pb (Fig. 6c) plots. When looking at the Rb-Co (Fig. 6d), K₂O/Na₂O-K₂O + Na₂O (Fig. 7a; Paterne et al., 1988), Zr/Rb-Th/Rb (Fig. 7b) and Ce/TiO-TiO₂ (Fig. 7c) plots, the Nebrodi samples also exhibit a strong relation to the Aeolian Islands. In contrast, the lapilli collected at Nebrodi II were predominantly within the Sicily domain (Figs. 6 and 7; Paterne et al., 1988). A similar result was obtained for the lapilli using the Pb/Hf-Pb (Fig. 6c) and Zr/Rb-Th/Rb (Fig. 7b) diagram. The Lipari IIB event (epoch VI after Forni et al., 2013) and Vulcano events were closest to the soil data when using the Ce/Nd-Sr/Rb and Ce/La-Sr/Rb plots (Fig. 8c and d). In the Th-Th/U plot, the Lipari IIB event was even the only one that overlaps with the data of the soil samples (Fig. 8e).

All glasses showed similar levels of incompatible trace element enrichment reflected in their spidergrams and are up to > 800 times more enriched than in the primitive mantle. This enrichment is particularly given for Rb, Ba Th, and U. The profiles are characterised by a trough at Nb and Ta and a pronounced depletion in Ti (Fig. 5). The volcanic clasts, however, do not exhibit this Ti depletion. The glasses indicate a light rare earth element (LREE) enrichment relative to the heavy rare earth elements. Using the LA-ICP-MS analyses, the origin of the glass particles, pumice-like material and volcanic clasts can be fairly

Table 5
Identified minerals in the fraction < 32 µm using DRIFT.

Site	Horizon	Kaolinite	Gibbsite	Chlorite	ITM ^a	Illite (Mica)	Quartz	Smectite	Okt. (Mg/Fe)	AlMgOH	Amphibole
Nebrodi I	A1	x	x	?	(x)	x	x	(x)			x
	A2	x	x	(x)	(x)	x	x	(x)			
	A3	x	(x)			(x)	x	(x)			
	A4	x	?		(x)	x	x	(x)			
	AB	x	(x)		(x)	x	x	(x)			
	Bw	x	?				x				
Nebrodi II	A1	x	(x)		(x)	x		(x)		(x)	
	A2	x	x	(x)	(x)		x	(x)	(x)		
	2BA	?	x				x				
	2Bw	(x)	x	(x)	(x)	(x)	(x)	(x)		(x)	
	3BC	?	?		(x)		x	(x)			
	4BC	?	?		(x)	(x)	(x)	(x)			
Nebrodi III	A1	(x)	x		(x)	x	(x)	(x)		x	
	A2	x	x	?		x	x	x		(x)	
	Bw	x	x	x	(x)	x	x	(x)			
	2BCg	x	x	?	(x)	x	(x)			x	
	2BC	x	x	?	(x)	x	x	x		x	
	3BC	x	x		(x)	x	(x)	(x)	x	x	
Nebrodi IV	A1	x	?		?	x	x				x
	A2	x	?				x				x
	2Btm	x			(x)	(x)			(x)		
	3Co	?	x	?	?			x			x
	4Co	x	(x)		(x)	(x)	(x)				
	5Co	x	?		(x)		x				
	6C	(x)			(x)		x				
Sila I	A1	x	x	(x)	x	x	(x)		x	(x)	
	A2	x	x		x	(x)	(x)	(x)			(x)
	Bw	x	x		(x)	(x)	(x)	(x)			x
	2Bw	x	x	?	?						x
	2C	x	x		(x)	(x)					x
Sila II	A1	x	x	(x)	x	x	(x)		x	(x)	
	A2	x	x		x	(x)	(x)	(x)			(x)
	Bw	x	x		(x)	(x)	(x)	(x)			x
	2Bw	x	x	?	?						x
	2C	x	x		(x)	(x)					x

? = traces questionable, x = present in significant amount, (x) = low amount.

^a ITM = imogolite-type material, henceforth referred to as the sum of imogolite and proto-imogolite allophane.

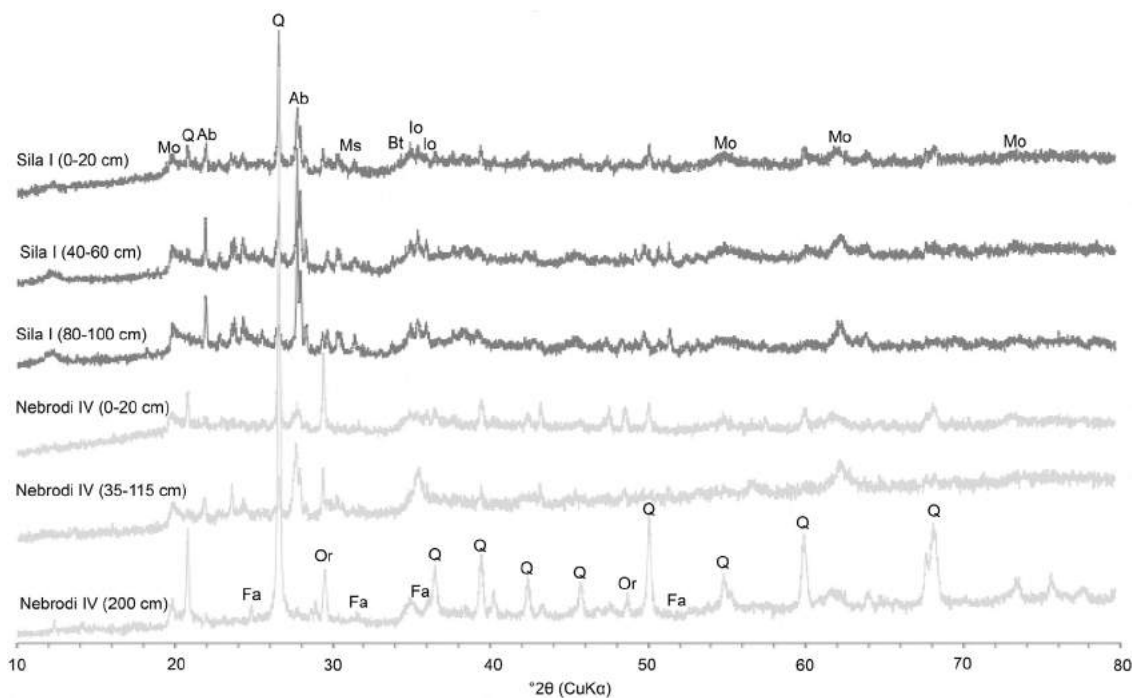


Fig. 4. X-ray diffraction patterns of six selected samples. Associated diffraction peaks are labelled as quartz (Q), albite (Ab), montmorillonite (Mo), iron oxide (Io), muscovite (Ms), biotite (Bt) and fayalite (Fa).

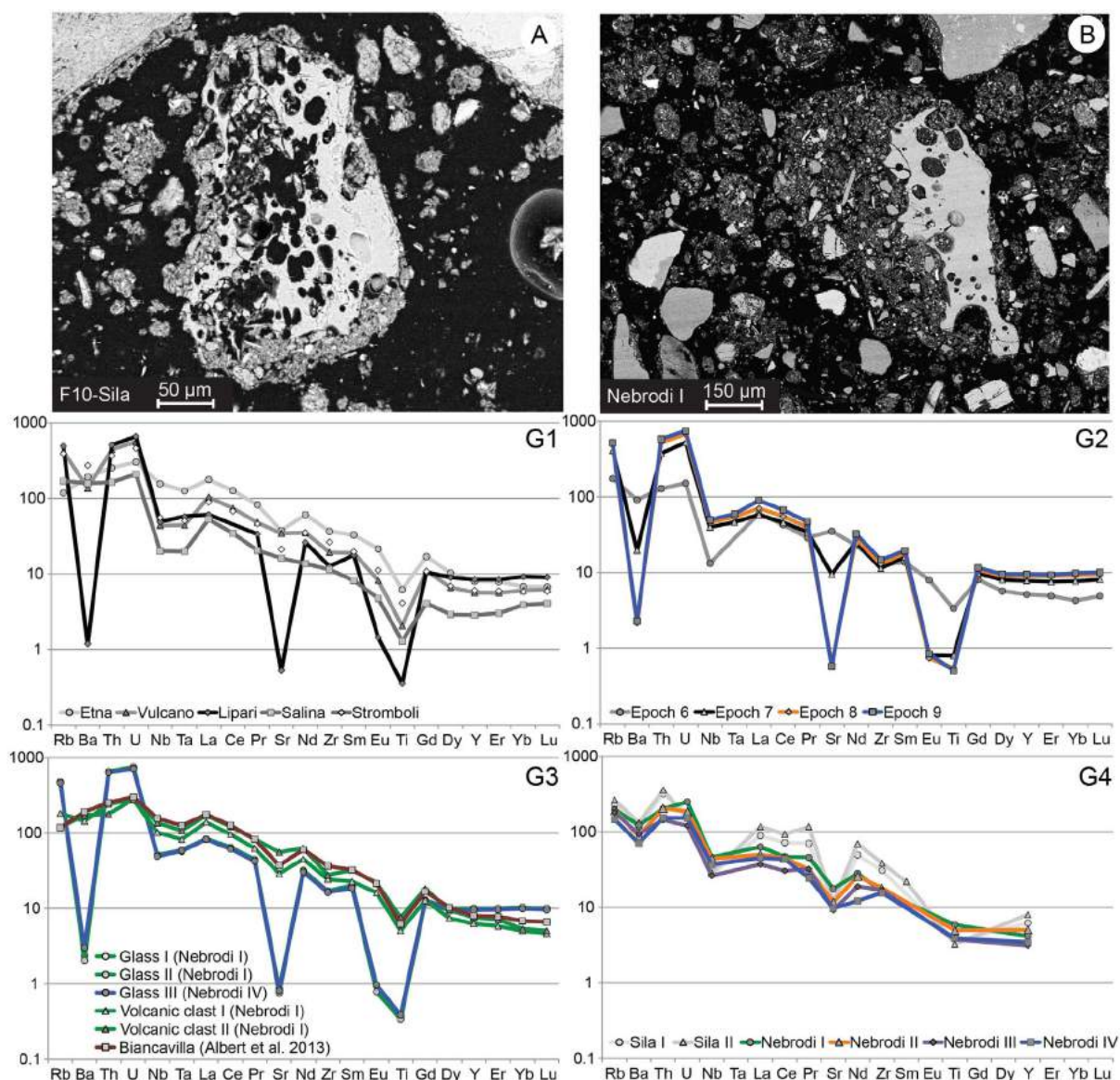


Fig. 5. SEM images of strongly weathered vesicular glass fragments of (A) Sila (Scarciglia et al., 2008) and (B) Nebrodi. Primitive mantle (Sun and McDonough, 1989) normalised data of G1) trace elements of volcanic glasses of the Aeolian Islands (Albert et al., 2017), G2) average composition of the Lipari volcanic epochs (Forni et al., 2013), G3) measured volcanic glasses and clasts in the Nebrodi soil profiles together with the Biancavilla deposits (Etna; Albert et al., 2013) and G4) average trace element composition of the investigated soil profiles.

well allocated by comparing them with data published by Forni (2011) and Albert et al. (2013, 2017). The glasses and clasts suggest an origin from the Aeolian Islands (although from different eruptive epochs) and the pumice-like material seems to fit well with a particular flank eruption of the Etna (the Biancavilla ignimbrites and Unit D Plinian fall deposits; Fig. 5).

3.5. Radiocarbon ages of OM

Age data of already published soil charcoal data are compiled in Table 7. The ages vary from modern to about 14 ka BP. Additional charcoal fragments, using the APOx preparation technique, did not result in higher ages (Table 7). Furthermore, nine soil samples were investigated (Table 8) that showed an overall age range from 319 to 9662 cal BP. The ages increased with soil depth at all sites. They showed that the oldest organic matter fractions that could be detected in the soils have a Holocene age. Maximum ages for the Nebrodi and Sila mountains from the H_2O_2 -resistant soil organic matter fraction were in the range of 8–10 ka BP. The ages in the topsoil varied in the range of about 500–1800 ka BP at all sites.

3.6. Weathering indices

Weathering indices are given in Table 9. An undisturbed soil evolution would be characterised by increasingly weathered and leached horizons towards the surface. This is partially given for profile Nebrodi I. The sites Nebrodi II to IV however showed some discontinuities with less weathered material in the uppermost and lowermost horizons. Sila I and II had only little variation along the profile. The weathering indices used here do not always provide a conclusive signal where the $(K + Ca)/Ti$ ratio indicates an increasingly weathered material towards the surface, while the CIW, CIA and PIA weathering indices showed less variations. In fact, these last three indices indicate less weathered material at the top and, thus, reflect the layering of the soil material. All weathering indices strongly correlated (highly significant; using the Spearman rank correlation) with each other. The weakest, but still highly significant correlation was between the $(K + Ca)/Ti$ ratio and the index B and the CIA ($R = 0.45$; $p < 0.01$) and the strongest between the index B and the CIA ($R = 0.999$; $p < 0.01$). In all these correlations, the ‘bedrock’ sample of the Nebrodi sites was an outlier.

Compared to the CIA, CIW and PIA indices, the WIP is known to

better cope with inhomogeneities in soils (Price and Velbel, 2003). Therefore, the WIP weathering index (using Fig. 9 as a basis) was used for an age estimate (Table 10). According to these estimates, the ash deposits in the Nebrodi mountains have an average age of about 70 ka and those in the Sila mountains about 49 ka (and 45 ka – with a considerable variability – when using the data of Scarciglia et al., 2008). The glass fragments found in the Sila soils would indicate even a lower age (between modern up to about 24 ka). Using the WIP, the volcanic deposits on the Nebrodi mountains seem to be older than those on the Sila mountains.

4. Discussion

4.1. Soil chemical and mineralogical properties indicate volcanic origin

The investigated regions of Nebrodi and Sila are considered to be suitable for distal tephra sedimentation due to their proximity to the Aeolian Arc and Mount Etna. Although the criteria for Andosols were not always fulfilled, andic-like and vitric properties could be observed in many places. Similar to other studies conducted on volcanic soils in southern Italy (Pichler, 1981; Pichler, 1984; Mirabella et al., 2005; Scarciglia et al., 2008; Egli et al., 2008; Vingiani et al., 2014), the total chemical composition of major and trace elements showed a dominance of SiO₂ and Al₂O₃ (Table 4). On average, the soils of the Nebrodi mountains had a slightly higher SiO₂ value (58.2%) compared to Sila area (53.0%). This is in agreement with the values reported in Scarciglia et al. (2008) and Vingiani et al. (2014). Kaolinite or halloysite were commonly found in all the investigated soils. Kaolinite and halloysite are typically found in volcanic soils and were presumably formed through the weathering sequence: glass > halloysite > kaolinite (Mirabella et al., 2005; Egli et al., 2008). Gibbsite is similarly produced by chemical weathering of aluminium-rich rocks (Glenn and Nash, 1964). Smectite-like clay minerals were also found, particularly in the A-horizon. According to Sumner (1999), Mirabella et al. (2005), Egli et al. (2008) and De Rosa et al. (2016), smectite is often found in volcanic soils, possibly created through hydrothermal processes. The DRIFT analysis also revealed the presence of imogolite (typically in the A and B horizons) — a typical short-range order (poorly crystalline) mineral found in volcanic soils that were formed from ashes/tephra (Sumner, 1999). The clay assemblages confirm the volcanic origin of the soils.

4.2. Origin of the volcanic deposits

Given the locations of Nebrodi and Sila, several volcanic areas (Fig. 7d) could potentially contribute volcanic material to the soils. The main challenge in determining the origin of these deposits is to find a method that can differentiate the volcanoes from each other while excluding influences due to alteration. The chemical composition of the soils and of the potential volcanic sources (Pichler, 1967; Scarciglia et al., 2008; Pelle et al., 2013; Vingiani et al., 2014) can be used for a forensic analysis especially the element ratios Th/Rb vs Zr/Rb, TiO₂ vs Ce/TiO₂ and K₂O/Na₂O vs K₂O + Na₂O were useful for alteration material. We also considered currently inactive volcanic systems (e.g. only Etna and Stromboli are presently active). Th-Co (Hastie et al., 2007) is unaffected by the enrichment and depletion of potassium or sodium in soils, making it a good indicator of the geochemistry of the original source. All the soils investigated here fall into the high-K calc-alkaline series (Fig. 8a; Peccerillo, 2005). This allowed us to exclude several volcanic centers based on their petrochemical affinity, such as Na-alkaline and transitional series (Sardinia, Sicily, Sicily Channel), crustal anatectic (Elba, Giglio), K-alkaline (Tuscany, Umbria, Ernice-Roccamonfina, Vultur) and tholeiitic (Montferro) sources. Only the Aeolian Arc, Roman Province and part of Campania in southern Italy display similar geochemistry (Keller et al., 1978; Pichler, 1981; Paterne et al., 1988; Narcisi and Vezzoli, 1999; Peccerillo, 2005; Forni, 2011;

Albert et al., 2017). Mount Etna was initially assumed to be a major source due to its close proximity to the research areas and its enormous eruption rates during the past four centuries (Condomines and Tanguy, 1995). However, while the lapilli layers do seem to be derived from Etna (Figs. 5 and 6), the generally alkaline to tholeiitic series volcanism (Peccerillo, 2005) does not fit with the rest of the soil data (Fig. 8a). Albert et al. (2013) analysed volcanic glasses from the Biancavilla ignimbrites and Unit D Plinian fall deposits of Mt. Etna. These deposits can be ascribed to the explosive activity (about 17–19 ka BP) within the predominantly effusive and mildly explosive (Strombolian) volcanic history of Mount Etna. The explosive eruptions from Etna are considered responsible for widespread ash dispersals throughout the central Mediterranean region, producing marker tephra layers. Compared to other eruptions from Mt. Etna, the chemical composition of the Biancavilla ignimbrites is more evolved and acidic. The Biancavilla ignimbrites and Unit D Plinian fall deposits have a SiO₂ content in the range of about 60–64% and a Na₂O + K₂O content in the range of 8.9–9.9% (Albert et al., 2013). According to our LA-ICP-MS analyses, part of the volcanic particles (pumice) can be most likely ascribed to this Biancavilla ignimbrites and Plinian eruptions. Mt. Etna therefore has contributed to the volcanic deposits of the Nebrodi mountains and maybe also to the deposits in the Sila mountains.

The high-K calc-alkaline to shoshonite series composition of the soils (Fig. 8a) are, however, also typical for island arcs and subduction magmatism (Joplin, 1968; Morrison, 1980; Pichler, 1981) and match Campania and Aeolian Arc volcanism. This is demonstrated in the Ti/Nb – Ti/Zr, Rb-Co, Ce/TiO₂ – TiO₂ plots (Fig. 6a and d and Fig. 7c). Zr/Rb versus Th/Rb and K₂O/Na₂O versus K₂O + Na₂O (Fig. 7a; Paterne et al., 1988) also indicate that the soils of Nebrodi and Sila were strongly affected by the Aeolian Arc during their pedogenesis. This agrees well with Scarciglia et al. (2008) who suggested that the volcanic ash fragments of the Sila uplands derive from the Aeolian Arc, particularly from Lipari as the main source. However, as described above, the chemistry of the lapilli strongly differs from the soil (Table 4). The analysed lapilli fragments found in the soil of Nebrodi II appear to derive from Sicily (Fig. 6a–d and Fig. 7a, c) suggesting input from Mount Etna. In a next step, a discrimination between the different volcanoes of the Aeolian Arc was undertaken.

According to Pichler (1967), the volcanic archipelago of the seven Aeolian Islands has always been separated into two groups based on their chemical composition. The first group (A) consists of the islands of Lipari, Salina, Filicudi, Alicudi and Panarea-Basiluzzo, while the other (B) includes the islands of Vulcano and Stromboli. Group A is characterised by a normal-calk-alkaline magma, except for the high-K calc-alkaline (to shoshonitic) volcanic activity epochs II, V, VI and VII (Fig. 10) of Lipari (Pichler, 1981; Forni et al., 2013). Group B has a potassium-rich calc-alkaline magma development (Pichler, 1981). According to several studies (e.g. Joplin, 1968; Munno et al., 1980; Pichler, 1981; Bertagnini et al., 2008), the islands Stromboli and Vulcano clearly differentiate themselves from the rest of the Aeolian volcanoes due to their strong shoshonitic signatures (Joplin, 1968; Bertagnini et al., 2008; De Astis et al., 2013; Francalanci et al., 2013). Shoshonites are basaltic rocks rich in potassium and classified as trachyandesite (Joplin, 1968; Munno et al., 1980; Pichler, 1981). The majority of the Nebrodi samples fit the field of trachyandesite. This is in contrast to the Sila samples that seem to be related to the rhyolite/dacite field (Fig. 8b). Dacite and andesite rocks are typical for the epochs IV, V and VI, whereas the epochs VII–IX of Lipari are dominated by dacite to rhyolite effusive rocks (Forni et al., 2013). The eruptive history of Vulcano predominantly consists of shoshonites, basalts and a minor amount of trachyte (-andesite) (De Astis et al., 2013). From a forensic point of view, the most likely volcanic sources of the investigated samples are several epochs of Lipari and Vulcano. Based on the data of Pichler (1984), the investigated samples are chemically close to Vulcano and Lipari phase IIB and the epochs V and VI of Lipari (Fig. 10; Forni et al., 2013). Taking into account that the Nebrodi samples even

Table 6
Major, minor and trace elements data measured by LA-ICP-MS on glass shards from Nebrodi soil samples.

Profile	Nebrodi I			Nebrodi I	Nebrodi IV	
Horizon	A2 (20–50 cm)			A4 (90–130 cm)	A1 (0–20 cm)	
Material	Glass I (n = 5)	Glass II (n = 3)	Volcanic clast I (n = 2)	Volcanic clast II (n = 6)	Glass III (n = 3)	Pumice I (n = 2)
Major elements (wt-%)						
SiO ₂	71.17 ± 0.16	72.20 ± 0.07	54.86 ± 1.55	54.00 ± 1.78	72.03 ± 0.85	52.48 ± 4.28
TiO ₂	0.08 ± 0.00	0.07 ± 0.00	1.10 ± 0.03	1.65 ± 0.22	0.08 ± 0.01	0.81 ± 0.07
Al ₂ O ₃	13.82 ± 0.16	13.34 ± 0.10	22.11 ± 3.54	15.9 ± 1.61	13.53 ± 0.39	23.41 ± 2.15
FeO	1.64 ± 0.10	1.54 ± 0.01	7.10 ± 3.07	7.70 ± 1.33	1.61 ± 0.03	9.57 ± 0.05
MnO	0.07 ± 0.00	0.06 ± 0.00	0.21 ± 0.15	0.17 ± 0.05	0.07 ± 0.01	0.26 ± 0.02
MgO	0.04 ± 0.00	0.04 ± 0.00	1.68 ± 0.17	2.70 ± 1.00	0.06 ± 0.02	2.63 ± 0.01
CaO	0.81 ± 0.05	0.75 ± 0.03	2.81 ± 1.95	6.83 ± 1.86	0.74 ± 0.06	4.66 ± 2.09
Na ₂ O	4.36 ± 0.01	4.07 ± 0.04	4.24 ± 2.86	4.75 ± 0.58	4.03 ± 0.23	0.54 ± 0.02
K ₂ O	5.02 ± 0.11	4.92 ± 0.10	2.88 ± 0.61	3.29 ± 0.47	4.83 ± 0.24	2.63 ± 0.12
Total	97.0	97.0	97.0	97.0	97.0	97.0
Trace elements (µg/g)						
V	0.9 ± 0.31	0.6 ± 0.03	128.0 ± 84.70	237.1 ± 58.08	2.9 ± 2.53	179.9 ± 3.4
Co	0.4 ± 0.09	0.3 ± 0.05	15.8 ± 11.97	18.1 ± 2.95	0.9 ± 0.77	21.5 ± 0.8
Rb	302.5 ± 8.27	304.4 ± 2.59	116.5 ± 59.12	75.7 ± 11.56	293.4 ± 13.85	227.7 ± 12.9
Sr	18.3 ± 1.93	16.0 ± 0.15	614.8 ± 354.51	1179.7 ± 127.62	17.2 ± 0.54	262.8 ± 83.1
Y	45.6 ± 0.71	45.1 ± 0.61	28.7 ± 0.42	34.8 ± 8.87	43.5 ± 1.35	153.4 ± 77.4
Zr	189.6 ± 1.50	187.2 ± 3.26	272.6 ± 131.10	310.5 ± 36.85	183.0 ± 5.93	112.3 ± 9.6
Nb	36.5 ± 0.71	35.7 ± 0.73	72.7 ± 33.56	97.1 ± 18.01	34.9 ± 0.11	34.7 ± 2.5
Cs	16.9 ± 0.48	17.1 ± 0.25	5.2 ± 6.23	1.8 ± 0.22	16.6 ± 0.60	10.0 ± 1.3
Ba	16.6 ± 1.01	14.3 ± 0.15	1009.1 ± 430.13	1214.0 ± 186.90	21.1 ± 5.93	606.7 ± 76.3
La	58.0 ± 0.61	57.2 ± 0.47	95.5 ± 4.99	117.9 ± 17.56	56.7 ± 1.76	442.8 ± 233.9
Ce	115.1 ± 2.77	111.4 ± 0.71	171.1 ± 5.75	217.9 ± 41.85	109.4 ± 3.61	391.1 ± 173.8
Pr	12.3 ± 0.34	12.0 ± 0.20	17.3 ± 0.62	23.0 ± 4.78	11.7 ± 0.31	72.4 ± 35.8
Nd	43.5 ± 0.84	42.3 ± 0.33	61.2 ± 2.70	86.0 ± 18.84	40.9 ± 2.03	257.0 ± 128.6
Sm	9.0 ± 0.13	8.5 ± 0.36	10.2 ± 0.27	14.4 ± 3.67	8.3 ± 0.82	45.0 ± 22.1
Eu	0.2 ± 0.01	0.1 ± 0.03	2.7 ± 0.52	3.7 ± 0.32	0.2 ± 0.04	10.6 ± 5.9
Gd	7.7 ± 0.11	7.1 ± 0.15	7.7 ± 0.17	10.9 ± 2.86	7.5 ± 0.69	38.2 ± 18.8
Tb	1.1 ± 0.03	1.1 ± 0.02	1.0 ± 0.01	1.3 ± 0.32	1.1 ± 0.15	5.0 ± 2.8
Dy	7.4 ± 0.20	7.0 ± 0.21	5.5 ± 0.01	7.0 ± 1.97	7.0 ± 0.10	24.9 ± 11.4
Ho	1.5 ± 0.03	1.4 ± 0.08	1.0 ± 0.03	1.3 ± 0.34	1.5 ± 0.04	4.2 ± 2.0
Er	4.8 ± 0.09	4.8 ± 0.22	2.8 ± 0.12	3.4 ± 1.11	4.7 ± 0.24	10.8 ± 5.3
Tm	0.7 ± 0.02	0.7 ± 0.02	0.4 ± 0.02	0.4 ± 0.12	0.7 ± 0.02	1.3 ± 0.6
Yb	5.0 ± 0.18	5.1 ± 0.27	2.5 ± 0.10	2.6 ± 0.65	4.9 ± 0.13	7.7 ± 3.6
Lu	0.7 ± 0.02	0.7 ± 0.04	0.3 ± 0.00	0.4 ± 0.10	0.7 ± 0.01	1.1 ± 0.4
Hf	6.7 ± 0.07	6.8 ± 0.27	5.6 ± 2.21	6.2 ± 1.01	6.6 ± 0.47	2.3 ± 0.3
Ta	2.4 ± 0.01	2.3 ± 0.07	3.4 ± 1.62	4.4 ± 0.78	2.4 ± 0.05	1.5 ± 0.2
Pb	30.8 ± 1.48	32.3 ± 2.61	43.6 ± 41.73	17.4 ± 0.70	30.2 ± 0.62	76.2 ± 16.3
Th	55.7 ± 0.25	54.0 ± 0.41	20.6 ± 1.14	15.3 ± 1.19	53.9 ± 1.75	18.4 ± 5.1
U	15.9 ± 0.44	15.1 ± 0.27	5.9 ± 0.73	5.9 ± 0.86	15.0 ± 0.19	9.5 ± 3.8

showed a stronger inclination to Lipari using the Th – Th/U plot (Fig. 8e), we suggest that Lipari is the main source for both sites.

Several horizons seemed to be purely composed of volcanic material while some were a mixture (volcanic material mixed with the in situ parent material). Given a known ‘parent material’ at the sites of interest, the proportion of volcanic material in the soils of Nebrodi and Sila can be roughly estimated. Having a mixture of two different materials, their proportion can be estimated by using inert components under the prevailing weathering conditions (Sommer et al., 2000). Based on the available data and using the concept of weathering indices, Al₂O₃ and TiO₂ were used as tracers. Using a mass balance approach, we have:

$$a\text{Al}_2\text{O}_3(\text{pm}) + b\text{Al}_2\text{O}_3(\text{v}) = c\text{Al}_2\text{O}_3(\text{fe}) \quad (7)$$

$$a\text{TiO}_2(\text{pm}) + b\text{TiO}_2(\text{v}) = c\text{TiO}_2(\text{fe}) \quad (8)$$

$$a + b = 1 \quad (9)$$

where *a* is the relative proportion of the parent material and *b* is the relative proportion of the volcanic source (Aeolian Islands; Lipari; data from Mirabella et al., 2005 and Peccerillo, 2005). The letter *c* denotes the weathering coefficient of the soil; Al₂O₃(pm), Al₂O₃(v), TiO₂(pm) and TiO₂(v) are the contents of the parent material (pm) and volcanic source (v). Al₂O₃(fe) and TiO₂(fe) are the contents in the fine earth of

the soil. Solving the three linear equations with three unknown results in (Sommer et al., 2000):

$$c = \frac{\text{TiO}_2(\text{v})[\text{Al}_2\text{O}_3(\text{pm}) - \text{Al}_2\text{O}_3(\text{v})] - \text{Al}_2\text{O}_3(\text{v})[\text{TiO}_2(\text{pm}) - \text{TiO}_2(\text{v})]}{\text{TiO}_2(\text{fe})[\text{Al}_2\text{O}_3(\text{pm}) - \text{Al}_2\text{O}_3(\text{v})] - \text{Al}_2\text{O}_3(\text{fe})[\text{TiO}_2(\text{pm}) - \text{TiO}_2(\text{v})]} \quad (10)$$

and

$$a = \frac{c\text{Al}_2\text{O}_3(\text{fe}) - \text{Al}_2\text{O}_3(\text{v})}{\text{Al}_2\text{O}_3(\text{pm}) - \text{Al}_2\text{O}_3(\text{v})} \quad (11)$$

Due to the high heterogeneity of the soils, it is difficult to assign a single parent material: in the case of Nebrodi II, four different substrates along the profile were defined and for Nebrodi IV even six (Tables 2 and 4; Fig. 2d). In such cases, we assumed that the horizon directly underlying the ash is indicative of the ‘parent material’ (the likelihood seems to be greatest that ash deposits were mixed with this layer). In several cases (Table 11), the source material of the topsoil and parts of the subsoil seem to originate up to 100% from Lipari. In general, the proportion of ash increases towards the surface, matching the macromorphological examinations (Fig. 2). In addition, we also calculated the proportion of the Biancavilla ignimbrites and Unit D Plinian fall deposits on the soil composition (A horizons). Compared to Lipari, the geochemical overlap of the Biancavilla eruptions with the

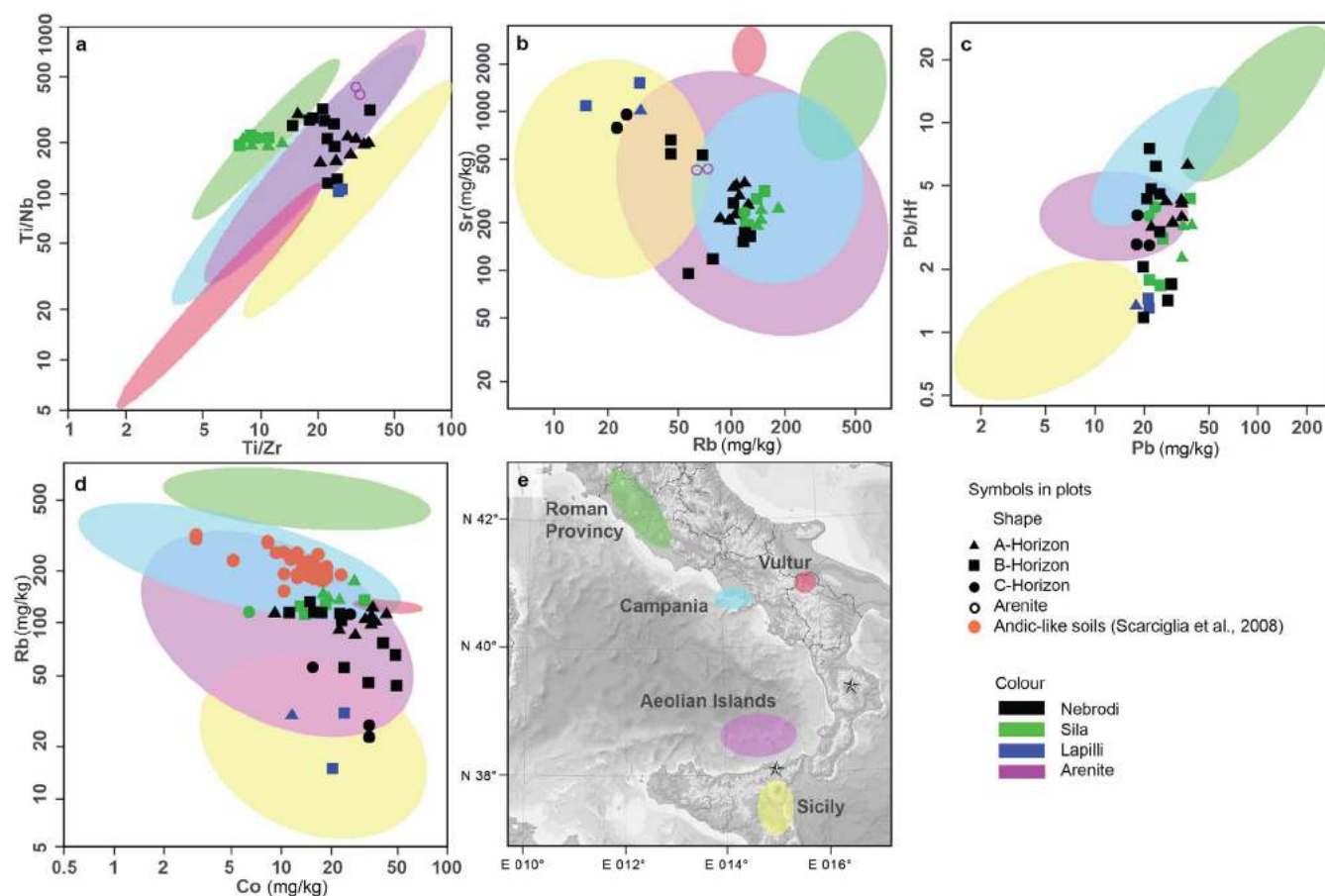


Fig. 6. Geochemical forensics based on a comparison between the a) Ti/Nb-ratio and Ti/Zr-ratio, b) Sr vs Rb, c) Pb/Hf-ratio vs Pb and d) Rb vs Co. e) The coloured fields are used as a reference for the corresponding volcanic areas based on data of Peccerillo (2005). The two stars mark the locations of the investigation sites Nebrodi and Sila mountains. In addition, the values given in Scarciglia et al. (2008) are also plotted. (For interpretation of the references to colour in this figure legend, the reader is referred to the web version of this article.)

investigated soils is small. At some sites, the Biancavilla ignimbrites and Unit D Plinian fall deposits may explain up to 80% of the main geochemical composition, while at other sites they are absent. The explanatory power of the Biancavilla ignimbrites and Unit D Plinian fall deposits on the geochemical composition of the soils seems therefore lower compared to the Lipari effusiva. It is, however, still very likely that the Biancavilla and Plinian eruptions have contributed (to a smaller extent) to the volcanic deposits on the Sila and Nebrodi mountains. Due to bioturbation, erosion and chemical weathering, such volcanic deposits are partially mixed with older volcanic deposits. It seems that the predominant source of volcanogenic material are the Aeolian Islands with some contributions from the Etna.

4.3. Age estimates from weathering indices

Scarciglia et al. (2008) estimated the age of the volcanic deposits in the Sila mountains (start of formation of ando-like soils) by radiocarbon dating charcoal. Three charcoal fragments were taken from mineral horizons of three different soil profiles (samples from a surface horizon, a buried horizon and from a subsurface horizon), yielding ages between 3383–3355 to 254–33 ka cal BP (Table 7). However, clay coatings found in the ando-like soil horizons together with their stratigraphic position overlying a rubified soil of the last Interglacial imply an older, not clearly defined time range, from the Late Pleistocene to the Holocene. Based on this, the authors hypothesised that the volcanic ash contributions probably derived from the Aeolian Arc explosive activity spanning the last 30 ka. Pelle et al. (2013) refined this interpretation, suggesting a slightly older input of pyroclastics dating back to the last 42 ka.

Our approach, by using the H_2O_2 -resistant organic matter fraction as an approximate indicator for the start of soil formation (Favilli et al., 2009a, 2009b) gave an age of about 8.2 ka cal BP for the Sila volcanic ash deposits and about 9.6 ka cal BP for the Nebrodi ash deposits (Table 8). The $\delta^{13}C$ values of the H_2O_2 -resistant carbon indicate in most cases C4 plants, except for Nebrodi I and III. This might be due either to a fractionation during adsorption or due to a former cultivation with C3 plants which has been quite common in Sicily since the Islamic period (Egli et al., 2013). While older than the radiocarbon data (3.1 ka BP) of Scarciglia et al. (2008) and estimates from archaeological finds in the same soils (\leq ca. 5.8 ka BP; Pelle et al., 2013), our H_2O_2 -resistant radiocarbon results still indicate a purely Holocene age (Table 8). Recent charcoal dating in these soils has yielded ages of up to 5 ka in the A horizon and up to about 14 ka cal BP in the underlying B horizon (Moser et al., 2017; Table 7), hinting again that the ash deposits must already have been present in the Late Pleistocene. In general, ^{14}C -ages of charcoal increased with increasing depth due to bioturbation, transport in macropores and accumulation of aeolian deposits on top. Remote aeolian transport of macrocharcoal can be usually excluded (Carcaillet and Brun, 2000; Lynch et al., 2004; Favilli et al., 2010).

To help refine the chronology of these soils, we also estimated the age of the volcanic deposits using an empirical relation to the WIP weathering indices (Fig. 9). These ages could then be correlated to the activity phases of the volcanoes of the Aeolian Arc (Fig. 10). Compared to other weathering indices, the WIP better copes with inhomogeneities of the samples (Price and Velbel, 2003). Soil genesis on the Sila mountains started between 45–49 ka BP based on WIP-derived ages and seems to have been influenced by the Aeolian Arc explosive activities (Table 10) over at least the last about 50 ka (Table 11). This fits nicely

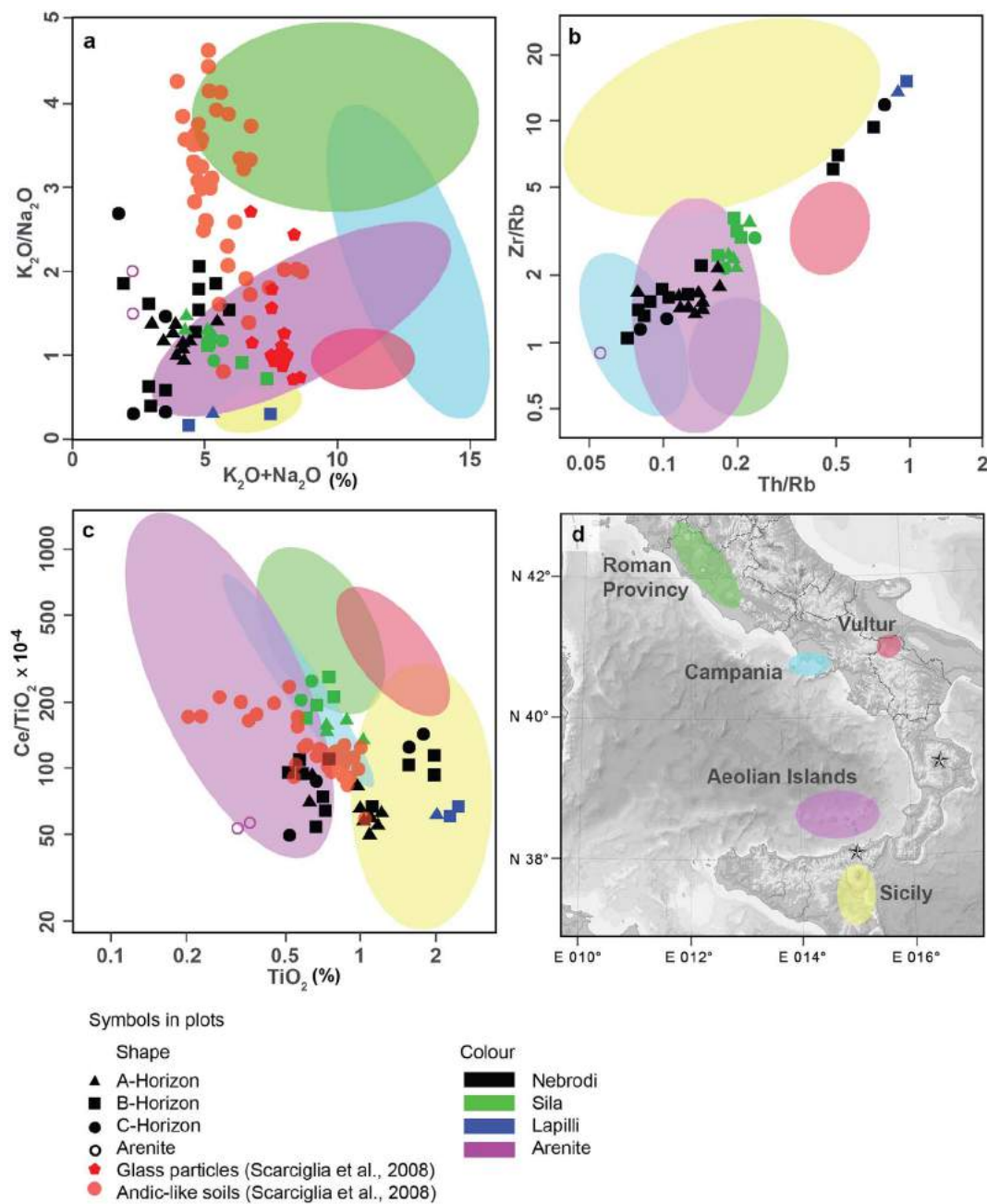


Fig. 7. Geochemical forensics based on a comparison between a) the alkali ratio (K_2O/Na_2O) vs total alkali diagram ($K_2O + Na_2O$) according to Paternite et al. (1988), b) Zr/Rb- vs Th/Rb-ratio and c) Ce/ TiO_2 -ratio vs TiO_2 . d) The coloured fields are used as a reference for the corresponding volcanic areas based on data of Peccerillo (2005). The two stars mark the locations of the investigation sites Nebrodi and Sila mountains. In addition, the values given in Scarciglia et al. (2008) are also plotted. (For interpretation of the references to colour in this figure legend, the reader is referred to the web version of this article.)

with the first estimates done by Scarciglia et al. (2008) and Pelle et al. (2013). On the Nebrodi mountains, the influence of the Aeolian Arc seems to have started even earlier (70 ka BP). The geochemistry (major and trace elements) of volcanic clasts (Table 6), furthermore, fits best with the eruption epoch 6 of Lipari (mostly between 81 and 92 ky BP; Forni, 2011). The glass components in the soils seem to have a younger age and fit nicely with the eruption epochs 7–9 (< 70–1 ka BP). The pumice-like components can be attributed to the Biancavilla and Plinian eruptions (ca. 17–19 ka BP; Albert et al., 2013).

The apparent inconsistencies between the radiocarbon dates and geochemical indices-estimated ages can have several reasons. It seems that a considerable part of the volcanic deposits has its origin in older eruptive epochs of the Pleistocene (roughly between 80 and 90 ka PB; Table 10). Between the Late Pleistocene and Holocene, several

additional eruptive epochs of the Aeolian Islands (epochs 7–9, according to Forni, 2011) and Etna (particularly the Biancavilla and Plinian eruptions; Albert et al., 2013) have occurred. The dated charcoal pieces fall into this second period. Charcoal and soil organic matter of the earlier phase was most likely not conserved (it furthermore would be out of the dating range of ^{14}C). The fate of soil organic matter also depends on the strong chemical interactions during weathering. Decay of soil organic matter on 10 ka timescales or mineral transformation and surface properties changes may have released strongly bound organic phases (Torn et al., 1997; Kleber et al., 2007). It is, furthermore, likely that macro-charcoal is not that stable in these environments (only very few samples had an age of > 8 ka; Moser et al., 2017; Table 7). This is probably related to a bad preservation of charcoal. De Lafontaine et al. (2011) suggested that the permineralization process increases the

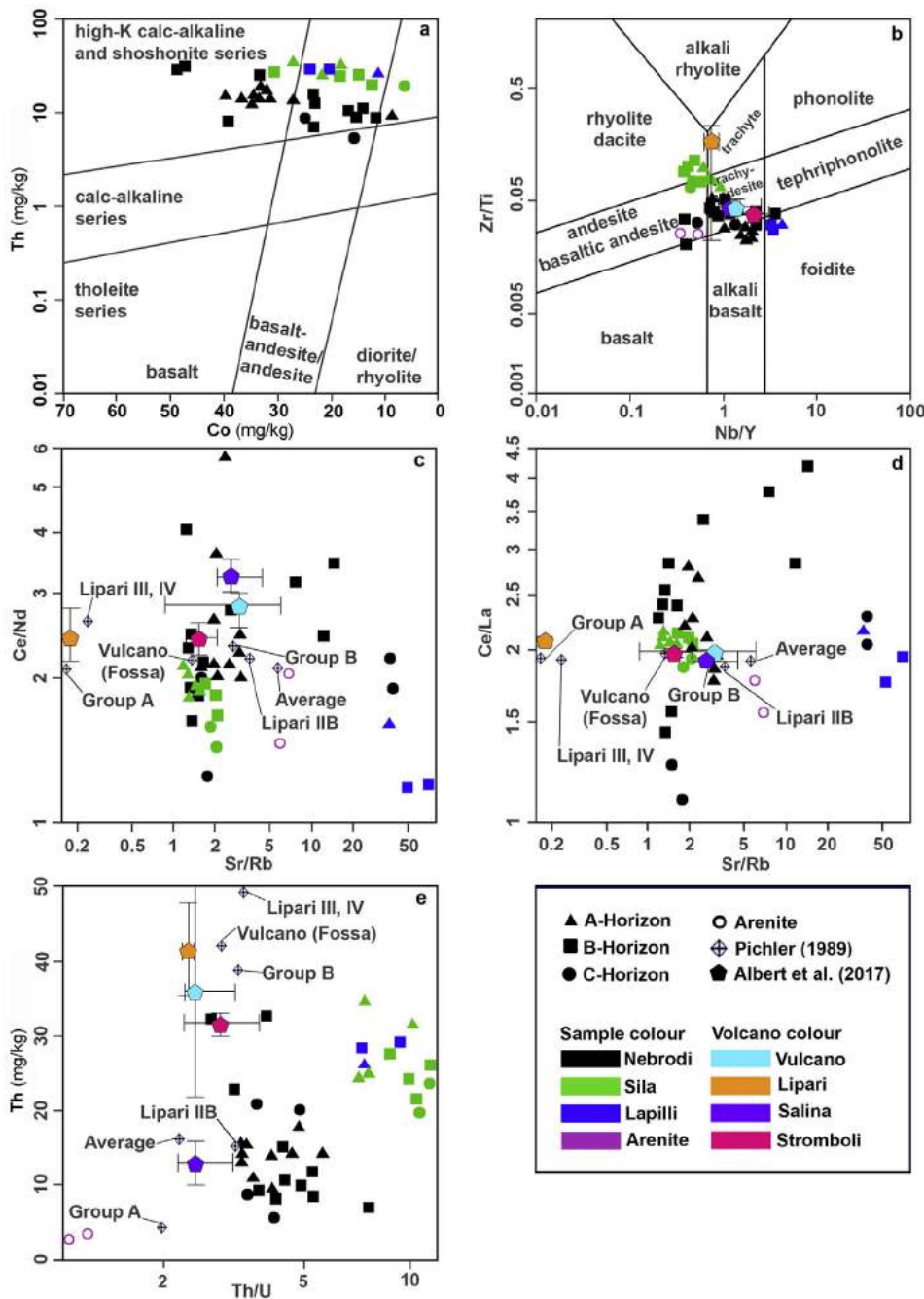


Fig. 8. Geochemical forensics based on a) the Co-Th plot after Hastie et al. (2007), b) Zr/Ti-ratio against Nb/Y-ratio plot after Pearce (1996), c) and d) Ce/Nd-ratio and Ce/La-ratio vs the Sr/Rb-ratio and e) Th vs Th/U-ratio. Group A includes the Aeolian Islands Lipari, Salina, Fillicudi, Alicudi, Panare-Basiluzzo and Group B Lipari IB, III, IV (equals the epochs I, VIII and IX after Forni et al. (2013)), Vulcano and Stromboli (Pichler, 1989).

density of charcoal particles and thus offers a protection against subsequent degradation. This fossilisation process consists in concealing wood structures by massive mineral filling inside the cavities. Charcoal fragments are, furthermore, well preserved in acidic environments (Weiner et al., 1993; Karkanas et al., 2000). Under only slightly acidic conditions (as at the investigation sites), the preservation is therefore not optimal.

By cross-referencing the estimated time windows based on the WIP, the calculated ages would fit best with the eruption epochs of Vulcano, Lipari and Alicudi (Fig. 10), and partially with Stromboli. Forni et al. (2013) described the epoch V of Lipari as recurrent hydromagmatic explosions and the epoch VI of Lipari as Vulcanian-type explosive phases. De Astis et al. (2013) stated that the eruptions of epoch III of Vulcano were effusive and coupled with a hydromagmatic phase. All of these epochs had a high-K calc-alkaline volcanism, although Vulcano had a tendency towards a shoshonite composition (De Astis et al., 2013;

Forni et al., 2013). Based on these findings, the epochs VI–IX of Lipari were probably the main sources for the Sila soils with the epoch VI of Lipari together with some input of the Etna influencing Nebrodi. Volcanism from Vulcano cannot be fully excluded from having contributed to the volcanic deposits of the study areas.

5. Conclusions

Using a multi-method approach, the origin and age of soils formed from volcanic deposits in southern Italy could be tentatively determined. When comparing soil material with volcanic deposits, the main geochemical composition may be used as a forensic indicator. However, due to weathering and leaching processes, the composition of soils might be altered. It is therefore strongly recommended to use alternative tracers for determining the origin of volcanic deposits such as relatively ‘immobile’ elements and their ratios among each other (e.g.

Table 7

Radiocarbon dates of charcoal found in the soils of the Sila highland. Datasets are from Moser et al. (2017), Scarciglia et al. (2008) and new measurements.

Soil profile	Lab reference	Horizon	Charcoal (Taxon)	C-14 age (y BP)	$\delta^{13}\text{C}$ (‰)	Calibrated age 2 σ (95.4%)
Moser et al. (2017)						
CL1	KIA45420	A2	Pinus group sylvestris	1051 ± 25	-24.80 ± 0.14	1051–930
	KIA45421	A3	Deciduous <i>Quercus</i>	4200 ± 30	-25.10 ± 0.15	4843–4627
	KIA47441(1)	A3	Pinus group sylvestris	2430 ± 30	-21.91 ± 0.11	2699–2354
	KIA47441(2)	A3	n.i.	2695 ± 30	-23.44 ± 0.19	2850–2755
	KIA50234(1)	A3	Pinus group sylvestris	3000 ± 40	-23.86 ± 0.13	3316–3080
	KIA50234(2)	A3	n.i.	3020 ± 25	-21.63 ± 0.14	3337–3083
	KIA48518	2Bw1	Deciduous <i>Quercus</i>	4065 ± 30	-24.30 ± 0.17	4799–4437
	KIA48519(1)	2Bw1	Deciduous <i>Quercus</i>	4305 ± 25	-24.52 ± 0.20	4960–4832
	KIA48519(2)	2Bw1	n.i.	4355 ± 30	-24.36 ± 0.15	5032–4851
	KIA48520	2Bw1	Pinus group sylvestris	8895 ± 45	-23.79 ± 0.17	10193–9794
	POZ-59596	A1	Pinus group sylvestris	125 ± 30		273–10
	POZ-59597	A2	Pinus group sylvestris	155 ± 30		285–modern
	KIA48512	A2	Deciduous <i>Quercus</i>	2845 ± 25	-27.77 ± 0.19	3056–2872
	KIA48513(1)	Bw	<i>Abies</i>	6760 ± 30	-24.22 ± 0.13	7666–7576
KIA48513(2)	Bw	n.i.	6675 ± 30	-24.81 ± 0.13	7591–7489	
KIA48514	Bw	<i>Juniperus</i>	6975 ± 35	-24.08 ± 0.22	7926–7705	
POZ-59598	Bw3	<i>Juniperus</i>	8270 ± 50		9430–9091	
CL3	KIA48516	2Ab	<i>Abies</i>	8170 ± 50	-24.93 ± 0.14	9269–9010
	KIA48515	2Ab	Deciduous <i>Quercus</i>	8920 ± 100	-26.74 ± 0.11	10242–9695
	KIA48517	2Bwb	Deciduous <i>Quercus</i>	8820 ± 55	-22.56 ± 0.12	10158–9682
CL4	KIA48507	A	<i>Abies</i>	3465 ± 35	-23.97 ± 0.10	3834–3640
	KIA48508(1)	2Bw	<i>Abies</i>	8430 ± 40	-24.88 ± 0.12	9530–9324
	KIA48508(2)	2Bw	n.i.	8525 ± 50	-24.06 ± 0.16	9554–9453
	KIA48509	2Bw	<i>Juniperus</i>	12180 ± 60	-21.52 ± 0.20	14245–13835
	KIA48510	2Bt	<i>Abies</i>	7245 ± 36	-24.06 ± 0.26	8164–7982
CL5	POZ-59591	Ap	<i>Fagus sylvatica</i>	230 ± 30		421–modern
	POZ-59592	Bw1	Pinus group sylvestris	330 ± 30		473–308
	KIA48050	Bw2	<i>Cornus</i>	2015 ± 25	-28.16 ± 0.21	2039–1895
	KIA48051(1)	Bw2	<i>Juniperus</i>	2865 ± 30	-24.85 ± 0.14	3072–2879
	KIA48051(2)	Bw2	n.i.	2740 ± 30	-24.24 ± 0.12	2920–2765
	KIA48051(3)	Bw2	n.i.	2465 ± 30	-25.03 ± 0.25	2713–2379
	KIA48051(4)	Bw2	n.i.	2805 ± 30	-23.38 ± 0.25	2995–2804
	POZ-59593	Bw2	<i>Abies</i>	2475 ± 30		2720–2380
	POZ-59595	C	<i>Juniperus</i>	5215 ± 35		6173–5908
	BETA - 320186	C	<i>Juniperus</i>	6480 ± 40	-24.80 ± 0.00	7470–7310
	BETA - 320187	Ab	Leguminosae	810 ± 30	-22.80 ± 0.00	781–681
	KIA48052(1)	Ab	Leguminosae	1250 ± 25	-24.10 ± 0.20	1273–1084
	KIA48052(2)	Ab	n.i.	1240 ± 25	-22.48 ± 0.13	1265–1075
	BETA - 320188	ABb	<i>Abies</i>	4130 ± 30		4821–4532
	KIA48053(1)	ABb	Deciduous <i>Quercus</i>	3510 ± 30	-23.69 ± 0.15	3867–3697
	KIA48053(2)	ABb	n.i.	3455 ± 30	-23.99 ± 0.15	3828–3640
	KIA48054	ABb	<i>Juniperus</i>	3810 ± 80	-25.05 ± 0.23	4420–3981
Scarciglia et al. (2008)						
C1	DSA983		n.i.	342 ± 16		457–320
C2	DSA985		n.i.	3135 ± 18		3383–3355
C3	DSA986		n.i.	92 ± 24		254–modern
New measurements						
CL4	60–80 (1)	2Bw	n.i.	3565 ± 22	-22.0 ± 1.0	3960–3734
	60–80 (2)	2Bw	n.i.	3620 ± 24	-26.3 ± 1.0	4059–3852
CL5	80–90	Bw2	n.i.	6568 ± 26	-28.8 ± 1.0	7555–7427

n.i. = not identified.

Table 8

Radiocarbon dating of the H₂O₂-resistant soil organic matter at the Nebrodi and Sila sites together with one additional site (CL5, Sila, according to Moser et al., 2017).

Soil	Horizon	Depth (cm)	Material	C-14 age (y BP)	$\delta^{13}\text{C}$ (‰)	Calibrated ages (cal BP)	
						1 σ (68.2%)	2 σ (95.4%)
Nebrodi I	A1	0–20	Volcanic soil	470 ± 30	-14.0 ± 1.0	525–505	541–493
	A2	20–50	Volcanic soil	1565 ± 35	-7.7 ± 1.0	1521–1411	1538–1381
Nebrodi III	A1	0–50	Volcanic soil	2850 ± 35	-12.7 ± 1.0	3004–2884	3066–2867
	A2	50–75	Volcanic soil	4562 ± 29	-15.9 ± 1.0	5315–5085	5437–5057
	Bw	75–110	Volcanic soil	8607 ± 35	-21.2 ± 1.0	9595–9531	9662–9524
Nebrodi IV	A1	0–20	Volcanic soil	1810 ± 30	-17.4 ± 1.0	1810–1709	1823–1628
Sila I	A1	0–20	Volcanic soil	725 ± 30	-19.8 ± 1.0	686–663	725–570
	Bw	40–60	Volcanic soil	7345 ± 33	-28.0 ± 1.0	8195–8051	8292–8030
Sila II	A1	0–20	Volcanic soil	380 ± 30	-19.0 ± 1.0	500–333	505–319
CL5	Ab	130–150	Volcanic soil	1608 ± 23	-22.1 ± 1.0	1545–1419	1553–1415

Table 9

Comparison of several chemical weathering indices along the investigated soil profiles: Index B (Kronberg and Nesbitt, 1981); molar (K + Ca)/Ti ratio (Egli et al., 2008); CIA = chemical index of alteration (Nesbitt and Young, 1982); CIW = chemical index of weathering (Harnois, 1988); PIA = plagioclase index of alteration (Fedo et al., 1995); WIP = weathering index of Parker (Parker, 1970; Price and Velbel, 2003); CPA = chemical proxy of alteration (Buggle et al., 2011).

Site	Horizon	Index B (–)	(K + Ca)/Ti (–)	CIA (%)	CIW (%)	PIA (%)	WIP (–)	CPA (%)
Nebrodi I	A1	0.33	3.30	67.2	73.2	70.5	42.0	84.3
	A2	0.30	2.91	69.9	76.3	73.9	41.9	85.6
	A3	0.30	2.93	70.4	76.7	74.4	40.8	86.1
	A4	0.31	2.99	69.5	75.4	73.1	43.8	85.0
	AB	0.29	5.06	70.7	79.2	76.3	47.8	87.0
	Bw	0.31	5.56	68.8	78.1	74.7	47.5	86.9
Nebrodi II	A1	0.33	4.14	67.4	73.9	71.1	40.0	87.4
	A2	0.28	3.11	71.6	77.0	75.2	36.6	88.6
	2BA	0.21	1.44	79.0	81.9	81.2	33.0	89.1
	2Bw	0.20	1.47	79.9	82.0	81.5	31.0	89.6
	3BC	0.27	3.25	72.8	81.7	79.1	23.6	87.5
	4BC	0.23	2.45	77.4	84.9	83.3	18.0	91.6
Nebrodi III	A1	0.33	5.53	67.5	77.0	73.3	48.6	83.4
	A2	0.25	2.59	75.0	81.8	80.0	42.0	87.4
	Bw	0.24	2.87	76.1	82.5	80.9	42.9	88.5
	2BCg	0.32	5.76	68.3	78.8	75.0	49.2	83.7
	2BC	0.31	6.44	69.4	80.4	76.7	47.7	85.9
	3BC	0.28	4.47	72.1	82.7	79.7	43.1	88.3
Nebrodi IV	A1	0.35	4.28	64.5	73.0	68.9	42.7	82.0
	A2	0.26	2.49	74.4	81.5	79.5	32.8	88.6
	2Btm	0.25	1.98	75.2	78.3	77.4	33.0	88.9
	3Co	0.33	3.03	67.5	69.4	68.5	44.5	84.7
	4Co	0.23	1.70	77.2	78.7	78.3	29.0	89.5
	5Co	0.32	3.66	68.1	77.3	73.7	34.3	84.5
Sila I	6C	0.24	2.67	76.1	85.7	83.6	17.5	92.3
	A1	0.32	5.65	67.6	74.3	71.5	45.3	86.4
	A2	0.32	6.04	67.8	74.8	71.9	46.2	87.3
	Bw	0.34	8.78	66.1	72.3	69.4	53.7	86.1
	2Bw	0.35	8.65	65.2	71.2	68.3	55.4	85.8
	2C	0.38	10.96	61.8	68.0	64.4	59.5	84.0
Sila II	A1	0.29	4.82	71.2	77.4	75.2	45.9	88.2
	A2	0.31	6.64	69.2	74.8	72.6	49.1	88.1
	Bw	0.36	9.78	63.9	68.9	66.3	57.4	84.5
	2Bw	0.37	10.37	63.0	67.5	65.0	64.1	82.1
Lapilli ^a	2C	0.36	10.21	63.8	68.7	66.1	58.5	84.8
	2BA	0.42	2.64	58.3	60.8	59.1	67.4	75.7
	2Bw	0.48	3.43	52.2	54.6	52.4	75.1	71.5
Bedrock ^b	2Bw	0.35	1.92	64.6	65.9	65.2	60.0	79.2
		0.81	66.91	18.7	19.4	16.4	104.4	85.6

^a Lapilli of the Nebrodi II site.

^b Bedrock average of the Monti Nebrodi sites.

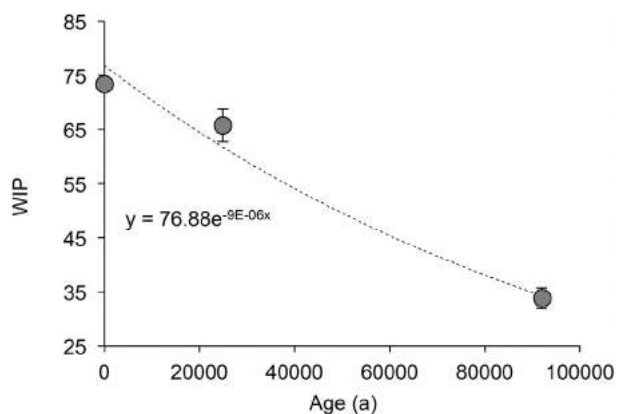


Fig. 9. Chronosequence based on data of Mirabella et al. (2005) that was used to estimate the ages of the volcanic deposits using the WIP (weathering index of Parker).

Table 10

Age estimation using the WIP (Parker, 1970; Price and Velbel, 2003). Data from Mirabella et al. (2005) was used for calibration (chemical data and numeric age indications are given) due to its close proximity to the investigation sites and favourable volcanic area. The calculation is based on the chemical composition of the A and AB (or Bw) horizons. The other horizons were excluded because they contain arenite, marl, lapilli (from the Etna) or granite (local bedrock). In addition, the timing of deposition was estimated using the chemical composition of volcanic clasts and glasses based on LA-ICP-MS measurements and SEM-EDS data (new and published data (Scarciglia et al., 2008; Vingiani et al., 2014)) and comparing them with the timing of eruptions and the evolution of the chemical composition (Si, Ti, REE) of eruptiva (Forni, 2011; Albert et al., 2013, 2017).

Site	Estimated soil ages (ka BP; based on WIP)	Estimated ages of volcanic deposits (ka BP; based on LA-ICP-MS)
Nebrodi I	62.3 ± 7.5	92–81; < 70
Nebrodi II	77.5 ± 6.9	
Nebrodi III	61.0 ± 8.8	
Nebrodi IV	80.0 ± 20.6	
Average Nebrodi	70.2 ± 11.9	92–81; < 70
Sila I	51.6 ± 10.4	
Sila II	46.6 ± 12.7	
Average Sila	49.1 ± 10.8	
Sila ^a		
Min	15.6	
Max	66.7	
average	45.3 ± 11.1	
Glass fragments Sila ^a		
Min	modern	< 70
Max	23.7	92–81

^a Chemical data from Scarciglia et al. (2008), Vingiani et al. (2014).

Nb/Y vs Zr/Ti) or other trace elements (Co, Th) and rare earth elements (Ce, La). Besides the main geochemical composition (bulk soil), detailed geochemical data (major compounds, trace elements and REE) individual glass particles and volcanic clasts may contain important information about their origin (provided that geochemical data of the origin material exist). Immobile and trace elements systematics revealed that a large part of the volcanic sediments deposited at the investigated sites (Nebrodi and Sila mountains) most likely originate from the Aeolian Islands (Lipari, Vulcano). Larger particles (lapilli) in the Nebrodi soils have their origin from eruptions of the Etna. To better identify the source of origin isotopic ratios (e.g. ¹⁴³Nd/¹⁴⁴Nd vs ⁸⁷Sr/⁸⁶Sr or ²⁰⁸Pb/²⁰⁴Pb vs ²⁰⁶Pb/²⁰⁴Pb) should be investigated to better cope with weathering processes. LA-ICP-MS and SEM-EDS measurements gave a clear hint that several sources exist: not only the Aeolian Islands but also specific eruption epochs of the Etna (Biancavilla) contributed to the deposits.

The age estimate of these deposits has some limitations. Since radiocarbon dating appears to only give minimum ages (Early Holocene or Late Pleistocene) in this setting, we suggested that weathering indices and the chemical composition of volcanic glasses and clasts can be helpful for establishing a semi-quantitative dating and chronology. Our weathering index approach, combined with the geochemical fingerprinting, implies that large parts of the soils derive from the epochs VI to IX of Lipari, with possible influence from Vulcano (or Stromboli). This again shows that the volcanic soils consist of multiple deposits giving rise to a complex landscape evolution for the last 50 ka in the Sila mountains and 70 ka in the Nebrodi mountains. Although the age estimates seem reasonable, the results should be evaluated in the future by other, if possible numerical dating techniques.

The geochemical fingerprinting method used here could identify the sources of the deposits relatively precisely. While the weathering index-derived ages remain speculative, they do represent an improvement on previous chronologies in the area.

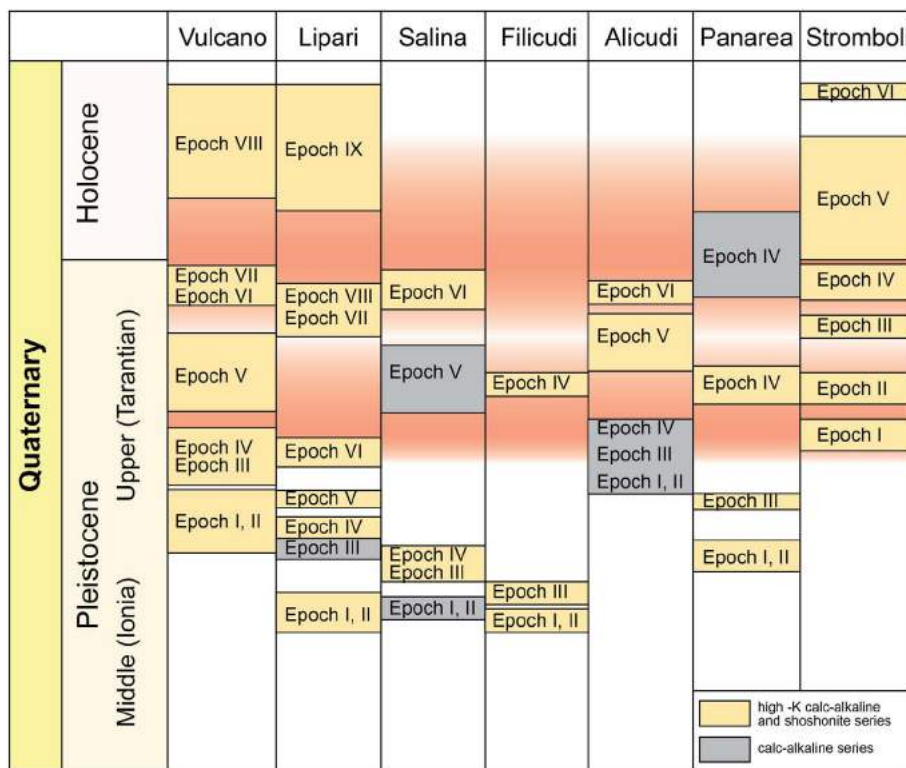


Fig. 10. Active periods of Aeolian Arc volcanism (in grey and yellow) according to Pichler (1989) and updated after Forni et al. (2013), De Astis et al. (2013), Lucchi et al. (2013a, 2013b, 2014a, 2014b) and Francalanci et al. (2013). The estimated age ranges of the volcanic deposits at the investigation sites (Sila and Nebrodi) using the WIP (weathering index after Parker) and chemical composition of glass particles, pumice and volcanic clasts are indicated in red stripes. (For interpretation of the references to colour in this figure legend, the reader is referred to the web version of this article.)

Table 11

Mass balance calculations (fine earth) and estimation of the volcanic proportion in the soil layers using several potential sources: 1)–3) Aeolian islands, Lipari (different eruption epochs) and 4) Biancavilla ignimbrite and Plinian eruptions, Etna.

Site	Horizon	Soil depth cm	Al ₂ O ₃ kg/m ²	TiO ₂ kg/m ²	¹ Volcanic proportion Lipari (epoch 6)	² Volcanic proportion (Lipari, < 50 ka; Albert et al., 2017)	³ Volcanic proportion (Lipari; > ca. 30 ka; Mirabella et al., 2005)	⁴ Volcanic proportion Biancavilla(Albert et al., 2013)
Nebrodi I	A1	0–20	35.03	2.08	100%	0%	100%	80%
	A2	20–50	58.91	3.42	100%	0%	100%	76%
	A3	50–90	79.45	4.58	100%	0%	100%	75%
	A4	90–130	88.66	5.08	100%	0%	100%	74%
	AB	130–140	29.85	1.01	28%	0%	15%	6%
	Bw	140–160	57.66	2.03	46%	0%	25%	11%
Nebrodi II	A1	0–15	28.42	1.52	47%	25%	63%	0%
	A2	15–50	68.64	3.84	31%	16%	42%	0%
	2BA	50–65	31.87	2.07	0%	0%	0%	0%
Nebrodi III	2Bw	65–90	30.85	1.84	0%	0%	0%	0%
	A1	0–50	112.83	3.72	18%	0%	10%	4%
Nebrodi IV	A2	50–75	55.71	2.65	100%	100%	100%	46%
	Bw	75–110	91.08	3.81	100%	72%	70%	30%
	A1	0–20	23.96	1.2	65%	37%	84%	0%
	A2	20–35	20.29	1.13	41%	23%	53%	0%
Sila I	2Btm	35–115	170.78	11.51	0%	0%	0%	0%
	2C	115–135	35.86	2.34	0%	0%	0%	0%
	A1	0–20	39.22	1.45	85%	0%	63%	35%
	A2	20–40	43.9	1.56	76%	0%	56%	31%
	Bw	40–60	54.62	1.42	5%	0%	4%	2%
Sila II	2Bw	60–80	65.53	1.82	21%	0%	14%	7%
	2C	80–100	57.09	1.45	0%	0%	0%	0%
	A1	0–20	40.9	1.49	85%	0%	65%	38%
	A2	20–40	39.38	1.2	49%	0%	35%	19%
	Bw	40–60	48.65	1.23	6%	0%	4%	2%
2Bw	60–80	60.52	1.4	0%	0%	0%	0%	
	2C	80–100	49.39	1.22	0%	0%	0%	0%

¹ Average composition (data from Forni, 2011)

Al₂O₃: 169 ± 4.9 g/kg

TiO₂: 6.7 ± 0.5 g/kg.

² Average composition (data from Albert et al., 2017)

Al₂O₃: 131 ± 6.8 g/kg

TiO₂: 1.0 ± 0.4 g/kg.

³ Average composition (data from Mirabella et al., 2005)

Al₂O₃: 170 ± 27.2 g/kg

TiO₂: 7.9 ± 6.2 g/kg.

⁴ Using the Biancavilla ignimbrite and unit D Plinian fall deposits (Etna) as origin (Albert et al., 2013)

Al₂O₃: 172 ± 3.7 g/kg

TiO₂: 11.4 ± 1.9 g/kg.

Acknowledgements

This research was supported by the Swiss National Science Foundation (SNSF) project grant no. 200021_162338/1. We are, furthermore, indebted to two unknown reviewers for their helpful comments on an earlier version of the manuscript.

References

- Albert, P.G., Tomlinson, E.L., Lane, C.S., Wulf, S., Smith, V.C., Coltelli, M., Keller, J., Lo Castro, D., Manning, C.J., Müller, W., Menzies, M.A., 2013. Late glacial explosive activity on Mount Etna: implications for proximal–distal tephra correlations and the synchronisation of Mediterranean archives. *J. Volcanol. Geotherm. Res.* 265, 9–26.
- Albert, P.G., Tomlinson, E.L., Smith, V.C., Di Traglia, F., Pistolesi, M., Morris, A., Donato, P., De Rosa, R., Sulpizio, R., Keller, J., Rosi, M., Menzies, M., 2017. Glass geochemistry of pyroclastic deposits from the Aeolian Islands in the last 50 ka: a proximal database for tephrochronology. *J. Volcanol. Geotherm. Res.* 336, 81–107.
- Beckhoff, B., Kanngießer, B., Langhoff, N., Wedell, R., Wolff, H., 2006. *Handbook of Practical X-ray Fluorescence Analysis*. Springer, Berlin.
- Bertagnini, A., Métrich, N., Francalanci, L., Landi, P., Tommasini, S., Conticelli, S., 2008. Volcanology and magma geochemistry of the present-day activity: constraints on the feeding system. In: Calvari, S., Inguaggiato, S., Puglisi, G., Ripepe, M., Rosi, M. (Eds.), *The Stromboli Volcano: An Integrated Study of the 2002–2003 Eruption*. American Geophysical Union, Washington, D. C., pp. 19–37.
- Bourne, A.J., Albert, P.G., Matthews, I.P., Trincardi, F., Wulf, S., Asiola, A., Blockley, S.P.E., Keller, J., Lowe, J.J., 2015. Tephrochronology of core PRAD 1-2 from the Adriatic Sea: insights into Italian explosive volcanism for the period 200–80 ka. *Quat. Sci. Rev.* 116, 28–43.
- Brock, F., Higham, T., Ditchfield, P., Bronk Ramsey, C., 2010. Current pretreatment methods for AMS radiocarbon dating at the Oxford radiocarbon accelerator unit (ORAU). *Radiocarbon* 52, 103–112.
- Bronk Ramsey, C., 2001. Development of the radiocarbon calibration program. *Radiocarbon* 43, 355–363.
- Bronk Ramsey, C., 2009. Bayesian analysis of radiocarbon dates. *Radiocarbon* 51, 337–360.
- Buggle, B., Glaser, B., Hambach, U., Gerasimenko, N., Markovic, S., 2011. An evaluation of geochemical weathering indices in loess-paleosol studies. *Quat. Int.* 240, 12–21.
- Carcaillet, C., Brun, J.-J., 2000. Changes in landscape structure in the northwestern Alps over the last 7000 years: lessons from soil charcoal. *J. Veg. Sci.* 11, 705–714.
- Cirrincone, R., Fazio, E., Fiannacca, P., Ortolano, G., Pezzino, A., Punturo, R., 2015. The Calabria-Peloritani Orogen, a composite terrane in Central Mediterranean; its overall architecture and geodynamic significance for a pre-Alpine scenario around the Tethyan basin. *Periodico Minerale* 84-3B (Special Issue), 701–749.
- Condomines, M., Tanguy, J.C., 1995. Magma dynamics at Mt Etna: constraints from U–Th–Ra–Pb radioactive disequilibrium and Sr isotopes in historical lavas. *Earth Planet. Sci. Lett.* 132, 25–41.
- Costantini, E., Dazzi, C. (Eds.), 2013. *The Soils of Italy*. Springer, Dordrecht, Heidelberg, New York, London.
- Dahms, D., Favilli, F., Krebs, R., Egli, M., 2012. Soil weathering and accumulation rates of oxalate-extractable phases derived from alpine chronosequences of up to 1 Ma in age. *Geomorphology* 151, 99–113.
- De Astis, G., Lucchi, F., Dellino, P., La Volpe, L., Tranne, C.A., Frezzotti, M.L., Peccerillo, A., 2013. Chapter 11 Geology, volcanic history and petrology of Vulcano (central Aeolian archipelago). In: Lucchi, F., Peccerillo, A., Keller, J., Tranne, C.A., Rossi, P.L. (Eds.), *The Aeolian Islands Volcanoes*. The Geological Society of Londonpp. 281–349.
- De Rosa, R., Donato, P., Scarciglia, F., 2016. On the origin and post-depositional history of widespread massive ash deposits: the case of Intermediate Brown Tuffs (IBT) of Lipari (Aeolian Islands, Italy). *J. Volcanol. Geotherm. Res.* 327, 135–151.
- Egli, M., Fitze, P., 2000. Formulation of pedologic mass balance based on immobile elements: a revision. *Soil Sci.* 165, 437–443.
- Egli, M., Nater, M., Mirabella, A., Raimondi, S., Plötz, M., Alioth, L., 2008. Clay minerals, oxyhydroxide formation, element leaching and humus development in volcanic soils. *Geoderma* 143, 101–114.
- Egli, M., Gristina, L., Wiesenberg, G., Martin Civantos, J.M., Rotolo, A., Novara, A., Brandová, D., Raimondi, S., 2013. From pedologic indications to archaeological reconstruction: deciphering land use in the Islamic period in the Baida district (northwestern Sicily). *J. Archaeol. Sci.* 40, 2670–2685.
- Eusterhues, K., Rumpel, C., Kögel-Knabner, I., 2005. Stabilization of soil organic matter isolated via oxidative degradation. *Org. Geochem.* 36, 1567–1575.
- Favilli, F., Egli, M., Cherubini, P., Sartori, F., Haerberli, W., Delbos, E., 2008. Comparison of different methods of obtaining a resilient organic matter fraction in Alpine soils. *Geoderma* 245, 355–369.
- Favilli, F., Egli, M., Brandová, D., Ivy-Ochs, S., Kubik, P., Cherubini, P., Mirabella, A., Sartori, G., Giaccai, D., Haerberli, W., 2009a. Combined use of relative and absolute dating techniques for detecting signals of Alpine landscape evolution during the late Pleistocene and early Holocene. *Geomorphology* 112, 48–66.
- Favilli, F., Egli, M., Brandová, D., Ivy-Ochs, S., Kubik, P.W., Maisch, M., Cherubini, P., Haerberli, W., 2009b. Combination of numerical dating techniques using ¹⁰Be in rock boulder and ¹⁴C of resilient soil organic matter for reconstructing the chronology of glacial and periglacial processes in a high alpine catchment during the late Pleistocene and early Holocene. *Radiocarbon* 51, 537–552.
- Favilli, F., Cherubini, P., Collenberg, M., Egli, M., Sartori, G., Schoch, W., Haerberli, W., 2010. Charcoal fragments of Alpine soils as an indicator of landscape evolution during the Holocene in Val di Sole (Trentino, Italy). *The Holocene* 20, 67–79.
- Fedo, C.M., Nesbitt, H.W., Young, G.M., 1995. Unraveling the effects of potassium metasomatism in sedimentary rocks and paleosols, with implications for paleo-weathering conditions and provenance. *Geology* 23, 921–924.
- Fisher, R.V., Schmincke, H.U., 1984. *Pyroclastic Rocks*. Springer, Berlin.
- Forni, F., 2011. *Petrology and Geochemistry of Lipari Island (Aeolian Archipelago): Constraints on Magma Genesis and Evolution*. PhD thesis University of Bologna, Italy.
- Forni, F., Lucchi, F., Peccerillo, A., Tranne, C.A., Rossi, P.L., Frezzotti, M.L., 2013. Chapter 10 Stratigraphy and geological evolution of the Lipari volcanic complex (central Aeolian archipelago). In: Lucchi, F., Peccerillo, A., Keller, J., Tranne, C.A., Rossi, P.L. (Eds.), *The Aeolian Islands Volcanoes*. The Geological Society of Londonpp. 213–279.
- Francalanci, L., Lucchi, F., Keller, J., De Astis, G., Tranne, C.A., 2013. Chapter 13 Eruptive volcano-tectonic and magmatic history of the Stromboli volcano (north-eastern Aeolian archipelago). In: Lucchi, F., Peccerillo, A., Keller, J., Tranne, C.A., Rossi, P.L. (Eds.), *The Aeolian Islands Volcanoes*. The Geological Society of Londonpp. 397–471.
- Giaccio, B., Isaia, R., Sulpizio, R., Zanchetta, G., 2008. Explosive volcanism in the central Mediterranean area during the late Quaternary-linking sources and distal archives. *J. Volcanol. Geotherm. Res.* 177, v–vii.
- Glenn, R.C., Nash, V.E., 1964. Weathering relationship between gibbsite, kaolinite, chlorite, and expandable layer silicates in selected soils from the lower Mississippi Coastal Plain. *Clays Clay Miner. Proc.* 12, 539–548.
- Guillon, M., Meier, D.L., Allan, M.M., Heinrich, C.A., Yardley, B.W.D., 2008. SILLs: a MATLAB-based program for the reduction of laser ablation ICP–MS data of homogeneous materials and inclusions. In: Sylvester, P. (Ed.), *Laser Ablation ICP–MS in the Earth Sciences: Current Practices and Outstanding Issues*. Mineral. Mineralogical Association of Canada Short Course Series Vol. 40. pp. 328–333.
- Harnois, L., 1988. The CIW index: a new chemical index of weathering. *Sediment. Geol.* 55, 319–322.
- Hastie, A.R., Kerr, A.C., Pearce, J.A., Mitchell, S.F., 2007. Classification of altered volcanic island arc rocks using immobile trace elements: development of the Th–Co discrimination diagram. *J. Petrol.* 48, 2341–2357.
- IUSS Working Group WRB, 2015. *World Reference Base for Soil Resources 2014, Update 2015. International Soil Classification System for Naming Soils and Creating Legends for Soil Maps*. World Soil Resources Reports 106 FAO, Rome.
- Johannes, A., 1937. *A descriptive petrography of the igneous rocks*. In: *Introduction, Textures, Classifications, and Glossary*. Vol. 1 The University of Chicago Press, Chicago, Illinois.
- Joplin, G.A., 1968. The shoshonite association: a review. *J. Geol. Soc. Aust.* 15, 275–294.
- Karkanas, P., Bar-Yosef, O., Goldberg, P., Weiner, S., 2000. Diagenesis in prehistoric caves: the use of minerals that form in situ to assess the completeness of the archaeological record. *J. Archaeol. Sci.* 27, 915–929.
- Keller, J., Ryan, W.B.F., Ninkovich, D., Altherr, R., 1978. Explosive volcanic activity in the Mediterranean over the past 200,000 yr as recorded in deep-sea sediments. *Geol. Soc. Am. Bull.* 89, 591–604.
- Kleber, M., Sollins, P., Sutton, R., 2007. A conceptual model of organo-mineral interactions in soils: self-assembly of organic molecular fragments into zonal structures on mineral surfaces. *Biogeochemistry* 85, 9–24.
- Kronberg, G.L., Nesbitt, H.W., 1981. Quantification of weathering of soil chemistry and soil fertility. *J. Soil Sci.* 32, 453–459.
- de Lafontaine, G., Couillard, P., Payette, S., 2011. Permineralization process promotes preservation of Holocene macrofossil charcoal in soils. *J. Quat. Sci.* 26, 571–575.
- Le Pera, E., Sorriso-Valvo, M., 2000. Weathering and morphogenesis in a Mediterranean climate Calabria, Italy. *Geomorphology* 34, 251–270.
- Lucchi, F., Tranne, C.A., Peccerillo, A., Keller, J., Rossi, P.L., 2013a. Chapter 12 Geological history of the Panarea volcanic group (eastern Aeolian archipelago). In: Lucchi, F., Peccerillo, A., Keller, J., Tranne, C.A., Rossi, P.L. (Eds.), *The Aeolian Islands Volcanoes*. The Geological Society of Londonpp. 351–395.
- Lucchi, F., Gertisser, R., Keller, J., Forni, F., De Astis, G., Tranne, C.A., 2013b. Chapter 9 Eruptive history and magmatic evolution of the island of Salina (central Aeolian archipelago). In: Lucchi, F., Peccerillo, A., Keller, J., Tranne, C.A., Rossi, P.L. (Eds.), *The Aeolian Islands Volcanoes*. The Geological Society of Londonpp. 155–211.
- Lucchi, F., Santo, A.P., Tranne, C.A., Peccerillo, A., Keller, J., 2014a. Chapter 8 Volcanism, magmatism, volcano-tectonic and sea-level fluctuations in the geological history of Filicudi (western Aeolian archipelago). In: Lucchi, F., Peccerillo, A., Keller, J., Tranne, C.A., Rossi, P.L. (Eds.), *The Aeolian Islands Volcanoes*. The Geological Society of Londonpp. 113–153.
- Lucchi, F., Peccerillo, A., Tranne, C.A., Rossi, P.L., Frezzotti, M.L., Donati, D., 2014b. Chapter 7 Volcanism, calderas and magmas of the Alicudi composite volcano (western Aeolian archipelago). In: Lucchi, F., Peccerillo, A., Keller, J., Tranne, C.A., Rossi, P.L. (Eds.), *The Aeolian Islands Volcanoes*. The Geological Society of Londonpp. 83–111.
- Lynch, J.A., Clark, J.S., Stocks, B.J., 2004. Charcoal production, dispersal, and deposition from Fort Providence experimental fire: interpreting fire regimes from charcoal record in boreal forests. *Can. J. For. Res.* 34, 1642–1656.
- McKeague, J.A., Brydon, J.E., Miles, N.M., 1971. Differentiation of forms of extractable iron and aluminum in soils. *Soil Sci. Soc. Am. Proc.* 35, 33–38.
- Mirabella, A., Egli, M., Raimondi, S., Giaccai, D., 2005. Origin of clay minerals in soils on pyroclastic deposits in the island of Lipari (Italy). *Clay Clay Miner.* 53, 410–422.
- Mizota, C., van Reeunwijk, L.P., 1989. Clay mineralogy and chemistry of soils formed in volcanic material in diverse climate regions. In: *International Soil Reference and Information Centre. Soil Monograph Vol. 2 (Wageningen)*.
- Morrison, G.W., 1980. Characteristics and tectonic setting of the shoshonite rock association. *Lithos* 13, 97–108.
- Moser, D., Di Pasquale, G., Scarciglia, F., Nelle, O., 2017. Holocene mountain forest changes in central Mediterranean: soil charcoal data from the Sila Massif (Calabria, southern Italy). *Quat. Int.*. <http://dx.doi.org/10.1016/j.quaint.2017.01.042>. (under

- review).
- Munno, R., Rossi, G., Tadini, C., 1980. Crystal chemistry of kimzeyite from Stromboli, Aeolian Islands, Italy. *Am. Mineral.* 65, 188–191.
- Narcisi, B., Vezzoli, L., 1999. Quaternary stratigraphy of distal tephra layers in the Mediterranean an overview. *Glob. Planet. Chang.* 21, 31–50.
- Nesbitt, H.W., Young, G.M., 1982. Early Proterozoic climates and plate motions inferred from major element chemistry of lutites. *Nature* 299, 715–717.
- Parker, A., 1970. An index for weathering for silicate rocks. *Geol. Mag.* 107, 29–147.
- Paterne, M., Guichard, F., Labeyrie, J., 1988. Explosive activity of the south Italian volcanoes during the past 80,000 years as determined by marine tephrochronology. *J. Volcanol. Geotherm. Res.* 34, 153–172.
- Paterne, M., Guichard, F., Duplessy, J.C., Siani, G., Sulpizio, R., Labeyrie, J., 2008. A 90,000–200,000 yrs marine tephra record of Italian volcanic activity in the Central Mediterranean Sea. *J. Volcanol. Geotherm. Res.* 177, 187–196.
- Pearce, J.A., 1996. A user's guide to basalt discrimination diagrams. In: Wyman, D.A. (Ed.), *Trace Element Geochemistry of Volcanic Rocks: Applications for Massive Sulphide Exploration*. Geological Association of Canada, Short Course Notes Vol. 12. pp. 79–113.
- Peccerillo, A., 2005. *Plio-Quaternary Volcanism in Italy*. Springer, Berlin.
- Pelle, T., Scarciglia, F., Di Pasquale, G., Allevato, E., Marino, D., Robustelli, G., La Russa, M.F., Pulice, I., 2013. Multidisciplinary study of Holocene archaeological soils in an upland Mediterranean site: natural versus anthropogenic environmental changes at Cecita Lake, Calabria, Italy. *Quat. Int.* 303, 163–179.
- Peters, D., Pettke, T., 2017. Evaluation of major to ultra-trace element bulk rock chemical analysis of nanoparticulate pressed powder pellets by LA-ICP-MS. *Geostand. Geoanal. Res.* 41, 5–28.
- Pettke, T., Oberli, F., Audetat, A., Guillong, M., Simon, A., Hanley, J., Klemm, L.M., 2012. Recent developments in element concentration and isotope ratio analysis of individual fluid inclusions by laser ablation single and multiple collector ICP-MS. *Ore Geol. Rev.* 44, 10–38.
- Pichler, H., 1967. Neue Erkenntnisse über Art und Genese des Vulkanismus der Äolischen Inseln (Sizilien). *Geologische Rundschau Stuttgart* 57, 102–126.
- Pichler, H., 1981. *Sammlung Geologischer Führer* 69, Lipari, Vulcano, Stromboli, Tyrrhenisches Meer Italienische Vulkan-Gebiete III. Gebrüder Bornträger, Berlin-Stuttgart.
- Pichler, H., 1984. *Sammlung Geologischer Führer Ätna, Sizilien. Italienische Vulkan-Gebiete IV. Gebrüder Bornträger, Berlin-Stuttgart.*
- Pichler, H., 1989. *Sammlung Geologischer Führer: Italienische Vulkangebiete V. Mte. Vulture, Äolische Inseln II (Saline, Filicudi, Alicudi, Panarea), Mti. Iblei, Capo Passero, Ustica, Pantelleria und Linosa. Gebrüder Bornträger, Berlin-Stuttgart.*
- Plante, A.F., Chenu, C., Balabane, M., Mariotti, A., Righi, D., 2004. Peroxide oxidation of clay associated organic matter in a cultivation chronosequence. *Eur. J. Soil Sci.* 55, 471–478.
- Price, J.R., Velbel, M.A., 2003. Chemical weathering indices applied to weathering profiles developed on heterogeneous felsic metamorphic parent rocks. *Chem. Geol.* 202, 397–416.
- Reimer, P.J., Bard, E., Bayliss, A., Beck, J.W., Blackwell, P.G., Bronk Ramsey, C., Buck, C.E., Cheng, H., Edwards, R.L., Friedrich, M., Grootes, P.M., Guilderson, T.P., Hafflidason, H., Hajdas, I., Hatté, C., Heaton, T.J., Hoffmann, D.L., Hogg, A.G., Hughen, K.A., Kaiser, K.F., Kromer, B., Manning, S.W., Nui, M., Reimer, R.W., Richards, D.A., Scott, E.M., Southon, J.R., Staff, R.A., Turney, C., van der Plicht, J., 2013. IntCal13 and Marine13 radiocarbon age calibration curves 0–50,000 years cal BP. *Radiocarbon* 55, 1869–1887.
- Sandri, L., Costa, A., Selva, J., Tonini, R., Macedonio, G., Folch, A., Sulpizio, R., 2016. Beyond eruptive scenarios: assessing tephra fallout hazard from Neapolitan volcanoes. *Sci Rep* 6 (24271), 1–13.
- Scarciglia, F., De Rosa, R., Vecchio, G., Apollaro, C., Robustelli, G., Terrasi, F., 2008. Volcanic soil formation in Calabria (southern Italy): the Cecita Lake geosol in the late Quaternary geomorphological evolution of the Sila uplands. *J. Volcanol. Geotherm. Res.* 177, 101–117.
- Siddig, A.A., Ellison, A.M., Ochs, A., Villar-Leeman, C., Lau, M.K., 2015. How do ecologists select and use indicator species to monitor ecological change? Insights from 14 years of publication in ecological indicators. *Ecol. Indic.* 60, 223–230.
- Soil Survey Division Staff, 2010. *Keys to Soil Taxonomy*. US Department of Agriculture (USDA) and National Resource Conservation Service (NRCS), Washington.
- Sommer, M., Halm, D., Weller, U., Zarei, M., Stahr, K., 2000. Lateral podzolization in a granite landscape. *Soil Sci. Soc. Am. J.* 64, 1434–1442.
- Stiles, C.A., Mora, C.I., Driesse, S.G., 2003. Pedogenetic processes and domain boundaries in an arid soil chronosequence: evidence from titanium and zirconium distribution and morphology. *Geoderma* 116, 279–299.
- Sulpizio, R., Zanchetta, G., Caron, B., Dellino, P., Mele, D., Giaccio, B., Insinga, D., Paterne, M., Siani, G., Costa, A., Macedonio, G., Santacroce, R., 2014. Volcanic ash hazard in the Central Mediterranean assessed from geological data. *Bull. Volcanol.* 76, 866.
- Sumner, M.E. (Ed.), 1999. *Handbook of Soil Science*. CRC press, Boca Raton.
- Sun, S.S., McDonough, W.F., 1989. Chemical and isotopic systematics of oceanic basalts; implications for mantle composition and processes. In: Saunders, A.D., Norry, M.J. (Eds.), *Magmatism in the Ocean Basins*. Geological Society Special Publication Vol. 42. Blackwell Scientific, Oxford, pp. 313–345.
- Thomas, M.F.H., 2011. *Sedimentology and Basin Context of the Numidian Flysch Formation; Sicily and Tunisia*. Doctoral Thesis 85.
- Torn, M.S., Trumbore, S.E., Chadwick, O.A., Vitousek, P.M., Hendricks, D.M., 1997. Mineral control of soil organic carbon storage and turnover. *Nature* 389, 170–173.
- Tuttolomondo, T., Licata, M., Leto, C., Bonsangue, G., Gargano, M.L., Venturella, G., La Bella, S., 2014. Popular uses of wild plant species for medicinal purposes in the Nebrodi Regional Park (north-eastern Sicily, Italy). *J. Ethnopharmacol.* 157, 21–37.
- Vingiani, S., Scarciglia, F., Mileti, F.A., Donato, P., Terribile, F., 2014. Occurrence and origin of soils with andic properties in Calabria (southern Italy). *Geoderma* 232, 500–516.
- Weiner, S., Goldberg, P., Bar-Yosef, O., 1993. Bone preservation in Kebara Cave, Israel, using on-site Fourier transform infrared spectrometry. *J. Archaeol. Sci.* 20, 613–627.
- Wood, R.E., Douka, K., Boscato, P., Haeserts, P., Sinityn, A., Higham, T.F.G., 2012. Testing the ABOx-SC method: dating known-age charcoals associated with the Campanian ignimbrite. *Quat. Geochronol.* 9, 16–26.
- Zimmerer, M.J., Lafferty, J., Coble, M.A., 2016. The eruptive and magmatic history of the youngest pulse of volcanism at the Valles caldera: implications for successfully dating late quaternary eruptions. *J. Volcanol. Geotherm. Res.* 310, 50–57.



Denudation variability of the Sila Massif upland (Italy) from decades to millennia using ^{10}Be and $^{239+240}\text{Pu}$

Gerald Raab¹ | Fabio Scarciglia² | Kevin Norton³ | Dennis Dahms⁴ | Dagmar Brandová¹ | Raquel de Castro Portes¹ | Marcus Christl⁵ | Michael E. Ketterer⁶ | Annina Ruppli¹ | Markus Egli¹

¹Department of Geography, University of Zurich, Zurich, Switzerland

²Department of Biology, Ecology and Earth Sciences (DiBEST), University of Calabria, Arcavacata di Rende, Italy

³School of Geography, Environment and Earth Sciences, Victoria University of Wellington, Wellington, New Zealand

⁴Department of Geography, University of Northern Iowa, Cedar Falls, Iowa

⁵Department of Physics, ETH Zurich, Zurich, Switzerland

⁶Chemistry and Biochemistry, Northern Arizona University, Flagstaff, Arizona

Correspondence

Gerald Raab, Department of Geography, University of Zurich, Winterthurerstrasse 190, 8057 Zurich, Switzerland.

Email: gerald.raab@geo.uzh.ch

Funding information

Schweizerischer Nationalfonds zur Förderung der Wissenschaftlichen Forschung, Grant/Award Number: 200021_162338/1 IZKOZ2_147421 IZKOZ2_170715/1; SNSF grant for a Short Research Visit, Grant/Award Number: IZKOZ2_147421; Royal Society Te Apārangi Rutherford Discovery Fellowship; SNSF Visiting International Fellowship, Grant/Award Number: IZKOZ2_170715/1

Abstract

Landscapes and soils evolve in non-linear ways over millennia. Current knowledge is incomplete as only average denudation (or erosion) rates are normally estimated, neglecting the temporal discontinuities of these processes. The determination of regressive and progressive phases of soil evolution is important to our understanding of how soils and landscapes respond to environmental changes. The Sila Massif (Italy) provides a well-defined geomorphological and geological setting to unravel temporal variations in soil redistribution rates. We used a combination of in situ cosmogenic radionuclide measurements (^{10}Be) along top (residual rock) height profiles, coupled with fallout radionuclides ($^{239+240}\text{Pu}$) in soils, to model soil denudation rates over the last 100 ka. We measured rates prior to the Last Glacial Maximum (LGM) of $\leq 30 \text{ t km}^{-2} \text{ yr}^{-1}$ ($\sim 0.036 \text{ mm yr}^{-1}$). Following the LGM, during the transition from the Pleistocene to the Holocene, these rates increased to $\sim 150\text{--}200 \text{ t km}^{-2} \text{ yr}^{-1}$ and appeared to be above soil production rates, causing regressive soil evolution. For the last ~ 50 years, we even describe erosion rates of $\geq 1,000 \text{ t km}^{-2} \text{ yr}^{-1}$ ($\sim 1.23 \text{ mm yr}^{-1}$) and consider human impact as the decisive factor for this development. Consequently, the natural soil production rates cannot cope with the current erosion rates. Thus, a distinct regressive phase of soil formation exists, which will give rise to shallowing of soils over time. Overall, our multimethod approach traced denudation and erosion histories over geologic and human timescales and made a new archive to soil science and geomorphology accessible.

KEYWORDS

cosmogenic nuclides, fallout radionuclides, landscape evolution, soil erosion rates, top formation

1 | INTRODUCTION

Earth's surface landscapes are known to form in complex and non-linear ways over thousands of years—this is particularly the case for soils. In a coevolutional model, soil formation is regarded to be discontinuous over time and conceptualised by 'progressive' or 'regressive' process groups (Johnson & Watson-Steger, 1987; Sommer, Gerke, & Deumlich, 2008) that are caused by changing environmental conditions. Periods with dominantly progressive processes (e.g., soil

deepening and weathering) alternate with periods with dominantly regressive processes (e.g., erosion) due to fast and substantial changes in drivers. Soils can only form if the rate of their production is higher than the rate of soil loss. Soil formation (F_{soil}) can be expressed by

$$F_{\text{soil}} = P_{\text{soil}} - D_{\text{soil}}, \quad (1)$$

where P_{soil} is the soil production and D_{soil} the soil denudation. Progressive phases occur when soil production is greater than soil denudation,

and regressive phases occur when soil denudation rates are greater than soil production. Denudation fluxes (D) consist of chemical weathering fluxes (W) and physical erosion fluxes (E):

$$D_{\text{soil}} = W_{\text{soil}} + E_{\text{soil}}, \quad (2)$$

where W_{soil} is the chemical weathering fluxes (leaching losses) and E_{soil} is the soil erosion. Chemical and physical weathering and mineral transformation contribute to progressive soil formation, whereas strong erosion leads to regressive development and thereby to surface denudation. Often, soil erosion is almost equal to denudation. Dixon and von Blanckenburg (2012), Reeves and Rothman (2014), and several others have demonstrated that soil erosion is the driving force

for denudation in agricultural landscapes and hill country. In steep mountainous terrain, mass wasting dominates. Soil erosion (catchment-wide to profile-related data) is mostly in the range of 0.5–0.9 D_{soil} (Dixon & von Blanckenburg, 2012):

$$0.5 \cdot D_{\text{soil}} \leq E_{\text{soil}} \leq 0.9 \cdot D_{\text{soil}}. \quad (3)$$

Changes in soil-forming factors can be very abrupt across space and time in mountain landscapes, either because of catastrophic natural events or by human influences (e.g., land use changes and agriculture intensification; Egli & Poulencard, 2016). The concern about soil erosion increases worldwide. Also in Europe (Figure 1a), there is a need to understand erosion processes to establish mitigation measures. This

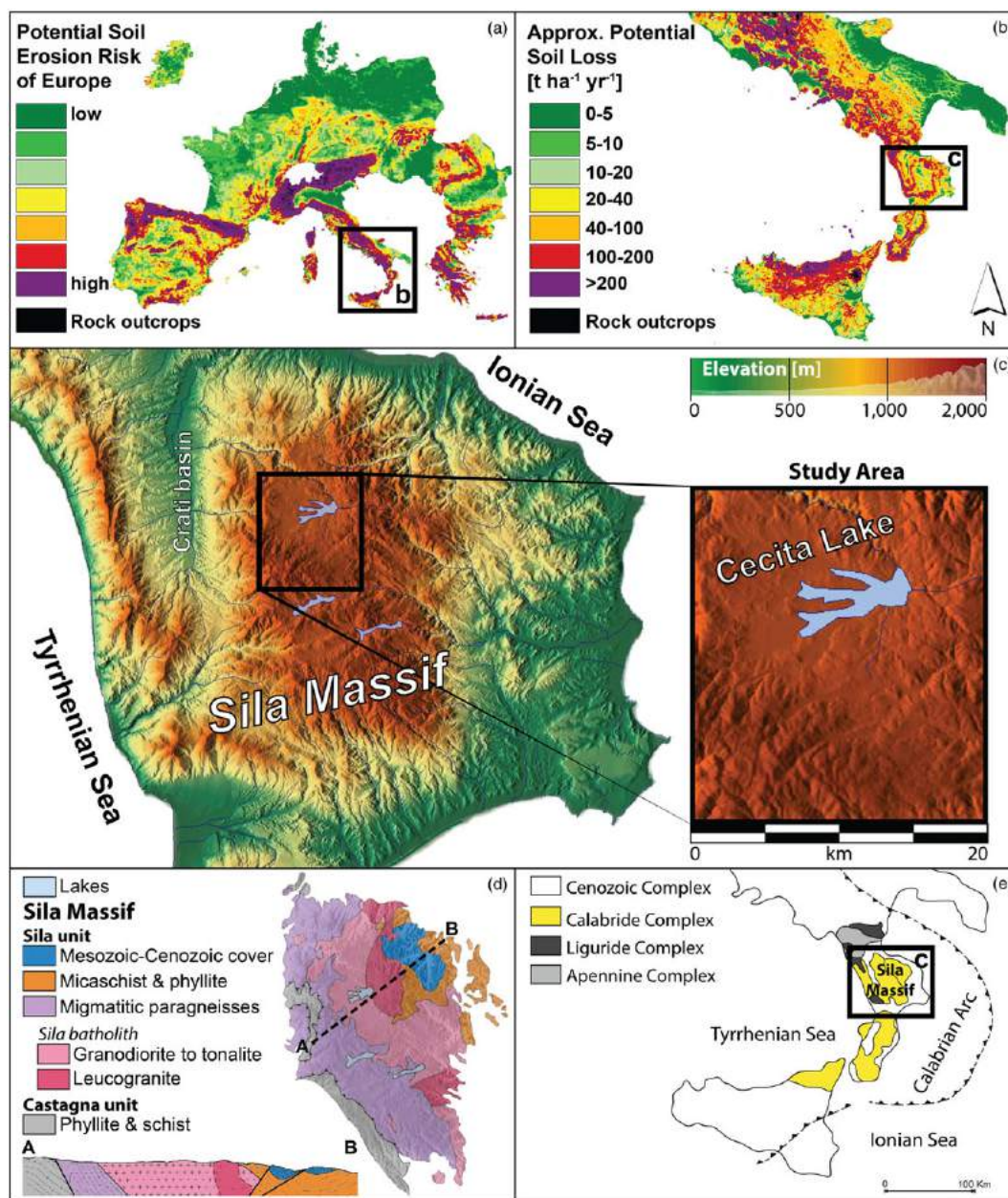


FIGURE 1 (a) Potential soil erosion risk map of Europe (black square: southern Italy), modified after van der Knijff, Jones, and Montanarella (2000). (b) Approximate potential soil loss in southern Italy (van der Knijff, Jones, & Montanarella, 1999). (c) Topographic map of the Sila Massif and the study area near the Cecita Lake, based on data of the Geoportale Nazionale (Ministero dell'Ambiente, Italy). (d) Geological overview of the Sila Massif based on von Eynatten, Tolosana-Delgado, Karius, Bachmann, and Caracciolo (2015) and Liotta et al. (2008). (e) Geological framework of the Sila Massif after Vespasiano et al. (2015) [Colour figure can be viewed at wileyonlinelibrary.com]

is particularly the case for countries such as Italy with a large proportion of mountainous and landscapes having steep slopes (Figure 1b). Several recent studies attempt to compare erosion rates over various time periods in order to estimate rates of various geomorphic processes (e.g., Bellin, Vanacker, & Kubik, 2014; Kirchner et al., 2001). These studies, however, often used catchment-wide approaches (e.g., Bartley, Croke, Brainbridge, Austin, & Kuhnert, 2015; Ibbeken & Schleyer, 1991) and, thus, cannot distinguish soil erosion from denudation as a general degradation process, which is a combination of (soil and rock) erosion, weathering, and mass wasting. Qualitative or quantitative estimates of erosion rates over different timescales have been reported for river sediment yields (Bartley et al., 2015; Kirchner et al., 2001), for lake and marine sedimentation (Mourier, Poulencard, Carcaillet, & Williamson, 2010), and for speleothem growth rates (Clift, Wan, & Blusztajn, 2014). Under specific conditions, the quantification of soil erosion over a few millennia has been possible to high precision through the use of lake sediment records (Bajard et al., 2017).

Up to now, deciphering the temporal development of soil erosion or denudation (and related soil production) over millennia has been difficult (Bajard et al., 2017; Boardman & Poesen, 2007; Poesen, 2018), and our knowledge in this field remains incomplete and fragmented. Neglecting the fact that soil erosion processes are discontinuous over time weakens the understanding of a modern degradation mechanism that has a huge economic and environmental impact (Pimentel, 2006).

Soil denudation and erosion are driven by tectonic activity, local geology, surface topography, climate, and anthropogenic and biotic activities (Smithson et al., 2008). In order to estimate soil erosion over longer time periods, an area has to be selected that predominantly traces soil erosion and not mass wasting or rock (or saprolite) erosion. Thus, archives have to be investigated that optimally preserve this temporal information. Intense erosion- and denudation-affected landscapes can be identified by the presence of boulder fields or 'tor and bornhardt' landforms (Migoń, 2013; Twidale, 2002). These landscapes usually exhibit tower-like or dome-shaped, often castellated residual rocks (tors) that appear to grow from surrounding gentle landforms. We hypothesise that tors are a key for deciphering the evolution of surface lowering rates over time. Where surface lowering is primarily linked to a decrease in soil volume, soil erosion or denudation rates can be deduced. Rock tors (linked to the bedrock) and boulders (detached from the bedrock) usually have a higher physical resistance than the surrounding more easily weatherable (saprolite) material. In an eroding landscape, tors consequently progressively extend above their surrounding landscape surfaces. The rate at which a tor extends further above its landscape is an indicator of the rate of (soil) denudation of the surrounding surface.

Through the use of cosmogenic radionuclide techniques, the exposure of tors and boulders can be dated. Several authors estimated the exposure ages of such landforms. In most cases, however, only samples at the top of tors/boulders were analysed (e.g., Bierman & Caffee, 2001; Darmody et al., 2008; Gunnell et al., 2013). A more detailed sampling design has very rarely been applied (Heimsath, Chappell, Dietrich, Nishiizumi, & Finkel, 2001; Wakasa, Matsuzaki, Tanaka, & Matsukura, 2006). The ^{10}Be exposure ages obtained from

the vertical profile of tor surfaces should allow us to determine their exhumation rates and consequently to calculate surface lowering (soil denudation) and related soil erosion rates over varying and long time intervals (virtually continuous and over millennia). To understand the dynamics of surface lowering and related soil erosion, it would be helpful to compare past erosion rates with present-day rates. Actual (average) rates can be determined with nuclear fallout radionuclides (Lal, Tims, Fifield, Wasson, & Howe, 2013; Meusburger et al., 2016). Isotopes of plutonium ($^{239+240}\text{Pu}$) are an efficient tool in tracing soil erosion and accumulation (Alewell, Pitois, Meusburger, Ketterer, & Mabit, 2017).

This combined approach should enable us to compare past long-term soil denudation rates with the present-day soil erosion rates. This gives us a hint about the future surface development. We thus had the following research questions:

1. How did soil denudation and, thus, soil erosion rates vary over late Pleistocene-to-Holocene time?
2. How did soils develop over time? Can progressive and regressive phases be detected?
3. How do current soil erosion rates compare to past rates?

2 | STUDY AREA

The Sila Massif upland in Calabria, southern Italy, was chosen (Figure 1c), because of its ideal geomorphological and geological setting (Figure 1d). The tectonic massif started forming during the active subduction of the Ionian Basin along the Calabrian Arc (Figure 1e) in the Oligocene (Rossetti et al., 2001). Several tectonic phases uplifted the Sila Massif mainly during the Miocene to the late Pleistocene (Olivetti, Cyr, Molin, Faccenna, & Granger, 2012). The relief and drainage systems are nowadays controlled by N-S, E-W, and NW-SE trending faults (Molin, Pazzaglia, & Dramis, 2004; Spina, Galli, Tondi, Critelli, & Cello, 2007).

The solitary position and surrounding steep slopes (Figure 1c) make the plateau an independent rock mass system. The old landscape of the Sila upland has been affected by long-term deep weathering processes (Figure 2) and subsequent erosion (Scarciglia, 2015; Scarciglia et al., 2016). As a consequence of weathering, granitic boulder fields, tors, and bornhardt landforms have developed here (Scarciglia, 2015). The present-day landscape has many tor and bornhardt landforms and is generally characterised by wide, gently rolling to flat palaeosurfaces ranging from 1,000 to 1,700 m asl. They represent remnants of old planation landforms that were shaped since the Pliocene to the Pleistocene (Molin et al., 2004; Sorriso-Valvo, 1993).

Soils are predominately Cambisols and Umbrisols and occasionally Leptosols, Fluvisols, Regosols, and Andosols (Scarciglia, Le Pera, & Critelli, 2005a). The soils are affected by volcanic ash input, which derives mostly from the Lipari Islands, and started to form during the Pleistocene (Raab et al., 2017). The overall soil thickness can reach 80–100 cm whereby the upper A, A1, or Ap horizons are about 10–35 cm thick (Table 1). Bt and Bw horizons are found in 30- to 60-cm depth. Above the C horizon, in about 60–75 cm, a Bw2 and

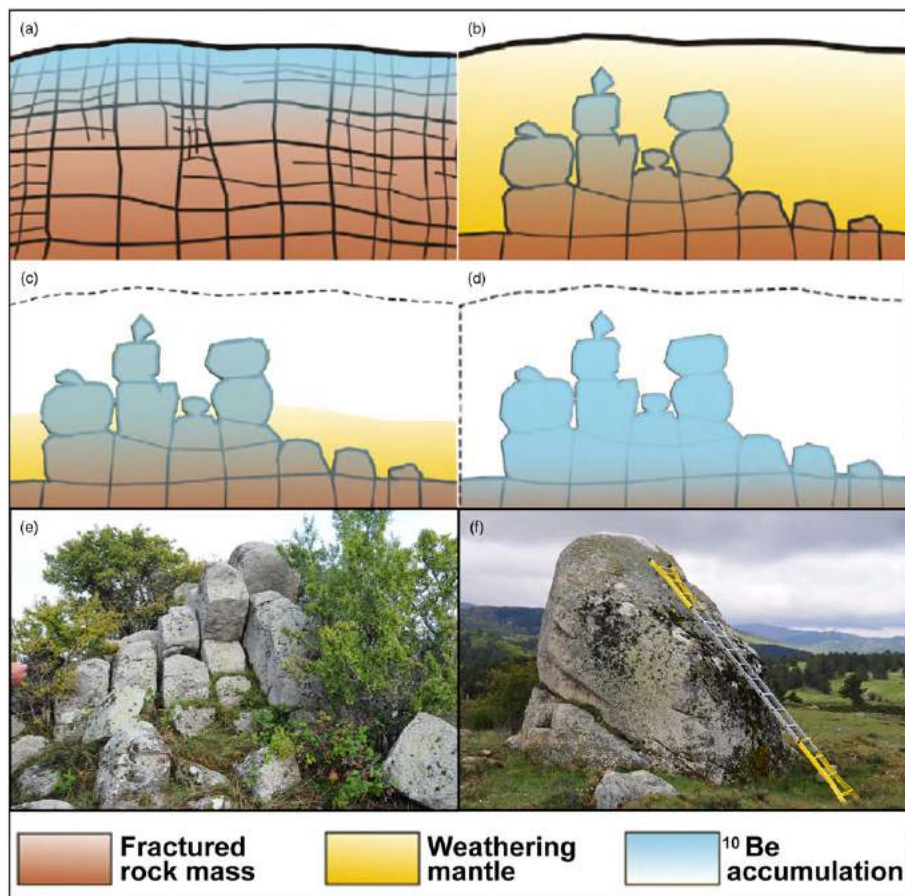


FIGURE 2 Weathering scheme of a rock surface (Migoñ, 2013). It starts with (a) rock fracturing, followed by (b) the formation of a deep weathering mantle and (c) erosion of the weathering mantle over time until (d) present-day surface has established. The bluish colour indicates the hypothesised increasing accumulation of ^{10}Be over time. (e,f) A local example of this process [Colour figure can be viewed at wileyonlinelibrary.com]

CB (t) is quite common (Scarciglia, Le Pera, Vecchio, & Critelli, 2005b; Raab et al., 2017).

The vegetation cover of the Sila upland plateau consists of grassland, conifers (pines and firs), and deciduous trees (beech; Scarciglia, Le Pera, & Critelli, 2005a; Sorriso-Valvo, 1993). The present-day temperate climate is typical for upland Mediterranean zones having an annual average temperature of 9–12°C and an annual precipitation of 1,000–1,800 mm (Le Pera & Sorriso-Valvo, 2000).

3 | MATERIALS AND METHODS

3.1 | General procedure

A multimethodological approach was chosen to address our research questions. We used the following methods to obtain soil denudation (erosion) rates for the Sila plateau:

- Vertical sampling of tors and determination of the speed of their long-term exhumation rate to derive soil denudation rates using in situ ^{10}Be .
- Sampling of soils near the tors. This was done with the purpose to obtain quantitative current (last 50 years) and indicative mid-

term (decade/century) soil erosion rates by using the fallout radionuclides $^{239+240}\text{Pu}$ and stable carbon isotopes ($\delta^{13}\text{C}$).

In addition, larger scale catchment-wide erosion values (based on ^{10}Be measurements on fluvial sediments) are available for this area and are used for comparison (Olivetti et al., 2012).

3.2 | Sampling of tors for in situ ^{10}Be dating and long-term soil denudation

We sampled three tors having a height of some metres (Figure 3, Table S1). The sampling was carried out (Figure 3b,c) at different heights on the tors in order to assess their possibly multistep exhumation through time. In total, we took six 1- to 3-kg samples of rock per tor at increasing heights from the base, using an electrical stone saw, hammer, and chisel. We sampled the uppermost 1–3 cm of the rock surface and documented the sample thickness (Table S1).

Principally, the longer the surface is exposed to cosmic rays, the more in situ ^{10}Be is accumulated. Due to the fact that ^{10}Be also penetrates the soil surface and that consequently some tors may already have interacted with cosmic rays before they appear at the surface, we also sampled tors below the surface (up to 40 cm) to account for

TABLE 1 Soil features of the Sila Massif upland

Label	Horizon	Depth (cm)	Munsell colour (moist)	Structure	Texture	Organic matter (%)	pH (-)	Sand (%)	Silt (%)	Clay (%)
Scarciglia, Le Pera, Vecchio, and Critelli (2005b):							(H ₂ O)			
P1	A1	0–5/10	10YR 2/2	m, C, m SB	SL	9.3	5.4	56.4	35.6	8.0
	A2	5/10–55	10YR 2/2	m/c AB	L	3.1	5.8	44.6	45.4	10.0
	Bw	55–75	10YR 4/4	m SB	SL	1.0	6.0	59.4	30.6	10.0
	C	75–110+			SG					
P2	A	0–10	10YR 4/2	m SB, vc C	LS					
	Bw1 + Bw2 + Bw3	10–125	10YR 5/4–4/4	m/c SB	LS	0.6	6.1	75.4	16.6	8.0
	Bw4	125–158	10YR 4/2	c SB	LS	1.1	6.1	68.4	19.6	12.0
	2Ab	158–190	10YR 2/2	c AB	SL	3.2	6.2	55.8	32.2	12.0
	2Bwb	190–230	10YR 6/6	m SB	LS	0.5	6.5	75.4	18.2	6.0
	2BC	230–260+	10YR 6/6	m SB	LS					
P3	Oi	0–5								
	A1	5–20/30	10YR 2/2	C C, m SB	L	5.7	5.7	54.6	37.4	8.0
	A2	20/30–45	10YR 2/2	c AB	L	5.4	6.1	46.0	45.0	9.0
	A3	45–60/65	10YR 3/2	f SB	L	3.7	5.9	46.8	45.2	8.0
	2Bw1	60/65–80	7.5YR 4/3	c SB	L	0.9	6.4	57.0	35.0	8.0
	2Bw2	80–100	7.5YR 4/4	c SB	SL	0.6	6.2	61.8	28.2	10.0
	2BC	100–120+	7.5YR 5/4	m SB	SL					
P4	Oi	0–2								
	A	2–25	10YR 3/3	c C, m AB	LS	3.6	5.8	80.6	17.4	2.0
	R	25–60+								
P5	A	0–30/38	10YR 4/4	m C, m SB	L	3.1	5.0	42.6	43.8	13.6
	Bt	30/38–60	7.5YR 4/6	c AB	L	0.9	5.5	37.8	36.6	25.6
	CBt	60–75	7.5YR 4/3	m SB	SL	0.4	5.6	74.4	10.0	15.6
	C	75–100+			S					
Raab et al. (2017):							(CaCl ₂)			
Sila I	A1	0–20	10YR 3/4			10.1	4.8	37.1	38.0	24.9
	A2	20–40	10YR 3/4			6.7	5.0	-	-	-
	Bw	40–60	10YR 4/6			1.3	5.0	60.7	33.4	5.9
	2Bw	60–80	10YR 6/4			1.4	5.1	-	-	-
	2C	80–100	10YR 6/3			0.7	4.9	70.9	22.4	6.7
Sila II	A1	0–20	10YR 3/4			9.0	5.1	-	-	-
	A2	20–40	10YR 3/4			6.1	5.0	-	-	-
	Bw	40–60	10YR 4/6			3.3	5.1	-	-	-
	2Bw	60–80	10YR 6/4			0.9	5.2	-	-	-
	2C	80–100	10YR 6/3			0.9	5.2	-	-	-

Note. The profiles P1–P5 are south of Cecita Lake (near Location 2) and Sila I and II are at Location 1 (Figure 3). Structure: AB: angular blocky; SB: subangular blocky; C: crumbly; f: fine; m: medium; c: coarse; vc: very coarse. Texture: L: loam; SL: sandy loam; LS: loamy sand; S: sand; SG: sandy gravel.

this early subsurface ¹⁰Be accumulation (Figure 3d). The GPS position of each of the sampling sites was recorded and verified with topographic maps. Both the geometry of each tor and the topographic shielding by the surrounding terrain influence the amount of cosmic radiation received at each location. We corrected for these effects, by measuring the dip of the rock surface, its direction, and topographic shielding.

3.3 | Laboratory procedure for surface exposure dating (¹⁰Be)

The sampled rock material was crushed and the 0.6- to 0.25-mm fraction collected (Kohl & Nishiizumi, 1992). The material was then treated

using standard procedures: aqua regia for 36 hr to eliminate iron oxides, carbonates, and organic material; 1 hr treatment with 0.4% hydrogen fluoride (HF) and a floatation system (Kitchener, 1984) to physically separate feldspar and mica components from quartz; and final leaching with 4% HF (7–21 days). A ⁹Be carrier solution (Scharlau, BE03460100) was added to 20–30 g of pure quartz and dissolved in 40% HF. Be was isolated using anion and cation exchange columns (von Blanckenburg, Belshaw, & O'Nions, 1996), and the obtained Be (OH)₂ was calcinated for 2 hr at 850°C to BeO and mixed with Nb powder (and transferred to targets). The targets were measured at the ETH Laboratory of Ion Beam Physics Accelerator Mass Spectrometry facility using the ¹⁰Be standard S2007N with a nominal value of ¹⁰Be/⁹Be = 28.1 × 10⁻¹² (Christl et al., 2013; Kubik & Christl, 2010).

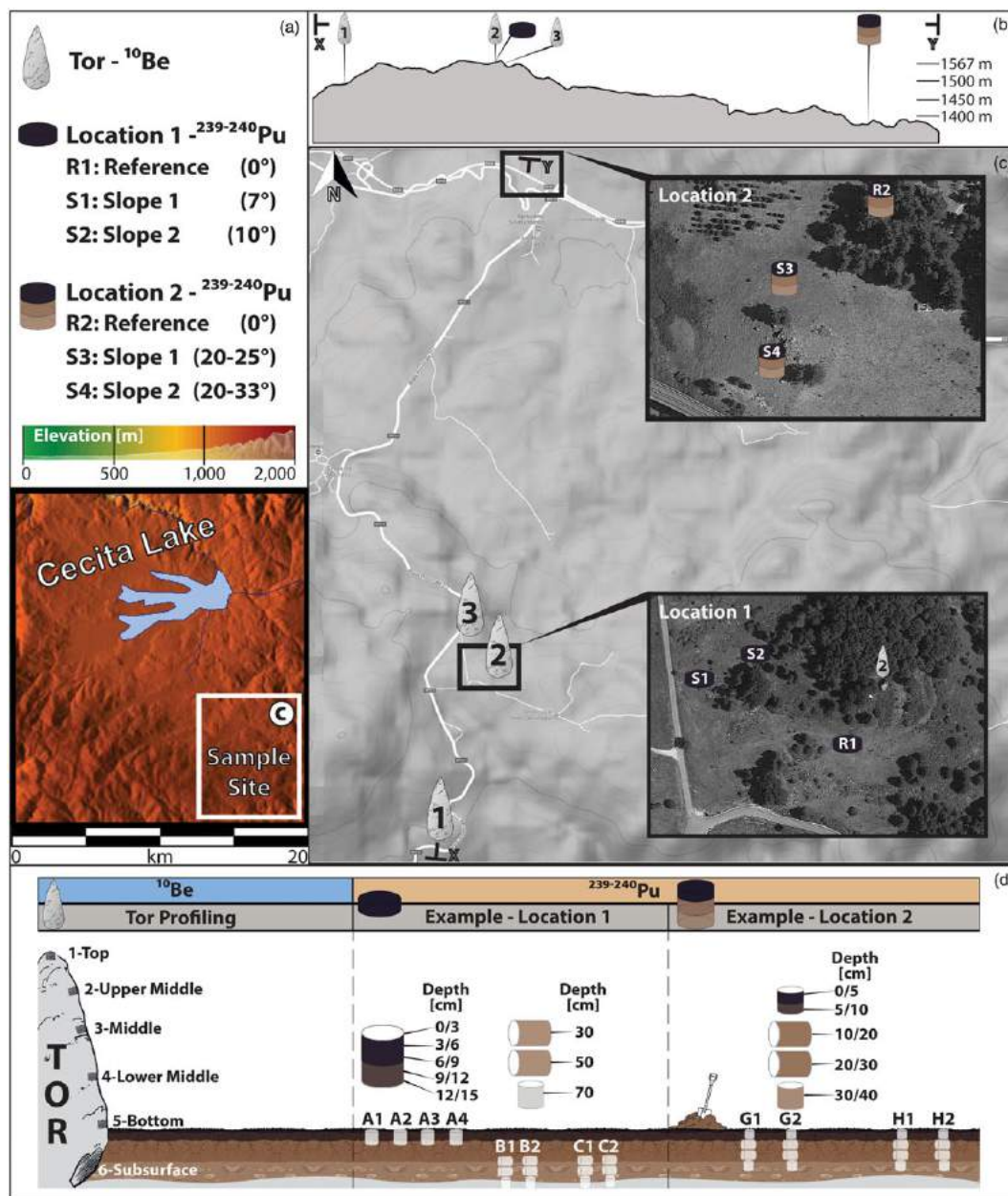


FIGURE 3 (a) Legend for the map symbols and sampling site within the study area. (b) X and Y mark the start and end points of the elevation profile (Google Earth, 2017). (c) Position of the sampled tors (Google Maps, 2017), with close-ups of the soil pits of Locations 1 and 2 (Google Earth, 2017). (d) Illustration of the individual sampling procedure in the field for ¹⁰Be (five samples per tor) and ²³⁹⁺²⁴⁰Pu (with four replicates for each sampling site) [Colour figure can be viewed at wileyonlinelibrary.com]

S2007N has been calibrated to the Nishiizumi standard ICN01-5-1 with a revised nominal value of 2.709×10^{-11} (Nishiizumi et al., 2007). The 1σ error of S2007N is 2.7% (Christl et al., 2013). Measured ¹⁰Be/⁹Be ratios were corrected for ¹⁰Be contributed by the Be carrier (blank value: $3 \pm 0.87 \text{ E-15}$).

¹⁰Be exposure ages were calculated using the cosmogenic nuclide online calculator v2.3 (Balco et al., 2008) with a sea-level high-latitude ¹⁰Be production rate of 4.01 (¹⁰Be atoms gram SiO₂⁻¹ yr⁻¹; Borchers et al., 2016), a ¹⁰Be half-life of $1.387 \pm 0.012 \text{ Ma}$ (Chmeleff, von Blanckenburg, Kossert, & Jakob, 2010; Korschinek, Bergmaier, Faestermann, Gerstmann, & Remmert, 2010), a production rate correction for latitude and altitude (Lal, 1991; Stone, 2000), and a correction for sample thickness (Brown, Edmond, Raisbeck, Yiou, &

Desgarceaux, 1992) using an effective radiation attenuation length of 160 g cm^{-2} (Gosse & Phillips, 2001) and a rock density of 2.7 g cm^{-3} . We tested for various rock erosion rates (0, 1, and 2 mm kyr^{-1}) to cover a greater range of potential variability and, thus, ages and applied no correction for snow.

3.4 | Determination of surface lowering and soil denudation/erosion rates using ¹⁰Be

Ages calculated assuming a rock erosion rate of $0\text{--}1 \text{ mm kyr}^{-1}$ were used for model fitting (height vs. age). Best regression fits were obtained with a polynomial (third order) and a logistic model (Lichter, 1998),

$$f(t) = \frac{a}{(1 + e^{b(t-c)})} + d, \quad (4)$$

where $f(t)$ is the height (m; lowered surface), as a function of time, a the range of height (m), t the time (yr), b the slope coefficient (-), c the time of the maximal rate of change (yr), and d the asymptotic value (m). By taking the error ranges of the ^{10}Be measurements into account (external error), we modelled the height-age relation using Monte Carlo simulations and the previously noted regression fits.

The mathematical derivation of these functions then provided rates in form of surface lowering (SL) (mm yr^{-1}) and, thus, the amount of soil denudation over each time interval. To do this, the age of the rock's initial appearance at the surface (early subsurface ^{10}Be accumulation; t_s) had to be taken into account.

$$\frac{\partial f(t-t_s)}{\partial t} = SL(t). \quad (5)$$

The soil denudation rates ($t \text{ km}^{-2} \text{ yr}^{-1}$), which are mostly due to soil erosion (see Equation (3)), were then obtained by

$$D_{\text{soil}} = E_{\text{soil}} = SL(t) \times \rho_s \times 1,000, \quad (6)$$

with ρ_s as the soil bulk density of 0.82 t m^{-3} .

3.5 | Short- and mid-term soil erosion

We used $^{239+240}\text{Pu}$ for the assessment of the current (last few decades) soil redistribution rates. Because they were emitted during the nuclear weapon tests of the mid-20th century (maximum in 1963–1964), Pu isotopes provide an average soil redistribution rate for the last ~50 years (Wallbrink & Murray, 1993). Soil redistribution rates are calculated on the basis of the differences in Pu activity (Bq m^{-2}) between a local flat reference site and inclined investigation sites (e.g., eroding slopes). It is expected that the 'erosion' sites have a lower Pu activity than the 'reference' site. The signature of stable carbon isotopes and total soil organic carbon content allowed us to qualitatively indicate mid-term disturbances in soils (Zollinger et al., 2015). Due to fractionation during organic matter decomposition, an enrichment of ^{13}C together with a decrease in the C content with increasing soil depth is expected (Schaub & Alewell, 2009).

We choose undisturbed reference soil locations with a flat topography and slopes of varying angles in close proximity as erosion/accumulation sites. We sampled four replicate soils at each of the reference (R) and erosion sites (S1–S4; Figure 3d). In total, three sampling series at two locations were undertaken, whereby Location 1 is associated with Tor 2 for better comparability (Figure 3c). Samples were collected using a 5-cm-diameter core sampler. Soil cores were taken at 3- to 5-cm increments from 0- to 20-cm depths and at higher increments below 20-cm depth (to a maximum depth of 70 cm at Location 1 and to 40 cm at Location 2) at all erosion and reference sites. The soil cores were also used to determine soil bulk densities. A total of 156 soil samples were analysed for Pu and C isotopes.

3.6 | Determination of $^{239+240}\text{Pu}$ in soil samples

The measurement of Plutonium isotopes ($^{239+240}\text{Pu}$) was performed at Northern Arizona University using a Thermo X Series II quadrupole inductively coupled plasma mass spectrometry (ICP-MS) instrument equipped with a high-efficiency desolvating sample introduction system (APEX HF, ESI Scientific, Omaha, NE, USA). A detection limit of $0.1\text{-Bq kg}^{-1} \text{ }^{239+240}\text{Pu}$ was obtained for samples of ~1 g of dry-ashed material (16 hr, 550°C). The measurement error was 1% to 3% for $^{239+240}\text{Pu}$ activities $>1 \text{ Bq kg}^{-1}$. Prior to ICP-MS analysis, the samples were dry ashed and spiked with ~0.005 Bq of a ^{242}Pu tracer (licensed solution from NIST). Pu was leached with 16-mol L^{-1} nitric acid overnight at 80°C and was subsequently separated from the solution using a Pu-selective TEVA resin (Ketterer, Zhang, & Yamada, 2011). The masses 235, 238, 239, 240, and 242 were recorded. Taking the mass bias factor and the UH^+/H^+ ratio into account, the individual mass ratios were corrected and the $^{240}\text{Pu}/^{239}\text{Pu}$ atom ratios determined. Data quality was evaluated through the analysis of blanks (soils or rocks devoid of Pu), duplicates, and control samples having known $^{239+240}\text{Pu}$ activities.

3.7 | $^{239+240}\text{Pu}$ activity conversion into soil redistribution rates

As a basis for the calculation of soil accumulation or erosion rates, the inventory (I) of the $^{239+240}\text{Pu}$ activities (Bq m^{-2}) has to be determined by using the equation

$$I = \frac{1}{A} \sum_i M_i C_i, \quad (7)$$

where A is the horizontal cross-sectional area (m^2), M_i the mass (kg) of the i th sample depth increment, and C_i the activity (Bq kg^{-1}) of the i th subsample depth increment.

Soil redistribution rates were then obtained when the isotope inventory for an eroding point was compared with a local reference inventory where neither soil erosion nor soil accumulation is expected. Two different models were used to convert $^{239+240}\text{Pu}$ inventories into soil redistribution rates:

1. The profile distribution model after Walling and He (1999) and Zhang, Higgitt, and Walling (1990):

$$I'(x) = I_{\text{ref}} \left(1 - e^{-\frac{M_x}{h_0}}\right), \quad (8)$$

where $I'(x)$ is the amount of the isotope inventory (Bq m^{-2}) above the depth (x), I_{ref} the reference inventory (Bq m^{-2} ; Location 1), M_x the mass (kg m^{-2}) between top and actual depth (x), and h_0 the profile shape factor (kg m^{-2}). The soil erosion rate E_{soil} ($\text{t km}^{-2} \text{ yr}^{-1}$) was calculated using

$$E_{\text{soil}} = \frac{10}{t-t_0} \times \ln \left(\frac{I_{\text{ref}} - I_{\text{inv}}}{I_{\text{ref}}} \right) \times h_0 \times 100, \quad (9)$$

where t is the yr of sampling (2015 and 2016), $t_0 = 1,963$ (maximum peak of thermonuclear weapon testing), and I_{inv} is the investigation site inventory (Bq m^{-2}).

2. The inventory method according to Lal et al. (2013) calculating the loss of soil, L (Bq m^{-2}):

$$L = \frac{1}{\alpha P} \times \ln \left(1 - \frac{I_{\text{ref}} - I_{\text{inv}}}{I_{\text{ref}}} \right) \quad (10)$$

where α is the coefficient of the least squares exponential fit of the profile depth to activity after Alewell, Meusburger, Juretzko, and Mabit (2014) and P is the particle size correction factor. For both models, a p value of 1, 1.2 (Walling & He, 1999), and 1.5 (Lal et al., 2013) was used.

3.8 | Soil sample preparation, organic C, and stable carbon isotopes

Soil samples were oven dried at 70°C for 48 hr before being sieved to <2 mm (fine earth). Soil density was obtained from the dry weight of the 100-cm³ soil cores. Oven-dried fine earth samples were then fine milled. The organic carbon (C_{org}) contents were obtained by measuring 0.1-g finely milled soil material in tin capsules with a Leco® C-H-N elemental analyser (Leco TruSpec Micro Analyser) at the Zurich University of Applied Sciences. The EDTA standard (CAS No: 20824-56-0) and the Soil-Leco (Part No: 502-308) were used for standardisation.

The $\delta^{13}\text{C}$ isotopic ratios were measured with a Picarro analyser for isotopic CO_2 (Combustion Module Cavity Ring-Down Spectroscopy, Sunnyvale, California, USA). Instrumental precision is <0.1‰. Soil powder (milled fine earth) was weighed (~0.1 g) into tin capsules and combusted at 950°C. The released CO_2 was measured with a Cavity Ring-Down Spectroscopy analyser (G2131-i). We used an internal standard (30B00GW9 Chernozem 2013) for every six samples to correct for potential drift (<0.5‰) in the C and $\delta^{13}\text{C}$ values.

4 | RESULTS AND DISCUSSION

4.1 | Ancient surface denudation and long-term soil redistribution— ^{10}Be

The 18 collected rock samples (Table S1) provided 15 exposure ages ranging from 10 ± 2 to 106 ± 12 ka (Table S2). The applied different rock erosion rates (0, 1, and 2 mm kyr⁻¹) exerted only a minor influence (average 2.6 ka) on the calculated exposure ages (Figure 4). With a rock erosion of 1 mm kyr⁻¹, Tor 1 has an age of 37 ± 4 ka at 4 m above ground and Tor 3 an age of 36 ± 3 ka at 3.5 m above ground. Tor 2 yielded older overall ages (~100 ka) than Tor 1 and Tor 3, due to its greater height with 5.6 m. The vertical profile sampling series of each tor showed an increasing age trend (Figure 4a,c,e) along with higher ^{10}Be concentrations (Figure 4g) towards the tors' top surfaces. The increase in the ^{10}Be concentration with tor height reflects the conceptual idea that tors are exhumed over time at our study area. The tor assemblage shows consistent exhumation trends. The average exhumation rates were 0.054 ± 0.027 , 0.052 ± 0.026 , and 0.050 ± 0.026 mm yr⁻¹, respectively. Obstacles that could have led to abrupt changes of the ^{10}Be signal (e.g., exfoliation) were not observed in field. Samples taken to determine early subsurface ^{10}Be accumulation had similar atom counts as the bottom-most tor surface

samples. Based on these indifferent results, we can assume that the surface lowering has occurred in a similar manner across the plateau. The calculated exhumation rates, therefore, represent a net soil denudation that is almost equal to soil erosion (Equations (3) and (6)).

Soil denudation/erosion rates over time were modelled by using the surface ages (and, thus, the tors' exhumation rates; Figure 4b,d,f). The rates are in the range of 50–300 t km⁻² yr⁻¹ for the last 25 ka (Figure 4b,f). Due to the greater size of Tor 2 and, thus, older ages (Figure 4c), its model provides insight over the last 100 ka and indicates rates of 0–130 t km⁻² yr⁻¹ (Figure 4d). By combining the information derived from all tors, we constructed a relatively detailed time sequence for the last ~100 ka (Figure 4h).

The total soil denudation rates have clearly changed over time. The lowest rates were calculated for the period 100–20 ka BP. Higher rates are seen before 100 ka BP and after 20 ka BP. Soil erosion rates showed a maximum of about 250 t m⁻² yr⁻¹ (about 0.31-mm yr⁻¹ soil material) at the transition from the Pleistocene to the Holocene. Minimum rates were measured around 50–100 ka BP with about 0–0.12 mm yr⁻¹. Based on earlier geomorphological and pedological investigations, Scarciglia (2015) and Scarciglia et al. (2016) estimated the average erosion rates for the Sila upland to be in the range of <0.01–0.05 to 0.10–0.21 mm yr⁻¹. With a soil density of approximately 0.82 g cm⁻³, the soil erosion rates vary between 8 and 170 t km⁻² yr⁻¹. These values fit well with the rates that we obtained.

Our values are also consistent with uplift-driven Pleistocene–Holocene erosion rates (0.04–0.6 mm yr⁻¹; about 30–490 t km⁻² yr⁻¹), estimated for various areas of the southern Apennines (north of Calabria; Amato, Aucelli, & Cinque, 2003; Gioia, Martino, & Schiattarella, 2011; Martino, Nico, & Schiattarella, 2009). Catchment-wide average erosion rates of the steep slopes at the border of the Sila upland are given in Olivetti et al. (2012). These rates vary between 0.08 and 0.92 mm yr⁻¹ (expressed on the basis of quartz with a density of 2.6 g cm⁻³) or about 216–2,480 t km⁻² yr⁻¹. Catchment-based erosion rates, however, include all erosion processes, not all of which are related to soil.

4.2 | Qualitative soil erosion estimates— $\delta^{13}\text{C}$

The $\delta^{13}\text{C}$ values of all soil sites (Table S3) increase with soil depth and range between –28‰ and –25‰ (Figure 5). In contrast, total C_{org} decreases with depth. Therefore, all investigated soil profiles exhibit a negative linear correlation between $\delta^{13}\text{C}$ and C_{org} . The negative correlation of C_{org} and $\delta^{13}\text{C}$ can qualitatively indicate the extent of mid-term disturbances in soils (Zollinger et al., 2015). However, when only erosion (and no accumulation or mixing) occurs, the depth trends of C_{org} and $\delta^{13}\text{C}$ still remain similar. The lowest correlations ($\rho = -0.87$) are calculated for flat surfaces (0°) of the R sites and slightly higher correlations ($\rho = -0.89$ to -0.93) for slopes. We also obtained a C_{org} content of <0.5% at 40–70 cm, whereas the $\delta^{13}\text{C}$ values showed a large variability (most likely due to increasing accuracy problems with a low carbon content). These $\delta^{13}\text{C}$ values were not considered for the correlation calculations. In contrast to findings of Zollinger et al. (2015), our $\delta^{13}\text{C}$ trends did not indicate any particular disturbances that could be directly related to erosion/accumulation.

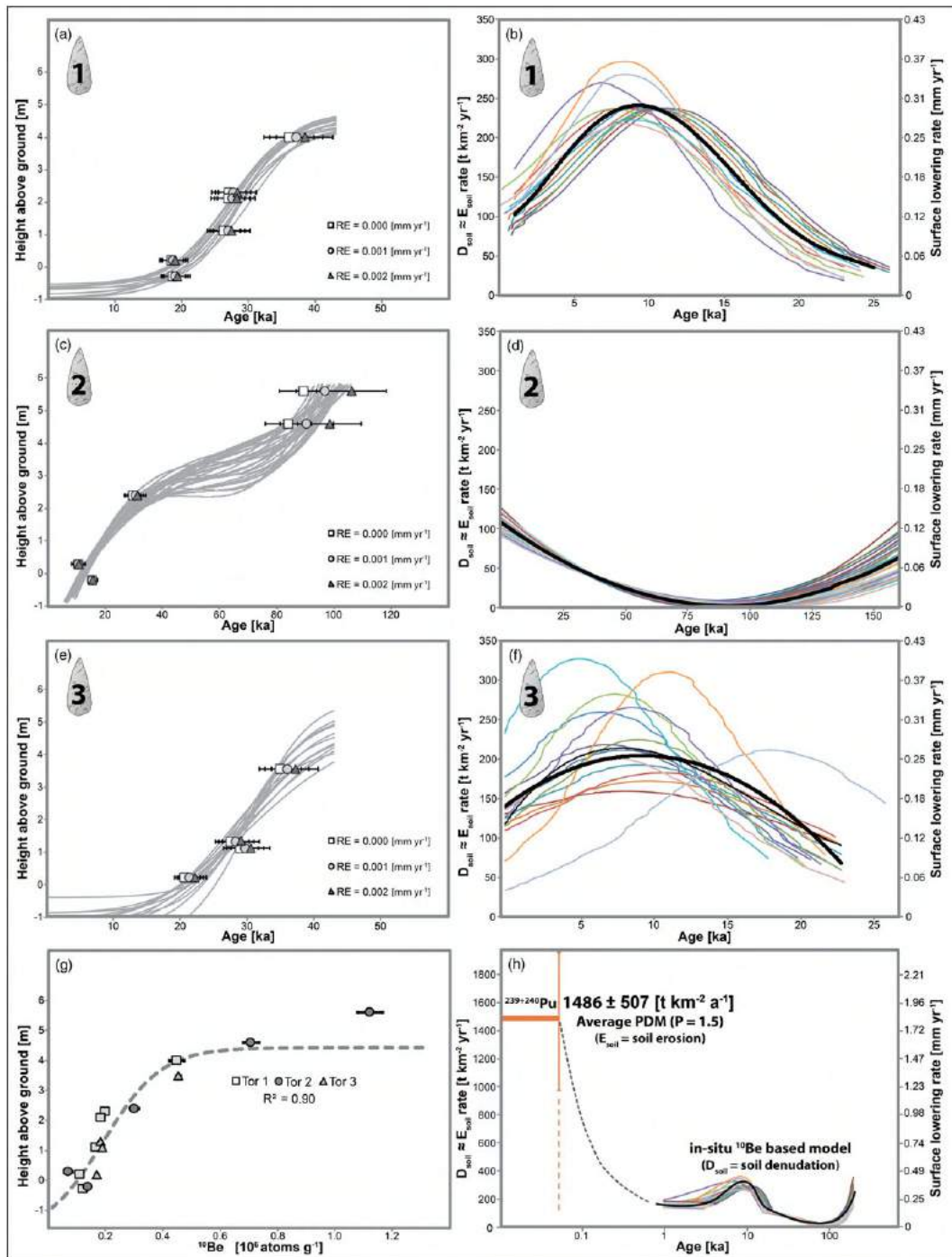


FIGURE 4 Exposure ages (^{10}Be) as a function of tor height and derived soil denudation/erosion rates (using a Monte Carlo simulation) for Tor 1 (a,b), Tor 2 (c,d), and Tor 3 (e,f). ^{10}Be concentrations as a function of height (with a related trend curve) of all samples are plotted in (g). Temporal evolution of soil denudation/erosion rates (h) using both, ^{10}Be and $^{239+240}\text{Pu}$ data. For simplicity, soil erosion is assumed to be almost equal to soil denudation (see Equations (2), (3), and (6)) [Colour figure can be viewed at wileyonlinelibrary.com]

4.3 | Modern soil erosion rates of the Sila upland— $^{239+240}\text{Pu}$

The $^{240}\text{Pu}/^{239}\text{Pu}$ atomic ratios of all samples (Figure 6a) lie within the characteristic signature of the fallout in the northern hemisphere (0.180 ± 0.014 ; Kelly et al., 1999) and do not indicate contributions or influences from any regional source(s). Reference and

erosion sites have a similar and consistent $^{240}\text{Pu}/^{239}\text{Pu}$ signals throughout all depth increments. Only a few samples of Location 1 have slightly higher values (up to 0.248 ± 0.0045).

The $^{239+240}\text{Pu}$ activity distributions (Figure 6b) along the profiles of Location 2 are consistent with observed trends in the literature, where higher activities were reported to occur near the surface and exponentially decrease with depth (Alewell et al.,

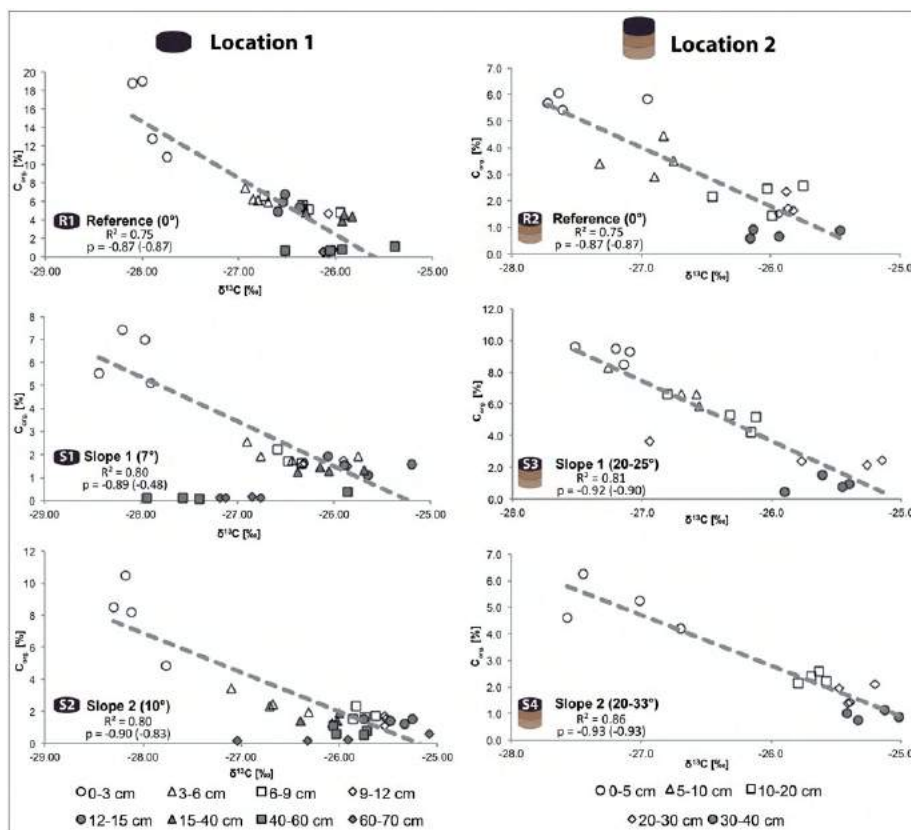


FIGURE 5 Correlation between C_{org} (organic carbon content) and $\delta^{13}C$ values as indicator of soil disturbance/stability. Below a concentration of 0.5% of C_{org} , $\delta^{13}C$ could not be measured accurately enough; these values were not considered for the correlation [Colour figure can be viewed at wileyonlinelibrary.com]

2014; Portes et al., 2018; Lal et al., 2013, Meusburger et al., 2016; Zollinger et al., 2015). In contrast, Location 1 has an unusual Pu depth trend, although similar activity trends were reported by Ketterer et al. (2004) and Frielinghaus and Vahrson (1998). At Location 1, bioturbation (visible in the field) seems to have been one cause for the unusual Pu depth trend. The $\delta^{13}C$ data however indicate (Figure 5) that not only bioturbation but also other processes such as a translocation with colloids (clays) may have contributed. The pH values of the soils (Table 1) are in the appropriate range to indicate that clay migration is reasonable. To a limited extent, Pu is also involved in soil-forming processes (Bunzel, Kracke, & Schimmak, 1995).

Nevertheless, the Pu total inventory (Figure 6b) reflects the expected erosional behaviour signal of the study sites, where a lower activity was measured on slopes than on flat surfaces. The highest total inventory of $176 \pm 18 \text{ Bq m}^{-2}$ was determined for R1. This quantity was used as basis for the profile distribution model and inventory method. Our $^{239+240}\text{Pu}$ data indicate soil erosion at all investigated sites (Figure 6c, Table 2). Interestingly, the $^{239+240}\text{Pu}$ activity ($\sim 0.8 \text{ Bq kg}^{-1}$) at Location 2 in the topsoil is quite similar to the site R1 at 15-cm depth ($\sim 0.7 \text{ Bq kg}^{-1}$; Figure 6b). We assume that the soil at Location 2 has lost part of its uppermost layer (first $\sim 15 \text{ cm}$) in the recent past. Observations of erosion rims (sometimes $>30 \text{ cm}$; with traces of clay coatings on the rock) between the present-day soil surface and boulders or tors also indicate recent erosion events (Scarciglia, 2015).

Furthermore, the soil erosion rates (Figure 6c) of Location 2 are distinctly higher than those of Location 1. The erosion rates at Site 1 vary from 1,000 to 2,100 $\text{t km}^{-2} \text{ yr}^{-1}$ whereas erosion rates range from 1,200 to over 3,500 $\text{t km}^{-2} \text{ yr}^{-1}$ at Site 2. Soil erosion rates are also found to be higher along steeper hill slopes (Figure 6d). The fact that soils of Location 2 have steeper slopes and are shallower compared with Location 1 further supports our assumption that Location 2 has recently lost part of its uppermost layer.

In general, the recent soil erosion rates in the Sila upland (on slopes) with about 1,000 to more than 3,000 $\text{t km}^{-2} \text{ yr}^{-1}$ are very high. According to Alewell, Egli, and Meusburger (2015), soil erosion rates in alpine areas at intensively used slopes ranged from 600 to 3,000 $\text{t km}^{-2} \text{ yr}^{-1}$. Such rates are certainly not compatible with a sustainable use of soils.

4.4 | Past progressive and regressive soil formation

To estimate tolerable rates of soil erosion/denudation, it is important to know the soil production/formation rates that are counteracting soil loss processes (Alewell et al., 2015; McFadden, 2013). Several empirical investigations show that the rate of soil production or soil formation is a function of time (e.g., Alewell et al., 2015; Anderson, Dietrich, & Brimhall, 2002). According to Alewell et al., average soil production rates in alpine areas for relatively old soils ($>10\text{--}18 \text{ ka}$) range around 54–113 $\text{t km}^{-2} \text{ yr}^{-1}$. Production rates for young soils ($>1\text{--}10 \text{ ka}$) are between 119 and 248 $\text{t km}^{-2} \text{ yr}^{-1}$, and rates for very

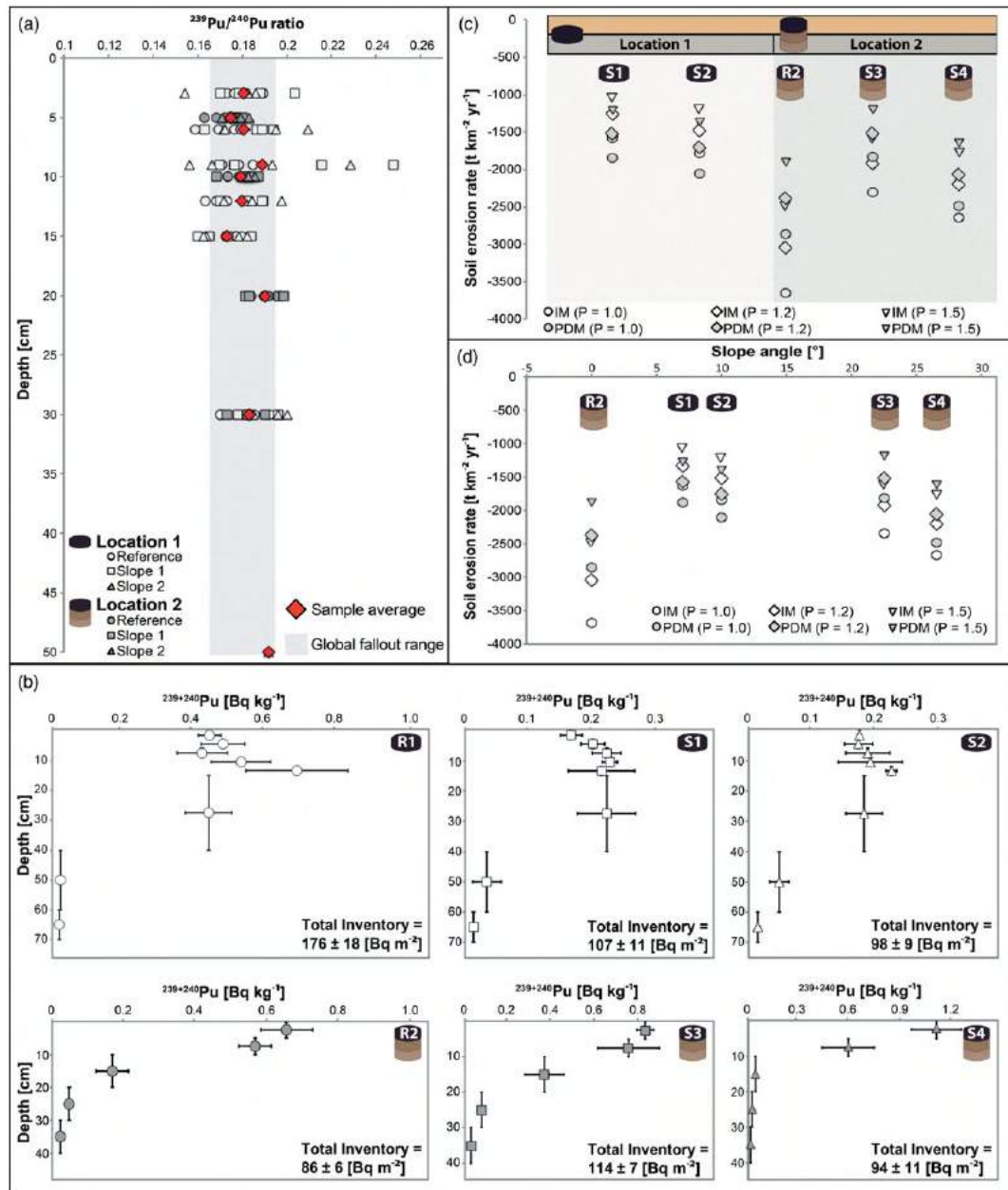


FIGURE 6 (a) $^{240}\text{Pu}/^{239}\text{Pu}$ ratio of the soil samples as a function of soil depth. The average for each depth increment is given in red. The grey area indicates the global fallout range (0.180 ± 0.014) of the northern hemisphere (Kelly, Bond, & Beasley, 1999). (b) Depth activity profiles (\pm standard error) of the investigated sites. (c) Calculated annual soil erosion using different particle size correction factors ($p = 1.0, 1.2, \text{ and } 1.5$) for the inventory method (IM; R Lal et al., 2013) and the profile distribution model (PDM; Walling & He, 1999; Zhang et al., 1990). (d) Calculated soil erosion ranges in relation to the slope angle [Colour figure can be viewed at wileyonlinelibrary.com]

young soils (≤ 1 ka) are between 415 and $881 \text{ t km}^{-2} \text{ yr}^{-1}$. Dixon and von Blanckenburg (2012) estimated a maximum soil production rate in the range of 320 – $450 \text{ km}^{-2} \text{ yr}^{-1}$, whereas Alewell et al. (2015) and Larsen et al. (2014) set this value much higher (for very young soils or highly eroding sites up to $2,000 \text{ t km}^{-2} \text{ yr}^{-1}$). The average soil denudation rates for the Sila plateau over the last 20 ka are about $145 \text{ t km}^{-2} \text{ yr}^{-1}$.

Overall, the soil denudation/erosion rates have strongly varied in the Sila mountains. At the transition from the Pleistocene to the Holocene, we observe rates of up to $300 \text{ t km}^{-2} \text{ yr}^{-1}$. This fits well with findings of Zanchetta, Borghini, Fallick, Bonadonna, and Leone (2007) and Tinner et al. (2009) who showed that a higher

frequency of forest fires occurred at the onset of the Holocene. The presence of organised human societies since the Bronze Age in southern Italy and the Baleari Islands, around 4,000 cal BP, was detected by a repeated increase in fire events, which are most likely of anthropogenic origin (Peréz-Obiol & Sadori, 2007). Pollen analyses of the Lago Grande di Monticchio clearly show that the Apennine mountain chain was increasingly influenced by forest clearance and agricultural activity over the last 2,000 years (Allen, Watts, McGee, & Huntley, 2002)—a phenomenon that is also documented in the Sila upland by pedological, charcoal, and historical data (Moser, Di Pasquale, Scarciglia, & Nelle, 2017; Pelle et al., 2013; Scarciglia et al., 2008).

TABLE 2 Calculated soil erosion rates of $^{239+240}\text{Pu}$ investigated soil pits of Location 1 (S1 and S2) and Location 2 (S3, S4, and R2) after Lal et al. (2013), Walling and He (1999), and Zhang et al. (1990) applying diverse particle size correction factors (PM)

		Inventory method (IM)			Profile distribution model (PDM)		
		PM = 1 ($\text{t km}^{-2} \text{yr}^{-1}$)	PM = 1.2 ($\text{t km}^{-2} \text{yr}^{-1}$)	PM = 1.5 ($\text{t km}^{-2} \text{yr}^{-1}$)	PM = 1 ($\text{t km}^{-2} \text{yr}^{-1}$)	PM = 1.2 ($\text{t km}^{-2} \text{yr}^{-1}$)	PM = 1.5 ($\text{t km}^{-2} \text{yr}^{-1}$)
S1	Average	-1,585	-1,320	-1,056	-1,881	-1,568	-1,254
	Std. error	13.5	13.2	11.8	19.3	17.6	15.8
S2	Average	-1,813	-1,511	-1,209	-2,098	-1,748	-1,398
	Std. error	14.0	12.8	11.5	16.1	14.7	13.2
S3	Average	-2,307	-1,922	-1,538	-1,832	-1,527	-1,221
	Std. error	45.4	41.5	37.1	40.3	36.8	32.9
S4	Average	-2,640	-2,200	-1,760	-2,478	-2,065	-1,652
	Std. error	39.9	36.5	32.6	36.1	33.0	29.5
R2	Average	-3,649	-3,041	-2,433	-2,853	-2,378	-1,902
	Std. error	55.6	50.7	45.4	47.9	43.8	39.1
Total Average		-2,399	-1,999	-1,599	-2,228	-1,857	-1,486
Std. error		46	42	38	38	35	31

Note. Figure 6 provides a more graphical display.

Our compiled soil formation and soil production rates (Figure 7a,b) of Mediterranean to alpine climates demonstrate that several regressive soil evolutionary phases must have occurred at the investigated site. Only young soils (>1–10 ka) with high soil production rates would have been able to cope with the relatively high soil erosion rates ($\sim 300 \text{ t km}^{-2} \text{ yr}^{-1}$) at the Pleistocene–Holocene transition. Only very young ($\leq 1 \text{ ka}$) and shallow soils ($\sim 20 \text{ cm}$) have such high soil production rates that would equal the observed soil erosion rates for the last 50 years ($\geq 1,000 \text{ t km}^{-2} \text{ yr}^{-1}$).

Based on our dataset, we estimated (very roughly) the counterpart of soil denudation over time (Figure 7c). The study area received ash input from volcanic eruptions on the Lipari Islands (Raab et al., 2017) several-times (with three major eruptions) during the last 15 to 90 ka (that corresponds approximately to the duration of soil formation). Soil aggradation by ashes is also supported by field evidence (Scarciglia, 2015). The fresh and unweathered material serves as new substrate and counteracts soil erosion as explained in Ugolini and Dahlgren (2002). With each new ash input, the soil production rate increases drastically for roughly 800 years to a magnitude range of $\geq 1,000 \text{ t km}^{-2} \text{ yr}^{-1}$ (Figure 7b,c). Due to the rejuvenation of the soil parent material, the soil production remained $>100 \text{ t km}^{-2} \text{ yr}^{-1}$ for about 10 ka (Figure 7b,c). Although these estimates are only approximate, they nonetheless show that progressive phases of soil formation, presumably (vitric) Cambisols, occurred between about 55–30 ka BP and 20–15 ka BP (Figure 7c,d). The two dominating soil-forming processes were probably transformation through chemical weathering and addition of new material (volcanic glass and minerals) as well as decomposing (dead) plant tissue. We see that regressive phases prevail particularly during the last 15–20 ka where soil denudation rates increased to about $300 \text{ t km}^{-2} \text{ yr}^{-1}$ and were, as an average, about 50–100 $\text{t km}^{-2} \text{ yr}^{-1}$ higher than soil production rates (Figure 7c,d).

4.5 | Present situation and outlook

Although a large part of the Sila Massif is a forested national park, it is partly used for arable crops and livestock (sheep and cattle) and still records the effects of intensive land use of the recent past. Where intense grazing still exists or where arable farming still occurs, soil erosion rates are high. On flat surfaces and where human impacts are low (e.g., with forest cover), conditions close to steady state (Figure 7d) may be established between soil production and soil denudation (Scarciglia et al., 2016). The Pu data indicate soil erosion rates on slopes of $\geq 1,000 \text{ t km}^{-2} \text{ yr}^{-1}$. These rates appear to be considerably higher than during the past 10–60 ka (Figure 7d).

Conforti et al. (2013) concluded that intensive land use and annual crops have greatly contributed to the sediment input of the nearby Crati basin (Figure 1c). Bajard et al. (2017) demonstrated that deforestation already in medieval times has led to erosion rates in mountain areas of the European Alps of $1,000 \text{ t km}^{-2} \text{ yr}^{-1}$. Arable farming even caused erosion rates of up to $1,230 \text{ t km}^{-2} \text{ yr}^{-1}$. Vanacker, Bellin, Molina, and Kubik (2014) stated that a decreasing vegetation cover leads to an exponential increase in total erosion rates. The results of Hewawasam, von Blanckenburg, Schaller, and Kubik (2003) suggest that soil is lost 10–100 times faster on agricultural land. It is therefore reasonable to assume that the episode of higher soil erosion rates (detected by the Pu isotopes) is caused by human impact (e.g., overgrazing, pasture, and deforestation).

Our understanding of the Sila upland is that soil erosion rates of about $200\text{--}300 \text{ t km}^{-2} \text{ yr}^{-1}$ are the natural maximum. This natural maximum might be climate driven when looking at the timing of the increase in denudation/erosion (post-Last Glacial Maximum [LGM]; Figures 4h and 7d). The increase in denudation rates at the transition from a cold to a warm period (climate change) has also been reported by Schaller et al. (2016). The sea surface temperature of the

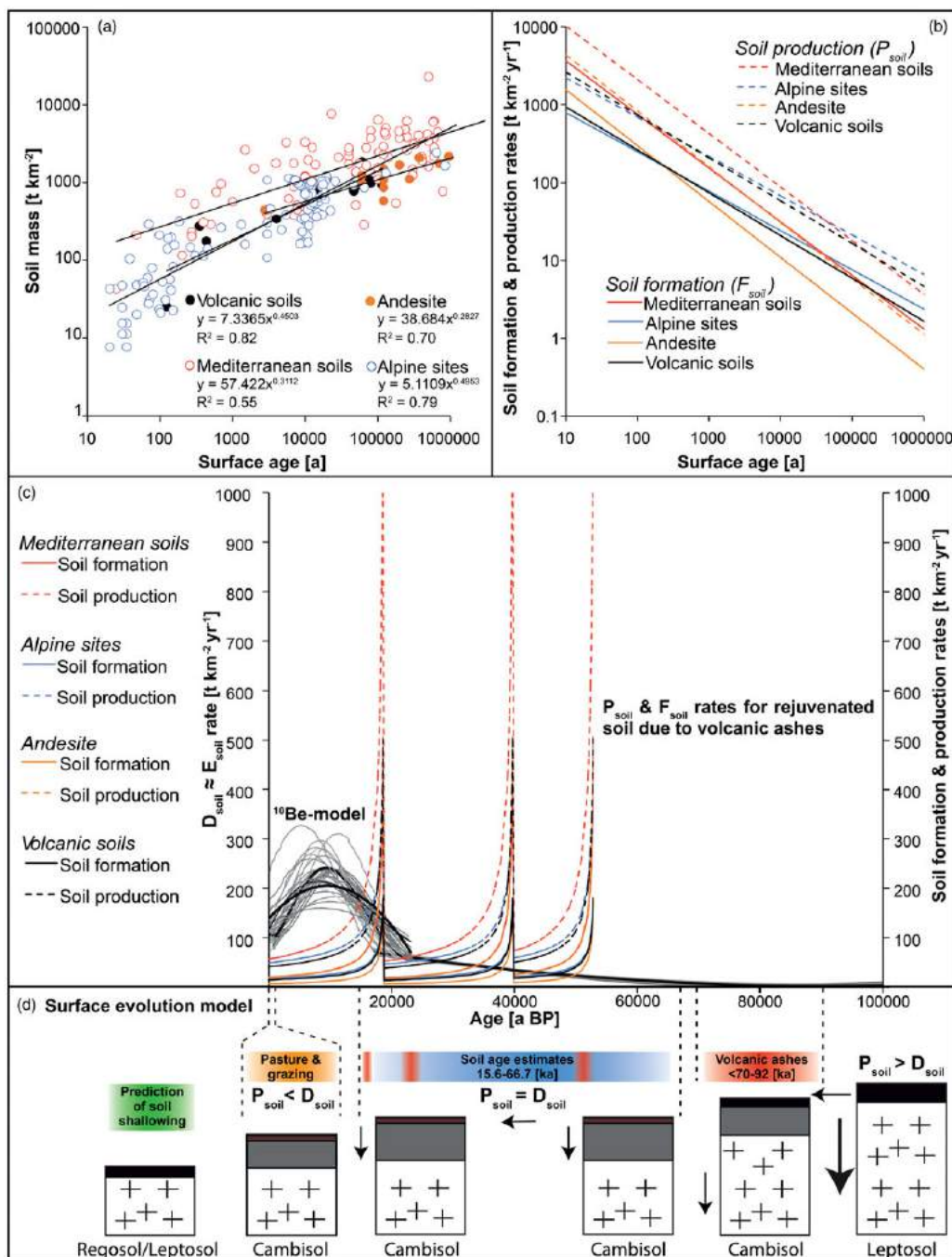


FIGURE 7 (a) Correlation between soil mass and surface age using chronosequences of volcanic, Mediterranean (and andesitic), and alpine soils after Egli et al. (2008, 2014, and references therein) and Alewell et al. (2015). (b) Mathematical derivation of the regression functions is given in (a). This derivation gives soil formation and production rates (Alewell et al., 2015) over time. (c) Comparison between soil denudation/erosion (black and grey lines; ¹⁰Be-model) and soil formation/production rates (coloured lines) for the last 50 ka. Soil formation and production rates are derived from the regression curves given in Figure 7b. Over the entire soil formation period, three volcanic eruption periods (Lipari Islands) with subsequent ash input have occurred and led to a rejuvenation of the soils (Raab et al., 2017; Ugolini & Dahlgren, 2002). This gave rise to a sharp increase in the soil production and soil formation rate. (d) Conceptual model: Reconstruction of past and prediction of future soil evolution based on (c) and results from Raab et al. (2017) [Colour figure can be viewed at wileyonlinelibrary.com]

Tyrrhenian Sea (Figure 1c) started to rise ~18 ka BP; it reached its maxima around 8.9–8.4 ka BP (Cacho et al., 2001). This trend is similar to our denudation/erosion rates model (Figure 7c). Also, rapid environmental changes with increased moisture availability and biomass production in southern Italy (Lago Grande di Monticchio) were reported by Allen et al. (1999), starting ~15 ka ago. The abrupt warming and increase in precipitation after the LGM (Bølling transition) have

probably led to the increase in denudation/erosion up to its natural maximum around 9 ka ago.

The present-day use of the landscape often results in high erosion rates, which disrupts the balance between the natural removal of surface material and soil production. Steady-state conditions cannot be expected in such a situation. Therefore, the upland of the Sila Massif is now in a distinctly regressive phase with respect to soils. If the

current regressive phase of soil formation continues then Cambisols will—over long-time periods (century to millennia)—transform into a rockier landscape (Figure 7d) with very shallow Leptosols (soil depth < 5 cm) or Regosols (see Alewell et al., 2015).

5 | CONCLUSIONS

Our multi-isotope approach has allowed us to decipher new archives containing a long-term history of the surface evolution of the Sila upland plateau, Italy. This novel approach has shown that the exhumation rates of tors (as determined by surface exposure dating) give valuable insight into the temporal evolution of surface denudation and, thus, of soil erosion. Using the exposure age of tor surfaces, we were able to trace soil denudation and erosion over for the last 100 ka. Through the use of $^{239+240}\text{Pu}$, we were able to extrapolate the time series to the present. The correlation between $\delta^{13}\text{C}$ and total C_{org} did not provide any further, useful information about erosion.

We detected extremely low rates from MIS6/MIS5 (130–80 ka; Lisiecki, 2005) to the LGM (~21 ka), mostly below $30 \text{ t km}^{-2} \text{ yr}^{-1}$ (about 0.036 mm yr^{-1}). Over this period, continuous soil formation seemed to have occurred (progressive phase), also stimulated by a volcanic ash input from the Lipari Islands. However, soil erosion rates strongly increased at the transition from the Pleistocene to the Holocene, with the effect that total denudation rates were faster than soil production rates giving rise to a regressive phase of soil evolution. The rapid warming and accompanied increasing moisture at this time are a plausible cause for this. The strong increase in soil erosion during the Holocene and particularly during the last few decades is largely due to human impact. The $^{239+240}\text{Pu}$ data suggest soil erosion rates for the last five decades ($\geq 1,000 \text{ t km}^{-2} \text{ yr}^{-1}$; about 1.22 mm yr^{-1}) that are far above the natural rates of soil production. This will definitely lead to a distinct decrease in soil depth and with time to a landscape with shallower soils and rockier surface.

We showed that tors and boulders are a useful archive to reconstruct surface processes and soil erosion events. Together with Pu isotopes, this archive could be extended to the recent past and a relatively detailed chronology was obtained. Denudation processes could therefore be traced back from human to more geological timescales.

ACKNOWLEDGMENTS

This research was supported by the Swiss National Science Foundation (SNSF - Schweizerischer Nationalfonds zur Förderung der Wissenschaftlichen Forschung) project Grant 200021_162338/1. Special thanks go to Rahel Wanner of the ZHAW for the CHN measurements and Moritz Reisser for his help in the laboratory. Kevin Patrick Norton was supported by a SNSF Visiting International Fellowship (IZKOZ2_170715/1) and the Royal Society Te Apārangi Rutherford Discovery Fellowship. Fabio Scarciglia was supported by a SNSF grant for a Short Research Visit (IZKOZ2_147421). Finally, we thank three anonymous reviewers and Kristina Hippe for their constructive suggestions.

ORCID

Gerald Raab  <http://orcid.org/0000-0002-3063-6806>

REFERENCES

- Alewell, C., Egli, M., & Meusburger, K. (2015). An attempt to estimate tolerable soil erosion rates by matching soil formation with denudation in Alpine grasslands. *Journal of Soils and Sediments*, 15(6), 1383–1399. <https://doi.org/10.1007/s11368-014-0920-6>
- Alewell, C., Meusburger, K., Juretzko, G., Mabit, L., & Ketterer, M. E. (2014). Suitability of $^{239+240}\text{Pu}$ and ^{137}Cs as tracers for soil erosion assessment in mountain grasslands. *Chemosphere*, 103, 274–280. <https://doi.org/10.1016/j.chemosphere.2013.12.016>
- Alewell, C., Pitois, A., Meusburger, K., Ketterer, M., & Mabit, L. (2017). $^{239+240}\text{Pu}$ from “contaminant” to soil erosion tracer: Where do we stand?. *Earth-Science Reviews*, 172, 107–123. <https://doi.org/10.1016/j.earscirev.2017.07.009>
- Allen, J. R. M., Brandt, U., Brauer, A., Hubberten, H. W., Huntley, B., Keller, J., ... Zolitschka, B. (1999). Rapid environmental changes in southern Europe during the last glacial period. *Nature*, 400, 740–743. <https://doi.org/10.1038/23432>
- Allen, J. R. M., Watts, W. A., McGee, E., & Huntley, B. (2002). Holocene environmental variability – the record from Lago Grande di Monticchio, Italy. *Quaternary International*, 88, 69–80. [https://doi.org/10.1016/S1040-6182\(01\)00074-X](https://doi.org/10.1016/S1040-6182(01)00074-X)
- Amato, A., Aucelli, P. P. C., & Cinque, A. (2003). The long-term denudation rate in the Southern Apennines Chain (Italy): A GIS-aided estimation of the rock volumes eroded since middle Pleistocene time. *Quaternary International*, 101–102, 3–11. [https://doi.org/10.1016/S1040-6182\(02\)00087-3](https://doi.org/10.1016/S1040-6182(02)00087-3)
- Anderson, S. P., Dietrich, W. E., & Brimhall, G. H. (2002). Weathering profiles, mass-balance analysis, and rates of solute loss: Linkages between weathering and erosion in a small, steep catchment. *Geological Society of America Bulletin*, 114(9), 1143–1158. [https://doi.org/10.1130/0016-7606\(2002\)114<1143:WPMBAA>2.0.CO;2](https://doi.org/10.1130/0016-7606(2002)114<1143:WPMBAA>2.0.CO;2)
- Bajard, M., Poulencard, J., Sabatier, P., Develle, A. L., Giguet-Covex, C., Jacob, J., ... Arnaud, F. (2017). Progressive and regressive soil evolution phases in the Anthropocene. *Catena*, 150, 39–52. <https://doi.org/10.1016/j.catena.2016.11.001>
- Balco, G., Stone, J. O., Lifton, N. A., & Dunai, T. J. (2008). A complete and easily accessible means of calculating surface exposure ages or erosion rates from ^{10}Be and ^{26}Al measurements. *Quaternary Geochronology*, 8, 174–195. <https://doi.org/10.1016/j.quageo.2007.12.001>
- Bartley, R., Croke, J., Brainbridge, Z. T., Austin, J. M., & Kuhnert, P. M. (2015). Combining contemporary and long-term erosion rates to target erosion hot-spots in the Great Barrier Reef, Australia. *Anthropocene*, 10(1–2), 1–12. <https://doi.org/10.1016/j.ancene.2015.08.002>
- Bellin, N., Vanacker, N., & Kubik, P. W. (2014). Denudation rates and tectonic geomorphology of the Spanish Betic Cordillera. *Earth and Planetary Science Letters*, 390, 19–30. <https://doi.org/10.1016/j.epsl.2013.12.045>
- Bierman, P. R., & Caffee, M. (2001). Slow rates of rock surface erosion and sediment production across the Namib Desert and escarpment, Southern Africa. *American Journal of Science*, 301(4–5), 326–358. <https://doi.org/10.2475/ajs.301.4-5.326>
- von Blanckenburg, F., Belshaw, N. S., & O’Nions, R. K. (1996). Separation of ^9Be and cosmogenic ^{10}Be from environmental materials and SIMS isotope dilution analysis. *Chemical Geology*, 129, 93–99. [https://doi.org/10.1016/0009-2541\(95\)00157-3](https://doi.org/10.1016/0009-2541(95)00157-3)
- Boardman, J., & Poesen, J. (2007). *Soil erosion in Europe*. Chichester: John Wiley & Sons Ltd. <https://doi.org/10.1002/0470859202>
- Borchers, B., Marrero, S., Balco, G., Caffee, M., Goehring, B., Lifton, N., ... Stone, J. (2016). Geological calibration of spallation production rates in the CRONUS-Earth project. *Quaternary Geochronology*, 31, 188–198. <https://doi.org/10.1016/j.quageo.2015.01.009>
- Brown, E. T., Edmond, J. M., Raisbeck, G. M., Yiou, F., & Desgarceaux, S. (1992). Effective attenuation length of cosmic rays producing ^{10}Be and ^{26}Al in quartz: Implications for surface exposure dating. *Geophysical Research Letters*, 9, 369–372. <https://doi.org/10.1029/92GL00266>

- Bunzel, K., Kracke, W., & Schimmak, W. (1995). Migration of fallout $^{239+240}\text{Pu}$, ^{241}Am and ^{137}Cs in the various horizons of a forest soil under pine. *Journal of Environmental Radioactivity*, 28, 17–34. [https://doi.org/10.1016/0265-931X\(94\)00066-6](https://doi.org/10.1016/0265-931X(94)00066-6)
- Cacho, I., Grimalt, J. O., Canals, M., Sbaiffi, L., Shackleton, N. J., Schönfeld, J., & Zahn, R. (2001). Variability of the western Mediterranean Sea surface temperature during the last 25,000 years and its connection with the Northern Hemisphere climatic changes. *Paléo*, 16, 40–52. <https://doi.org/10.1029/2000PA000502>
- Chmeleff, J., von Blanckenburg, F., Kossert, K., & Jakob, D. (2010). Determination of the ^{10}Be half-life by multicollector ICP-MS and liquid scintillation counting. *Nuclear Instruments and Methods in Physics Research Section B: Beam Interaction with Materials and Atoms*, 268, 192–199. <https://doi.org/10.1016/j.nimb.2009.09.012>
- Christl, M., Vockenhuber, C., Kubik, P. Q., Wacker, L., Lachner, J., Alfimov, V., & Synal, H. A. (2013). The ETH Zurich AMS facilities: Performance parameters and reference materials. *Nuclear Instruments and Methods in Physics Research B*, 294, 29–38. <https://doi.org/10.1016/j.nimb.2012.03.004>
- Clift, P. D., Wan, S., & Blusztajn, J. (2014). Reconstructing chemical weathering, physical erosion and monsoon intensity since 25 Ma in the northern South China Sea: A review of competing proxies. *Earth Science Reviews*, 130, 86–102. <https://doi.org/10.1016/j.earscirev.2014.01.002>
- Conforti, M., Buttafuoco, G., Leone, A. P., Aucelli, P. P. C., Robustelli, G., & Scarciglia, F. (2013). Studying the relationship between water-induced soil erosion and soil organic matter using Vis-NIR spectroscopy and geomorphological analysis: A case study in southern Italy. *Catena*, 110, 44–58. <https://doi.org/10.1016/j.catena.2013.06.013>
- Darmody, R. G., Thorn, C. E., Seppälä, M., Campbell, S. W., Li, Y. K., & Harbor, J. (2008). Age and weathering status of granite tors in Arctic Finland (~68°N). *Geomorphology*, 94, 10–23. <https://doi.org/10.1016/j.geomorph.2007.04.006>
- van der Knijff JM, Jones RJA, Montanarella L. (1999). Soil erosion risk assessment in Italy. European Soil Bureau. EUR 19044 EN.
- van der Knijff JM, Jones RJA, Montanarella L. (2000). Soil erosion risk assessment in Europe. European Soil Bureau. EUR 19044 EN.
- Dixon, J. L., & von Blanckenburg, F. (2012). Soils as pacemakers and limiters of global silicate weathering. *Comptes Rendus Geoscience*, 344(11), 597–609. <https://doi.org/10.1016/j.crte.2012.10.012>
- Egli, M., Mirabella, A., Nater, M., Alioth, L., & Raimondi, S. (2008). Clay minerals, oxyhydroxide formation, element leaching and humus development in volcanic soils. *Geoderma*, 143, 101–114. <https://doi.org/10.1016/j.geoderma.2007.10.020>
- Egli, M., Norton, K., & Dahms, D. (2014). Soil formation rates on silicate parent material in alpine environments: Different approaches—different results? *Geoderma*, 213, 320–333. <https://doi.org/10.1016/j.geoderma.2013.08.016>
- Egli, M., & Poulencard, J. (2016). Soils of mountainous landscapes. In *International Encyclopedia of Geography: People, the Earth, Environment and Technology*, 1–10. <https://doi.org/10.1002/9781118786352.wbieg0197>
- von Eynatten, H., Tolosana-Delgado, R., Karius, V., Bachmann, K., & Caracciolo, K. (2015). Sediment generation in humid Mediterranean setting: Grain-size and source-rock control on sediment geochemistry and mineralogy (Sila Massif, Calabria). *Sedimentary Geology*, 336, 68–80. <https://doi.org/10.1016/j.sedgeo.2015.10.008>
- Frielinghaus, M., & Vahrson, W. G. (1998). Soil translocation by water erosion from agricultural cropland into wet depressions (morainic kettle holes). *Soil and Tillage Research*, 46, 23–30. [https://doi.org/10.1016/S0167-1987\(98\)80104-9](https://doi.org/10.1016/S0167-1987(98)80104-9)
- Gioia, D., Martino, C., & Schiattarella, M. (2011). Long- to short-term denudation rates in the southern Apennines: Geomorphological markers and chronological constraints. *Geologica Carpathica*, 62(1), 27–41. <https://doi.org/10.2478/v10096-011-0003-1>
- Google Earth. (2017). Version 7.3.2.5491 (July 10, 2017). Calabria Italy: Sila Massif.
- Google Maps. (2017). Retrieved from <https://www.google.com/maps/@39.3261099,16.527087,11.57z>
- Gosse, J. C., & Phillips, F. M. (2001). Terrestrial in situ produced cosmogenic nuclides: Theory and application. *Quaternary Science Reviews*, 20, 1475–1560. [https://doi.org/10.1016/S0277-3791\(00\)00171-2](https://doi.org/10.1016/S0277-3791(00)00171-2)
- Gunnell, Y., Jarman, D., Braucher, R., Calvet, M., Delmas, M., Leanni, L., ... Keddaouche, K. (2013). The granite tors of Dartmoor, Southwest England: Rapid and recent emergence revealed by Late Pleistocene cosmogenic apparent exposure ages. *Quaternary Science Reviews*, 61, 62–76. <https://doi.org/10.1016/j.quascirev.2012.11.005>
- Heimsath, A. M., Chappell, J., Dietrich, W. E., Nishiizumi, K., & Finkel, R. C. (2001). Late Quaternary erosion in southeastern Australia: A field example using cosmogenic nuclides. *Quaternary International*, 83, 169–185. [https://doi.org/10.1016/S1040-6182\(01\)00038-6](https://doi.org/10.1016/S1040-6182(01)00038-6)
- Hewawasam, T., von Blanckenburg, F., Schaller, M., & Kubik, P. W. (2003). Increase of human over natural erosion rates in tropical highlands constrained by cosmogenic nuclides. *Geology*, 31, 597–600. [https://doi.org/10.1130/0091-7613\(2003\)031<0597:IOHONE>2.0.CO;2](https://doi.org/10.1130/0091-7613(2003)031<0597:IOHONE>2.0.CO;2)
- Ibbeken, H., & Schleyer, R. (1991). *Source and sediment: A case study of provenance and mass balance at an active plate margin (Calabria, Southern Italy)*. Heidelberg: Springer. <https://doi.org/10.1007/978-3-642-76165-2>
- Johnson, D. L., & Watson-Stegner, D. (1987). Evolution model of pedogenesis. *Soil Science*, 143, 349–366.
- Kelly, J. M., Bond, L. A., & Beasley, T. M. (1999). Global distribution of Pu isotopes and ^{237}Np . *The Science of the Total Environment*, 237–238, 483–500. [https://doi.org/10.1016/S0048-9697\(99\)00160-6](https://doi.org/10.1016/S0048-9697(99)00160-6)
- Ketterer, M. E., Hafer, K. M., Link, C. L., Kolwaite, D., Wilson, J., & Mietelski, J. W. (2004). Resolving global versus local/regional Pu sources in the environment using sector ICP-MS. *Journal of Analytical Atomic Spectrometry*, 19, 241–245. <https://doi.org/10.1039/B302903D>
- Ketterer, M. E., Zhang, J., & Yamada, M. (2011). Application of transuranics as tracers and chronometers in the environment. In M. Baskaran (Ed.), *Handbook of environmental isotope geochemistry (Advances in Isotope Geochemistry)*. Heidelberg: Springer. <https://doi.org/10.1007/978-3-642-10637-8>
- Kirchner, J. W., Finkel, R. C., Riebe, C. S., Granger, D. E., Clayton, J. L., King, J. G., & Megahan, W. F. (2001). Mountain erosion over 10 yr, 10 ky, and 10 my time scales. *Geology*, 29(7), 591–594. [https://doi.org/10.1130/0091-7613\(2001\)029<0591:MEQYKY>2.0.CO;2](https://doi.org/10.1130/0091-7613(2001)029<0591:MEQYKY>2.0.CO;2)
- Kitchener, J. A. (1984). The froth flotation process: Past, present and future—in brief. In K. J. Ives (Ed.), *The scientific basis of flotation (Vol. 75) NATO ASI Series (Series E: Applied Sciences)*. Dordrecht: Springer. https://doi.org/10.1007/978-94-009-6926-1_2
- Kohl, C., & Nishiizumi, K. (1992). Chemical isolation of quartz for measurement of in-situ-produced cosmogenic nuclides. *Geochimica Cosmochimica Acta*, 56, 3583–3587. [https://doi.org/10.1016/0016-7037\(92\)90401-4](https://doi.org/10.1016/0016-7037(92)90401-4)
- Korschinek, G., Bergmaier, A., Faestermann, T., Gerstmann, U. C., & Rimmert, A. (2010). A new value for the half-life of ^{10}Be by heavy-ion elastic recoil detection and liquid scintillation counting. *Nuclear Instruments and Methods in Physics Research Section B: Beam Interaction with Materials and Atoms*, 268, 187–191. <https://doi.org/10.1016/j.nimb.2009.09.020>
- Kubik, P. W., & Christl, M. (2010). ^{10}Be and ^{26}Al measurements at the Zurich 6 MV Tandem AMS facility. *Nuclear Instruments and Methods B*, 268, 880–883. <https://doi.org/10.1016/j.nimb.2009.10.054>
- Lal, D. (1991). Cosmic ray labelling or erosion surfaces: In situ nuclide production rates and erosion models. *Earth and Planetary Science Letters*, 104, 424–439. [https://doi.org/10.1016/0012-821X\(91\)90220-C](https://doi.org/10.1016/0012-821X(91)90220-C)
- Lal, R., Tims, S. G., Fifield, L. K., Wasson, R. J., & Howe, D. (2013). Applicability of Pu-239 as a tracer for soil erosion in the wet-dry tropics of northern Australia. *Nuclear Instruments and Methods in Physics Research Section B*, 294, 577–583. <https://doi.org/10.1016/j.nimb.2012.07.041>

- Larsen, I. J., Almond, P. C., Eger, A., Stone, J. O., Montgomery, D. R., & Malcolm, B. (2014). Rapid soil production and weathering in the Western Alps, New Zealand. *Science*, 1244908. <https://doi.org/10.1126/science.1244908>, 637–640.
- Le Pera, E., & Sorriso-Valvo, M. (2000). Weathering and morphogenesis in a Mediterranean climate, Calabria, Italy. *Geomorphology*, 34(3), 251–270. [https://doi.org/10.1016/S0169-555X\(00\)00012-X](https://doi.org/10.1016/S0169-555X(00)00012-X)
- Lichter, J. (1998). Rates of weathering and chemical depletion in soils across a chronosequence of Lake Michigan sand dunes. *Geoderma*, 85, 255–282. [https://doi.org/10.1016/S0016-7061\(98\)00026-3](https://doi.org/10.1016/S0016-7061(98)00026-3)
- Liotta, D., Caggianelli, A., Kruhl, J. H., Festa, V., Prosser, G., & Langoe, A. (2008). Multiple injections of magmas along a Hercynian mid-crustal shear zone (Sila Massif, Calabria, Italy). *Journal of Structural Geology*, 30, 1202–1217. <https://doi.org/10.1016/j.jsg.2008.04.005>
- Lisiecki, L. E., & Raymo, M. E. (2005). A Pliocene-Pleistocene stack of 57 globally distributed benthic $\delta^{18}\text{O}$ records. *Paleoceanography*, 20, PA1003. <https://doi.org/10.1029/2004PA001071>
- Martino, C., Nico, G., & Schiattarella, M. (2009). Quantitative analysis of InSAR digital elevation models for identification of areas with different tectonic activity in southern Italy. *Earth Surface Processes and Landforms*, 34, 3–15. <https://doi.org/10.1002/esp.1681>
- McFadden, L. D. (2013). Strongly dust-influenced soils and what they tell us about landscape dynamics in vegetated arid lands of the southwestern United States. *Geological Society of America Special Papers*, 500, 501–532. [https://doi.org/10.1130/2013.2500\(15\)](https://doi.org/10.1130/2013.2500(15))
- Meusburger, K., Mabit, L., Ketterer, M., Park, J. H., Sandor, T., Porto, P., & Alewell, C. (2016). A multi-radionuclide approach to evaluate the suitability of $^{239+240}\text{Pu}$ as soil erosion tracer. *Science of the Total Environment*, 566, 1489–1499. <https://doi.org/10.1016/j.scitotenv.2016.06.035>
- Migoń, P. (2013). Weathering and hillslope development. In J. F. Shroder (Ed.), *Treatise on geomorphology* (Vol. 4) (pp. 159–178). San Diego: Academic Press. <https://doi.org/10.1016/B978-0-12-374739-6.00075-0>
- Molin, P., Pazzaglia, F. J., & Dramis, F. (2004). Geomorphic expression of active tectonics in a rapidly-deforming fore-arc, Sila Massif, Calabria, Southern Italy. *American Journal of Science*, 304, 559–589. <https://doi.org/10.2475/ajs.304.7.559>
- Moser, D., Di Pasquale, G., Scarciglia, F., & Nelle, O. (2017). Holocene mountain forest changes in central Mediterranean: Soil charcoal data from the Sila Massif (Calabria, southern Italy). *Quaternary International*, 457, 113–130. <https://doi.org/10.1016/j.quaint.2017.01.042>
- Mourier, B., Poulencard, J., Carcaillet, C., & Williamson, D. (2010). Soil evolution and subalpine ecosystem changes in the French Alps inferred from geochemical analysis of lacustrine sediments. *Journal of Paleolimnology*, 44(2), 571–587. <https://doi.org/10.1007/s10933-010-9438-0>
- Nishiizumi, K., Imamura, M., Caffee, M. W., Southon, J. R., Finkel, R. C., & McAnich, J. (2007). Absolute calibration of ^{10}Be AMS standards. *Nuclear Instruments & Methods in Physics Research Section B-Beam Interactions with Materials and Atoms*, 258, 403–413. <https://doi.org/10.1016/j.nimb.2007.01.297>
- Olivetti, V., Cyr, A. J., Molin, P., Faccenna, C., & Granger, D. E. (2012). Uplift history of the Sila Massif, southern Italy, deciphered from cosmogenic ^{10}Be erosion rates and river longitudinal profile analysis. *Tectonics*, 31, 1–19. <https://doi.org/10.1029/2011TC003037>
- Pelle, T., Scarciglia, F., Di Pasquale, G., Allevato, E., Marino, D., Robustelli, G., ... Pulice, I. (2013). Multidisciplinary study of Holocene archaeological soils in an upland Mediterranean site: Natural versus anthropogenic environmental changes at Cecita Lake, Calabria, Italy. *Quaternary International*, 303, 163–179. <https://doi.org/10.1016/j.quaint.2013.04.003>
- Pérez-Obiol, R., & Sadori, L. (2007). Similarities and dissimilarities, synchronisms and diachronisms in the Holocene vegetation history of the Balearic Islands and Sicily. *Vegetation History and Archaeobotany*, 16(4), 259–265. <https://doi.org/10.1007/s00334-006-0038-x>
- Portes, R., Dahms, D., Brandová, D., Raab, G., Christl, M., Kühn, P., ... Egli, M. (2018). Evolution of soil erosion rates in alpine soils of the Central Rocky Mountains using fallout Pu and $\delta^{13}\text{C}$. *Planetary Science Letters*, 496, 258–269. <https://doi.org/10.1016/j.epsl.2018.06.002>
- Pimentel, D. (2006). Soil erosion: A food and environmental threat. *Environment, Development and Sustainability*, 8(1), 119–137. <https://doi.org/10.1016/j.epsl.2004.07.031>
- Poesen, J. (2018). Soil erosion in the Anthropocene: Research needs. *Earth Surface Processes and Landforms*, 43, 64–84. <https://doi.org/10.1002/esp.4250>
- Raab, G., Halpern, D., Scarciglia, F., Raimondi, S., Norton, K., Pettke, T., ... Egli, M. (2017). Linking tephrochronology and soil characteristics in the Sila and Nebrodi mountains, Italy. *Catena*, 158, 266–285. <https://doi.org/10.1016/j.catena.2017.07.008>
- Reeves, D., & Rothman, D. H. (2014). Diffusion and kinetic control of weathering layer development. *Geofluids*, 14, 128–142. <https://doi.org/10.1111/gfl.12056>
- Rossetti, F., Faccenna, C., Goffé, B., Monié, P., Argentieri, A., Funicello, R., & Mattei, M. (2001). Alpine structural and metamorphic signature of the Sila Piccola Massif nappe stack (Calabria, Italy): Insights for the tectonic evolution of the Calabrian Arc. *Tectonics*, 20, 112–133. <https://doi.org/10.1029/2000TC900027>
- Scarciglia, F. (2015). Weathering and exhumation history of the Sila upland plateaus, southern Italy: A geomorphological and pedological perspective. *Journal of Soils and Sediments*, 15, 1278–1291. <https://doi.org/10.1007/s11368-014-0923-3>
- Scarciglia, F., Critelli, S., Borrelli, L., Coniglio, S., Muto, F., & Perri, F. (2016). Weathering profiles in granitoid rocks of the Sila Massif uplands, Calabria, southern Italy: New insights into their formation process and rates. *Sedimentary Geology*, 336, 46–67. <https://doi.org/10.1016/j.sedgeo.2016.01.015>
- Scarciglia, F., De Rosa, R., Vecchio, G., Apollaro, C., Robustelli, G., & Terrasi, F. (2008). Volcanic soil formation in Calabria (southern Italy): The Cecita Lake geosol in the late Quaternary geomorphological evolution of the Sila uplands. *Journal of Volcanology Geothermal Research*, 177, 101–117. <https://doi.org/10.1016/j.jvolgeores.2007.10.014>
- Scarciglia, F., Le Pera, E., & Critelli, S. (2005a). Weathering and pedogenesis in the Sila Grande Massif (Calabria, south Italy): From field scale to micromorphology. *Catena*, 61, 1–29. <https://doi.org/10.1016/j.catena.2005.02.001>
- Scarciglia, F., Le Pera, E., Vecchio, G., & Critelli, S. (2005b). The interplay of geomorphic processes and soil development in an upland environment, Calabria, South Italy. *Geomorphology*, 69, 169–190. <https://doi.org/10.1016/j.geomorph.2005.01.003>
- Schaller, M., Ehlers, T. A., Stor, T., Torrent, J., Lobato, L., Christl, M., & Vockenhuber, C. (2016). Spatial and temporal variations in denudation rates derived from cosmogenic nuclides in four European fluvial terrace sequences. *Geomorphology*, 274, 180–192. <https://doi.org/10.1016/j.geomorph.2016.08.018>
- Schaub, M., & Alewell, C. (2009). Stable carbon isotopes as an indicator for soil degradation in an alpine environment (Urseren Valley, Switzerland). *Rapid Communications Mass Spectrometry*, 23, 1499–1507. <https://doi.org/10.1002/rcm.4030>
- Smithson, P., Addison, K., & Atkinson, K. (2008). *Fundamentals of the physical environment: Fourth edition* (Vol. 65). (pp. 234–235). New York: Routledge. https://doi.org/10.1111/j.1745-7939.2009.01167_1.x
- Sommer, M., Gerke, H. H., & Deumlich, D. (2008). Modelling soil landscape genesis—A “time split” approach for hummocky agricultural landscapes. *Geoderma*, 145, 480–493. <https://doi.org/10.1026/j.geoderma.2008.01.012>
- Sorriso-Valvo, M. (1993). The geomorphology of Calabria. A sketch. *Geografia Fisica e Dinamica Quaternaria*, 16, 75–80.
- Spina, V., Galli, P., Tondi, M., Critelli, S., & Cello, G. (2007). Kinematics and structural properties of an active fault zone in the Sila Massif (Northern Calabria, Italy). *Bollettino Della Società Geologica Italiana*, 126, 427–438.
- Stone, J. O. (2000). Air pressure and cosmogenic isotope production. *Journal of Geophysical Research*, 105, 753–759. <https://doi.org/10.1029/2000JB900181>

- Tinner, W., van Leeuwen, J. F. N., Colombaroli, D., Vescovi, E., van der Knapp, W. O., Henne, D. P., ... La Mantia, T. (2009). Holocene environmental and climatic changes at Gorgo Basso, a coastal lake in southern Sicily, Italy. *Quaternary Science Reviews*, 28, 1498–1510. <https://doi.org/10.1016/j.quascirev.2009.02.001>
- Twidale, C. R. (2002). The two-stage concept of landform and landscape development involving etching: Origin, development and implications of an idea. *Earth-Science Reviews*, 57(1–2), 37–74. [https://doi.org/10.1016/S0012-8252\(01\)00059-9](https://doi.org/10.1016/S0012-8252(01)00059-9)
- Ugolini, F. C., & Dahlgren, R. A. (2002). Soil development in volcanic ash. *Global Environmental Research*, 6(2), 69–82.
- Vanacker, V., Bellin, N., Molina, A., & Kubik, P. W. (2014). Erosion regulation as a function of human disturbances to vegetation cover: A conceptual model. *Landscape Ecology*, 29(2), 293–309. <https://doi.org/10.1007/s10980-013-9956-z>
- Vespasiano, G., Apollaro, C., De Rosa, R., Muto, F., Larosa, S., Fiebig, J., ... Marini, L. (2015). The Small Spring Method (SSM) for the definition of stable isotope–elevation relationships in northern Calabria (Southern Italy). *Applied Geochemistry*, 63, 333–346. <https://doi.org/10.1016/j.apgeochem.2015.10.001>
- Wakasa, S., Matsuzaki, H., Tanaka, Y., & Matsukura, Y. (2006). Estimation of episodic exfoliation rates of rock sheets on a granite dome in Korea from cosmogenic nuclide analysis. *Earth Surface Processes and Landforms*, 31, 1246–1256. <https://doi.org/10.1002/esp.1328>
- Wallbrink, P. J., & Murray, A. S. (1993). Use of fallout radionuclides as indicators of erosion processes. *Hydrological Processes*, 7, 297–304. <https://doi.org/10.1002/hyp.3360070307>
- Walling, D., & He, Q. (1999). Improved models for estimating soil erosion rates from cesium-137 measurements. *Journal of Environmental Quality*, 28, 611–622. <https://doi.org/10.2134/jeq1999.00472425002800020027x>
- Zanchetta, G., Borghini, A., Fallick, A. E., Bonadonna, F. P., & Leone, G. (2007). Late Quaternary palaeohydrology of Lake Pergusa (Sicily, southern Italy) as inferred by stable isotopes of lacustrine carbonates. *Journal of Palaeolimnology*, 38, 227–239. <https://doi.org/10.1007/s10933-006-9070-1>
- Zhang, X., Higgitt, D. L., & Walling, D. E. (1990). A preliminary assessment of the potential for using caesium-137 to estimate rates of soil erosion in the Loess Plateau of China. *Hydrological Science Journal*, 35, 43–252. <https://doi.org/10.1080/02626669009492427>
- Zollinger, B., Alewell, C., Kneisel, C., Meusburger, K., Brandová, D., Kubik, P., ... Egli, M. (2015). The effect of permafrost on time-split soil erosion using radionuclides (^{137}Cs , $^{239+240}\text{Pu}$, meteoric ^{10}Be) and stable isotopes ($\delta^{13}\text{C}$) in the eastern Swiss Alps. *Journal of Soils and Sediments*, 15(6), 1400–1419. <https://doi.org/10.1007/s11368-014-0881-9>

SUPPORTING INFORMATION

Additional supporting information may be found online in the Supporting Information section at the end of the article.

How to cite this article: Raab G, Scarciglia F, Norton K, et al. Denudation variability of the Sila Massif upland (Italy) from decades to millennia using ^{10}Be and $^{239+240}\text{Pu}$. *Land Degrad Dev*. 2018;29:3736–3752. <https://doi.org/10.1002/ldr.3120>

Climate and relief-induced controls on the temporal variability of denudation rates in a granitic upland

Gerald Raab,^{1*} Markus Egli,¹ Kevin Norton,² Dennis Dahms,³ Dagmar Brandová,¹ Marcus Christl⁴ and Fabio Scarciglia⁵

¹ Department of Geography, University of Zurich, Zurich, Switzerland

² School of Geography, Environment and Earth Sciences, Victoria University of Wellington, Wellington, New Zealand

³ Department of Geography, University of Northern Iowa, Cedar Falls, IA USA

⁴ Department of Physics, ETH, Zurich, Zurich, Switzerland

⁵ Department of Biology, Ecology and Earth Sciences (DiBEST), University of Calabria, Arcavacata di Rende (CS), Italy

Received 31 October 2018; Revised 29 May 2019; Accepted 29 May 2019

*Correspondence to: Gerald Raab, Department of Geography, University of Zurich, Winterthurerstrasse 190, 8057 Zurich, Switzerland. E-mail: gerald.raab@geo.uzh.ch

ESPL

Earth Surface Processes and Landforms

ABSTRACT: How soil erosion rates evolved over the last about 100 ka and how they relate to environmental and climate variability is largely unknown. This is due to a lack of suitable archives that help to trace this evolution. We determined *in situ* cosmogenic beryllium-10 (¹⁰Be) along vertical landforms (tors, boulders and scarps) on the Sila Massif to unravel their local exhumation patterns to develop a surface denudation model over millennia.

Due to the physical resistance of tors, their rate of exhumation may be used to derive surface and, thus, soil denudation rates over time. We derived soil denudation rates that varied in the range 0–0.40 mm yr⁻¹. The investigated boulders, however, appear to have experienced repositioning processes about ~20–25 ka BP and were therefore a less reliable archive. The scarps of the Sila upland showed a rapid bedrock exposure within the last 8–15 ka. Overall, the denudation rates increased steadily after 75 ka BP but remained low until about 17 ka BP. The exhumation rates indicate a denudation pulse that occurred about 17–5 ka BP. Since then the rates have continuously decreased.

We identify three key factors for these developments – climate, topography and vegetation. Between 75 and 17 ka BP, climate was colder and drier than today. The rapid changes towards warmer and humid conditions at the Pleistocene–Holocene transition apparently increased denudation rates. A denser vegetation cover with time counteracted denudation.

Topography also determined the extent of denudation rates in the upland regime. On slopes, denudation rates were generally higher than on planar surfaces. By determining the exhumation rates of tors and scarps, soil erosion rates could be determined over long timescales and be related to topography and particularly to climate. This is key for understanding geomorphic dynamics under current environmental settings and future climate change. © 2019 John Wiley & Sons, Ltd.

KEYWORDS: granite landscape; Sila Massif; tor; denudation; cosmogenic nuclides

Introduction

Landscape surfaces can be very dynamic and are often driven by environment- and climate-induced changes. Although there are numerous and detailed climate archives, few attempts have been done so far to quantify soil denudation rates over time (e.g. Bajard *et al.*, 2017), due to a deficiency in continuous *in situ* records. Catchment-wide approaches are more commonly used to infer average surface lowering and denudation rates. However, such approaches make the coupling with specific landscape sites (e.g. slopes, ridges, planes) or environmental conditions difficult, as landscapes may not evolve uniformly or linearly. To understand landscape evolution more comprehensively, new approaches and (*in situ*) archives are needed that preserve the temporal signal of surface lowering over time. A recent study (Raab *et al.*, 2018) indicated that geomorphic forms of granite landscapes (Figure 1) may preserve the

denudation signal over time. Here, we explore the potential of a variety of granite landforms such as boulders, tors or scarps in more detail.

The distinction between these three landforms may appear straightforward, but the contrary is often the case. Scarps can be associated with cliffs, steep slopes or with displaced landforms (e.g. faults, landslides) that are commonly seen as bedrock outcrops along vertical or inclined surfaces that lack more detailed definition. Boulders are generally seen as rounded rock masses detached from bedrock with a diameter greater than 256 mm (Bates and Jackson, 1987) but sizes vary greatly from 25 cm to over 33 m in diameter. Boulders have also been defined as just ‘more-or-less’ rounded, isolated or clustered masses of standing rock (Linton, 1955).

The most ambiguous term of all of these is the ‘tor’. Most famous for describing the castellated granite landscape of Dartmoor (UK), the word is broadly used for large residual

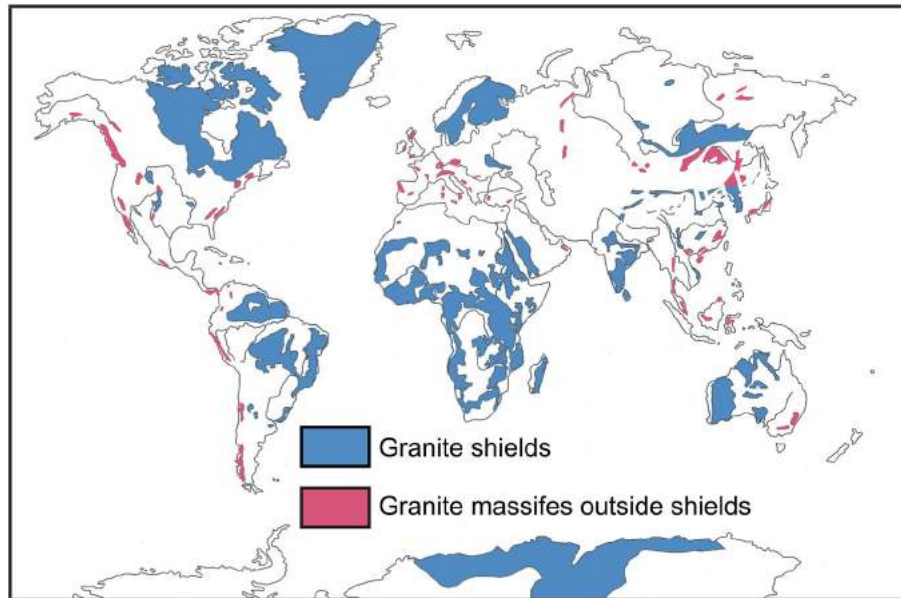


Figure 1. Granite landscapes around the world, differentiated between ancient shields and exhumed massifs. The map is modified after Migoñ (2006). [Colour figure can be viewed at wileyonlinelibrary.com]

rocks (tower-like or dome-shaped), often castellated landforms (Linton, 1955). They characteristically have rounded summits or form convex ridges and seldom exceed 10–15 m in height (Migoñ, 2006). Thomas (1965) described them as spherically weathered boulders which are still rooted in bedrock.

Although such granitic landscapes are ubiquitous, the geomorphic literature mostly contains conceptual models with little empirical data (Linton, 1955; Migoñ, 2006; and references cited therein). The timing and the forces that enable the formation of granitic outcrops are more often qualitatively described rather than quantitatively assessed (e.g. Twidale, 2002; Phillips *et al.*, 2006). Depending on local conditions, boulders, tors and scarps may form within the saprolite. Rock tors and boulders have higher physical resistance than the surrounding soils or saprolite that are more easily weathered (Migoñ and Vieira, 2014). Therefore, in an eroding landscape, tors are exhumed over time by the lowering of the surrounding surface, through surface denudation rates, D_{Surface} ; denudation processes consisting of W , weathering [i.e. conversion of bedrock to loose (erodible) material] and E , physical erosion (transport of mobile material by e.g. wind, water):

$$D_{\text{Surface}} = W + E \quad (1)$$

Thus, the rate of exhumation can be used to indicate denudation of the surrounding surface. Few studies have quantified the temporal development of particular landscape features (e.g. Gunnell *et al.*, 2013; Heimsath *et al.*, 2001). So far, granitic landforms such as tors, boulders and scarps have rarely been used as an environmental archive to trace rates of surface and relief development (Raab *et al.*, 2018).

Vertical age profiles along tor surfaces allow the determination of their exhumation history and subsequently the calculation of surface denudation rates over several time intervals (continuous and over millennia; Heimsath *et al.*, 2001; Wakasa *et al.*, 2006; Raab *et al.*, 2018). Applying the same technique to boulders and scarps enlarges the possibilities and enables comparisons among local formation patterns. Consequently, we use tors, boulders and scarps of a granitic landscape to explore surface lowering over time and, by extrapolation, past denudation rates of the surrounding landscape (predominantly erosion). Due to the fact that tors, boulders and scarps are more physically and chemically resistant than the saprolite or soil, surface

denudation causes their exhumation over time. By deriving *in situ* beryllium-10 (^{10}Be) surface exposure ages along these geomorphic landforms, we attempt to trace rates of surface lowering and, thus, soil denudation rates during the Holocene and part of the Pleistocene. We assume that denudation rates vary on both temporal and spatial scales. On eroding landscapes (and depending on the topographic position of tors, boulders or scarps), the signal intensity will most likely vary. Climate and vegetation patterns will have substantially varied over time (last 10–100 ka) in many parts of mid-latitude environments. We therefore hypothesize that calculated soil erosion rates can be linked to both the topographic position and to general patterns of climate and vegetation variability.

Study Area

The Sila Massif in Calabria (Italy) is an ideal geological and topographic setting for our study (Figure 2) with tors, boulders and rock scarps. Vegetation here consists of grassland, conifer (pine, fir) and deciduous trees (beech) (Sorriso-Valvo, 1993; Scarciglia *et al.*, 2005a, 2005b). The present-day moist and temperate climate is typical for upland Mediterranean zones with an annual average temperature of 9 to 12°C and annual precipitation of 1000 to 1800 mm (Le Pera and Sorriso-Valvo, 2000). The landscape of the box-shaped plateau is characterized by wide-flat to gently-rolling paleosurfaces ranging between 1000 m and 1700 m above sea level (a.s.l.) that are bordered by steep slopes. The relief and drainage systems are controlled by north–south (N–S), east–west (E–W) and northwest–southeast (NW–SE) trending faults (Molin *et al.*, 2004; Spina *et al.*, 2007).

The geological setting (Figure 2b) of the Sila upland plateau was created by the uplift of the Paleozoic plutonic and metamorphic basement rocks of the Calabride complex and its Miocene-to-Pleistocene sedimentary cover. Regional tectonic uplift has affected a relatively large area and caused the isolation of the Sila upland through a number of tectonic phases (Molin *et al.*, 2004; Olivetti *et al.*, 2012). The last uplift phase occurred around 300–400 ka BP (Olivetti *et al.*, 2012). The acceleration of regional uplift here resulted in a number of uplift rate estimates: between 0.6 and 1 mm yr⁻¹ (Olivetti *et al.*, 2012), between 0.52 and 0.88 mm yr⁻¹ (Corbi *et al.*, 2009), and 0.65 mm yr⁻¹ (Bintanja *et al.*, 2005).

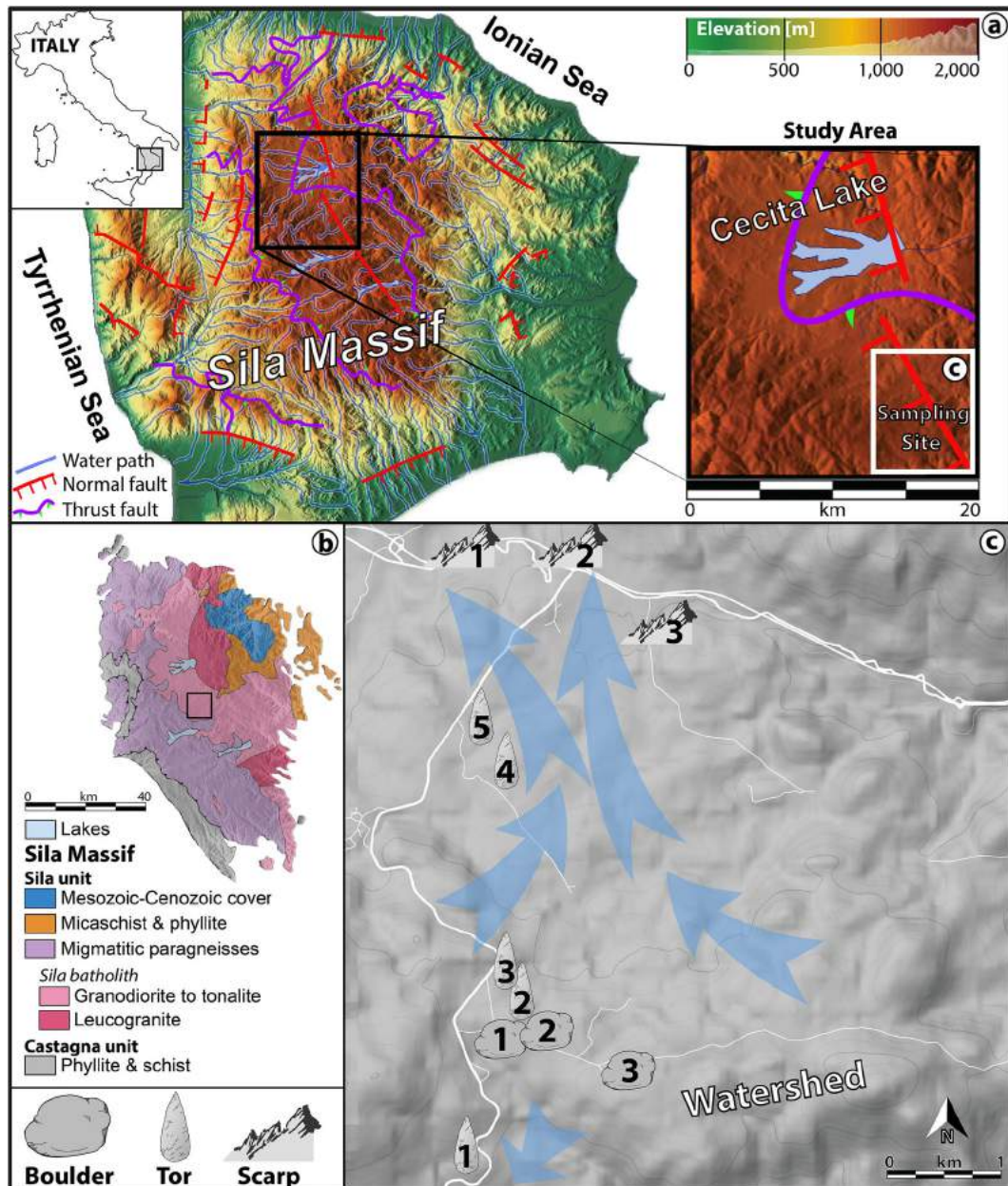


Figure 2. (a) Topographic map of the Sila Massif in southern Italy (after Raab *et al.*, 2018). The sampling site of the study area near the Cecita Lake is marked as a white box (Geoportale Nazionale, Ministero dell'Ambiente, Italy). Additionally, normal and thrust faults are indicated (Olivetti *et al.*, 2012). (b) Geological overview map of the Sila Massif according to Liotta *et al.* (2008) and von Eynatten *et al.* (2015). The black frame indicates the sampling site. (c) Detailed position of sampled boulders, tors and bedrocks plotted on a Google map (2017) surface model together with possible drainage patterns (blue arrows) on the basis of the steepness factors from Olivetti *et al.* (2012). [Colour figure can be viewed at wileyonlinelibrary.com]

For such uplift rates, the weathering model of Thomas (1997) suggests that grus weathering slightly dominates over saprolite formation. Le Pera and Sorriso-Valvo (2000) described the local 50–60 m thick weathering mantle as 'arenite' and 'clayed grus'. Both saprolite and grus weathering mantles are identified in this region (Scarciglia *et al.*, 2016). As a consequence of local long-term deep weathering processes followed by exhumation, granitic boulder fields, tors and steep scarps have developed here which are represented by a large assortment of granitic outcrops of different sizes and shapes. Various forms depicted in the weathering scheme of Migoñ (2013) are present (Raab *et al.*, 2018). Tors and outcrops with chessboard-like joint structures are found mostly along ridge crests but also occur in slightly undulating areas and isolated small topographic basins.

Tors are free-standing rock outcrops that remain attached to the underlying bedrock and usually have heights of 4 to 6 m. Some collapsed tors occur as elongated boulders with lengths of 8 m or more. Boulders, however, hardly exceed diameters

of more than 2.5 m and vary from nearly perfectly rounded to half-moon shapes. Boulders are found in clusters or as single isolates on low-angle relief surfaces. They are spread across the plateau but are more often found along gentle ridges (Scarciglia, 2015). Scarps are found throughout the plateau on rather steep to gently sloping surfaces.

Materials and Methods

Sampling sites and experimental design

Our sampling area is in the centre of the Sila massif (Figure 2a) and provides an ideal mix of all required geomorphic landforms: close proximity (Figure 2c) within a well-defined spatial area with relatively small altitudinal differences. At the centre of the sampling area is a small north-oriented basin with planation surfaces that are surrounded by gently-undulated ridges. Its

highest extent in the south acts as a divide between the northward-draining upland basin (e.g. Cecita Lake) and the southern drainage to the lowlands. Extensively-scarped slopes are mainly found in the northern basin. Tors and boulders are spread all-over, but are concentrated on the surrounding ridges.

We sampled tors from different topographic positions. Steeper slopes were investigated using one tor at the southern part of the watershed, one at the northern part and one on the ridge itself. These tors were compared to two tors nearer the basin centre with gentler slopes and to three boulders along the watershed ridge.

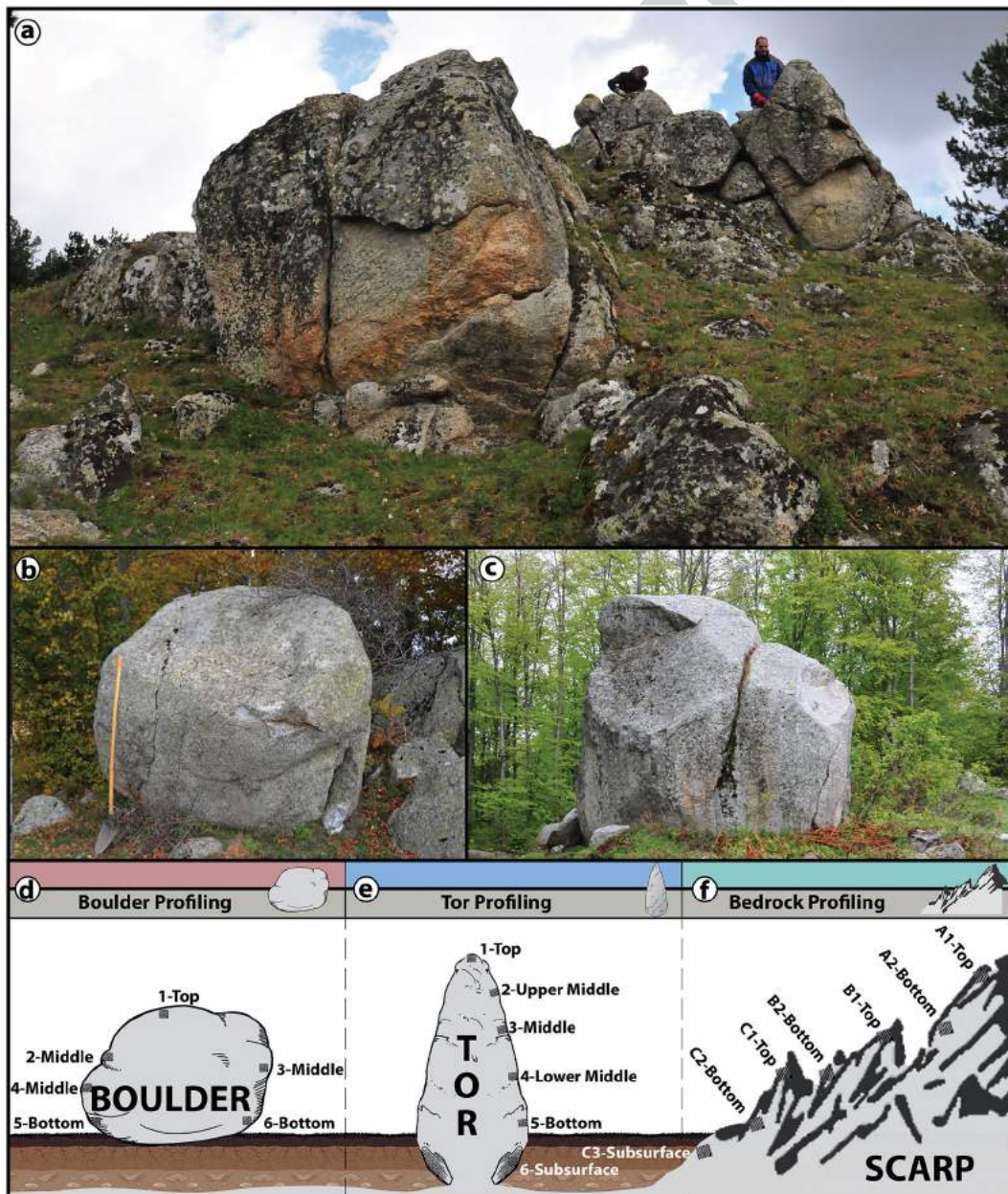
To determine surface denudation in this landscape, our ^{10}Be sampling focused on surface exposures along vertical rock profiles (Figure 3). According to our hypotheses, we expected to detect different formation and exhumation patterns:

- the vertical sampling of tors should reveal the landscape's denudation rates and changes over time and as a function of their topographic position

- boulders will have a more complex exhumation process, because of their detachment from the bedrock
- scarps probably provide the timing of relatively young denudation processes

Sampling of rocks for *in situ* ^{10}Be dating

We sampled five tors, three boulders and three scarps (Table I). An average of six 1–3 kg samples per tor were taken at different heights in order to assess the timing of their progressive, possibly multistep, exhumation through time. Given their uneven morphology, two of the three scarps were investigated in more detail with up to seven samples. The sampling was carried out with an electric stone saw, hammer and chisel. Because cosmic rays are distinctly attenuated within the rock, production of cosmogenic isotopes is highest directly at the surface. We therefore sampled the uppermost 1–3 cm of the rock surface



Colour online, B&W in print

Figure 3. The sampling strategies for the individual landscape features (a) scarps, (b) boulders and (c) tors, are drawn in (d), (e) and (f). [Colour figure can be viewed at wileyonlinelibrary.com]

Table 1. Sample characteristics of the investigated profiles along boulders, tors and scarps

Samples series	Coordinates [WGS84]		Ground elevation (m a.s.l.)	Rock type ^b (-)	Sample thickness (cm)	Height aboveground (m)	Dip direction of rock surface (deg)	Dip angle of rock surface (deg)	Shielding factor (-)
	Latitude (°N)	Longitude (°E)							
<i>Boulder 1</i>									
1-Top	39° 16' 51.6"	16° 32' 20.4"	1572	Granodiorite	2.00	2.25	040	10	0.999
2-Middle	39° 16' 51.6"	16° 32' 20.4"	1572	Granodiorite	3.00	1.28	325	70	0.613
3-Middle	39° 16' 51.6"	16° 32' 20.4"	1572	Granodiorite	3.00	1.02	250	80	0.879
4-Middle	39° 16' 51.6"	16° 32' 20.4"	1572	Granodiorite	3.00	0.76	345	85	0.558
5-Bottom	39° 16' 51.6"	16° 32' 20.4"	1572	Granodiorite	3.00	0.25	342	90	0.498
6-Bottom	39° 16' 51.6"	16° 32' 20.4"	1572	Granodiorite	3.00	0.10	220	70	0.490
<i>Boulder 2</i>									
1-Top	39° 16' 51.6"	16° 32' 20.7"	1572	Granodiorite	2.00	1.70	360	12	0.998
3-Middle	39° 16' 51.6"	16° 32' 20.7"	1572	Granodiorite	3.00	1.20	170	70	0.782
6-Bottom	39° 16' 51.6"	16° 32' 20.7"	1572	Granodiorite	9.50	-0.20	300	70	0.612
<i>Boulder 3</i>									
1-Top	39° 16' 35.6"	16° 32' 58.1"	1567	Granodiorite	1.00	1.40	047	7	1.000
6-Bottom	39° 16' 35.6"	16° 32' 58.1"	1567	Granodiorite	1.50	0.25	160	70	0.677
<i>Tor 1^a</i>									
1-1-Top	39° 16' 06.7"	16° 32' 07.8"	1504	Granodiorite	2.00	4.00	150	10	0.999
1-2-Upper middle	39° 16' 06.7"	16° 32' 07.8"	1504	Granodiorite	3.00	2.30	270	80	0.589
1-3-Middle	39° 16' 06.7"	16° 32' 07.8"	1504	Granodiorite	2.50	2.10	250	80	0.544
1-4-Lower middle	39° 16' 06.7"	16° 32' 07.8"	1504	Granite	1.80	1.10	285	90	0.498
1-5-Bottom	39° 16' 06.7"	16° 32' 07.8"	1504	Granodiorite	2.00	0.20	290	40	0.473
1-6-Subsurface	39° 16' 06.7"	16° 32' 07.8"	1504	Granodiorite	1.00	-0.28	270	85	0.509
<i>Tor 2^a</i>									
2-1-Top	39° 16' 52.4"	16° 32' 22.9"	1572	Granodiorite	2.00	5.60	115	32	0.972
2-2-Upper middle	39° 16' 52.4"	16° 32' 22.9"	1572	Granodiorite	3.00	4.60	115	80	0.654
2-3-Middle	39° 16' 52.4"	16° 32' 22.9"	1572	Granodiorite	1.50	3.30	225	70	0.704
2-4-Lower middle	39° 16' 52.4"	16° 32' 22.9"	1572	Granodiorite	2.00	2.40	245	60	0.771
2-5-Bottom	39° 16' 52.4"	16° 32' 22.9"	1572	Granodiorite	3.00	0.30	360	90	0.501
2-6-Subsurface	39° 16' 52.4"	16° 32' 22.9"	1572	Granodiorite	9.50	-0.20	300	70	0.724
<i>Tor 3^a</i>									
3-1-Top	39° 17' 01.6"	16° 32' 17.0"	1569	Granodiorite	2.00	3.50	358	10	0.999
3-2-Upper middle	39° 17' 01.6"	16° 32' 17.0"	1569	Granodiorite	3.00	2.10	170	85	0.504
3-3-Middle	39° 17' 01.6"	16° 32' 17.0"	1569	Granodiorite	2.00	1.30	165	90	0.498
3-4-Lower middle	39° 17' 01.6"	16° 32' 17.0"	1569	Granodiorite	4.00	1.10	165	90	0.498
3-5-Bottom	39° 17' 01.6"	16° 32' 17.0"	1569	Granodiorite	2.00	0.20	170	80	0.607
3-6-Subsurface	39° 17' 01.6"	16° 32' 17.0"	1569	Granodiorite	3.00	-0.40	170	90	0.601
<i>Tor 4</i>									
4-1-Top	39° 17' 56.9"	16° 32' 20.6"	1465	Granite	3.00	3.60	030	44	0.926
4-2-Upper middle	39° 17' 56.9"	16° 32' 20.6"	1465	Granite	3.00	2.00	170	80	0.612
4-3-Middle	39° 17' 56.9"	16° 32' 20.6"	1465	Granodiorite	3.00	1.55	170	80	0.612
4-4-Lower middle	39° 17' 56.9"	16° 32' 20.6"	1465	Granodiorite	3.00	0.85	170	80	0.612
4-5-Bottom	39° 17' 56.9"	16° 32' 20.6"	1465	Granite	3.00	0.38	170	80	0.612
4-6-Subsurface	39° 17' 56.9"	16° 32' 20.6"	1465	Granite	3.00	-0.30	170	80	0.612
<i>Tor 5</i>									
5-1-Top	39° 18' 02.4"	16° 32' 12.4"	1475	Granite	2.00	2.40	088	26	0.986
5-2-Upper middle	39° 18' 02.4"	16° 32' 12.4"	1475	Granite	1.50	1.60	071	21	0.969
5-3-Middle	39° 18' 02.4"	16° 32' 12.4"	1475	Granite	3.00	1.40	081	30	0.964
5-4-Lower middle	39° 18' 02.4"	16° 32' 12.4"	1475	Granite	2.20	1.10	029	11	0.983
5-5-Bottom	39° 18' 02.4"	16° 32' 12.4"	1475	Granodiorite	1.80	0.26	160	55	0.845
5-6-Subsurface	39° 18' 02.4"	16° 32' 12.4"	1475	Granodiorite	1.80	-0.20	164	76	0.528
<i>Scarp 1</i>									
C1-Top	39° 19' 06.1"	16° 32' 12.8"	1360	Granite	3.00	1.49	285	10	0.932
<i>Scarp 2</i>									
A1-Top	39° 19' 06.4"	16° 32' 35.2"	1394	Granite	2.50	0.50	210	50	0.890
A2-Bottom	39° 19' 06.4"	16° 32' 35.2"	1394	Granite	2.50	0.10	110	80	0.534
B1-Top	39° 19' 06.4"	16° 32' 35.2"	1393	Granite	2.50	2.00	270	30	0.977
B2-Bottom	39° 19' 06.4"	16° 32' 35.2"	1393	Granite	2.50	1.00	270	90	0.492
C1-Top	39° 19' 06.4"	16° 32' 35.2"	1393	Granite	2.50	2.30	105	10	0.997
C2-Bottom	39° 19' 06.4"	16° 32' 35.2"	1393	Granite	2.50	1.10	210	70	0.714
C3-Subsurface	39° 19' 06.4"	16° 32' 35.2"	1393	Granite	2.50	-0.35	200	70	0.710
<i>Scarp 3</i>									
A1-Top	39° 18' 43.2"	16° 33' 22.3"	1422	Granite	1.30	0.75	228	28	0.982
A2-Bottom	39° 18' 43.2"	16° 33' 22.3"	1413	Granite	2.00	0.20	195	30	0.978
B1-Top	39° 18' 43.2"	16° 33' 22.3"	1413	Granite	1.50	0.95	233	12	0.993

(Continues)

Table 1. (Continued)

Samples series	Coordinates [WGS84]		Ground elevation (m a.s.l.)	Rock type ^b (–)	Sample thickness (cm)	Height aboveground (m)	Dip direction of rock surface (deg)	Dip angle of rock surface (deg)	Shielding factor (–)
	Latitude (°N)	Longitude (°E)							
B2-Bottom	39° 18′ 43.2″	16° 33′ 22.3″	1413	Granite	1.50	0.15	055	40	0.991
C1-Top	39° 18′ 43.2″	16° 33′ 22.3″	1413	Granite	1.50	0.87	240	10	0.992
C2-Bottom	39° 18′ 43.2″	16° 33′ 22.3″	1413	Granite	3.00	0.64	240	30	0.977
C3-Subsurface	39° 18′ 43.2″	16° 33′ 22.3″	1413	Granite	1.80	–0.20	210	35	0.967

^aData from Raab *et al.* (2018).

^bClassification after Middlemost (1994).

(Table I). Since tors may have already interacted with cosmogenic rays before they appear at the ground surface, we also sampled belowground (up to 40 cm deep) to account for possible early subsurface ¹⁰Be accumulation. This was necessary in order to constrain the exhumation models. The position (latitude, longitude, altitude) of the sampling sites was recorded with global positioning system (GPS) and verified with topographic maps. Standard corrections were made for the geometry of the rock samples and the effect of topographic shielding at each location (Gosse and Philips, 2001).

Surface exposure dating laboratory procedure – ¹⁰Be

The rock sample material was crushed and about 0.4 kg of the 0.6–0.25 mm fraction was collected and treated according to standard procedures (Kohl and Nishiizumi, 1992). The selected fraction was treated with *aqua regia* for up to 36 hours and iron oxides, organic material and carbonates were eliminated. The remaining mineral assemblage underwent a one hour-treatment with 0.4% hydrogen fluoride (HF). Afterwards we used a flotation system (Kitchener, 1984) to physically separate mica and feldspar components from quartz. Any remaining contaminants were removed with 4% HF leaching cycles (7–21 days). About 20–30 g of the obtained pure quartz were spiked with a ⁹Be-carrier solution (Scharlau, BE03460100) and together dissolved in 40% HF. We isolated Be by using anion and cation exchange columns followed by selective pH precipitation (von Blanckenburg *et al.*, 1996). The resulting beryllium hydroxide (Be(OH)₂) was calcinated to beryllium oxide (BeO) for two hours at 850°C and mixed with niobium (Nb) powder before pressing it into copper (Cu)-targets. The ETH Laboratory of Ion Beam Physics accelerator mass spectrometry (AMS) facility measured the targets. ETH used ¹⁰Be standard S2007 N with a nominal value of ¹⁰Be/⁹Be = 28.1 × 10^{–12} calibrated to the Nishiizumi standard ICN01-5-1 with a revised nominal value of 2.709 × 10^{–11} (Christl *et al.*, 2013; Kubik and Christl, 2010; Nishiizumi *et al.*, 2007). The 1σ error of S2007 N is 2.7% (Christl *et al.*, 2013). The measured ¹⁰Be/⁹Be ratios were corrected for the ¹⁰Be contribution of the Be-carrier (¹⁰Be/⁹Be blank ratio: 3.00 ± 0.87 × 10^{–15}). Exposure ages were calculated using the cosmogenic nuclide online calculator v2.3 (Balco *et al.*, 2008). The programme uses a ¹⁰Be half-life of 1.387 ± 0.0012 Ma (Chmeleff *et al.*, 2010; Korschinek *et al.*, 2010) and a sea level high latitude ¹⁰Be production rate of 4.01 ¹⁰Be-atoms g^{–1} SiO₂ yr^{–1} (Borchers *et al.*, 2016). The production rate was corrected for latitude and altitude after the scaling scheme of Stone (2000) and further corrected for the sample thickness according to the depth profile of Brown *et al.* (1992) with an effective radiation attenuation length of 160 g cm^{–2} of Gosse and Philips (2001) and a constant rock density of 2.7 g cm^{–3}. A variety of rock surface erosion rates were tested with no correction for snow. Related effects of

geomagnetic field variations on the ¹⁰Be ages are assumed to be negligible (Masarik *et al.*, 2001; Pigati and Lifton, 2004).

Determination of surface denudation rates (D_{Surface})

Ages were calculated on the basis of a rock surface erosion rate between 0 and 0.002 mm yr^{–1}, typical for cold (alpine) granite regions (Small *et al.*, 1999), and were subsequently used for modelling the exhumation rate (height versus age). Best regression fits were obtained with a polynomial (third order) or a logistic function (Lichter, 1998) given by

$$f(t) = \frac{a}{(1 + e^{b(t-c)})} + d \quad (2)$$

where $f(t)$ is the height in metres (lowered surface), as a function of time, a is the range of height in metres, t time in years, b the slope coefficient, c the time of the maximal rate of change in years, and d the asymptotic value in metres. The height–age relation of the exhuming tors was then modelled by taking the error ranges of the ¹⁰Be measurements into account (external error), using Monte Carlo simulations and the previously noted regression fits.

The mathematical derivative of these functions then provided the rates of surface lowering and, thus, surface denudation (D_{Surface}) in millimetres per year. For this calculation, it was necessary to account for the age of the rocks' initial surface appearance (early subsurface ¹⁰Be accumulation; t_s), as follows:

$$\frac{D_{\text{Surface}}}{\partial t} = \frac{\partial f(t-t_s)}{\partial t} \quad (3)$$

Results

Tors

The 30 samples collected from tors (Table I) resulted in 24 ages ranging from 11 ± 2 ka to 106 ± 12 ka (Table II). Application of various surface erosion rates (0, 0.001, 0.002 mm yr^{–1}) resulted only in minor differences (about 2.6 ka) in the exposure ages. Use of a surface erosion rate of 0.002 mm yr^{–1} resulted in the following age–height relationships: 38 ± 4 ka at 4 m for tor #1, 106 ± 12 ka at 5.6 m for tor #2, 37 ± 4 ka at 3.5 m for tor #3, 32 ± 3 ka at 3.6 m for tor #4 and 33 ± 3 ka at 2.4 m for tor #5 (Figure 4).

The series of vertical profile samples from the five tors showed a general increase in ¹⁰Be concentration with increasing height above the surrounding ground surfaces (Figure 4f). We observed no obvious morphologic features that would indicate the presence of abrupt changes to the ¹⁰Be signal (e.g. exfoliation). Samples taken below the present-day surface to determine early subsurface ¹⁰Be accumulation had similar atom counts to those samples taken from the land-surface level at the base of the tors.

Table II. Calculated exposure ages (\pm external uncertainty) based on ^{10}Be concentration (\pm error) and different rock surface erosion rates ($E_0 = 0.000 \text{ mm yr}^{-1}$, $E_1 = 0.001 \text{ mm yr}^{-1}$, $E_2 = 0.002 \text{ mm yr}^{-1}$)

	^{10}Be		Heights (m)	Calculated exposure ages of different rock surface erosion rates		
	Concentration ($\text{E}+4 \text{ atoms g}^{-1}$)	Error (%)		E_0 (a)	E_1 (a)	E_2 (a)
<i>Boulder 1</i>						
1-Top	30.24 \pm 1.64	5.4	2.25	23000 \pm 2341	23448 \pm 2434	23919 \pm 2535
2-Middle	31.47 \pm 1.27	4.0	1.28	39258 \pm 3742	40582 \pm 4003	42032 \pm 4303
3-Middle	69.83 \pm 2.80	4.0	1.02	61382 \pm 5880	64733 \pm 6553	68625 \pm 7399
4-Middle	34.40 \pm 3.41	9.9	0.76	47197 \pm 6243	49129 \pm 6775	51287 \pm 7405
5-Bottom	28.40 \pm 2.11	7.4	0.25	43504 \pm 4977	45134 \pm 5364	46937 \pm 5817
6-Bottom	50.10 \pm 2.97	5.9	0.10	78674 \pm 8339	84265 \pm 9603	91069 \pm 11315
<i>Boulder 2</i>						
1-Top	26.52 \pm 1.36	5.1	1.70	21643 \pm 2168	22038 \pm 2249	22454 \pm 2336
6-Bottom	16.73 \pm 0.85	5.1	-0.20	23519 \pm 2348	23984 \pm 2443	24475 \pm 2546
<i>Boulder 3</i>						
1-Top	64.35 \pm 1.77	2.8	1.40	49367 \pm 4483	51502 \pm 4886	53903 \pm 5367
6-Bottom	7.03 \pm 0.35	5.0	0.25	7828 \pm 776	7878 \pm 786	7930 \pm 797
<i>Tor 1^a</i>						
1-1-Top	44.99 \pm 2.51	5.6	4.00	36094 \pm 3716	37215 \pm 3954	38434 \pm 4224
1-2-Upper middle	19.95 \pm 0.78	3.9	2.30	27097 \pm 2561	27717 \pm 2682	28376 \pm 2814
1-3-Middle	18.42 \pm 0.71	3.8	2.10	26987 \pm 2542	27602 \pm 2661	28255 \pm 2791
1-4-Lower middle	16.60 \pm 0.67	4.0	1.10	26327 \pm 2502	26910 \pm 2616	27529 \pm 2740
1-5-Bottom	11.08 \pm 0.49	4.5	0.20	18479 \pm 1788	18763 \pm 1844	19059 \pm 1904
1-6-Subsurface	12.18 \pm 0.57	4.6	-0.28	18748 \pm 1831	— \pm —	— \pm —
<i>Tor 2^a</i>						
2-1-Top	112.44 \pm 4.39	3.9	5.60	89330 \pm 8576	96723 \pm 10097	106044 \pm 12269
2-2-Upper middle	70.94 \pm 2.70	3.8	4.60	83960 \pm 8016	90408 \pm 9332	98390 \pm 11161
2-4-Lower middle	30.12 \pm 1.49	4.9	2.40	29647 \pm 2946	30395 \pm 3098	31195 \pm 3267
2-5-Bottom	6.96 \pm 1.40	20.0	0.30	10518 \pm 2297	10609 \pm 2338	10703 \pm 2380
2-6-Subsurface	13.82 \pm 0.72	5.2	-0.20	15328 \pm 1538	— \pm —	— \pm —
<i>Tor 3^a</i>						
3-1-Top	45.45 \pm 1.04	2.3	3.50	34745 \pm 3097	35782 \pm 3287	36906 \pm 3501
3-3-Middle	18.18 \pm 0.56	3.1	1.30	27578 \pm 2518	28219 \pm 2638	28901 \pm 2770
3-4-Lower middle	19.73 \pm 0.57	2.8	1.10	28872 \pm 2616	29576 \pm 2747	30328 \pm 2892
3-5-Bottom	16.76 \pm 0.57	3.4	0.20	20882 \pm 1927	21248 \pm 1996	21931 \pm 2069
<i>Tor 4</i>						
4-1-Top	34.14 \pm 0.84	2.5	3.60	30556 \pm 2736	31353 \pm 2882	32207 \pm 3045
4-2-Upper middle	23.82 \pm 0.70	2.9	2.00	32088 \pm 2918	32963 \pm 3082	33906 \pm 3265
4-4-Lower middle	13.24 \pm 0.46	3.4	0.85	17775 \pm 1646	18038 \pm 1696	18313 \pm 1749
4-5-Bottom	8.58 \pm 0.30	3.5	0.38	11493 \pm 1062	11603 \pm 1083	11715 \pm 1104
<i>Tor 5</i>						
5-1-Top	37.73 \pm 1.31	3.5	2.40	31258 \pm 2903	32093 \pm 3062	32990 \pm 3240
5-2-Upper middle	31.23 \pm 1.50	4.8	1.60	26164 \pm 2578	26745 \pm 2695	27362 \pm 2823
5-4-Lower middle	33.04 \pm 1.11	3.4	1.10	27477 \pm 2538	28119 \pm 2659	28803 \pm 2793
5-5-Bottom	22.54 \pm 0.84	3.7	0.26	21661 \pm 2028	22057 \pm 2103	22472 \pm 2184
5-6-Subsurface	20.86 \pm 1.20	5.7	-0.20	31963 \pm 3314	32830 \pm 3499	33763 \pm 3706
<i>Scarp 1</i>						
C1-Top	15.05 \pm 0.81	5.4	1.49	14391 \pm 1459	14564 \pm 1494	14742 \pm 1532
<i>Scarp 2</i>						
A1-Top	11.16 \pm 0.67	6.0	0.50	10847 \pm 1134	10944 \pm 1154	11045 \pm 1176
B1-Top	13.30 \pm 0.54	4.0	2.00	11793 \pm 1117	11908 \pm 1139	12027 \pm 1163
B2-Bottom	7.36 \pm 0.39	5.3	1.00	12831 \pm 1296	12967 \pm 1323	13107 \pm 1353
C1-Top	12.00 \pm 0.43	3.3	2.30	11294 \pm 1037	11400 \pm 1057	11509 \pm 1077
C2-Bottom	9.51 \pm 0.39	4.1	1.10	11494 \pm 1091	11603 \pm 1112	11716 \pm 1134
C3-Subsurface	7.01 \pm 0.35	4.9	-0.35	8501 \pm 840	8561 \pm 852	8622 \pm 864
<i>Scarp 3</i>						
A1-Top	9.82 \pm 0.46	4.7	0.75	8393 \pm 819	8345 \pm 830	8511 \pm 842
B1-Top	14.04 \pm 0.88	6.2	0.95	11896 \pm 1262	12014 \pm 1287	12136 \pm 1313
C1-Top	9.78 \pm 0.52	5.4	0.87	8288 \pm 837	8345 \pm 848	8403 \pm 860
C2-Bottom	10.35 \pm 0.80	7.7	0.64	9014 \pm 1039	9081 \pm 1055	9150 \pm 1071

Note: Calculation was performed using the cosmogenic nuclide online calculator v2.3 (Balco *et al.*, 2008).

^aData from Raab *et al.* (2018).

Following Raab *et al.* (2018), we used the surface ages, and thus exhumation rates, of the individual tors to model the surface denudation rates (Figures 5b, 5d, 5f, 6b and 6d). We calculated average exhumation rates ($\approx D_{\text{Surface}}$) of $0.062 \pm 0.037 \text{ mm yr}^{-1}$, $0.044 \pm 0.023 \text{ mm yr}^{-1}$, $0.046 \pm 0.036 \text{ mm yr}^{-1}$, $0.062 \pm 0.035 \text{ mm yr}^{-1}$ and $0.036 \pm 0.031 \text{ mm yr}^{-1}$ for Tors

#1–#5, respectively (rock surface erosion rate of 0.002 mm yr^{-1}). From the greater heights and older ages of the samples from Tor #2, we were able to model soil denudation rates for the last ~100 ka. Tor #2 yielded unusually low soil denudation rates compared to the other tors. Between 20 and 25 ka BP (Figure 5d), however, Tor #2 exhibits similar results to the

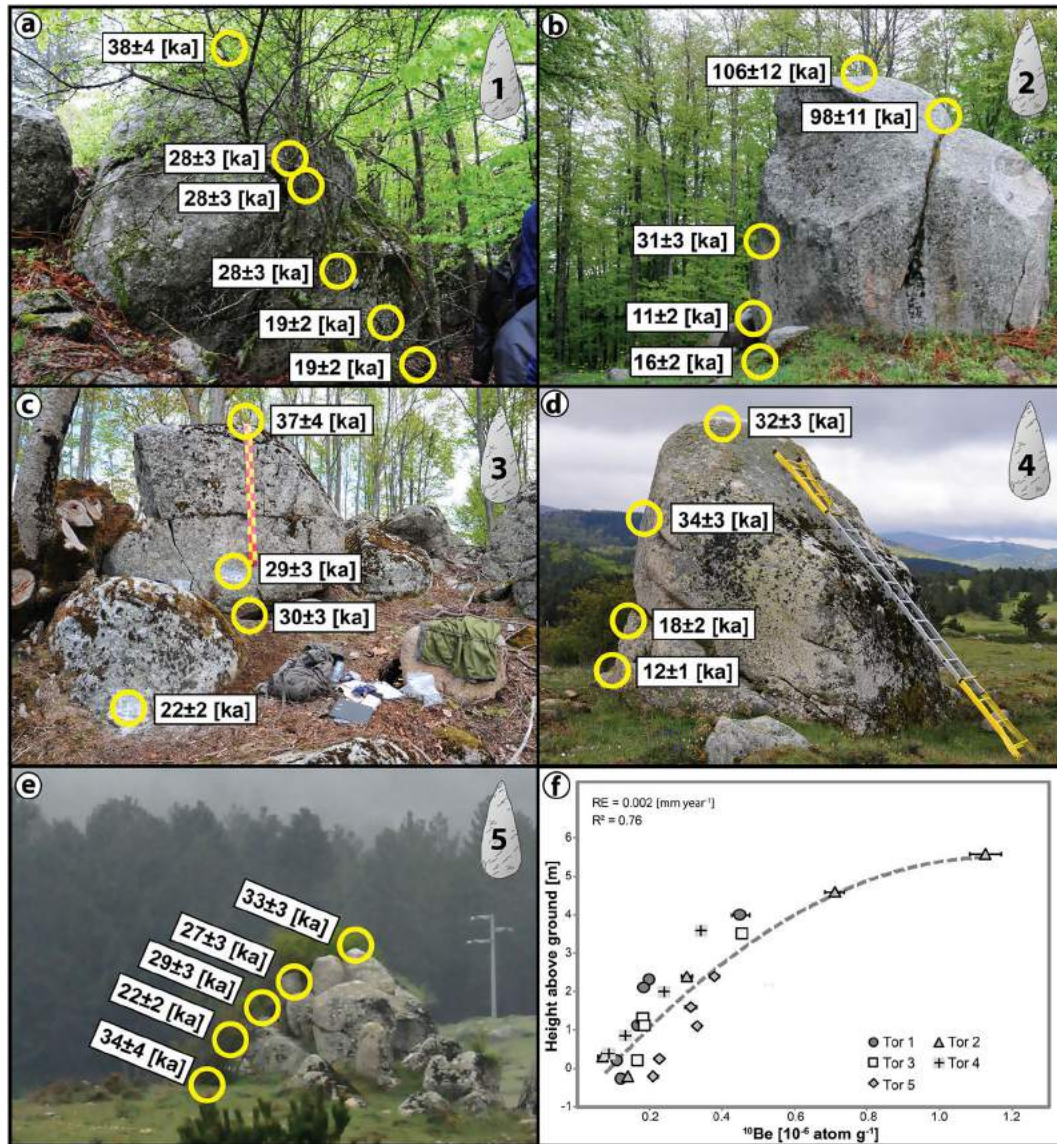


Figure 4. Exposure ages (a–e) along the tor profiles (Table II; $E_2 = 0.002$ mm yr $^{-1}$). The overall ^{10}Be concentrations as a function of height (with related trend curve) of all samples are plotted in (f). [Colour figure can be viewed at wileyonlinelibrary.com]

others. Tors #1 and #3 have similar slope angles ($\sim 6^\circ$ – 10°) and similar surface ages at similar heights. Both exhibit similar denudation rates (Figures 5b and 5f) in the range 0.05 – 0.37 mm yr $^{-1}$. The surface denudation rates derived from the exhumation rates of tors having slope angles of 0° to 2° (Tors #4 and #5) are slightly lower (0.06 – 0.22 mm yr $^{-1}$; Figures 6b and 6d).

Boulders

The 11 boulder samples (Table I) provided 10 surface exposure ages (Table II) that vary from 8 ± 1 ka to 91 ± 11 ka (Figure 7). The range of ages obtained from the boulders is similar to that of the tors, but all ages and ^{10}Be concentrations show broad variation at the same heights aboveground. The oldest age was from the sample taken at the bottom of Boulder #1, while the youngest ages were from the top of Boulder #2 and the bottom of Boulder #3. Using a surface erosion rate of 0.002 mm yr $^{-1}$, the top sample (1.4 m) of Boulder #3 resulted in an age of 54 ± 5 ka, similar to the ages (42 ± 4 to 68 ± 7 ka) of samples taken at the half total height (0.76–1.28 m) at Boulder #1. Boulder #2 gives nearly identical ages at the top (22 ± 2 ka) and at the bottom (24 ± 3 ka) despite a height difference of 1.7 m.

Scarps

The 15 samples taken along scarps (Table I) resulted in 11 measured ages ranging from 8 ± 1 ka to 15 ± 2 ka (Table II; Figure 8). Scarp #1 yielded the oldest age, but only one sample was measured here. Scarps #2 and #3 exhibit identical ages at their base (9 ± 1 ka). The ages slightly increase with height up to 13 ± 1 ka at Scarp #2. At Scarp #3, however, the top of the scarp still exhibited an age of 9 ± 1 ka while the ages at the bottom are similar to Boulder #3 (8 ± 1 ka). The larger number of successfully dated samples from Scarp #2 (six samples) enabled us to derive an age–height model and subsequently a soil denudation trend model, which integrated the results from the individual samples of Scarp #1 (one sample) and Scarp #3 (four samples). The denudation rates range from 0.06 to 0.40 mm yr $^{-1}$ with a peak denudation rate at c. 4 ka BP (Figures 6e and 6f).

Discussion

Tors

We see the increases in ^{10}Be concentrations with height (Figure 4f) as validation of our conceptual idea that tors were

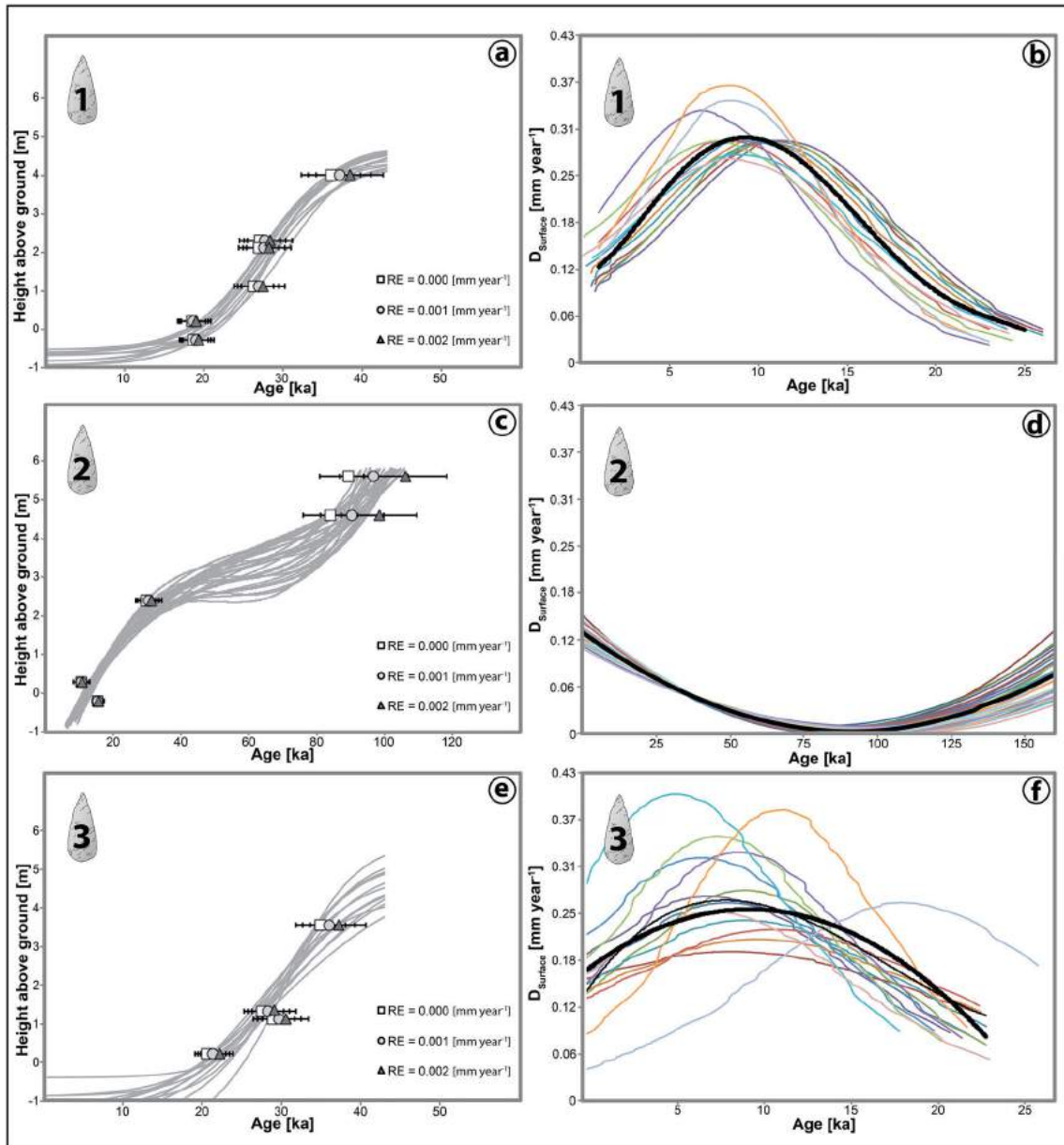


Figure 5. Trend of exposure ages as a function of tor height and derived soil denudation rates (D_{Surface}) using Monte Carlo simulations for Tor #1 (a and b), Tor #2 (c and d) and Tor #3 (e and f). RE = rock erosion. [Colour figure can be viewed at wileyonlinelibrary.com]

exhumed gradually over time (Figure 9). A search of the literature shows that surface denudation rates using granite tors are about $0.01\text{--}0.02\text{ mm yr}^{-1}$ for cold (alpine) regions (Small *et al.*, 1999) and $0.01\text{--}0.09\text{ mm yr}^{-1}$ in cool temperate climates (Heimsath *et al.*, 2001; Phillips *et al.*, 2006; Gunnell *et al.*, 2013). Our average exhumation rates ($0.03\text{--}0.10\text{ mm yr}^{-1}$) fit well to those reported from the Dartmoor tors (Gunnell *et al.*, 2013). Using river sediments as tracers, Olivetti *et al.* (2012) reported similar average erosion rates from cosmogenic ^{10}Be concentrations for the low-relief surfaces of the Sila upland (0.09 ± 0.01 to $0.13 \pm 0.01\text{ mm yr}^{-1}$). Our approach, however, allows us to not only report an average value, but also to capture the variations over a time span of about 100 ka.

The exhumation rates of tors depend on their topographic position. Tors found at similar topographic positions exhibit similar denudation trends. Tors #1 and #3 are positioned along backslopes and show higher overall rates (Figures 5b and 5d) than Tors #4 and #5 (Figures 6b and 6d), which are near the basin floor and along a lower surface gradient. These results show that tor archives can be used to decrypt differences in intensity and timing of denudation as well as variations among different

slope segments over millennia. The regional character of the Sila uplift (Molin *et al.*, 2004; Olivetti *et al.*, 2012) corresponds with these general exhumation trends.

Boulders

The complex age–elevation relationships imply that the boulders probably are not in their original position which supports our hypothesis that some boulders have moved. Because of these inconsistencies, we were unable to derive exhumation rates from these boulders. Re-location due to a collapse of a larger structure, rock spallation, exfoliation (Scarciglia *et al.*, 2005a, 2007) and toppling are plausible reasons for the various exposure ages. The selective local spheroidal weathering process is still continuing today (Scarciglia, 2015). A chemical weathering-driven multi-stage development of boulder landforms was proposed by Twidale (2002) through the formation of ‘corestones’ prior to exhumation (Migoñ and Prokop, 2013). This process is most notable in grus weathering environments, where the corestones emerge as boulders (Twidale and

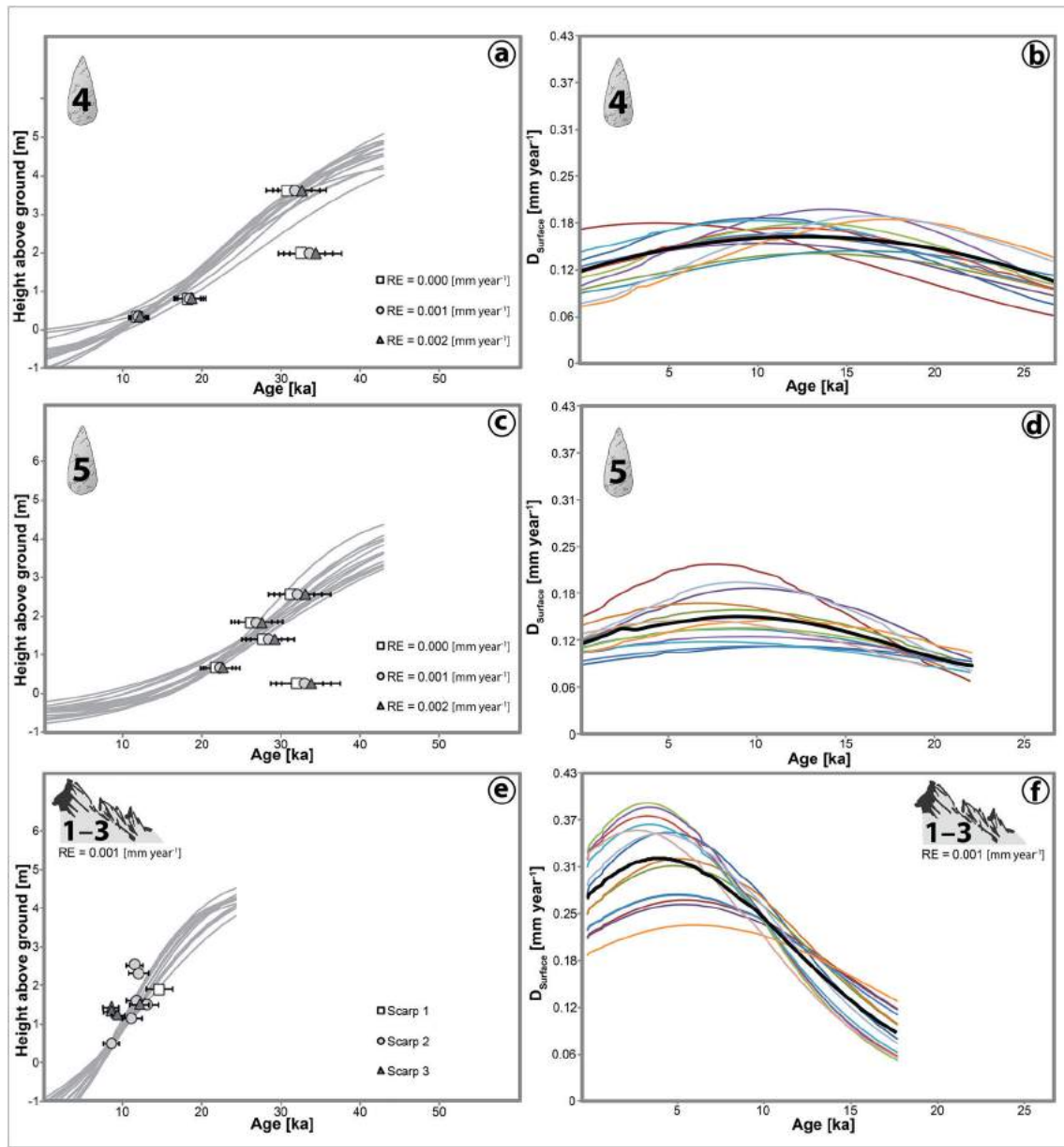


Figure 6. Exposure ages as a function of sample height/tors and scarps and derived surface denudation rates (D_{Surface}) using Monte Carlo simulations for Tor #4 (a and b), Tor #5 (c and d) and Scarps #1–#3 (e and f). RE = rock erosion. [Colour figure can be viewed at wileyonlinelibrary.com]

Romaní, 2005). The fast removal of material surrounding the corestones, via e.g. physical erosion, could also be a relevant factor that leads to the emergence of boulders, as it reduces the time needed for a continuous chemical weathering.

Depending on the boulders' positions within the rock mass and the intensity of the erosion process, a broad spectrum of exhumation events is likely, from gradual (Boulder #3) to abrupt (Boulder #2).

Early exposure of some boulder margins must have occurred ~90–100 ka ago. During this phase, the tor-based denudation rates were low (Figure 5d). Through constant denudation, progressively lower portions of boulders were exposed to cosmic rays. Thus, a second phase of exposure seems to have occurred ~50–70 ka ago (Figure 7; Table II) and coincides with the start of the increase in surface denudation found with tors (Figure 5d). The toppling or collapse of a larger structure may have caused **F10a** repositioning of the boulders ~20–25 ka ago (Figure 10), resulting in the younger ages found at the present-day boulder tops. A final denudation pulse, indicated by the extrapolated rates from the tors on the slopes on both sides of the watershed (Figures 5b and 5f), exposed even lower parts of some boulders

(e.g. Boulder #3) around 8 ± 1 ka. Because the boulder dataset is not conclusive, we propose that both processes, single corestone exhumation and toppling may be present.

Scarps

Based on the exhumation patterns of the scarps, the soil denudation rates range from 0.06 to 0.40 mm yr^{-1} and differ from the tor-based rates in two ways: (1) their maximum denudation rates are slightly higher than those of the tors (Figures 5b, 5f, 6b and 6d) and (2) the maximum soil denudation pulse seems to have occurred at about ~4 ka BP (Figure 6f). Note that the denudation peak seen for the tors of the slopes and the planes is around ~9–14 ka BP (Figures 5b, 5f, 6b and 6d). Denudation seems to have decreased along the slopes between ~4–9 ka BP while it increased at the scarp sites (Figures 5 and 6). The exposure ages found lower on the scarps indicate that they represent the final stage of surface evolution (Figure 11) and mark the final exhumation step of some tors (Figure 4d) and one boulder (Figure 7c). We see this as a confirmation of our initial **F11**

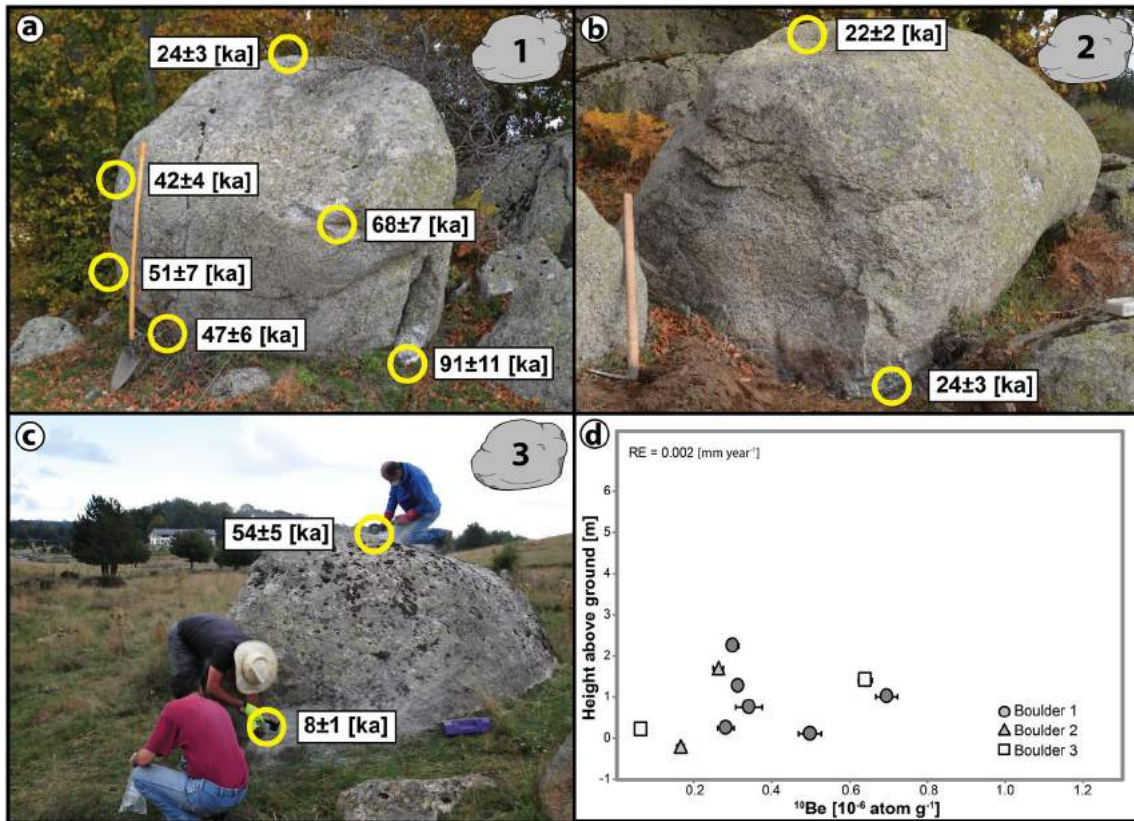


Figure 7. Exposure ages (a–c) along the boulder profiles (Table II; $E_2 = 0.002$ mm yr^{-1}). Their ^{10}Be concentrations are plotted as a function of height (d). [Colour figure can be viewed at wileyonlinelibrary.com]

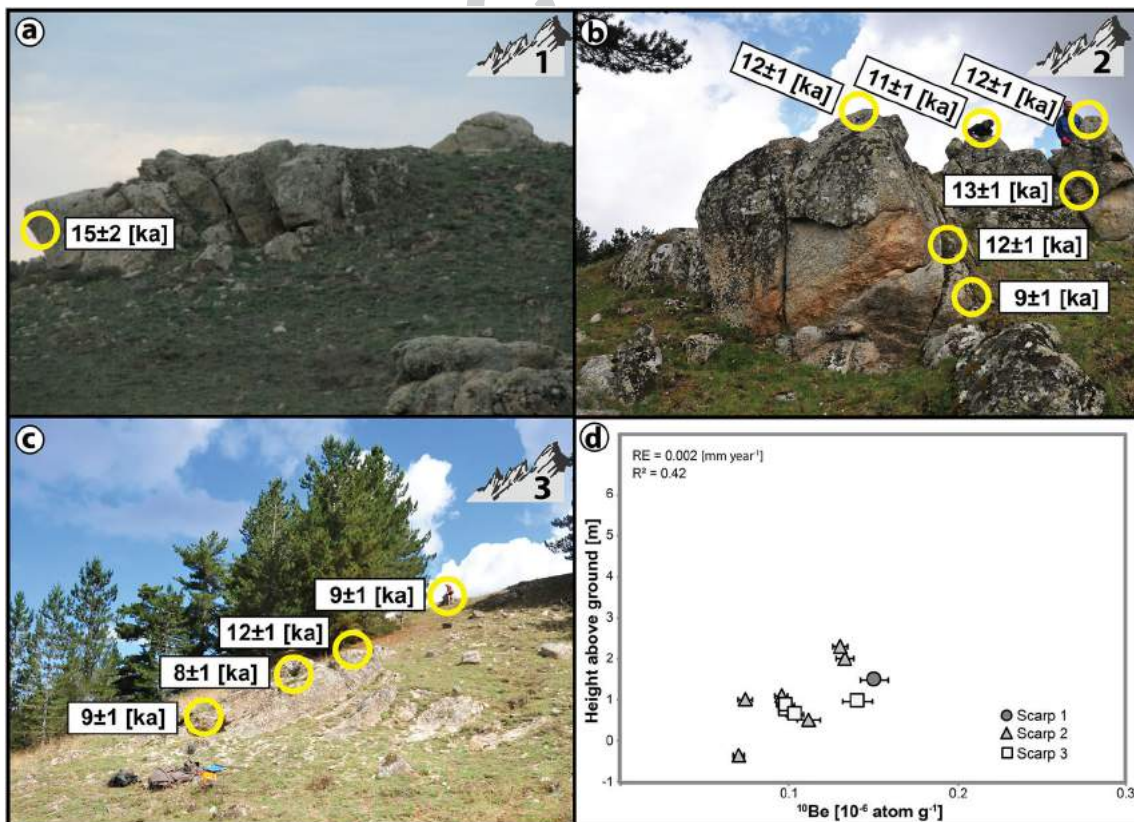


Figure 8. Exposure ages (a–c) of scarps (Table II; $E_1 = 0.002$ mm yr^{-1}). Their ^{10}Be concentrations are plotted as a function of height (with related trend curve) in (d). [Colour figure can be viewed at wileyonlinelibrary.com]

hypothesis, that scarps represent the youngest phase in surface evolution and differ in the timing of their formation when compared to the surrounding tors and boulders. This may be related

to an episode of latest-stage headward fluvial incision toward the surrounding summits, a process which Molin *et al.* (2004) and Olivetti *et al.* (2012) have not considered. This

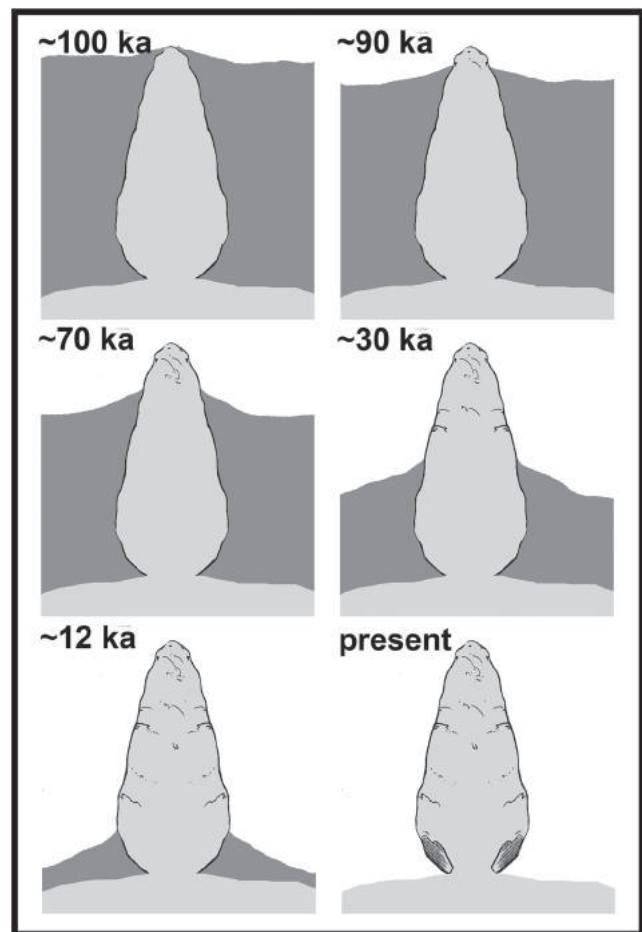


Figure 9. Concept of tor exhumation according to the surface exposure ages (e.g. Tor #2).

interpretation also fits the concept that plateau evolution is partly a hillslope process (e.g. back-stripping; Molin *et al.*, 2004; Olivetti *et al.*, 2012).

Topography and denudation rates

So far, we establish that tors provide characteristic denudation rates within a landscape that depends on their topographic position. Boulders are not suitable for such an approach because of their detachment from the bedrock and the associated complex multi-stage exposure timing. Scarps provide only denudation trends for the most recent surface processes with similar characteristics as tors along slopes. We compare the individual modelled average denudation rates with their topographic position (Figure 12). To do this, we subdivided the relief of the study site into five distinct sections, based on their surface angle and position within the plateau (Figure 12a).

The 'ridgetops' of the watershed (Tor #2) mark the highest elevation with a minimum age of 100 ka. Exposure ages of nearby boulders indicate that some have started to form simultaneously (Figure 2c). It appears that weathered material was transferred from the ridgetops to the 'slopes' on both the north-east (Tor #3) and the southwest (Tor #1) of the ridge. These two slope sections formed no later than 60 ka after the ridgetop. The drainage and thus material transport along the southern slope (Tor #1) are directed towards the lowland (Figure 2) while the material of the northern slope (Tor #2) moves toward the small upland planes and basins where it can be partially re-deposited. The Tors #4 and #5 are positioned in close proximity to a small local depression. Although these tors have only a

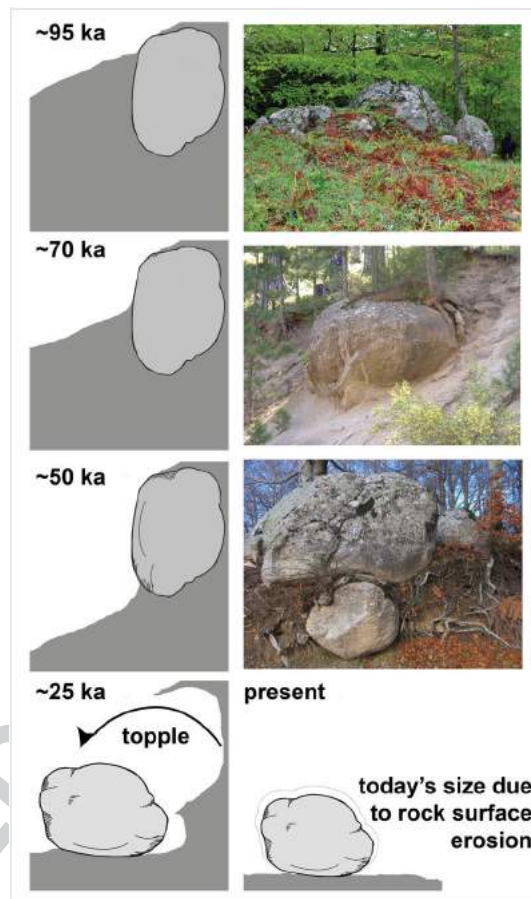


Figure 10. Proposed timing of events for some boulders (e.g. Boulder #1). [Colour figure can be viewed at wileyonlinelibrary.com]

minimum age difference of 5 ka to those on the slopes, their denudation trends are less pronounced (Figure 12b). We interpret the lower trends as a result of exhumation buffering through sediment re-deposition. Material influx has possibly counteracted denudation at Tors #4 and #5 to slow the pace of their exhumation (Figures 6b and 6d). In summary, we see that D_{Surface} started to increase at 50–75 ka BP on the ridges (Figure 5d), corresponding to the proposed second (70 ka BP) and third (50 ka BP) phases of boulder exposure (Figure 10). A subsequent phase of denudation is indicated at about 10–25 ka from the ^{10}Be ages of the tors. This correlates with the initiation of the toppling (e.g. collapse of larger structure) period apparent from some of the boulders (Figure 10).

Both tors and boulders are absent at the scarp sites and all are significantly older than the scarps. We propose that, during the major D_{Surface} pulse (~5–15 ka BP), the slopes were strongly eroded and that the modern surfaces started to be exposed to cosmic rays at about 12 ± 1 ka (Figure 8). As the denudation rates of the surrounding area began to decrease at about 9 ± 1 ka (Figure 12b), the production of loose material also must have decreased. Due to this reduction in sediment production, it is reasonable to assume that the fluvial system of the inner plateau removed the remaining regolith rather quickly, which resulted in a rapid exposure of the scarps. The resulting sediment would then have been relocated to the surrounding flanks and in the basins at the foot of the massif (Perri *et al.*, 2012; Ruello *et al.*, 2017; Russo Ermolli *et al.*, 2018). The rapid removal of already disintegrated sediments would also explain the delayed increase in D_{Surface} at the hills between 8 and 4 ka BP (Figure 12b). Because of the significant decrease in D_{Surface} at the ridgetops beginning at $\sim 9 \pm 1$ ka (Figures 6e, 6f and 8), the youngest tor and boulder ages (bottom of Tor #2;

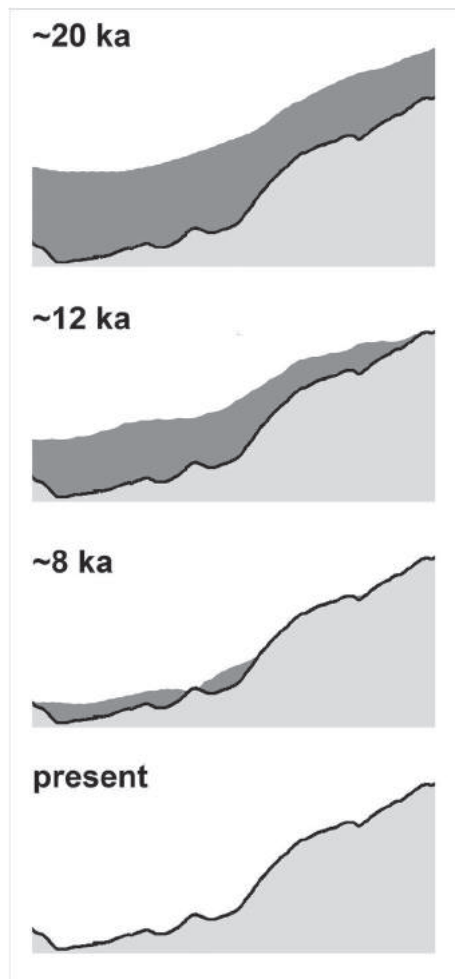


Figure 11. Conceptual model of surface lowering and exposure of scarps along the inner hills of the upland plateau.

Boulder #3; Figure 12a) match closely to those of the scarps of the hills. This suggests that the latest stage of the evolution of the Sila upland plateau was controlled by an initial episode of surface lowering followed by an early stage of river incision which then initiated erosion toward the summit of the landscape.

Responsible triggers for local denudation variations

Using the tors as an *in situ* archive, the temporal variations of the denudation rates are clearly detectable (Figures 5 and 6). Several factors determine rates of denudation, including surface topography, geology, tectonics, biosphere, human activity and climate (Smithson *et al.*, 2013). The temporal variability of the denudation rates thus suggests that the environmental drivers of landscape erosion also have changed. Furthermore, the detected changes depend on the topography, which indicates that the temporal trends depend on the relief position. Our approach and models enable us to investigate the causes of these variations over the last 100 ka (Figures 5, 6 and 12).

Because of the homogenous granitic basement (Figure 2b), abrupt lithological changes do not occur here. Therefore, other than weathering-induced changes in rock density due to saprolite formation and local tectonic effects (shear zones, fault gauges), no transition exists to move easily eroded rock types that would have contributed to an increased D_{Surface} . Tectonic forces lifted the upland to its present elevation and caused a disequilibrium that had to be counterbalanced by denudation. Over the course of the investigated time span (~100 ka), the Sila

Massif was uplifted by at least 50 m and possibly as much as 100 m (Bintanja *et al.*, 2005; Corbi *et al.*, 2009; Olivetti *et al.*, 2012). Our maximum denudation rate of 0.40 mm yr^{-1} (Figure 6f) would only result in a calculated absolute denudation of 40 m (in line with estimates of Scarciglia, 2015), but only if it had been constant over the entire time span. By comparing the uplift rates to the average exhumation trend ($0.05 \pm 0.03 \text{ mm yr}^{-1}$) of the vertical tor profiles, uplift appears even more dominant. Because the maximum D_{Surface} is not large enough to compensate the minimum uplift-rate, we argue that the Sila Massif uplift is still in disequilibrium, relative to its uplifting forces. Olivetti *et al.* (2012) also found the massif to be in a transient state of disequilibrium due to the strong and unsteady uplift that occurred 300–400 ka BP. Furthermore, our interpretation of erosion and accumulation agrees with Olivetti *et al.* (2012) who assumed that counterbalancing erosion processes (up to $\sim 0.92 \text{ mm yr}^{-1}$ along the massif flanks; average of $\sim 0.13 \text{ mm yr}^{-1}$ at plateau) are only effective along the massif flanks and that ‘pre-uplift’ erosion rates are conserved in the flat upland area.

Tectonic uplift processes here laid the ground work for a potential increase in D_{Surface} through accentuation of the relief leading to a predisposition toward erosion. Apparently, only the surrounding flanks appear to have responded (Olivetti *et al.*, 2012) as the low D_{Surface} values of the upland sites (Figures 5, 6 and 12) indicate that this area has not yet reacted to the tectonic uplift. We assume that the upland will remain relatively unaffected by the past uplift until the incision of creeks along the flanks become a dominant geomorphic process. The relatively young ages of the scarps suggest that this river incision is now at its earliest stage.

Furthermore, relief, climate and vegetation also affect soil erosion. Vegetation (‘biology’) is, however, not a fully independent factor because it depends on climate. Therefore, a climate effect on erosion always also includes, to a certain extent, vegetation (in the case that there is no anthropogenic impact). The uplift of the plateau also contributed to an environmental change in flora and fauna. The plateau began as a Miocene lowland 5 Ma ago, then evolved to a low-relief landscape ~ 2.6 Ma and finally to an upland at about 400 ka ago (Olivetti *et al.*, 2012). Based on pollen data, Fauquette and Combourieu-Nebout (2013) demonstrated that the Sila Massif had already reached a height of 1600 to 2100 m a.s.l. by 2.4 Ma. Furthermore, they described a change from a subtropical forest to an open-herbaceous biome as the uplift shifted the former humid climate towards a climate more dominated by stronger seasonal contrasts in temperature and precipitation. This change from a Thermomediterranean to an Oromediterranean and Altimediterranean altitudinal organization (Ozenda *et al.*, 1975; Bonin, 1981) has been identified in southern Calabria (Combourieu-Nebout, 1993).

In general, denudation forces are weaker under forest biomes and stronger in steppes, where the vegetation cover is temporally discontinuous (Allen *et al.*, 1999). Forest biomes dominated the mountain regions of southern Italy (Lago Grande di Monticchio) during the periods 100–75 ka BP and 14 ka BP to present, while steppes dominated shortly around 95 ka BP and between 75 and 14 ka (Figure 13; Allen *et al.*, 1999). No detailed investigation of the vegetation history is available for the Sila upland over the last 100 ka and so far, only palaeopedological investigations are available (Scarciglia *et al.*, 2005b, 2008). Detailed soil charcoal analyses at Cecita Lake has enabled the reconstruction of vegetation changes for the Holocene (Moser *et al.*, 2017). Fragments of charcoal in the soils surrounding Cecita Lake indicated the presence of an oak-dominated deciduous forest, which since has been replaced by mountain pine forest (Figure 13; Pelle *et al.*, 2013).

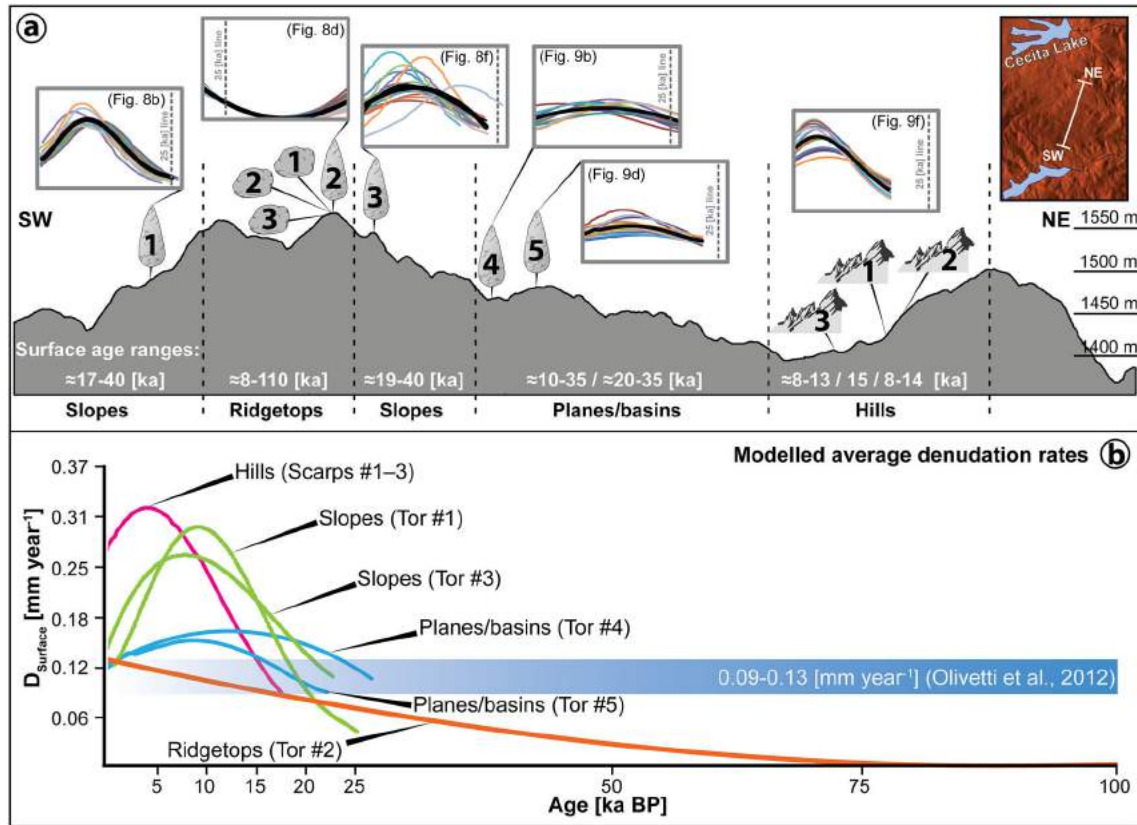


Figure 12. (a) Relation between surface topography and denudation rates along the southwest–northeast (SW–NE) investigation transect. (b) Comparison of modelled average denudation rates over time (Figures 8 and 9) of the different surface relief sections (e.g. ridgetops, slopes, planes/basins, hills) and average erosion rates (calculated from cosmogenic ¹⁰Be concentration using a material density of 2.6 g cm⁻³) after Olivetti *et al.* (2012). [Colour figure can be viewed at wileyonlinelibrary.com]

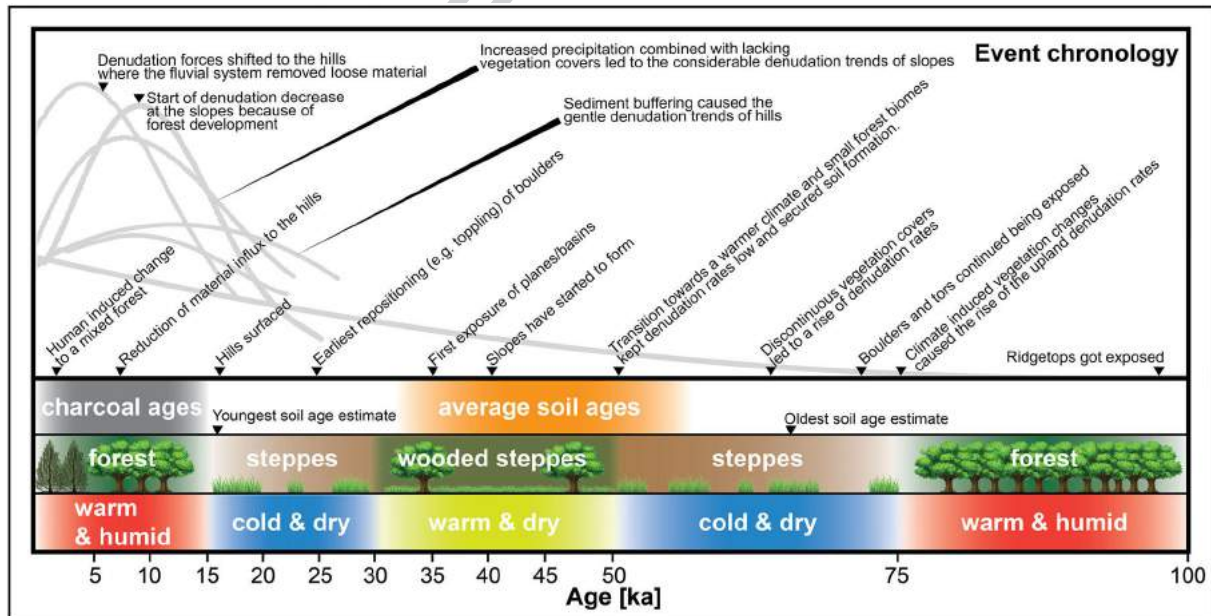


Figure 13. Model of local changes in climate (Allen *et al.*, 1999) and vegetation (Allen *et al.*, 1999; Pelle *et al.*, 2013) for the last 100 ka. This concept also includes soil and charcoal ages and major findings of Raab *et al.* (2017) and Moser *et al.* (2017) to complement the series of surface evolution events. [Colour figure can be viewed at wileyonlinelibrary.com]

Calibrated carbon-14 (¹⁴C) ages of charcoal samples only gave ages no older than 14 ka (Moser *et al.*, 2017), which correlate with our surface exposure ages of the hills (8–15 ka; Figure 12 a). These data are consistent with those obtained from pollen analyses of a nearby upland palaeolake (Trifoglietti) of the Coastal Chain, located about 50 km northwest of our study area. Joannin *et al.* (2012) found evidence of an increased

moisture from about 11 to 9.4 ka cal BP which could have enhanced erosion processes. At this site, a period with maximum humidity is recorded around 9.4–6.2 ka cal BP, followed by a general trend towards a drier climate until present. Previous soil age-estimates in the range 16–67 ka BP with an average of 45 ± 11 ka BP (Figure 13; Raab *et al.*, 2017) in the Sila upland correspond to the age of the slopes (~40 ka; Figure 12a).

Additionally, a relatively short warmer and drier climate pulse from 30 to 50 ka BP enabled wooded steppes to form here (Figure 13; Allen *et al.*, 1999) which would have slightly balanced the denuding processes through a denser root network that would have withheld soil and sediment. Furthermore, soil development is strongly linked with volcanic ash influx during this time (Raab *et al.*, 2018). Fertilization through volcanic ash-inputs (Pelle *et al.*, 2013; Raab *et al.*, 2017, 2018) may have enhanced this development at the upland, and might help explain the low D_{Surface} of Tor #2 (Figures 5d and 12b).

Studies of human activity in southern Italy indicate the presence of organized human societies since 6–7 ka BP (Scarciglia *et al.*, 2008; Pelle *et al.*, 2013; Russo Ermolli *et al.*, 2018). Allen *et al.* (1999) and Russo Ermolli *et al.* (2018) showed that the Apennine mountain chain and the Sant'Eufemia Plain (located southwest of the Sila Massif) experienced an increased influence of agricultural and forest clearance for the last 2 ka. A drastic increase in soil erosion has been recorded by Raab *et al.* (2018) due to more recent human activities.

Conclusions

Surface exposure dating (^{10}Be) along vertical rock profiles of granitic landscape forms (tors, boulders, scarps) revealed the temporal sequence of soil denudation processes and thus the controls on landscape evolution of the Sila Massif in southern Italy.

Tors provide a detailed insight into landscape evolution for the last 100 ka in southern Italy and allow us to more clearly understand and more effectively quantify the impacts that environmental factors have on landscape evolution here. We consider these granitic features to be a very useful *in situ* landscape archive that provide evidence of variable rates of soil denudation over time and as a function of topographic position. We see, furthermore, a great potential in this approach to trace and quantify over long periods of time the influence of climate variability on landscape denudation rates. This in turn is crucial for predicting the effect of future climate change on soil erosion rates. Our modelled soil denudation rates vary across a range of c. 0 to 0.37 mm yr^{-1} , with the highest rates occurring around 10–25 ka BP.

Boulders, however, may not remain at a stable position and are therefore less suitable for dating these landscape processes. The investigated boulders in the Sila upland evolved parallel to the tors, although some appear to have experienced changes in position about 20–25 ka BP, making the calculation of soil denudation rates difficult or impossible at this point in time. The investigated rock scarps in the Sila upland are relatively young (8–15 ka) and show a rather abrupt bedrock exposure, probably due to an increase of the denudation forces during the last 15 ka, with a maximum at ~5 ka BP. Thus, the scarps at the Sila upland represent the final stage of surface evolution, probably triggered by an initial river incision, while boulder and tors are remnants of an older landscape where surface lowering (denudation) prevailed.

By piecing together the evolution of the individual landforms, we are able to reconstruct a denudation chronology for the Sila upland for the last 100 ka and to relate it to environmental processes that appear to drive the evolution of this landscape. Climate induced vegetation changes around 75 ka BP and rapid changes towards warmer and more humid conditions around 15 ka BP appear responsible for the increases in denudation rates where we observed them. Increases in the density of vegetation cover (e.g. forest) from 30 to 50 ka BP and particularly after 15 ka BP appears to have counteracted erosion during these periods. Topography was apparently a secondary

factor controlling the extent of past variability in denudation rates in the upland. Our data suggest that slopes previously have experienced higher denudation rates than present-day planes and basins.

Overall, tors, boulder and scarps of granitic landscapes are excellent archives with which we may reconstruct environmental processes over time that may greatly improve our understanding of surface mass-flux processes.

Acknowledgements—This research was supported by the Swiss National Science Foundation (SNSF) project grant no. 200021_162338/1. Kevin Norton was supported by a SNSF Visiting International Fellowship (IZK0Z2_170715/1) and the Royal Society Te Apārangi Rutherford Discovery Fellowship and Fabio Scarciglia by a SNSF grant for a Short Research Visit (IZK0Z2_147421).

References

- Allen JRM, Brandt U, Brauer A, Hubberten HW, Hunley B, Keller J, Kraml M, Mackensen A, Mingram J, Negendank JFW, Nowaczyk NR, Oberhänsli H, Watts WA, Wulf S, Zolitschka B. 1999. Rapid environment changes in southern Europe during the last glacial period. *Nature* **400**: 740–743. <https://doi.org/10.1038/23432>.
- Bajard M, Poulenard J, Sabatier P, Develle AL, Giguet-Covex C, Jacob J, Crouzet C, David F, Pignol C, Arnaud F. 2017. Progressive and regressive soil evolution phases in the Anthropocene. *Catena* **150**: 39–52. <https://doi.org/10.1016/j.catena.2016.11.001>.
- Balco G, Stone JO, Lifton NA, Dunai TJ. 2008. A complete and easily accessible means of calculating surface exposure ages or erosion rates from ^{10}Be and ^{26}Al measurements. *Quaternary Geochronology* **8**: 174–195. <https://doi.org/10.1016/j.quageo.2007.12.001>.
- Bates RL, Jackson JA. 1987. *Glossary of Geology*, third edn. Alexandria, VA: American Geological Institute.
- Bintanja R, Roderik SW, Oerlemans J. 2005. Modelled atmospheric temperatures and global sea levels over the million years. *Nature* **437**: 125–128. <https://doi.org/10.1038/nature03975>.
- Bonin G. 1981. L'étagement de la végétation dans l'Apennin méridional. *Ecologia Mediterranea* **7**: 79–91.
- Borchers B, Marrero S, Balco G, Caffee M, Goehring B, Lifton N, Nishiizumi K, Phillips F, Schaefer J, Stone J. 2016. Geological calibration of spallation production rates in the CRONUS-Earth. *Quaternary Geochronology* **31**: 188–198. <https://doi.org/10.1016/j.quageo.2015.01.009>.
- Brown ET, Edmond JM, Raisbeck GM, Yiu F, Desgarceaux S. 1992. Effective attenuation length of cosmic rays producing ^{10}Be and ^{26}Al in quartz: implications for surface exposure dating. *Geophysical Research Letters* **9**: 369–372. <https://doi.org/10.1029/92GL00266>.
- Cacho I, Grimalt JO, Canals M, Sbaifi L, Shackleton NJ, Schönfeld J, Zahn R. 2001. Variability of the western Mediterranean Sea surface temperature during the last 25,000 years and its connection with the Northern Hemisphere climatic changes. *Paleoceanography* **16**: 40–52. <https://doi.org/10.1029/2000PA000502>.
- Chmeleff J, von Blanckenburg F, Kossert K, Jakob D. 2010. Determination of the ^{10}Be half-life by multicollector ICP-MS and liquid scintillation counting. *Nuclear Instruments and Methods in Physics Research Section B: Beam Interaction with Materials and Atoms* **268**: 192–199. <https://doi.org/10.1016/j.nimb.2009.09.012>.
- Christl M, Vockenhuber C, Kubik PQ, Wacker L, Lachner J, Alfimov V, Sval HA. 2013. The ETH Zurich AMS facilities: performance parameters and reference materials. *Nuclear Instruments and Methods in Physics Research B* **294**: 29–38. <https://doi.org/10.1016/j.nimb.2012.03.004>.
- Combourieu-Nebout N. 1993. Vegetation response to upper Pliocene glacial/interglacial cyclicity in the central Mediterranean. *Quaternary Research* **40**: 228–236. <https://doi.org/10.1006/qres.1993.1074>.
- Corbi F, Fubelli G, Lucá F, Muto F, Pelle T, Robustelli G, Scarciglia F, Drams F. 2009. Vertical movements in the Ionian margin of the Sila Massif (Calabria, Italy). *Bollettino della Società Geologica Italiana* **128**: 731–738. <https://doi.org/10.3301/IJG.2009.128.3.731>.
- Fauquette S, Combourieu-Nebout N. 2013. Palaeoaltitude of the Sila Massif (Southern Apennines, Italy) and distribution of the

- vegetation belts at ca. 2.4 Ma (Early Pleistocene). *Review of Palaeobotany and Palynology* **189**: 1–7. <https://doi.org/10.1016/j.revpalbo.2012.10.003>.
- Gosse JC, Philips FM. 2001. Terrestrial in situ produced cosmogenic nuclides: theory and application. *Quaternary Science Reviews* **20**: 1475–1560. [https://doi.org/10.1016/S0277-3791\(00\)00171-2](https://doi.org/10.1016/S0277-3791(00)00171-2).
- Gunnell Y, Jarman D, Braucher R, Calvet M, Delmas M, Leanni L, Bourlès D, Arnold M, Aumaitre G, Keddaouche K. 2013. The granites of Dartmoor, Southwest England: rapid and recent emergence revealed by Late Pleistocene cosmogenic apparent exposure ages. *Quaternary Science Reviews* **61**: 62–76. <https://doi.org/10.1016/j.quascirev.2012.11.005>.
- Heimsath AM, Chappell J, Dietrich WE, Nishiizumi K, Finkel RC. 2001. Late Quaternary erosion in southeastern Australia: a field example using cosmogenic nuclides. *Quaternary International* **83**: 169–185. [https://doi.org/10.1016/S1040-6182\(01\)00038-6](https://doi.org/10.1016/S1040-6182(01)00038-6).
- Joannin S, Brugiapaglia E, De Bealieu JL, Bernardo L, Magny M, Peyron O, Goring S, Vannièrè B. 2012. Pollen-based reconstruction of Holocene vegetation and climate in southern Italy: the case of Lago Trifoglietti. *Climate of the Past* **8**: 1973–1996.
- Kitchener JA. 1984. The froth flotation process: past, present and future – in brief. In *The Scientific Basis of Flotation*. Ives KJ (ed.), NATO ASI Series (Series E: Applied Sciences) 75. Springer: Dordrecht. https://doi.org/10.1007/978-94-009-6926-1_2
- Kohl C, Nishiizumi K. 1992. Chemical isolation of quartz for measurement of in-situ –produced cosmogenic nuclides. *Geochimica Cosmochimica Acta* **56**: 3583–3587. [https://doi.org/10.1016/0016-7037\(92\)90401-4](https://doi.org/10.1016/0016-7037(92)90401-4).
- Korschinek G, Bergmaier A, Faestermann T, Gerstmann UC, Remmert A. 2010. A new value for the half-life of ^{10}Be by heavy-ion elastic recoil detection and liquid scintillation counting. *Nuclear Instruments and Methods in Physics Research Section B: Beam Interaction with Materials and Atoms* **268**: 187–191. <https://doi.org/10.1016/j.nimb.2009.09.020>.
- Kubik PW, Christl M. 2010. ^{10}Be and ^{26}Al measurements at the Zurich 6 MV Tandem AMS facility. *Nuclear Instruments and Methods B* **268**: 880–883. <https://doi.org/10.1016/j.nimb.2009.10.054>.
- Le Pera E, Sorriso-Valvo M. 2000. Weathering and morphogenesis in a Mediterranean climate, Calabria, Italy. *Geomorphology* **34**(3): 251–270. [https://doi.org/10.1016/S0169-555X\(00\)00012-X](https://doi.org/10.1016/S0169-555X(00)00012-X).
- Li G, West AJ, Desmore AL, Jin Z, Zhang F, Wang J, Clark M, Hilton RG. 2017. Earthquakes drive focused denudation along a tectonically active mountain front. *Earth and Planetary Science Letters* **472**: 253–265. <https://doi.org/10.1016/j.epsl.2017.04.040>.
- Lichter J. 1998. Rates of weathering and chemical depletion in soils across a chronosequence of Lake Michigan sand dunes. *Geoderma* **85**: 255–282. [https://doi.org/10.1016/S0016-7061\(98\)00026-3](https://doi.org/10.1016/S0016-7061(98)00026-3).
- Linton DL. 1955. The problem of tors. *The Geographical Journal* **121**: 470–481.
- Liotta D, Caggianelli A, Kruhl JH, Festa V, Prosser G, Langoe A. 2008. Multiple injections of magmas along a Hercynian mid-crustal shear zone (Sila Massif, Calabria, Italy). *Journal of Structural Geology* **30**: 1202–1217. <https://doi.org/10.1016/j.jsg.2008.04.005>.
- Liu BY, Nearing MA, Risse LM. 1994. *Slope Gradient Effects on Soil Loss for Steep Slopes*. American Society of Agricultural and Biological Engineers: St Joseph, MI. <https://doi.org/10.13031/2013.28273>
- Lyell C. 1830. Review of principles of geology by Charles Lyell. *The Quarterly Review* **43**: 411–469.
- Masarik J, Frank M, Schaefer JM, Wieler R. 2001. Correction of in-situ cosmogenic nuclide production rates for geomagnetic field intensity variations during the past 800,000 years. *Geochimica et Cosmochimica Acta* **65**: 2995–3003.
- Middlemost EAK. 1994. Naming materials in the magma/igneous rock system. *Earth-Science Reviews* **37**: 215–224.
- Migoñ P. 2006. *Granite Landscapes of the World*. Oxford University Press: New York.
- Migoñ P. 2013. Weathering and hillslope development. In *Treatise on Geomorphology*, Shroder JF (ed.). Academic Press: San Diego, CA; volume **4**, 159–178. <https://doi.org/10.1016/B978-0-12-374739-6.00075-0>
- Migoñ P, Prokop P. 2013. Landforms and landscape evolution in the Myllem Granite Area, Meghalaya Plateau, northeast India. *Singapore Journal of Tropical Geography* **34**: 206–228.
- Migoñ P, Vieira G. 2014. Granite geomorphology and its geological controls, Serra da Estrela, Portugal. *Geomorphology* **226**: 1–14. <https://doi.org/10.1016/j.geomorph.2014.07.027>.
- Molin P, Pazzaglia FJ, Dramis F. 2004. Geomorphic expression of active tectonics in a rapidly-deforming fore-arc, Sila Massif, Calabria, southern Italy. *American Journal of Science* **304**: 559–589. <https://doi.org/10.2475/ajs.304.7.559>.
- Moser D, Di Pasquale G, Scarciglia F, Nelle O. 2017. Holocene mountain forest changes in central Mediterranean: soil charcoal data from the Sila Massif (Calabria, southern Italy). *Quaternary International* **457**: 113–130. <https://doi.org/10.1016/j.quaint.2017.01.042>.
- Nishiizumi K, Imamura M, Caffee MW, Southon JR, Finkel RC, McAnich J. 2007. Absolute calibration of ^{10}Be AMS standards. *Nuclear Instruments & Methods in Physics Research Section B-Beam Interactions with Materials and Atoms* **258**: 403–413. <https://doi.org/10.1016/j.nimb.2007.01.297>.
- Olivetti V, Cyr AJ, Molin P, Faccenna C, Granger DE. 2012. Uplift history of the Sila Massif, southern Italy, deciphered from cosmogenic ^{10}Be erosion rates and river longitudinal profile analysis. *Tectonics* **31**: 1–19. <https://doi.org/10.1029/2011TC003037>.
- Ozenda P. 1975. Sur les étages de végétation dans le montagnes du bassin méditerranéen. *Documents Cartographiques Ecologiques (Grenoble)* **16**: 1–32.
- Pelle T, Scarciglia F, Di Pasquale G, Allevato E, Marino D, Robustelli G, La Russa MF, Pulice I. 2013. Multidisciplinary study of Holocene archaeological soils in an upland Mediterranean site: natural versus anthropogenic environmental changes at Cecita Lake, Calabria, Italy. *Quaternary International* **303**: 163–179. <https://doi.org/10.1016/j.quaint.2013.04.003Sc>.
- Perri F, Critelli S, Dominici R, Muto F, Tripodi V, Ceramicola S. 2012. Provenance and accommodation pathways of late Quaternary sediments in the deep-water northern Ionian Basin, southern Italy. *Sedimentary Geology* **280**: 244–259.
- Phillips WM, Hall AM, Mottram R, Fifield LK, Sugden DE. 2006. Cosmogenic ^{10}Be and ^{26}Al exposure ages of tors and erratics, Cairngorm Mountains, Scotland: timescales for the development of a classic landscape of selective linear glacial erosion. *Geomorphology* **73**: 222–245. <https://doi.org/10.1016/j.geomorph.2005.06.009>.
- Pigati JS, Lifton NA. 2004. Geomagnetic effects on time-integrated cosmogenic nuclide production with emphasis on in situ ^{14}C and ^{10}B . *Earth and Planetary Science Letters* **226**: 193–205. <https://doi.org/10.1016/j.epsl.2004.07.031>.
- Raab G, Halpern D, Scarciglia F, Raimondi S, Norton K, Pettke T, Hermann J, de Castro PR, Aguilar Sanchez AM, Egli M. 2017. Linking tephrochronology and soil characteristics in the Sila and Nebrodi mountains, Italy. *Catena* **158**: 266–285. <https://doi.org/10.1016/j.catena.2017.07.008>.
- Raab G, Scarciglia F, Norton K, Dahms D, Brandová D, de Castro PR, Christl M, Ketterer ME, Ruppli A, Egli M. 2018. Denudation variability of the Sila Massif upland (Italy) from decades to millennia using ^{10}Be and $^{239+240}\text{Pu}$. *Land Degradation and Development* **29**(10): 3736–3752. <https://doi.org/10.1002/ldr.3120>.
- Ruello MR, Cinque A, Di Donato V, Molisso F, Terrasi F, Russo Ermolli E. 2017. Interplay between sea level rise and tectonics in the Holocene evolution of the St. Eufemia Plain (Calabria, Italy). *Journal of Coastal Conservation* **21**: 903–915. <https://doi.org/10.1007/s11852-017-0558-9>.
- Russo Ermolli E, Ruello MR, Cicala L, Di Lorenzo H, Moilso F, Pacciarelli M. 2018. An 8300-yr record of environmental and cultural changes in the Sant’Eufemia Plain (Calabria, Italy). *Quaternary International* **483**: 39–56.
- Scarciglia F. 2015. Weathering and exhumation history of the Sila Massif upland plateaus, southern Italy: a geomorphological and pedological perspective. *Journal of Soils and Sediments* **15**: 1278–1291. <https://doi.org/10.1007/s11368-014-0923-3>.
- Scarciglia F, Le Pera E, Critelli S. 2005a. Weathering and pedogenesis in the Sila Grande Massif (Calabria, south Italy): from field scale to micromorphology. *Catena* **61**: 1–29. <https://doi.org/10.1016/j.catena.2005.02.001>.
- Scarciglia F, Le Pera E, Vecchio G, Critelli S. 2005b. The interplay of geomorphic processes and soil development in an upland environment, Calabria, south Italy. *Geomorphology* **69**: 169–190. <https://doi.org/10.1016/j.geomorph.2005.01.003>.

- Scarciglia F, Le Pera E, Critelli S. 2007. The onset of the sedimentary cycle in a mid-latitude upland environment: weathering, pedogenesis and geomorphic processes on plutonic rocks (Sila Massif, Calabria). In *Sedimentary Provenance and Petrogenesis: Perspectives from Petrography and Geochemistry*, Arribas J, Critelli S, Johnsson MJ (eds), Geological Society of America Special Paper 420. Geological Society of America: Boulder, CO; 149–166. [https://doi.org/10.1130/2006.2420\(10\)](https://doi.org/10.1130/2006.2420(10))
- Scarciglia F, De Rosa R, Vecchio G, Apollaro C, Robustelli G, Terrasi F. 2008. Volcanic soil formation in Calabria (southern Italy): the Cecita Lake geosol in the late Quaternary geomorphological evolution of the Sila uplands. *Journal of Volcanology Geothermal Research* **177**: 101–117. <https://doi.org/10.1016/j.jvolgeores.2007.10.014>.
- Scarciglia F, Critelli S, Borrelli L, Coniglio S, Muto F, Perri F. 2016. Weathering profiles in granitoid rocks of the Sila Massif uplands, Calabria, southern Italy: new insights into their formation process and rates. *Sedimentary Geology* **336**: 46–67. <https://doi.org/10.1016/j.sedgeo.2016.01.015>.
- Small EE, Anderson RS, Hancock GS. 1999. Estimates of the rate of regolith production using ^{10}Be and ^{26}Al from an alpine hillslope. *Geomorphology* **27**: 131–150. [https://doi.org/10.1016/S0169-55x\(98\)00094-4](https://doi.org/10.1016/S0169-55x(98)00094-4).
- Smithson P, Addison K, Atkinson K. 2013. *Fundamentals of the Physical Environment – Fourth Edition*. London: Routledge.
- Sorriso-Valvo M. 1993. The geomorphology of Calabria. A sketch. *Geografia Fisica e Dinamica Quaternaria* **16**: 75–80.
- Spina V, Galli P, Tondi M, Critelli S, Cello G. 2007. Kinematics and structural properties of an active fault zone in the Sila Massif (northern Calabria, Italy). *Bollettino della Società Geologica Italiana* **126**: 427–438.
- Stone JO. 2000. Air pressure and cosmogenic isotope production. *Journal of Geophysical Research* **105**: 753–759. <https://doi.org/10.1029/2000JB900181>.
- Tansi C, Muto F, Critelli S, Iovine G. 2007. Neogene-Quaternary strike-slip tectonics in the central Calabrian Arc (southern Italy). *Journal of Geodynamics* **43**: 393–414. <https://doi.org/10.1016/j.jog.2006.10.006>.
- Thomas MF. 1965. Some aspects of the geomorphology of domes and tors in Nigeria. *Zeitschrift für Geomorphologie N.F.* **9**: 63–81.
- Thomas MF. 1997. Weathering and landslides in the humid tropics: a geomorphological perspective. *Journal of the Geosocial Society of China* **40**: 1–16.
- Twidale CR. 2002. The two-stage concept of landform and landscape development involving etching: origin, development and implications of an idea. *Earth Science Reviews* **57**: 37–74. [https://doi.org/10.1016/S0012-8252\(01\)00059-9](https://doi.org/10.1016/S0012-8252(01)00059-9).
- Twidale CR, Romani JRV. 2005. *Landforms and Geology of Granite Terrains*. Taylor & Francis: London.
- von Blanckenburg F, Belshaw NS, O’Nions RK. 1996. Separation of ^9Be and cosmogenic ^{10}Be from environmental materials and SIMS isotope dilution analysis. *Chemical Geology* **129**: 93–99. [https://doi.org/10.1016/0009-2541\(95\)00157-3](https://doi.org/10.1016/0009-2541(95)00157-3).
- von Eynatten H, Tolosana-Delgado R, Karius V, Bachmann K, Caracciolo K. 2015. Sediment generation in humid Mediterranean setting: grain-size and source-rock control on sediment geochemistry and mineralogy (Sila Massif, Calabria). *Sedimentary Geology* **336**: 68–80. <https://doi.org/10.1016/j.sedgeo.2015.10.008>.
- Wakasa S, Matsuzaki H, Tanaka Y, Matsukura Y. 2006. Estimation of episodic exfoliation rates of rock sheets on a granite dome in Korea from cosmogenic nuclide analysis. *Earth Surface Processes and Landforms* **31**: 1246–1256. <https://doi.org/10.1002/esp.1328>.

Supporting Information

Additional supporting information may be found online in the Supporting Information section at the end of the article.

TABLE S1. Input data for the CRONUS online calculator (Balco et al., 2008).

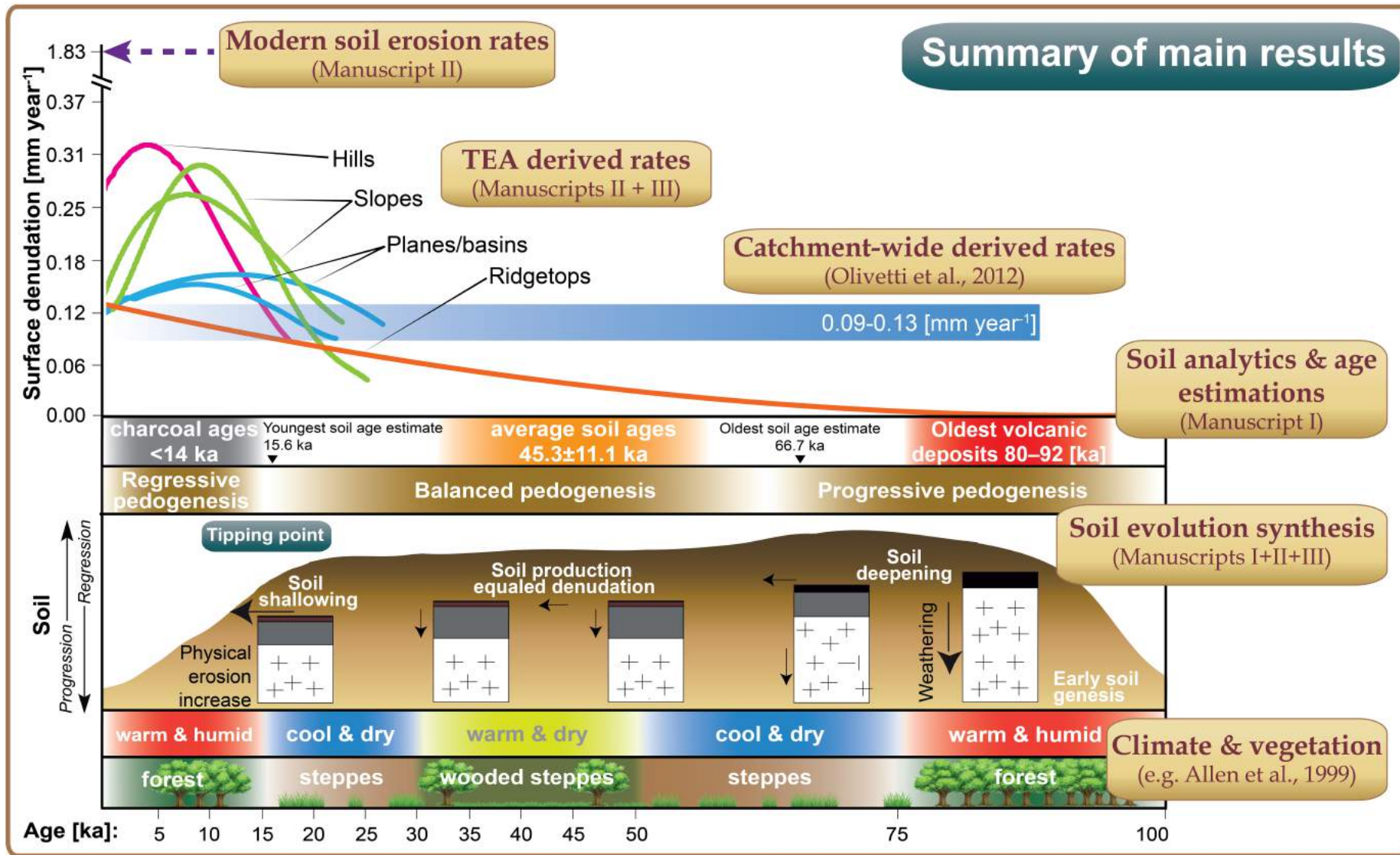


Figure 13: Manuscript I: Soil analytics and age estimations using radiocarbon dating, semi-quantitative and relative dating with chemical weathering indices and geochemical fingerprinting of volcanic ash (glass) deposits provided a basic geochronological understanding of the local soils. Manuscript II: Fallout radionuclide derived soil erosion rates for the last ~50 - 60 years are found to be significantly higher than rates of the last 100 ka derived from the TEA. Manuscript II + III: The TEA enabled the capturing of past surface denudation and soil erosion variations over multi-millennia (Holocene–Pleistocene) in contrast to catchment-wide derived rates (Olivetti et al. (2012)) which only provide average rates. In addition, the erosion differences of various angled surfaces (e.g. slopes and planes) could be captured. The combination of climate and vegetation data (Allen et al., 1999; Pelle et al., 2012) resulted in a local soil evolution model. The synthesis proposes the following evolutionary stages: early soil genesis and soil deepening prior to 70 ka was followed by a balanced pedogenesis which was disrupted around 15 ka by increased physical erosion.

5. DISCUSSION OF MAIN RESULTS

5.1. ALTERNATIVE SOIL AGE ESTIMATIONS

In Manuscript I we have taken the liberty of exploring other methods of assessing the local soil age than absolute soil dating (e.g. meteoric cosmogenic nuclides).

(i) The geo-forensic approach revealed first that literature-based radiocarbon ages of the Sila Upland vary from modern to about 14 ka BP (Table 7, Manuscript I). Newly dated soil organic matter in proximity to tors ranged at about 8 – 9.5 ka (Table 8, Manuscript I). These ages are equivalent to the exposure ages found at and below today's soil surface levels of tors (11 ± 2 ka), boulders (8 ± 1 ka) and scarps (8 ± 1 ka) (Manuscript II & III). Radiocarbon ages were indicative for the youngest local soil ages. Additionally performed chemical analyses of volcanic deposits and weathering trajectories identified a wider time window of local soil formation.

(ii) The geochemical signature of the primary (volcanic) material in soil enabled the determination of soil formation ages. This was achieved by comparing the unique geochemical fingerprint of past volcanic eruption material. Analysis of major, minor and trace (e.g. REEs) elements of volcanic glass particles allowed the best identification of the volcanic source and eruption phase and subsequently the time of deposition.

(iii) Chemical mass balance calculation from various soil horizons provided a further proportional connection of suitable eruptive

epochs. Highest proportional fits of the Lipari island (Aeolian Islands, Italy) indicated the age of the eruptive material, and subsequently the soil horizon, to be older than 30 ka and younger than 92 – 81 ka (epoch six of Lipari; Forni et al., 2013). In this context, the age of ~ 100 ka at the top of the largest Tor #2 (Manuscript II), potentially reflects the time of the earliest traceable soil formation.

(iv) Chemical weathering indices were used for semi-quantitative and relative dating. Semiquantitative dating was achieved by relating weathering data from the literature to numeric surface ages. Also the geochemical composition of similar source surfaces material could be successfully related to surface ages. This age estimation resulted in an average age of 45.3 ± 11.1 ka, with a lower and upper boundary of 15.6 and 66.7 ka (Table 10, Manuscript I). The calculated age range minimum of 15.6 ka correlates with the oldest radiocarbon ages found in the soil and youngest surface exposure ages of rock tors (Manuscript II & III). Also, four out of five tor tops started to be exposed at about 38 ± 4 to 32 ± 3 ka (Manuscript I & III), closely agreeing with the average age estimation from the semi-quantitative dating.

Overall, the three hypotheses of Manuscript I appear to be valid. The multi-method approach and connecting geochemical data with available literature data allowed soil age estimations.

However, not all landscapes possess handily-available (nearby) numerical data or soils that enable radiocarbon dating (e.g. lack of charcoal) that can be used for age calibrations. No radiocarbon ages were found for the prior steppes vegetation (Figure. 13, Manuscript III). Also, volcanic material is not a common soil feature in a non-volcanic area such as a granite upland plateau. Therefore, although the presented mix of methods provided a good age estimation, it was a rather specific combination suited for this investigation area. Moreover, the generated ages of relative and semi-quantitative dating are less specific than those of absolute dating and only provided a broad age range. In comparison, an absolute dating approach with the use of TCNs would have provided more specific results. However, this would have been associated with higher costs (e.g. AMS measurements fees) and time efforts (e.g. extraction of nuclides in the laboratory). But, by using literature data and standard soil investigation measurement techniques (e.g. XRF, XRD, DRIFT) and established mineralogical investigation tools (e.g. SED, LA-ICP-MS), estimation within the age ranges of nearby rock surface exposure ages could be achieved.

It could be concluded that by taking advantage of the area of interest local characteristics and available literature data, surface age estimations were more economically achieved. Therefore, although the relative dating resulted in a broader age range than absolute dating techniques, the

economic aspect might be more appealing to many researchers with limited funds.

5.2. TOR EXHUMATION APPROACH (TEA)

Manuscript II and III focused on the investigation of tors as new soil erosion archives. The hypotheses for Manuscript II were found to be partly valid:

(i) Exhumation rates of tors were successfully quantified and (ii) the concentration of tors increased with the heights above ground (Fig. 4, Manuscript II). The overall idea that tors are exhumed has been confirmed. The applied modelling allowed (iii) the determination of surface denudation and soil erosion trends over continuous time-intervals. (iv) In addition, the tor derived rates were in similar ranges as the catchment-based erosion rates (e.g. Olivetti et al., 2012). (v) The data provided by Manuscript I allowed the reconstruction of progressive and regressive phases of soil formation. (vi) However, soil erosion rates derived from modern tracing techniques (FRNs) were higher than the tor-based rates. The reason for this mismatch appears to be of anthropogenic origin. The strong increase is opposite to the tor-based model which showed a decrease since 10 – 5 ka BP.

Also, the hypotheses of Manuscript III are only partially valid: (i) Tors at similar topographic positions (slopes, planes) were shown to have similar surface denudation trends. In addition, slopes experienced higher soil erosion and surface denudation peaks than planes/basins or ridges.

(ii) Although vegetation and climate were similar around 75 to 50 ka and 30 to 15 ka, surface denudation rates were higher in the later (Fig. 13, Manuscript III). Therefore, the idea that time periods of equal environmental conditions result in similar soil erosion rates is invalid. The reason for this discrepancy is due to the neglect of varying soil production rates over time (Fig. 7, Manuscript II).

Soil age estimation on the basis of weathering indices from Manuscript I indicated an upper age range of 66.7 ka. Additionally, soil volcanic ages put the earliest soil formation at potentially around 92 – 81 ka. Young soils and soils rejuvenated due to volcanic ash input have the highest soil production rates (Fig. 7b, Manuscript II). Production rates during the time period 75 – 50 ka must have overcome soil erosion or kept the surface denudation (exhumation of tors) in a near steady-state condition. In the later stage (30 – 15 ka) soils were more mature, and production rates were lower. The last volcanic ash input was found to be prior to 30 ka. However, erosion rate increases were found at all transition phases (Fig. 13, Manuscript III)

(iii) The exhumation approach was further tested on unstable (boulders) and stable (scarps) landscape features. The comparison among tors, boulders and scarps revealed that tors are, so far, indeed uniquely providers of continuous soil erosion history. Bedrock outcrops of scarps represent only ages of the latest surface denudation peak at about 15 – 12 ka

(Fig. 12, Manuscript II), which fits the charcoal ages of Manuscript I.

Overall, the exhumation approach used on tors appears not to be transferable to other landscape features tested.

After evaluating the validity of the various hypotheses, the study aim about the suitability, capabilities and limitation of tors as soil erosion archive has to be reflected.

Suitability

The exhumation approach used on tors successfully provided soil erosion and surface denudation chronologies.

Among the three tested landscape features, tors provided the most consistent tracing of soil erosion and surface denudation rates. The granite tors of the Sila Massif recorded the temporal (soil) surface dynamics under changing environmental conditions over a continuous geological time-scale. Our overall hypothesis that exhumation rates of tors, determined with the use of TCNs, reflect soil erosion and surface denudation rates could be considered as valid.

However, objectively our study could only ascertain that the TEA was suitable at the lithology and conditions found at the Sila Massif upland. Similar areas (e.g. Serra da Estrela, Portugal) potentially lead to a comparative success. However, the performance in areas that do not meet the initial selection criteria for our study area (e.g. tectonically stable, consistent lithology, no large material influxes or glaciation etc.) remains unknown.

Hence, the TEA delivered (under the local conditions) the desired data needed to defragment the research field. Its suitability under different conditions still needs to be explored.

Capabilities

The TEA clearly provided a continuous soil surface evolution history over decamillennia at erosion sites (Manuscript II) as well as in transient depositional zones (Manuscript III). In addition, the topographic position of the tors revealed different denudation trends, which depended on the surface angle.

Controls of topography and slope angle on (soil) erosion rates are widely accepted (e.g. Liu et al., 1994; Montgomery & Brandon, 2002). The TEA has quantified this fact for the first time over a geological time-scale. The slope angle sensitivity is a quality that classical archives such as river sediment yields, lake sediments or speleothems are unable to preserve.

Long residence times of the surfaces of tors (e.g. Tor #2) indicated minor erosion rates or conditions close to steady-state, where soil production equals soil denudation. These conditions have been rarely demonstrated in studies, although they are often assumed in landscape evolution models (Phillips, 2010).

Also, the TEA enabled environmental literature data to be collaborated with soil erosion evolution over an unprecedented time-scale (Holocene—Pleistocene; Fig. 14). The combination of local environmental data about climate,

vegetation and soil allowed the creation of comprehensive surface evolution models. The captured surface denudation variations contributed to a deeper understanding on how landscapes react to environmental changes over longer time-scales. By being able to recognise the feedback effects of landscapes to environmental changes, predictions about future developments are achievable. The illustrated capabilities show a versatile use of the TEA for landscape research in the field of quantitative geomorphology.

Limitation

However, there are still some limitations to the approach. First of all, the archived period by tors was restricted by their individual heights. Only one out of five tors provided a historic log over 100 ka because of its height of about 6 m. Smaller tors of 3 to 4 m only reached half or a third of this age. Focusing investigations on very large tors would be reasonable, but they might not be present in the chosen landscape.

The distribution of tors in a landscape is an additional challenge. Tors provide less freedom of choice regarding sampling location compared to e.g. catchment-wide approaches. Also, the quantification of the total eroded material under steady-state phases cannot always be answered by the TEA alone; investigation of surrounding basins are necessary.

An undetermined hurdle for the TEA to become a universal approach is the influential role of past forces (e.g. glaciers, rock falls, exfoliation, strong abrasions or

surface shielding) that potentially can have changed the necessary isotopic signature.

In addition, there is a lack of a genuinely valid model or system that clearly establishes the genesis of tors. Although the world-wide presence of tors seems to be unrelated to environmental conditions, their formation and disintegration is still under-researched. There are several illustrated models that explain the formation of various tor rock types, but few that theorise their disintegration.

Our work contributed to the understanding and partly validated the model as proposed by Migoń (2013). Areas having a very different lithology (e.g. sandstone, schist) compared to the Sila Upland can be subjected to other processes than illustrated in Manuscript II. Therefore, the approach may need to be adjusted. Hence, until further testing is undertaken, the TEA success is currently restricted to particular granite-bearing landscapes.

In order to take full advantage of the approach, a good data set of past environmental parameters is necessary. Poorly characterised landscapes have to be preceded by numerous preliminary investigations about subjects such as the climate, vegetation or soil (see Manuscript I). The capability of the approach to develop a comprehensive landscape evolution model can be severely weaker in some areas. This could again limit its use to only carefully selected areas.

Because each tor offers a history of its specific location, only a set of tors can

provide an answer to the soil erosion evolution of an area. The dating technique used currently is still subject to a high financial and time effort. Considering that a minimum of four exposure ages are needed for any adequate modelling of one tor, this makes the approach relatively expensive. The prerequisite of either having an appropriate laboratory having the necessary know-how to perform surface exposure dating or the financial resources to outsource the task might hinder the approach that can be used by the majority of researchers. Besides the financial aspect, time can also be a restraining factor, as many research funds have an expiration date. It can take up to six months from field sampling to having a surface model – and this does not take into consideration the additional time necessary for preceding studies or laboratory issues.

This means that the TEA might only be able to be used by very few groups having the necessary resources at their disposal.

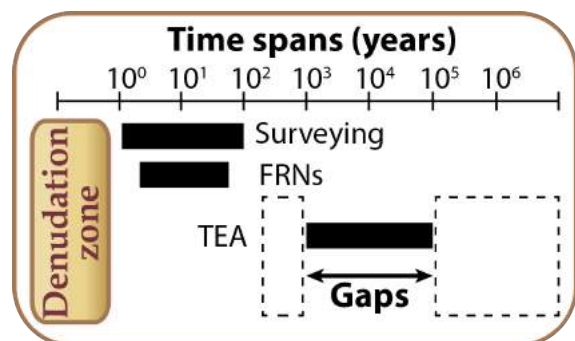


Figure 14: Contribution of the TEA to fill the proposed knowledge gap (Fig. 5). The remaining gaps still need adequate investigation techniques.

5.3. ANTHROPOGENIC SOIL EROSION?

We found in the Sila Massif that modern rates (the last 60 years) exceeded past rates by a factor of three to ten and more (Manuscript II). Human-induced actions e.g. deforestation and live-stock farming, were considered to be responsible. This seems to be alerting as these are common practises nowadays.

But it has to be considered that the FRN results are individual data points having quite a large variability (1,056 – 3,649 t km² yr⁻¹). The data set (and variability) could have been improved if it had a larger number of reference sites (e.g. Alewell et al., 2014) and more equal depth profiling increments (e.g. Porto et al., 2012).

Further investigations (Manuscript III) have shown that topography, climate and vegetation play a central role in the local surface evolution. The restoration of the upland by the increased vegetation appears to have caused the soil erosion to lessen continuously. In reverse, the reduction of this natural soil protective cover due to forest clearings (Allen et al., 2002) must have resulted in an increase of the erosion rates. The additional stress of farming (e.g. heavy animals pushing soil) accelerated this process.

In hindsight of the studies, human-induced actions were undoubtedly a local soil-erosion driver in recent years. However, the calculated extent of the modern rate increases should be considered with caution and improved by conducting additional FRN studies.

5.4. NATURAL DRIVER AND PREVENTOR OF SOIL EROSION

Although topography influenced the intensity of surface denudation rates (Manuscript III), the overall trends were similar. Except for the ridgetop, the highest elevated point in our study site, all tors show a decreasing surface denudation trend for approximately the last ten thousand years. Prior to this, rates steadily increased. We reasoned in Manuscript III that climate is the initiating driver, while vegetation prevented further increase and led to a reduction resulting in a developmental delay.

Changing climate is often found to be responsible for surface erosive processes. Accelerations of erosion are globally found under cooling (Hermann et al., 2013) as well as under warming (Nearing et al., 2004) climate conditions.

On the other hand, the impact of vegetation on soil erosion has rarely been investigated on geological time-scales. However, the fact that dense vegetation leads to a reduction in soil erosion was shown in short-term (few years) local studies (e.g. Mohammad & Adam, 2010; Zheng 2006) and also identified with rainfall simulations (e.g. Cerdá, 1999).

The results of our approach provide support for these investigations and indicate that vegetation plays a central role in regulating soil erosion. Therefore, vegetation should be considered more often in historic soil erosion investigations.

6. CONCLUSIONS

The aim of this thesis was to assess the suitability, capabilities and limitations of rock tors as a potential soil erosion and surface denudation archive. In addition, different techniques were tested for soil-age estimations. Radiocarbon ages of charcoal and soil organic material provided the minimum estimation of soil ages. Chemical weathering indices allowed the determination of a more concrete time span. Geochemical fingerprinting and source identification of allochthonous volcanic material in combination with chemical mass balance calculation of fine earth material further improved soil age estimations. Overall, the multi-method combination of relative and semi-quantitative dating techniques provided comparable age-results than when the surface exposure ages of surrounding rock surfaces were measured.

The tor-based work illustrates that the exhumation history of granite tors in an upland plateau comprehensively and easily enabled the determination of continuous soil erosion rates over geological time-scales (Holocene-Pleistocene). The modelling of vertical surface exposure age profiles along tors is considered to be a useful technique to capture surrounding surface variations. Additional qualities of tors include the quantification of their topographic influence on soil erosion and the capturing of steady-state alike conditions. Paleo-environmental data and prior soil investigations led to a local surface evolution model and an event

chronology. The approach contributed to an understanding of the local impact of certain environmental factors such as climate and vegetation. Although further studies are needed to validate the usability of the TEA in other landscape settings, the TEA has already demonstrated to be a promising tool to advance the research field.

7. OUTLOOK AND PERSPECTIVES

7.1. PROPOSED NEXT STEPS

The outcome of this work can only be seen as a starting point for further research on this topic. The approach was so far just tested in a very well-defined area. In order to understand more about its potentials and limitations, the TEA must be successively tested in more challenging environments.

In addition, the data density in the Sila Massive should be increased. For example, local soil ages could be dated using meteoric ^{10}Be dating to validate the approximated soil ages in Manuscript I. Steady-state conditions found in Tor #2 (Manuscript II) and the sediment buffering associated with Tor #4 and #5 (Manuscript III) could be explored in more detail (e.g. burial times) by factoring in an additional in-situ cosmogenic nuclide (e.g. ^{14}C). It would be also advisable to perform a mass balance among the surrounding basins and the upland of the Sila Massif. Records of transient deposition zones (e.g. lakes, rivers) and final deposition zones (e.g. marine sediments) should also be comparatively investigated.

Another step would be to assess the TEA in an area having a different lithology than granite (e.g. schist) and material influxes from other erosional areas. This would provide an understanding of how (strong) depositional phases potentially influence the retrievable information of tor archives. A successful investigation would also show the universal applicability of the approach in regarding different bedrock materials and the associated weathering. An investigation in this regard has already been started in the tor-schist dominated Otago upland on the southern island of New Zealand, and should soon be finished.

Because many tor provinces (especially in Europe) were subjected to glacial cycles, it would be advantageous to explore the influence of glacial forces on the exhumation process of tors and the exposure ages used for modelling. This could be achieved by a comparative study of isotope signatures between glaciated and never-glaciated tors in close proximity. The Serra da Estrela in Portugal offers such a dual setting. Incidentally, the mountain massif and the Sila Massif have very similar characteristics. Both sites have a plateau relief at about 1700 m a.s.l., granite tors and are positioned in close latitude ranges (Serra da Estrela: N40°19'; Sila: N39°22'). These are perfect conditions for additional comparative studies and facilitate the establishment of a broad soil erosion archive network.

Long-term consideration. There are about thirty well-explored and hundreds of

poorly-investigated tor provinces world-wide. Applying the tor exhumation approach on all of these can lead to a more detailed understanding of landscape evolution on a regional and later on a global scale.

7.2. BROADER APPLICABILITY AND VALUE

The specific mix of methods used at the Sila Upland for the relative and semi-quantitative dating of soils might not be identically feasible on other areas. However, the general concept of using calibrated weathering indices for soil age range estimations is new and can be transferred to other sites where numerical ages are available.

Presented limitations for the TEA should be considered chances for further research and new networks, not barriers. In particular, the resource intensity provides a great opportunity for new collaborations. Partnerships will probably make the TEA more affordable and more easily accessible to a larger array of people and institutions. To do so, one has to think about other beneficiaries and possible applications as well as the broader impacts of the generated data and models (Fig. 15). For example, the topographic dependent surface-lowering rates could be used to create past digital elevation models. The sensitivity of tors to slope angle and aspect ratio would allow an inverse modelling of the ancient landscape's elevations and its changes over time. In turn, such digital surface models could be useful in the understanding of changes in hydrological systems. Potential evaluations on past sediment streams might

provide hints of clogged river beds, eutrophication of water or water shortage. Again, this information could help anthropological studies to better understand migration patterns. This brief train of thought already illustrates a chain of various research fields that could benefit from this method.

A detailed understanding of the past allows a better prediction of the future. For example, nowadays alpine areas face a human-induced warming period (Cook et al., 2016) together with an increase of soil erosion (FOEN, 2014). It has also been found that the growth of lower vegetation (e.g. shrubs) rose to higher elevations over the last decades (Cannone et al., 2007), while, strong floras habitat losses are projected for the Pyrenees and Eastern Austrian Alps due to climate change in the coming c. 80 years (Engler et al., 2011). Speculatively, a similarity could be seen between the current alpine development and the past of the Sila Massif. Pursuing this idea, an increase of erosion over the next

millennia should be expected until the vegetation has caught up. With the increase in erosion, risks associated with soil can be expected to change. Such predictions are relevant for forest enterprises, environmental protection associations and consulting, tourism (alpine) and businesses, and the public outdoor-enthusiasts. Moreover, investigations to model the risk of climate change on soils in Alpine territories presented huge difficulties due to data unavailability of past developments (Bosco et al., 2009). This resulted in over-simplifications of computation, large uncertainties of estimated erosion rates and therefore demands better quantitative estimations of soil losses (Bosco et al., 2009). The TEA can potentially supply modellers with the lacking information.

In summary, there is a large array of potential partners for collaborations available. Reaching out to them might be essential in order to develop a global soil erosion archive.

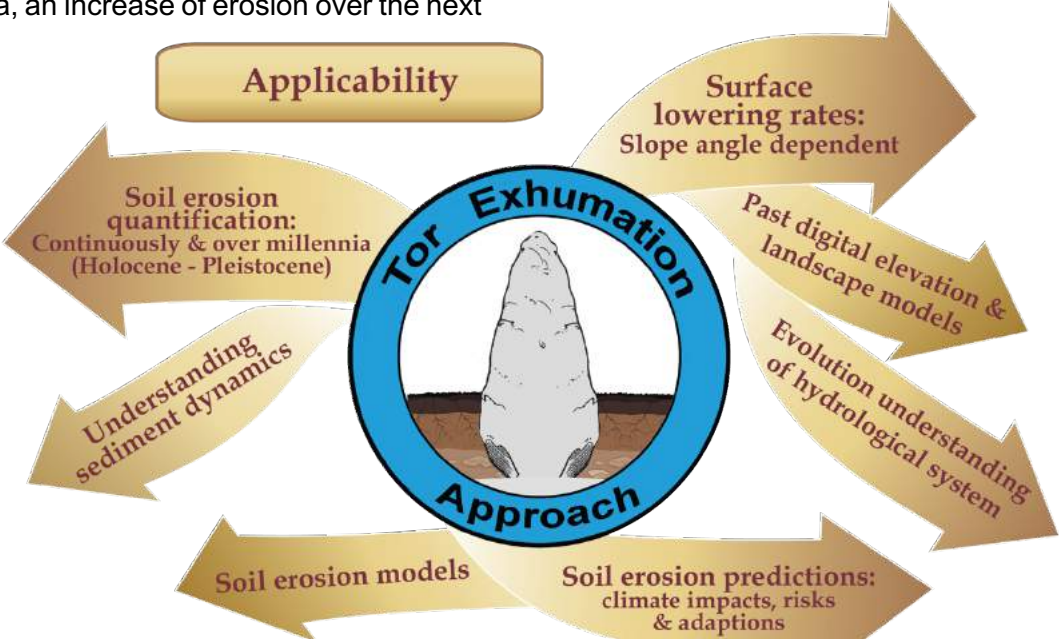


Figure 15: Ideas of applicability in a broader context.

REFERENCES

- Allen JRM, Brandt U, Brauer A, Hubberten HW, Hunley B, Keller J, Kraml M, Mackensen A, Mingram J, Negendank JFW, Nowaczyk NR, Oberhänsli H, Watts WA, Wulf S, Zolitschka B. 1999. Rapid environment changes in southern Europe during the last glacial period. *Nature* 400: 740-743. DOI: 10.1038/23432
- Allen JRM, Watts WA, McGee E, Huntley B. 2002. Holocene environmental variability – the record from Lago Grande di Monticchio, Italy. *Quaternary International* 88: 69–80. DOI: 10.1016/S1040-6182(01)00074-X
- Alewell C, Meusburger K, Juretzko G, Mabit L, Ketterer ME. 2014. Suitability of $^{239+240}\text{Pu}$ and ^{137}Cs as tracers for soil erosion assessment in mountain grasslands. *Chemosphere* 103: 274-280. DOI: 10.1016/j.chemosphere.2013.12.016
- Alewell C, Egli M, Meusburger K. 2015. An attempt to estimate tolerable soil erosion rates by matching soil formation with denudation in Alpine grasslands. *Journal of Soils and Sediments* 15 (6): 1383-1399. DOI: 10.1007/s11368-014-0920-6
- Alewell C, Pitois A, Meusburger K, Ketterer M, Mabit L. $^{239+240}\text{Pu}$ from “contaminant” to soil erosion tracer: Where do we stand? 2017. *Earth-Science Reviews* 172: 107-123. DOI: 10.1016/j.earscirev.2017.07.009
- Anderson SP, von Blanckenburg F, White AF. 2007. Physical and chemical controls on the Critical Zone. *Elements* 3 (5): 315-319. DOI: 10.2113/gselements.3.5.315
- Bajard M, Poulénard J, Sabatier P, Develle AL, Giguët-Covex C, Jacob J, Crouzet C, David F, Pignol C, Arnaud F. 2017. Progressive and regressive soil evolution phases in the Anthropocene. *Catena* 150: 39–52. DOI: 10.1016/j.catena.2016.11.001
- Blaikie P. 2016. *The political economy of soil erosion in developing countries*. Routledge
- Banwart SA, Bernasconi SM, Blum WE, de Souza DM, Chabaux F, Duffy C, Kercheva M, Krám P, Lair GJ, Lundin L, Menon M, Nikolaidis NP, Novak M, Panagos P, Ragnarsdóttir KV, Robinson DA, Rouseva S, de Ruiter, van Gaans P, Wenig I, White T, Zhang B. 2017. Soil functions in Earth's critical zone: key results and conclusions. In *Advances in Agronomy* 142: 1-27. DOI: 10.1016/bs.agron.2016.11.001
- Boardman J, Poesen J. (2007). *Soil erosion in Europe*. Chichester: John Wiley & Sons Ltd. DOI: 10.1002/0470859202
- Bouchard M, Jolicoeur S, 2000. Chemical weathering studies in relation to geomorphological research in southeastern Canada. *Geomorphology* 32 (3-4): 213–238. DOI: 10.1016/S0169-555X(99)00098-7
- Bosco C, Rusco E, Montanarella L, Panagos P. 2009. Soil erosion in the Alpine area: risk assessment and climate change. *Studi Trentini di scienze naturali* 85: 117-123.
- Brantley SL, White TS, White AF, Sparks D, Richter D, Pregitzer K, Derry L, Chorover J, Chadwick O, April R, Anderson S, Amundson R. 2006. *Frontiers in exploration of the Critical Zone: Report of a workshop sponsored by the National Science Foundation (NSF), 24-26 October 2005, Newark, DE, 30 pp.*
- Butzer KW. (1974). Accelerated soil erosion: a problem of man-land relationships. *Perspectives on environment* 13: 57-77.
- Cannone N, Sgorbati S, Guglielmin M. 2007. Unexpected impacts of climate change on alpine vegetation. *Frontiers in Ecology and the Environment* 5 (7) 360-364. DOI: 10.1890/1540-9295(2007)5[360:UIOCCO]2.0.CO;2

- Cerda A. 1999. Parent material and vegetation affect soil erosion in eastern Spain. *Soil Science Society of America Journal* 63 (2): 362-368. DOI: 10.2136/sssaj1999.03615995006300020014x
- Chmeleff J, von Blanckenburg F, Kossert K, Jakob D. 2010. Determination of the ^{10}Be half-life by multicollector ICP-MS and liquid scintillation counting. *Nuclear Instruments and Methods in Physics Research Section B: Beam Interactions with Materials and Atoms* 268 (2): 192-199. DOI: 10.1016/j.nimb.2009.09.012
- Christl M, Vockenhuber C, Kubik PW, Wacker L, Lachner J, Alfimov V, Sinal HA. 2013. The ETH Zurich AMS facilities: Performance parameters and reference materials. *Nuclear Instruments and Methods in Physics Research Section B: Beam Interactions with Materials and Atoms* 294: 29-38. DOI: 10.1016/j.nimb.2012.03.004
- Clift PD, Wan S, Blusztajn J. (2014). Reconstructing chemical weathering, physical erosion and monsoon intensity since 25 Ma in the northern South China Sea: A review of competing proxies. *Earth Science Reviews* 130: 86–102. DOI: 10.1016/j.earscirev.2014.01.002
- Cook J, Oreskes N, Doran PT, Anderegg WR, Verheggen B, Maibach EW, Carlton JS, Lewandosky S, Skuce AG, Green SA, Nuccitelli D, Jacobs P, Richardson M, Winkler B, Painting R, Rice K. 2016. Consensus on consensus: a synthesis of consensus estimates on human-caused global warming. *Environmental Research Letters*, 11(4): 048002. DOI: 10.1088/1748-9326/11/4/048002
- Crawford J. 2012. "What If the Worlds Soil Runs Out". *TIME*. December 14th.
- Delvaux B, Herbillon AJ, Vielvoye L. 1989. Characterization of a weathering sequence of soils derived from volcanic ash in Cameroon. Taxonomic, mineralogical and agronomic implications. *Geoderma* 45: 375–388. DOI: 10.1016/0016-7061(89)90017-7
- Dixon JL, von Blanckenburg F. (2012) Soils as pacemakers and limiters of global silicate weathering. *Comptes Rendus Geosciences* 344: 596-609. DOI: 10.1016/j.crte.2012.10.012
- Dunai TJ. 2010. *Cosmogenic Nuclides: Principles, concepts and applications in the Earth surface sciences*. Cambridge University Press. DOI: 10.1017/CBO9780511804519
- Dunai TJ, Lifton NA. 2014. The nuts and bolts of cosmogenic nuclide production. *Elements* 10: 347-350. DOI: 10.2113/gselements.10.5.347
- Dunne J, Elmore D, Muzikar P. 1999. Scaling factors for the rates of production of cosmogenic nuclides for geometric shielding and attenuation at depth on sloped surfaces. *Geomorphology* 27 (1-2): 3-11. DOI: 10.1016/S0169-555X(98)00086-5
- Ehlen J. 2005. Above the weathering front: contrasting approaches to the study and classification of weathered mantle. *Geomorphology* 67: 7-21. DOI: 10.1016/j.geomorph.2004.09.026
- Engler R, Randin CF, Thuiller W, Dullinger S, Zimmermann NE, Araújo MB, Pearman PB, Le Lay G, Piedallus C, Albert CH, Choler P, Coldea G, de Lamo X, Dirnböck T, Gégout JC, Gomez-Garcia D, Grytnes JW, Heegaard E, Høistad F, Nogués-Bravo D, Normand S, PusCas M, Sebastià MT, Stanisci A, Theurillat JP, Trivedi M, Vittoz P, Guisan A. 2011. 21st century climate change threatens mountain flora unequally across Europe. *Global Change Biology* 17 (7): 2330-2341. DOI: 10.1111/j.1365-2486.2010.02393.x
- Enters D, Dörfler W, Zolitschka B. 2008. Historical soil erosion and land-use change during the last two millennia recorded in lake sediments of Frickenhauser See, northern Bavaria, central Germany. *The Holocene* 18-2: 243-254. DOI: 10.1177/0959683607086762
- Federal Office for the Environment (FOEN). 2014. *Soil erosion in the Alps: Experience gained from case studies (2006-2013)*. Bern.

- Food and Agriculture Organization (FAO) of the United Nations. 2015. <http://www.fao.org/resources/infographics/infographics-details/en/c/284480/>. Accessed: June 17th 2019.
- Food and Agriculture Organization (FAO) of the United Nations. 2015. <http://www.fao.org/resources/infographics/infographics-details/en/c/284480/>. Accessed: June 17th 2019.
- Forni F, Lucchi F, Peccerillo A, Tranne CA, Rossi PL, Frezzotti ML. 2013. Chapter 10 Stratigraphy and geological evolution of the Lipari volcanic complex (central Aeolian archipelago). In: Lucchi F, Peccerillo A, Keller J, Tranne CA, Rossi PL. (Eds.), *The Aeolian Islands Volcanoes*: 213–279. The Geological Society of London. DOI: 10.1144/M37.10
- Gosse JC, Phillips FM. 2001. Terrestrial in situ cosmogenic nuclides: theory and application. *Quaternary Science Reviews* 20 (14): 1475-1560. DOI: 10.1016/S0277-3791(00)00171-2
- Graham RC, Rossi AM, Kenneth RH. 2010. Rock to regolith conversion: Producing hospitable substrates for terrestrial ecosystems. *GSA today* 20 (3): 4-9. DOI: 10.1130/GSAT57A.1
- Harnois L. 1988. The CIW index: a new Chemical Index of Weathering. – *Sedimentary Geology* 55: 319–322. DOI: 10.1016/0037-0738(88)90137-6
- Heimsath AM, Dietrich WE, Nishiizumi K, Finkel RC. 1999. Cosmogenic nuclides, topography, and the spatial variation of soil depth. *Geomorphology* 27: 151–172. DOI: 10.1016/S1040-6182(01)00038-6
- Heimsath AM, Chappell J, Dietrich WE, Nishiizumi K, Finkel RC. 2001a. Late Quaternary erosion in southeastern Australia: a field example using cosmogenic nuclides. *Quaternary International* 83–85: 169–185. DOI:
- Heimsath AM, Dietrich WE, Nishiizumi K, Finkel RC. 2001b. Stochastic processes of soil production and transport: erosion rates, topographic variation and cosmogenic nuclides in the Oregon coast range. *Earth Surface Processes and Landforms* 26: 531-552. DOI: 10.1002/esp.209
- Heimsath AM. 2006. Eroding the land: steady-state and stochastic rates and processes through a cosmogenic lens. *GSA Special Paper* 415: 111–129. DOI: 10.1130/2006.2415(07).
- Heimsath AM, DiBiase RA, Whipple KX. 2012. Soil production limits and the transition to bedrock-dominated landscapes. *Nature* 5: 210-214. DOI: 10.1038/ngeo1380
- Herman F, Seward D, Valla PG, Carter A, Kohn B, Willett SD, Ehlers TA. 2013. Worldwide acceleration of mountain erosion under a cooling climate. *Nature* 504 (7480): 423. DOI: 10.1038/nature12877
- Hu QH, Weng JQ, Wang JS. 2010. Sources of anthropogenic radionuclides in the environment: a review. *Journal of Environmental Radioactivity* 101: 426–437. DOI: 10.1016/j.jenvrad.2008.08.004.
- Ivy-Ochs S, Schaller M. 2009. Examining processes and rates of landscape change with cosmogenic radionuclides. *Radioactivity in the Environment* 16: 231-294. DOI: 10.1016/S1569-4860(09)01606-4
- Johnson DL, Watson-Stegner D. 1987. Evolution model of pedogenesis. *Soil Science* 143: 349–366. DOI: 10.1097/00010694-198705000-00005
- Ketterer ME, Hafer KM, Link CL, Kolwaite D, Wilson J, Mietelski JW. 2004. Resolving global versus local/regional Pu sources in the environment using sector ICP-MS. *Journal of Analytical Atomic Spectrometry* 19: 241–245. DOI: 10.1039/B302903D

- Kirchner JW, Finkel RC, Riebe CS, Granger DE, Clayton JL, King JG, Megahan, WF. 2001. Mountain erosion over 10 yr, 10 ky, and 10 my time scales. *Geology* 29 (7): 591–594. DOI: /10.1130/0091-7613(2001)029<0591:MEOYKY>2.0.CO;2
- Kohl CP, Nishiizumi K. 1992. Chemical isolation of quartz for measurement of in-situ-produced cosmogenic nuclides. *Geochimica et Cosmochimica Acta* 56(9): 3583-3587. DOI: 10.1016/0016-7037(92)90401-4
- Lal D. 1988. In situ-produced cosmogenic isotopes in terrestrial rocks. *Annual Review of Earth and Planetary Sciences* 16 (1): 355-388. DOI: 10.1146/annurev.ea.16.050188.002035
- Liu BY, Nearing MA, Risse LM. 1994. Slope gradient effects on soil loss for steep slopes. *Transactions of the ASAE* 37 (6): 1835-1840. DOI: 10.13031/2013.28273
- Mabit L, Benmansour M, Walling DE. 2008. Comparative advantages and limitations of the fallout radionuclides ¹³⁷Cs, ²¹⁰Pbex and ⁷Be for assessing soil erosion and sedimentation. *Journal of environmental radioactivity* 99 (12): 1799-1807. DOI: 10.1016/j.jenvrad.2008.08.009
- Masarik J, Beer J. 1999. Simulation of particle fluxes and cosmogenic nuclide production in the Earth's atmosphere. *Journal of Geophysical Research: Atmospheres* 104 (D10): 12099-12111. DOI: 10.1029/1998JD200091
- Migoń P, Lidmar-Bergström K. 2001. Weathering mantles and their significance for geomorphological evolution of central and northern Europe since the Mesozoic. *Earth-Science Reviews* 56 (1): 285-324. DOI: 10.1016/S0012-8252(01)00068-X
- Migoń P, Lidmar-Bergström, K. 2002. Deep weathering through time in central and NW Europe: problems of dating and interpretation of geological record. *Catena* 49: 25–40. DOI: 10.1016/S0341-8162(02)00015-2
- Migoń P, Thomas MF. 2002. Grus Weathering Mantles — Problems of Interpretation. *Catena* 49: 5–24. DOI: 10.1016/S0341-8162(02)00014-0
- Migoń P. (2006). *Granite Landscapes of the World (Vol. 2). Geomorphological Landscapes of the World.* Oxford University Press.
- Migoń P. 2013. Weathering and hillslope development. In J. F. Shroder (Ed.), *Treatise on geomorphology (Vol. 4)* (pp. 159–178). San Diego: Academic Press. DOI: 10.1016/B978-0-12-374739-6.00075-0
- Mohammad AG, Adam MA. 2010. The impact of vegetative cover type on runoff and soil erosion under different land uses. *Catena* 81 (2): 97-103. DOI: 10.1016/j.catena.2010.01.008
- Molin P, Pazzaglia FJ, Dramis F. 2004. Geomorphic expression of active tectonics in a rapidly-deforming fore-arc, Sila Massif, Calabria, Southern Italy. *American Journal of Science* 304: 559–589. DOI: 10.2475/ajs.304.7.559
- Montgomery DR, Brandon MT. 2002. Topographic controls on erosion rates in tectonically active mountain ranges. *Earth and Planetary Science Letters* 201(3-4): 481-489. DOI: 10.1016/S0012-821X(02)00725-2
- Mourier B, Poulénard J, Carcaillet C, Williamson D. 2010. Soil evolution and subalpine ecosystem changes in the French Alps inferred from geochemical analysis of lacustrine sediments. *Journal of Paleolimnology* 44 (2): 571–587. DOI: 10.1007/s10933-010-9438-0
- National Research Council (NRC). 2001. *Basic research opportunities in Earth Science.* National Academy Press, Washington, DC.
- Nearing MA, Pruski FF, O'neal MR. 2004. Expected climate change impacts on soil erosion rates: a review. *Journal of soil and water conservation* 59 (1): 43-50.

- Norton KP, von Blanckenburg F, Kubik PW. 2010. Cosmogenic nuclide-derived rates of diffusive and episodic erosion in the glacially sculpted upper Rhone Valley, Swiss Alps. *Earth Surface Processes and Landforms* 35: 651–662. DOI: 10.1002/esp.1961
- Norton KP, Von Blanckenburg F, DiBiase R, Schlunegger F, Kubik PW. 2011. Cosmogenic ^{10}Be -derived denudation rates of the Eastern and Southern European Alps. *International Journal of Earth Sciences* 100 (5): 1163-1179. DOI: 10.1007/s00531-010-0626-y
- Olivetti V, Cyr AJ, Molin P, Faccenna C, Granger DE. 2012. Uplift history of the Sila Massif, southern Italy, deciphered from cosmogenic ^{10}Be erosion rates and river longitudinal profile analysis. *Tectonics* 31: 1–19. DOI: 10.1029/2011TC003037
- Pelle T, Scarciglia F, Di Pasquale G, Allevato E, Marino D, Robustelli G, La Russa MF, Pulice I. 2013. Multidisciplinary study of Holocene archaeological soils in an upland Mediterranean site: natural versus anthropogenic environmental changes at Cecita Lake, Calabria, Italy. *Quaternary International* 303: 163-179. DOI: 10.1016/j.quaint.2013.04.003Sc
- Pérez-Obiol R, Sadori L. 2007. Similarities and dissimilarities, synchronisms and diachronisms in the Holocene vegetation history of the Balearic Islands and Sicily. *Vegetation History and Archaeobotany* 16 (4): 259-265. DOI: 10.1007/s00334-006-0038-x
- Phillips JD. 2010. The convenient fiction of steady-state soil thickness. *Geoderma*, 156 (3-4): 389-398. DOI: 10.1016/j.geoderma.2010.03.008
- Pimentel D, Harvey C, Resosudarmo P, Sinclair K, Kurz D, McNair M, Crist S, Shpritz L, Fitton L, Saffouri, Blair R. 1995. Environmental and Economic Costs of Soil Erosion and Conservation. *Science* 267: 1117–1123. DOI: 10.1126/science.267.5201.1117
- Pimentel D. 2006. Soil Erosion: A Food and Environmental Threat," *Environmental Development and Sustainability* 8: 119. DOI: 10.1007/s10668-005-1262-8
- Poesen J. 2018. Soil erosion in the Anthropocene: Research needs. *Earth Surface Processes and Landforms* 43: 64–84. DOI: 10.1002/esp.4250
- Portenga EW, Bierman PR. 2011. Understanding Earth's eroding surface with ^{10}Be . *GSA today* 21 (8): 4-10. DOI: 10.1130/G111A.1
- Porto P, Walling DE, Callegari G. 2013. Using ^{137}Cs and $^{210}\text{Pb}_{\text{ex}}$ measurements to investigate the sediment budget of a small forested catchment in southern Italy. *Hydrological Processes* 27 (6): 795-806. DOI: doi.org/10.1002/hyp.9471
- Richter DD, Markewitz D. 2001. *Understanding soil change: soil sustainability over millennia, centuries, and decades*. Cambridge University Press.
- Scarciglia F, Le Pera E, Critelli S. 2005. Weathering and pedogenesis in the Sila Grande Massif (Calabria, south Italy): From field scale to micromorphology. *Catena* 61: 1-29. DOI: 10.1016/j.catena.2005.02.001
- Scarciglia F, Le Pera E, Critelli S. 2007. The onset of the sedimentary cycle in a mid-latitude upland environment: weathering, pedogenesis and geomorphic processes on plutonic rocks (Sila Massif, Calabria). In: Arribas J, Critelli S, Johnsson MJ. (Eds.), *Sedimentary provenance and petrogenesis: Perspectives from petrography and geochemistry*. Geological Society of America Special Paper 420: 149-166. DOI: 10.1130/2006.2420(10)
- Schaller M, Blum JD, Ehlers TA. 2010a. Combining cosmogenic nuclides and major elements from moraine soil profiles to improve weathering rate estimates. *Geomorphology* 115: 117-128. DOI: 10.1016/j.geomorph.2009.09.040
- Schaller M, Ehlers TA, Blum JD. 2010b. Soil transport on a moraine foreslope. *Geomorphology* 115: 117-128. DOI: 10.1016/j.geomorph.2009.09.040

- Sommer M, Gerke HH, Deumlich D. 2008. Modelling soil landscape genesis – A “time split” approach for hummocky agricultural landscapes. *Geoderma* 145: 480-493. DOI: 10.1016/j.geoderma.2008.01.012
- United Nations (UN) News. 2017, September 12. Much of the planet’s land severely degraded owing to increased consumption, UN warns. Retrieved from: <https://news.un.org/en/story/2017/09/564752-much-planets-land-severely-degraded-owing-increased-consumption-un-warns>
- Von Blanckenburg F, Belshaw NS, O’Nions, RK. 1996. Separation of ^9Be and cosmogenic ^{10}Be from environmental materials and SIMS isotope dilution analysis. *Chemical Geology* 129 (1-2): 93-99. DOI: 10.1016/0009-2541(95)00157-3
- Wallbrink PJ, Murray AS. 1993. Use of fallout radionuclides as indicators of erosion processes. *Hydrological Processes* 7: 297–304. DOI: 10.1002/hyp.3360070307
- Wilding LP, Lin H. 2006. Advancing the frontiers of soil science towards a geoscience. *Geoderma* 131: 257-274. DOI: 10.1016/j.geoderma.2005.03.028
- Wieler R, Beer J, Leya I. 2013. The galactic cosmic ray intensity over the past 10^6 – 10^9 years as recorded by cosmogenic nuclides in meteorites and terrestrial samples. *Space science reviews*, 176 (1-4): 351-363. DOI: 10.1007/s11214-011-9769-9
- Yoo K, Mudd SM, Sanderman J, Amundson R, Blum A. 2009. Spatial patterns and controls of soil chemical weathering rates along a transient hillslope. *Earth and Planetary Science Letters* 288: 184–193. DOI: 10.1016/j.epsl.2009.09.021
- Zheng FL. 2006. Effect of vegetation changes on soil erosion on the Loess Plateau. *Pedosphere* 16 (4): 420-427. DOI: 10.1016/S1002-0160(06)60071-4

ACKNOWLEDGEMENTS

It would be foolish to assume that a doctorate is a purely individual achievement. Many people accompany one on this track. When I look back over the last three years, I see a large array of people that have helped me to make it an exciting and memorable journey. Although it seems to be an impossible task to name all of them, I will do my best to say, 'Thank you' to all of you.

First, I thank my main supervisor Markus Egli who gave me the great opportunity to conduct my doctoral research. I am grateful for the generous working environment he provided for me and the trust he gave me to carry out my duties. I am also grateful for the really wonderful support of our technicians Dagmar Brandová, Sandra Röthlisberger, Thomy Keller, Dmitry Tikhomirov and Tatjana Kraut — not to forget the help of our administrative personal Isabelle Wüest and Frank Hitzemann and our IT support Roya Soleymani Kohler. Your time and effort were invaluable in order for me to succeed.

Also, a part of lab and office who actively supported me during field work or interpreting data and formulating structured sentences out of (often) confusing puzzles of thoughts. Among other, this includes Fabio Scarciglia, Kevin Norton, Dennis Dahms and Raquel de Castro Portes. In addition, critical reflections from Max Maisch and Christine Alewell have repeatedly allowed me to see new perspectives of my work.

I also have to give my gratitude to Max Gero Boxleitner with whom I enjoyed many fruitful discussions. Overall, I was very lucky to be surrounded by a great mix of colleagues at the University of Zurich. Some of them are Alessandra Musso, Alessandro Cicoira, Alina Motschmann, Alysha Coppola, Barbara Strobl, Beatrice Gonzales Domingues, Cyrill Zosso, Emily Solly, Christoph Vogel, Cordula Friedli, Darshan Karki, Fabian Maier, Francesca Calitri, James Furguson, Juliane Hirte, Kavita Srivastava, Kirsti Hakala, Leonie Kiewit, Manuela Brunner, Marcus Schiedung, Moritz Reisser, Mirjam Studer, Nicholas Ofiti, Nico Mölg, Oliver Burkhard, Sanne Diek, Severin-Luca Bellè and Simon Etter.

Last but not least, I have to thank my family. First and foremost, my lovely partner Michaela Rußmann. I am thankful for her endurance of my long (nightly) work hours and numerous journeys and the resulting distance and loneliness. Such an endurance cannot be expected to be easily granted. I also say thank you to her side of the family who looked after my well-being at all times. Finally, a special thanks goes to my parents and their partners, my siblings and relatives who all kept believing in me.

APPENDICES

The original manuscripts I and II in the results section include all data for reproducibility. The following Table S1 includes background data of manuscripts III which has not found its way into the official printed version.

TABLE S1 Sample input data for CRONUS online calculator v2.3 (Baclo et al., 2008).

	Latitude	Longitude	Elev.	Press.	Thick.	Density	Shielding	Erosion	Be ¹⁰	+/-	Be AMS	Al ²⁶	+/-	Al AMS
	[DD]	[DD]	[m]	flag	[cm]	[g cm ⁻²]	[-]	[cm yr ⁻¹]	[atoms g ⁻¹]	[atoms g ⁻¹]	standard	[atoms g ⁻¹]	[atoms g ⁻¹]	standard
Boulder 1														
B1-1	39.28055556	16.53861111	1572	std	2.00	2.65	0.9993462	0.0001	302422.62	16444.97	07KNSTD	0.000E+00	0.000E+00	KNSTD
B1-2	39.28055556	16.53861111	1572	std	3.00	2.65	0.6130000	0.0001	314671.19	12678.05	07KNSTD	0.000E+00	0.000E+00	KNSTD
B1-3	39.28055556	16.53861111	1572	std	3.00	2.65	0.8790000	0.0001	698344.01	28025.36	07KNSTD	0.000E+00	0.000E+00	KNSTD
B1-4	39.28055556	16.53861111	1572	std	3.00	2.65	0.5577016	0.0001	344030.00	34058.48	07KNSTD	0.000E+00	0.000E+00	KNSTD
B1-5	39.28055556	16.53861111	1572	std	3.00	2.65	0.4980000	0.0001	284000.00	21100.00	07KNSTD	0.000E+00	0.000E+00	KNSTD
B1-6	39.28055556	16.53861111	1572	std	3.00	2.65	0.4900000	0.0001	501100.00	29700.00	07KNSTD	0.000E+00	0.000E+00	KNSTD
Boulder 2														
B2-1	39.30066667	16.53677778	1475	std	2.00	2.65	0.9981940	0.0001	265127.58	13619.24	07KNSTD	0.000E+00	0.000E+00	KNSTD
B2-6	39.30066667	16.53677778	1475	std	9.50	2.65	0.6124795	0.0001	167379.96	8476.94	07KNSTD	0.000E+00	0.000E+00	KNSTD
Boulder 3														
B3-1	39.27658333	16.54905556	1567	std	1.00	2.65	0.9926985	0.0001	643518.04	17707.34	07KNSTD	0.000E+00	0.000E+00	KNSTD
B3-6	39.27658333	16.54905556	1567	std	1.50	2.65	0.6765712	0.0001	70289.95	3519.21	07KNSTD	0.000E+00	0.000E+00	KNSTD
Tor 1*														
T1-1	39.26852778	16.5353	1504	std	2.00	2.65	0.9986884	0.0001	449874.32	25147.16	07KNSTD	0.000E+00	0.000E+00	KNSTD
T1-2	39.26852778	16.5353	1504	std	3.00	2.65	0.5894925	0.0001	199524.28	7799.75	07KNSTD	0.000E+00	0.000E+00	KNSTD
T1-3	39.26852778	16.5353	1504	std	2.50	2.65	0.5435041	0.0001	184225.52	7059.29	07KNSTD	0.000E+00	0.000E+00	KNSTD
T1-4	39.26852778	16.5353	1504	std	1.80	2.65	0.4981389	0.0001	165951.50	6692.59	07KNSTD	0.000E+00	0.000E+00	KNSTD
T1-5	39.26852778	16.5353	1504	std	2.00	2.65	0.4731655	0.0001	110791.03	4936.78	07KNSTD	0.000E+00	0.000E+00	KNSTD
T1-6	39.26852778	16.5353	1504	std	1.00	2.65	0.5092840	0.0001	121791.35	5659.59	07KNSTD	0.000E+00	0.000E+00	KNSTD

Tor 2*

T2-1	39.28138889	16.53972222	1572	std	2.00	2.65	0.9722750	0.0001	1124392.13	43924.80	07KNSTD	0.000E+00	0.000E+00	KNSTD
T2-2	39.28138889	16.53972222	1572	std	3.00	2.65	0.6539965	0.0001	709374.35	27041.14	07KNSTD	0.000E+00	0.000E+00	KNSTD
T2-4	39.28138889	16.53972222	1572	std	2.00	2.65	0.7713454	0.0001	301233.28	14884.82	07KNSTD	0.000E+00	0.000E+00	KNSTD
T2-5	39.28138889	16.53972222	1572	std	3.00	2.65	0.5009799	0.0001	69636.78	13956.20	07KNSTD	0.000E+00	0.000E+00	KNSTD
T2-6	39.28138889	16.53972222	1572	std	9.50	2.65	0.7240485	0.0001	138208.80	7185.71	07KNSTD	0.000E+00	0.000E+00	KNSTD

Tor 3*

T3-1	39.28378889	16.53804167	1569	std	2.00	2.65	0.9991864	0.0001	454498.55	10355.57	07KNSTD	0.000E+00	0.000E+00	KNSTD
T3-3	39.28378889	16.53804167	1569	std	2.00	2.65	0.4980073	0.0001	181842.79	5558.30	07KNSTD	0.000E+00	0.000E+00	KNSTD
T3-4	39.28378889	16.53804167	1569	std	4.00	2.65	0.4980073	0.0001	187255.52	5303.40	07KNSTD	0.000E+00	0.000E+00	KNSTD
T3-5	39.28378889	16.53804167	1569	std	2.00	2.65	0.6074053	0.0001	167649.82	5651.15	07KNSTD	0.000E+00	0.000E+00	KNSTD

Tor 4

T4-1	39.29915	16.53905556	1465	std	3.00	2.65	0.9259071	0.0001	341364.73	8407.53	07KNSTD	0.000E+00	0.000E+00	KNSTD
T4-2	39.29915	16.53905556	1465	std	3.00	2.65	0.6120609	0.0001	238184.52	6954.06	07KNSTD	0.000E+00	0.000E+00	KNSTD
T4-4	39.29915	16.53905556	1465	std	3.00	2.65	0.6120609	0.0001	132411.75	4613.81	07KNSTD	0.000E+00	0.000E+00	KNSTD
T4-5	39.29915	16.53905556	1465	std	3.00	2.65	0.6120609	0.0001	85754.31	2977.96	07KNSTD	0.000E+00	0.000E+00	KNSTD

Tor 5

T5-1	39.30066667	16.53677778	1475	std	2.00	2.65	0.9856913	0.0001	377258.38	13092.27	07KNSTD	0.000E+00	0.000E+00	KNSTD
T5-2	39.30066667	16.53677778	1475	std	1.50	2.65	0.9693221	0.0001	312258.09	14949.18	07KNSTD	0.000E+00	0.000E+00	KNSTD
T5-4	39.30066667	16.53677778	1475	std	2.20	2.65	0.9825776	0.0001	330359.20	11089.76	07KNSTD	0.000E+00	0.000E+00	KNSTD
T5-5	39.30066667	16.53677778	1475	std	1.80	2.65	0.8451667	0.0001	225439.13	8378.27	07KNSTD	0.000E+00	0.000E+00	KNSTD
T5-6	39.30066667	16.53677778	1475	std	1.80	2.65	0.5275316	0.0001	208559.19	11968.70	07KNSTD	0.000E+00	0.000E+00	KNSTD

Scarp 1

S1-C1	39.31836300	16.53688100	1360	std	3.00	2.65	0.9320623	0.0001	150470.00	8125.15	07KNSTD	0.000E+00	0.000E+00	KNSTD
-------	-------------	-------------	------	-----	------	------	-----------	--------	-----------	---------	---------	-----------	-----------	-------

Scarp 2

S2-A1	39.31843056	16.54310556	1393	std	2.50	2.65	0.8897977	0.0001	111550.88	6674.08	07KNSTD	0.000E+00	0.000E+00	KNSTD
S2-B1	39.31843056	16.54310556	1393	std	2.50	2.65	0.9769737	0.0001	132994.50	5378.45	07KNSTD	0.000E+00	0.000E+00	KNSTD
S2-B2	39.31843056	16.54310556	1393	std	2.50	2.65	0.4921216	0.0001	73626.48	3925.09	07KNSTD	0.000E+00	0.000E+00	KNSTD
S2-C1	39.31843056	16.54310556	1393	std	2.50	2.65	0.9971275	0.0001	129988.02	4307.61	07KNSTD	0.000E+00	0.000E+00	KNSTD
S2-C2	39.31843056	16.54310556	1393	std	2.50	2.65	0.7141295	0.0001	95121.77	3887.78	07KNSTD	0.000E+00	0.000E+00	KNSTD
S2-C3	39.31843056	16.54310556	1393	std	2.50	2.65	0.7104513	0.0001	70049.78	3450.22	07KNSTD	0.000E+00	0.000E+00	KNSTD

Scarp 3

S3-A1	39.31200000	16.55619444	1422	std	1.30	2.65	0.9815712	0.0001	98178.22	4595.24	07KNSTD	0.000E+00	0.000E+00	KNSTD
S3-B1	39.31200000	16.55619444	1422	std	1.50	2.65	0.9926985	0.0001	140365.89	8761.17	07KNSTD	0.000E+00	0.000E+00	KNSTD
S3-C1	39.31200000	16.55619444	1422	std	1.50	2.65	0.9921959	0.0001	97831.67	5236.45	07KNSTD	0.000E+00	0.000E+00	KNSTD
S3-C2	39.31200000	16.55619444	1422	std	3.00	2.65	0.9769043	0.0001	103476.92	7974.30	07KNSTD	0.000E+00	0.000E+00	KNSTD

CURRICULUM VITAE



PERSONAL DETAIL

RAAB, Gerald
26.01.1988
Steyr, Austria

EDUCATION

- Sept. 2013 – Nov. 2015 Master of Sciences in Earth Sciences, University of Technology Graz, Austria. Thesis title: “*Magmatic, Metamorphic and Tectonic Evolution of the Seckau Complex in the Area of the Sonntagskogel Mountain (Triebener Tauern, Province of Styria)*”
- Sept. 2012 – May 2013 Environmental Engineering, Aalto University Espoo, Finland
- Sept. 2009 – Aug. 2012 Bachelor of Sciences in Earth Sciences, University of Technology Graz, Austria
- June 2007 Matura, Federal Commercial Academy Steyr, Austria

DOCTORATE

- April 2016 – present Doctorate at the Department of Geography, University of Zurich, Switzerland
- Professional training:
May 2019 Visiting Researcher at the Institute of Geography and Regional Development, University of Wroclaw, Polen
- Aug. 2018 Climate Change Impacts on Sediment Dynamics: Measurement, Modelling and Management. IYFSWC Conference, Moscow, Russia
- Sept. 2017 International Geochronology Summer School — Dating Techniques in Environmental Research, Davos, Switzerland
- March 2017 Petrochronology: Methods and Application, University of Bern course at the European Geoscience Union Conference, Vienna, Austria
- Feb. 2017 Research stay at the School of Geography and Environmental and Earth Sciences, Victoria University of Wellington, New Zealand
- April 2016 Laser meets Mineral — Raman Spectroscopy and its Application in Geosciences and Related Field. Montan University of Leoben, Austria

<u>Transferable skills courses:</u>	Fund acquisition, research integrity, managing conflicts, project management, resource-oriented stress management, scientific writing, scientific publication — discover manage disseminate, successful fund acquisition and grant writing, time- and self-management, negotiation and moderation techniques, leadership skills for doctoral students
<u>Institutional responsibilities:</u>	
June 2016 – April 2019	Mittelbau (union) representative within the Faculty of Mathematics and Natural Science, University of Zurich, Switzerland
Sept. 2017 – May 2019	Laboratory focus group, Department of Geography, University of Zurich, Switzerland
<u>Conference contributions:</u>	
April 2019 (convener)	Visualizing Science. Short Course. EGU. Vienna. Austria
April 2019 (poster)	Going beyond average rates — Identifying responsible drivers for temporal and spatial denudation variations using in-situ ^{10}Be on a variety of granitic landscape features. EGU. Vienna. Austria
Aug. 2018 (oral)	“Modelling soil erosion dynamics over millennia using granite landforms, in-situ ^{10}Be and $^{239+240}\text{Pu}$ ”. The second international young scientists’ forum on soil and water conservation and ICCE symposium. Moscow. Russia
May 2018 (oral)	A story of granite landforms and surface denudation variations. Young Geomorphologist meeting. Stadtdendorf. Germany
April 2018 (poster)	Using granite landforms to decrypt soil erosion variations over millennia with in-situ ^{10}Be and $^{239+240}\text{Pu}$. EGU. Vienna. Austria
Aug. 2017 (oral)	Deciphering Landscape Archives of the Sila Massif by linking ^{10}Be & $^{239/240}\text{Pu}$. Goldschmidt. Paris. France
April 2017 (poster)	Tracing Landscape Evolution of the Sila Massif using ^{10}Be . EGU. Vienna. Austria
April 2017 (poster)	Linking tephrochronology and soil characteristics in the Sila and Nebrodi Mountains, Italy. EGU. Vienna. Austria

ADDITIONAL PUBLICATIONS

- Yu, F., Hunt, A., Egli, M., & **Raab, G.** (2019). Comparison and contrast in soil depth evolution for steady-state and stochastic erosion processes: Possible implications for landslide prediction. *Geochemistry, Geophysics, Geosystems*. DOI: 10.1029/2018GC008125
- Egli M., Hunt A., Dahms D., **Raab G.**, Derungs C., Raimondi S., & Yu F. (2018). Prediction of soil formation as a function of age using the percolation theory approach. *Front. Environ. Sci.* 6: 108. DOI: 10.33689/fenvs.2018.00108
- Portes R., Dahms D., Brandová D., **Raab G.**, Christl M., Kühn P., Ketterer M. & Egli M. (2018). Evolution of soil erosion rates in alpine soils of the Central Rocky Mountains using fallout Pu and $\delta^{13}C$. *Earth and Planetary Science Letters* 496: 258-269. DOI: 10.1016/j.epsl.2018.06.002
- Ganyushkin D., Chistyakov K., Volkov I., Bantcev D., Kunaeva E., Brandova D., **Raab G.**, Christl M., & Egli M. (2018). Palaeoclimate, glacier and treeline reconstruction based on geomorphic evidences in the Mongun-Taiga massif (south-eastern Russian Altai) during the Late Pleistocene and Holocene. *Quaternary International* 470: 26-37. DOI: 10.1016/j.quaint.2017.12.031
- Egli M., Hafner S., Derungs C., Ascher-Jenuß J., Camin F., Sartori G., **Raab G.**, Bontempo L., Paolini M., Ziller L., Bardelli T., Bardelli, T., Petrillo M. & Abiven S. (2016). Decomposition and stabilisation of Norway spruce needle-derived material in Alpine soils using a ^{13}C -labelling approach in the field. *Biogeochemistry* 131(3): 321-338. DOI: 10.1007/s10533-016-0281-x
- Höllén D., Klammer D., Letofsky-Papst I., **Raab G.**, & Dietzel M. (2016). Synthesis of hierarchically structured materials: microporous diatoms and nanoporous hydroxyaluminosilicate. *Nanotechnology for Environmental Engineering* 1(1): 9. DOI: 10.1007/s41204-016-0009-0
- Mogessie A., Hauzenberger C., Raic S., Schantl P., Belohlavek L., Ciriello A., Daghighi D., Fercher B., Goetschl K., Graber H., Mandl M., Preissegger V., **Raab G.**, Rauschenbusch F., Sattler T., Schorn S., Simic K., Wedenig M., Wiesmair S., Melcher F., Prochaska W., Mali H., Binder H., Dietmayer-Kräuter M., Friedman C., Haas M.M., Hampl F.J., Hanke G.E., Hasenburger W., Kaltenbock H.M., Onuk P., Pamsl A.R., Pongratz K., Schifko T., Schilli S.E., Schwabl S., Tauchner C., Wallner D., & Hentsche J. (2015). A Geological Excursion to the Mining Areas of South Africa. *Mitt.Österr.Miner.Ges.* 161: 175-219.
- Stüwe K., **Raab G.**, Rauschenbusch F., Piller E.W., & Claus P. (2015). Eine Geo-Reise durch Grönland. Weishaupt Verlag.